Neuroanatomical screening and analysis of transgenic and ENU induced mutagenised mice

A thesis written, composed and presented by

Mister Andrew Edwards, BSc, MRes

A student of Corpus Christi College
University of Oxford

Submitted for the rank

Doctor of Philosophy in Clinical Medicine

In the academic session

Trinity Term

MMXI

Dominus Illuminatio Mea

Abstract

Neuroanatomical screening and analysis of transgenic and ENU mutagenised mice

Andrew Edwards
The Wellcome Trust Centre for Human Genetics
Department of Clinical Medicine
Corpus Christi College, University of Oxford
D.Phil. Thesis
Trinity Term 2011

I have sought to discover genetic causes of neuroanatomical defects by conducting N-ethyl-N-nitrosourea mutagenesis and transgenic knock out screens in mice. The rationale behind this is that mutations causal to structural defects will be informative about developmental neurobiology and the biological basis of behaviour. Direct screening for behavioural abnormalities in mice has historically been arduous and yielded few findings due to small effect sizes and limited statistical power. My approach sought to bypass these problems by screening for highly penetrant morphological phenotypes. This thesis details my screens and the histological, genetic and behavioural characterisation of lines of interest. These include models of hydrocephalous, pyramidal cell layer ectopia, abnormal neurogenesis, corpus callosum agenesis, hippocampal enlargement, elevated cell death and hypomyelination.

Whilst N-ethyl-N-nitrosourea mutagenesis screening has been conducted since the twilight of the 20th century, systematic transgenic knock out screening is currently in its infancy. By discovering gene-phenotype associations through both approaches, I have been able to compare the relative yields, strengths and weaknesses of the two screening methods. Additionally, I have discussed the significant of the gene-phenotype associations produced from both screens.

Acknowledgements

I am extremely grateful for the abundance of help I received throughout my DPhil. Jonathan Flint is an excellent supervisor and was unfailingly supportive of my work. He ensured my projects were well directed and that I had all the resource required to thrive. Special thanks for reviewing my thesis drafts and tolerating my numerous dyslexia driven spelling errors.

David Keays and Guo-Jen Huang were key collaborators. From them, I learned most of my molecular and histological skills. Both were inspiring in their work ethic. When I left the lab at midnight, I could rest assured that GJ was still in the building and flying his remote controlled aeroplane whilst running gels. I am also thankful to James Cleak, Polinka Hernandez-Pliego, Stewart Davidson and my many, many, students who helped harvest and slice brains. Significantly less would have been achieved without their labours. Additionally, Jon Krohn and Tom Campbell helped write and debug the R scripts. Wei Yuan was also a huge help with SNP calling.

In terms of external collaborators, Helen Dawe and Mike Shaw helped process the tissue for scanning electron microscopy and were a pleasure to work alongside. At Experimental Psychology, Chris Barkus and David Bannerman provided exemplary training in behavioural testing and gave unflinching support. At the Sanger Institute, David Adams provided the resources for exome sequencing and witty repartee.

I am especially grateful to MRC Harwell, Sanger and Karen Steel for providing mice. I am also indebted to Le Fondation Jerome Lejeune, the Wellcome Trust and Corpus Christi College for providing me with funding. My special thanks to the animal technicians and NAKWOs who cared for my animals.

I would also like to thank Hannah Smith for being a wonderful friend and a dedicated student. The distractions of sushi and computer gaming were immensely appreciated. You'll do extremely well in life only to ruin it all by doing your own PhD and being far too successful…

Contributors

Academic supervisor

Professor Jonathan Flint

Wellcome Trust Principle Research Fellow
&
Michael Davys Professor of Neuroscience
At Merton College, University of Oxford

External collaborators

In alphabetical order

Doctor David Adams

1000 Genomes Project and Mouse Genomes Project,
Wellcome Trust Sanger Institute, University of Cambridge

Doctor David Bannerman

Wellcome Trust Senior Research Fellow, Department of Experimental Psychology,
University of Oxford

Professor Steve Brown

Director of the Mammalian Genetics Unit, Medical Research Council, Harwell

Professor Jamel Chelly

Directeur de recherche Centre National de Recherche Scientifique,
Institut Cochin, Université Paris Descartes, Paris, France

Doctor Helen Dawe & Professor Keith Gull

Lecturer in Cell Biology, University of Exeter
&
Wellcome Trust Principal Research Fellow
Sir William Dunn School of Pathology,
University of Oxford

Professor Karen Steel

Wellcome Trust Sanger Institute, University of Cambridge

Doctor David Keays

Research Fellow of the Institute of Molecular Pathology, Vienna, Austria

Doctors David Sunter, Jacqui White & Ramiro Ramirez-Solis

European Conditional Mouse Mutagenesis and Knockout Mouse Project, Wellcome Trust Sanger Institute, University of Cambridge

Internal collaborators

Doctors Guo-Jen Huang, Jérôme Nicod & Binnaz Yalcin

Post-doctoral researchers, Wellcome Trust Centre for Human Genetics

Technical assistance & others

Riddhi Benani, Amarjit Bhomra, Thomas Campbell, Joe Cook, Cormac Cosgrove, James Cleak, Stuart Davidson, Danica Fabrigar, Drew Hammond, Suzanne Ii, Jon Krohn, Peter Oliver, Emily Philips, Polinka Hernandez-Pliego, Mike Shaw, Hannah Smith, Martha Smith, Annis Stead, Abigail Tyre, Helen Whitley

Students, research assistants and post-doctoral researchers,
University of Oxford

Funding Contributors





Corpus Christi College



Experimental material suppliers





Table of contents

Abstract II

Acknowledgements III

List of contributors ..... IV-VI

List of Figures ..... XII-XIII

Publications XIV

Abbreviations ..... XV-XVI

Dedication XVII

Chapter 1: Introduction 2-24

Introduction 3-4

Methods used for finding genes which play a role in neurodevelopment and behaviour 5-9

ENU mutagenesis 5-6

ENU breeding strategy 6-7

KO screening 8-9

Justification and explanation of my experimental design 10-22

Background to my screens 10-20

My experimental design 21-22

Overview of thesis 23-24

Chapter 2: Materials and Methods 25-61

Introduction 26

Neuroanatomical screening, gene mapping and assessment of phenotypic hits 27-39

Sample collection and sectioning 27

Nissl staining 28

Scanning and anatomical assessment 28-29

Statistics and identification of mutants in ENU screen 30

Statistics and critical evaluation of lines in KO screen 31

Genetic mapping of phenotypic mutants in ENU screen 32-34

Sanger sequencing ENU induced mutations 35

Next generation sequencing and SNP calling of ENU lines 35-37
Scanning electron microscopy 38
Neurogenesis immunostaining 38
Git2 -/- Golgi staining and analysis 39
Behavioural methods 40-50
Order of tests and n numbers 40
Elevated plus maze 41
The open field maze 42
Y maze 43
Activity box 44
Food neophobia 45
Three chambered sociability box 46-47
Complex labyrinth maze 48
Accelerating rotarod 49
Running wheel 49
Inverted mesh grid grip test 50
Methods used for further analysis of *Jenna* mouse 51-57
BrdU labelling 51
Gallyas staining 51-53
In situ hybridisation 54-55
Juvenile and adult Immunohistochemistry 55-56
Apoptosis study 56
Quantification and statistics 56-57
Histological methods used to assess the cxcr4 conditional knockout 58
Cerebellar Gallyas staining 58
Golgi staining, dendritic spine analysis and Purkinje cell imaging 58
Genotyping 59-61
Chapter 3: ENU Mutagenesis Screen Results 62-95
Introduction 63
Detection and rederivation of phenotypic pedigrees 64-70
Mapping and analysis 71-89
PEDV50: The *Hydin* mouse 71-79

PED V76: The *Pinky* mouse 80-84
PED M23: The *Marble* mouse 85-89
Future work plans for *Pinky*, *Hydin* and *Marble* 90-94
Summary 95
Chapter 4: Sanger Transgenic Knock Out Screen Results 96-127
Introduction 97
Determining level of significance 98-99
Neuroanatomical screen: 6 week KO cohort 100-111
BL/6 background lines 102
Non-BL/6 background lines 103
Hits with evidence in the literature supporting a role in CNS 104-107
Hits with no current literature links to CNS development 108-109
Borderline hit genes 109-111
Neuroanatomical screen: 16 week KO cohort 112-116
Hits with evidence in the literature supporting a role in CNS 115-116
Comparing the KO cohorts 117-118
Further analysis of *Git2* KO mice 119-123
Neurogenesis and cortical thickness are elevated in *Git2* -/- 119-121
Synaptic spine density is increased in *Git2* -/- 122-123
Future work plans for the KO screening project 124-126
Summary 127
Chapter 5: Anatomical and Behavioural Assessment of Sanger ENU Mice 128-179
Introduction 129
Whirligig and *Diminuendo* neuroanatomy and physical phenotype 130-131
Whirligig behaviour 132-157
Choice of behavioural tests 132
Elevated plus maze 133-137
Open field 138-143
Y maze 144-146
Activity box 147-149
Food neophobia 150-151
Three chambered sociability box 152-157

Diminuendo behaviour ... 158-174
Choice of behavioural tests ... 158
Open field ... 159-163
Y maze ... 164-168
Complex labyrinth maze ... 169-171
Activity box ... 172-174
Future work plans for *Diminuendo* and *Whirligig* ... 175-177
Summary ... 178-179
Chapter 6: Additional Anatomical Assessment of the ENU Derived *Jenna* Mouse ... 180-198
Introduction ... 181
Structural defects in *Jenna* mouse superior colliculus ... 182-186
Gross structure ... 182-183
Laminar structure ... 184-186
Defective neuronal migration in *Jenna* superior colliculus ... 187-190
Neuron cell death in adult *Jenna* mutants ... 191-195
Future work plans for *Jenna* ... 196-197
Summary ... 198
Chapter 7: Analysis of *Sox1-Cre Cxcr4* Conditional Knock Out Mice ... 199-214
Introduction ... 200
Anatomical abnormalities ... 201-205
Behavioural defects ... 206-211
Future work plans for *Sox1-cre Cxcr4* ... 212-213
Summary ... 214
Chapter 8: Discussion ... 215-228
Introduction ... 216
Summary of the yield rates ... 217
Assessment of my neuroanatomical screening method ... 218-222
Strengths and weaknesses of my screens ... 223-226
My findings and their importance ... 229-237

Appendix 1: ENU screen Z-score plots 229-237
Appendix 2: KO screen non-CNS phenotypes (6 wks) 238
Appendix 3: KO screen gene expression (6 wks) 239
Appendix 4: KO screen non-CNS phenotypes (16 wks) 240
Appendix 5: KO screen gene expression (16 wks) 241
References 242-246

List of Figures

Figure 1: Harwell recessive ENU breeding strategy..... 7
Figure 2: Sanger KO strategy 9
Figure 3: Quantified neuroanatomical measurements 29
Figure 4: SNP calls versus read depth..... 37
Figure 5: Measuring dendritic spine density 39
Figure 6: Elevated plus maze protocol..... 41
Figure 7: Open field protocol 42
Figure 8: Y maze protocol 43
Figure 9: Photonic locomotion activity box protocol 44
Figure 10: Food neophobia protocol 45
Figure 11: Three chamber sociability box protocol 47
Figure 12: Complex labyrinth maze protocol 48
Figure 13: ABC developer solution composition and stock chemicals 53
Figure 14: Superior colliculus analysis box plotting protocol 57
Figure 15: Genotyping protocols 60
Figure 16: Phenotypic ENU pedigrees 65
Figure 17: ENU pedigrees featuring enlarged lateral ventricles 66
Figure 18: Affected ENU pedigree histology from quantitative screen 67
Figure 19: *Marble* line phenotypes prior to rederivation 69
Figure 20: *Marble* ectopia phenotype after rederivation 70
Figure 21: PEDV50 mutation interval 71
Figure 22: PEDV50 mutation is in hydin at V4858 73
Figure 23: Hydrocephalus in PEDV50/hy3 compound mutants 75
Figure 24: Infertility and reduced testicle weight in V4858E hydin mutants 76
Figure 25: V4858E hydin mutant sperm are tailless 77
Figure 26: Build up of globular debris in V4858E hydin mutant trachea 79
Figure 27: *Pinky* mutation interval 80
Figure 28: High quality SNPs in *Pinky* mutation interval 83
Figure 29: *Marble* mutation interval 85
Figure 30: High quality SNP in *Marble* mutation interval 86
Figure 31: *Marble Pik3r4* mutation creates premature stop codon 88
Figure 32: *Pik3r4* is expressed in CA1 of hippocampus 89
Figure 33: RT-PCR method..... 94
Figure 34: Q-Q plots for KO cohorts 99
Figure 35: All genes screened in 6 week old KO cohort 101
Figure 36: Hit genes on BL/6 KO lines (6 week cohort) 102
Figure 37: Hit genes on non-BL/6 KO lines (6 week cohort) 103
Figure 38: *Ube3b* -/- mouse brains feature microcephaly 107
Figure 39: Borderline non-Bl/6 hit genes in 6 week old 109
Figure 40: All genes screened in 16 week old KO cohort 113
Figure 41: Hit genes on BL/6 lines (16 week cohort) 114
Figure 42: Hit genes on non-BL/6 lines (16 week cohort) 114
Figure 43: Cortical thickness is affected by age 118
Figure 44: Neurogenesis and radiatum thickness in *Git2* and *Mbd2* mutants 120
Figure 45: CA1 spine density in *Git2* and *Mbd2* 123
Figure 46: Corpus callosum agenesis in *Whirligig* +/- mutant 130

Figure 47: Increased hippocampal area in *Diminuendo* homozygotes 131
Figure 48: *Whirligig* +/- make more Elevated plus maze arm entries 134
Figure 49: Elevated plus maze suggests reduced anxiety in *Whirligig* +/- 136
Figure 50: Open field suggests reduced anxiety in *Whirligig* +/- 139
Figure 51: Open field shows abnormal locomotion in *Whirligig* +/- 142
Figure 52: *Whirligig* +/- show lack of novelty preference in Y maze 144
Figure 53: Reduced exploration of Y maze novel arm by *Whirligig* +/- 146
Figure 54: Activity box results show *Whirligig* +/- are hyperactive 148
Figure 55: No significant difference in food neophobia in *Whirligig* +/- 151
Figure 56: *Whirligig* and WT animals respond differently to social cues 153
Figure 57: Neither *Whirligig* +/- or WT animals avoid stranger mice 156
Figure 58: Open field suggest WT anxiety levels in *Diminuendo* 160
Figure 59: *Diminuendo* homozygotes display backwards walking motion 162
Figure 60: *Diminuendo* hets display no first entry novelty preference 165
Figure 61: Reduced exploration of Y maze novel arm by *Diminuendo* 167
Figure 62: Exploration reduced in *Diminuendo* homozygotes 170
Figure 63: Activity box shows *Diminuendo* homozygotes are hyperactive 173
Figure 64: Summary of behavioural tests and findings 179
Figure 65: Increased superior colliculus exposure and length in *Jenna* 182
Figure 66: Reduced thickness of superior colliculus in *Jenna* +/- 183
Figure 67: Cell marker laminar structure is intact in *Jenna* +/- 185
Figure 68: Defects in *Jenna* +/- laminar myeloarchitecture 186
Figure 69: Defective neuronal migration in *Jenna* +/- superior colliculus 189
Figure 70: Loss of neurons in the SC of *Jenna* +/- 192
Figure 71: Increase in caspase staining in 7wk old *Jenna* +/- 195
Figure 72: Myeloarchitecture defects in *Sox1-Cre Cxcr4* -/- 202
Figure 73: Purkinje cell arborisation simplified in *Sox1-Cre Cxcr4* -/- 204
Figure 74: CA1 spine density in *Sox1-Cre Cxcr4* -/- mirrors WT 205
Figure 75: *Sox1-Cre Cxcr4* -/- mice perform poorly on rotarod 207
Figure 76: *Sox1-Cre Cxcr4* -/- mice are impaired on running wheel 208
Figure 77: *Sox1-Cre Cxcr4* -/- mice fail inverted mesh grip test 209
Figure 78: *Sox1-Cre Cxcr4* -/- mice display increased activity 211
Figure 79: Overview of ENU and KO screen yield (from chapters 3 & 4) 217

Publications

Edwards A, Treiber C, Breuss M, Pidsley R, Huang GJ, Cleak J, Oliver P, Flint J, Keays DA (2011) Cytoarchitectural disruption of the superior colliculus and an enlarged acoustic startle response in the *Tuba1a* mutant mouse. *Neuroscience*

Huang GJ, Smith AL, Gray DHD, Cosgrove C, Singer BH, **Edwards A**, Sim S, Parent JM, Johnsen A, Mott R, Mathis D, Klenerman P, Benoist C, Flint J (2010) A Genetic and Functional Relationship between T Cells and Cellular Proliferation in the Adult Hippocampus, *PLoS Biology*

Keays DA, Cleak J, Huang GJ, **Edwards A**, Braun A, Treiber CD, Pidsley R, Flint J (2010) The Role of *Tuba1a* in Adult Hippocampal Neurogenesis and the Formation of the Dentate Gyrus, *Developmental Neuroscience*

Koch S, Molchanova SM, Wright AK, **Edwards A**, Cooper JD, Taira T, Gillingwater TH, Tyynelä (2011) Mutations in Rps7 cause abnormal neuronal development and a spectrum of TRP53-dependent phenotypes, *Journal of Neuropathology and Experimental Neurology*

Keane TM, Goodstadt L, Danecek P, White MA, Wong K, Yalcin B, Heger A, Agam A, Slater G, Goodson M, Furrotte NA, Eskin E, Nellåker C, Whitley H, Cleak J, Janowitz D, Hernandez-Pliego P, **Edwards A**, Belgard TG, Oliver P, McIntyre RE, Bhomra A, Nicod J, Gan X, Yuan W, van der Weyden L, Steward CA, Balasubramaniam S, Stalker J, Mott R, Durbin R, Jackson I, Czechanski A, Guerra Assunção JA, Donahue LR, Reinholdt L, Payseur BA, Ponting CP, Birney E, Flint J, Adams DJ (2011) Sequence variants among 17 mouse genomes: Effect on phenotypes and gene regulation, *Nature*

Abbreviations

ANOVA	ANALYSIS OF VARIANCE
ASH	ASPM, SPD-2,HYDIN
ASR	ACOUSTIC STARTLE RESPONSE
BAC	BACTERIAL ARTIFICAL CHROMOSOME
BAM	BINARY ALIGNMENT MAP
BCIP	5-BROMO-4-CHLORO-3-INDOLYL PHOSPHATE
BrdU	5-BROMO-2'-DEOXYURIDINE
cM	CENTIMORGAN
CNS	CENTRAL NERVOUS SYSTEM
CSF	CEREBROSPINAL FLUID
DAB	3,3'-DIAMINOBENZIDINE TETRAHYDROCHLORIDE
DAPI	4',6-DIAMIDINO-2-PHENYLINDOLE
DCX	DOUBLECORTIN
DEPC	DIETHYLPYROCARBONATE
DIG	DIGOXIGENIN
DNA	DEOXYRIBONUCLEIC ACID
DPX	DISTYRENE, PLASTICISER AND XYLENE
dNTP	2'-DEOXY NUCLEOTIDE 5'-TRIPHOSPHATE
EDTA	ETHYLENEDIAMINE TETRA-ACETIC ACID
EPM	ELEVATED PLUS MAZE
ENU	*N*-ETHYL-*N*-NITROSOUREA
EUCOMM	EUROPEAN CONDITIONAL MOUSE MUTAGENESIS PROGRAM
Flp	FLIPPASE
FRT	FLIPPASE RECOGNITION TARGET
G1, 2 or 3	GENERATION 1, 2 OR 3
HCl	HYDROCHLORIC ACID
HET	HETEROZYGOUS
HOM	HOMOZYGOUS
IKMC	INTERNATIONAL KNOCKOUT MOUSE CONSORTIUM
IQ	INTELLIGENCE QUOTIENT
KO	KNOCKOUT
KOMP	KNOCK OUT MOUSE PROGRAM
LIS1	LISSENCEPHALY 1
MR	MENTAL RETARDATION
MRC	MEDICAL RESEARCH COUNCIL
MTC	MULTIPLE TEST CORRECTION
NBT	NITRO BLUE TETRAZOLIUM CHLORIDE
Neo	NEOMYCIN SELECTION MARKER
OCT	OPTIMAL CUTTING TEMPERATURE
OF	OPEN FIELD
PAG	PERIAQUADUCTAL GREY
PBS	PHOSPHATE BUFFERED SALINE
PFA	PARAFORMALDEHYDE
PCR	POLYMERASE CHAIN REACTION
PPI	PRE-PULSE INHIBITION OF THE ACOUSTIC STARTLE RESPONSE
QTL	QUANTITATIVE TRAIT LOCI

RNA	RIBONUCLEIC ACID
SAM	SEQUENCE ALIGNMENT MAP
SC	SUPERIOR COLLICULUS
SDS-PAGE	SODIUM DODECYL SULFATE POLYACRYLAMIDE GEL ELECTROPHORESIS
SEM	STANDARD ERROR OF THE MEAN
SEM	SCANNING ELECTRON MICROSCOPE
SNP	SINGLE NUCLEOTIDE POLYMORPHISM
SSC	SALINE SODIUM CITRATE BUFFER
UTR	UNTRANSLATED REGION
UV	ULTRAVIOLATE
WT	WILD TYPE
WTCHG	WELLCOME TRUST CENTRE FOR HUMAN GENETICS

Dedication

Without my parent's love and nourishment nothing would have been possible. I have happy memories of visiting the Royal Museum of Scotland with my father, sitting by the fish pools and exploring the natural science exhibits. He showed me the beauty of biology, the wonder of science and the kindness of people. Throughout my development, my mother was always there to encourage and inspire. She taught me the importance of hard work, love and integrity. I owe the shaping of my character, my strengths and my ideals to the finest people anyone could have hoped to have as parents. They gave me the perfect childhood. I love you both very much.

Additionally, I am eternally delighted to have met my best friend early in life. From the first time Eleanor spoke to me on the steps of the Swann Building on the 2nd of October 2002, she has been a constant source of support, courage and friendly rivalry. One of the reasons I wanted to do a DPhil was to rub it in her face. Alas, whilst I've been working in the lab she's been hugely successful: getting into the Guinness book of world records; running half-marathons; starting her own part time belly dancing business; getting herself a higher tax rate job focusing on thwarting climate change… I respect and admire you beyond comprehension. You are part of me, as we are all part of each other.



What was sundered and undone, shall be whole, the two made one

Chapter 1

An Introduction

The background, merits and goals of the projects

Introduction

The aim of this thesis is to find genetic mutations in mice which cause neuroanatomical defects. The rationale behind this is that such mutations will be informative about developmental neurobiology and the biological basis of behaviour.

Previously, screens in mice to find genes involved in behaviour have had relatively little success. This is because even null alleles make only a modest contribution to variation in a behavioural trait, often explaining only 10% of the variance in a segregating cross (Flint and Mott, 2008). The problem this poses for genetic screens is that hundreds of animals are needed simply to detect a locus.

In this thesis I considered one approach to deal with this problem: to screen for neuroanatomical phenotypes where the genetic effect is highly penetrant. Where these phenotypes are likely to affect brain function, it is reasonable to suppose that they may also affect behaviour. The idea to attempt this approach arose from previous work which identified an alpha tubulin mutant during a screen for hyperactivity. Once the mutation was cloned, it was noted that the mutant animals, nicknamed *Jenna*, had an overt neuroanatomical phenotype affecting the hippocampus (Keays *et al.*, 2007). This phenotype segregated as a fully penetrant dominant. By contrast the mutation accounted for only about 20% of the variation in locomotor hyperactivity, considerably complicating screening and genetic mapping.

Genetic screens fall into three broad categories: those that exploit naturally occurring variation (for example, searching for quantitative trait loci (QTLs) in crosses between inbred strains); those that introduce point mutations at random in the genome by mutagenesis and screen for phenotypic abnormalities that arise, mapping the location of any found in a segregating cross; and those that contrast the phenotypes of engineered mutants (typically null alleles) with wild type animals. The first two involve genetic mapping to identify the

relevant locus; the last requires no mapping, but does require access to a large cohort of null alleles, preferably genome wide. In this thesis I decided to compare the merits of mutagenesis and knockout (KO) screening.

The mutagenesis screen was conducted using N-ethyl-N-nitrosourea (ENU) mutagenised animals sourced from the MRC Harwell mutagenesis program. ENU induces many point mutations across the genome. As a consequence, there is diversity in the sites that can be mutagenised; splice sites, microRNAs, and protein coding regions (Acevedo-Arozena *et al.*, 2008). Similarly, there is great diversity in the types of mutation which can ensue. Mutations can be non-sense, missense, loss of function or gain of function. As a consequence, ENU mutagenesis mirrors the range of genetic defects that can underlie human pathology. Additionally, ENU mutagenesis makes no *a priori* assumptions about which genes may be involved in pathological processes. This allows for unexpected discoveries and avoids the biases of a candidate gene screening approach.

The KO screen was carried out using engineered mutants generated in a systematic program underway at the Sanger Institute. Whilst ENU mutagenesis screening can generate phenotypic hits, it can be extremely arduous to identify the causal mutation. The KO screen bypasses this problem as the causal gene is known. However, it does not mirror the rich spectrum of genetic defects which can affect humans. Consequently, ENU mutagenic and transgenic KO screening approaches complement each other's respective methodological weaknesses.

This chapter introduces the methods used for finding genes which play a role in neurodevelopment and behaviour. It also gives a justification and explanation of my experimental design. Lastly, I conclude the chapter with an overview of my thesis.

Methods used for finding genes which play a role in neurodevelopment and behaviour

ENU mutagenesis

In 1979, ENU was described as a potent mutagen in mice (Russell *et al.*, 1979). Unlike radiation or other chemical mutagens such as chlorambucil, ENU rarely induces deletions or inversions which span multiple genes and therefore allows for clear monogenic-phenotype associations (Balling, 2001). Mutations are caused through the alkylating moiety of ENU transferring its ethyl group to nitrogen and oxygen sites on any of the four deoxyribonucleotides (Acevedo-Arozena *et al.*, 2008). This ethyl group leads to point mutations at the affected base during DNA replication. Between 70 to 85% of ENU point mutations are AT to TA transversions or AT to GC transitions. In contrast, GC to CG transversion events are rarely seen.

To generate mutagenised pedigrees, two or three doses of 80-100mg/kg of ENU is administered by injection into the peritoneum of a male mouse which results in mutations in spermatagonia. This dose is sufficient to overwhelm DNA repair mechanisms. Higher doses are more likely to cause infertility or death as ENU is both highly toxic and carcinogenic (Weber *et al.*, 2000). Utilizing Harwell's ENU dosing regimen, a rate in excess of 1 new mutation per gene every 700 gametes is expected (Balling, 2001, Nolan *et al.*, 1997). This equates to 25-40 gene mutations and hundreds of intergenic mutations per mutagenised gamete (Keays *et al.*, 2006). Mutations result in nonsynonymous changes in 70% of instances. Of these, approximately 65% are missense changes and the remainder are nonsense or splice mutations (Acevedo-Arozena *et al.*, 2008). The mutations can occur anywhere in the genome, but the bias towards AT to TA over GC to CG transversion mutations means certain

genomic areas are more or less likely to be mutagenised depending on their base composition.

ENU breeding strategy

The ENU breeding program at Harwell MRC allows for the generation and assessment of both heterozygous and homozygous mutant animals. As illustrated in **Figure 1**, male C57BL/6J mice were exposed to ENU by injection into the peritoneum, resulting in random mutations in the spermatagonia. These mice were then mated with C3H/HeH females producing the first generation of mice (G1). G1 males were then mated with C3H/HeH females, resulting in the second generation of mice (G2). To produce homozygous animals, G2 females were backcrossed to the founding G1 male, producing a third generation (G3). Assuming half of the backcrossed G2 mothers are heterozygous for a mutation, the G3 should be a three eighths WT, four eights heterozygous and an eighth homozygous.

Figure 1: Harwell recessive ENU breeding strategy

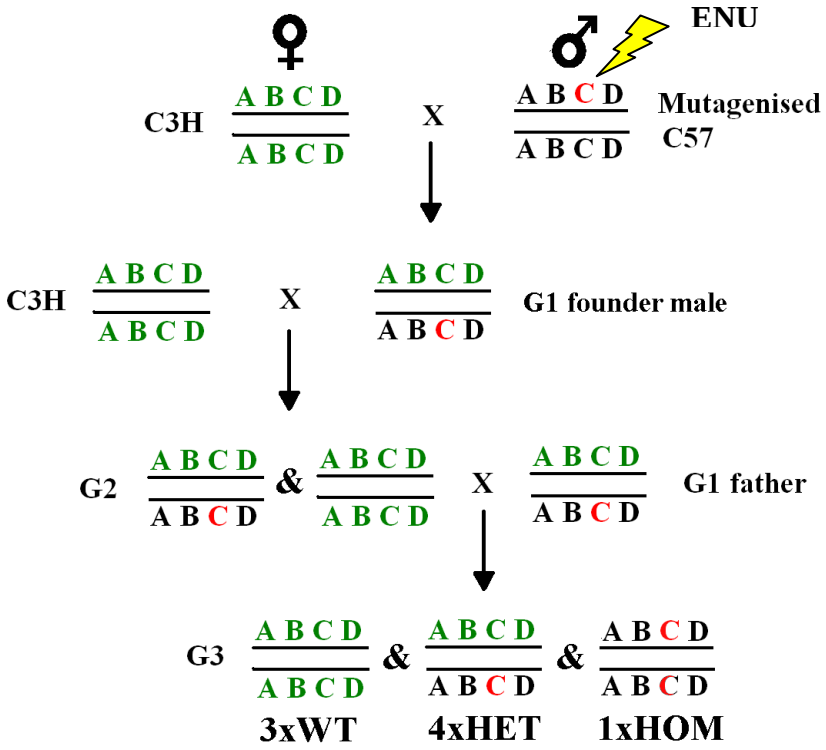


Figure 1. *ABCD represent a genetic sequence with the red C depicting a point mutation. The mutation is on the C57BL/6 (black) genetic background and not on the C3H/HeH (green), allowing it to be mapped using strain specific polymorphisms. Of the G3 animals produced, three eighths will be WT, half will be heterozygous, and one eighth will be the homozygous for a mutation.*

KO screening

The Sanger Institute is a participant in the International Knockout Mouse Consortium (IKMC) and generates KOs for the "European Conditional Mouse Mutagenesis" program (EUCOMM) and "Knockout Mouse Program" (KOMP) (Guan *et al.*, 2010). The IKMC aims to generate a KO for every gene in the genome.

As shown in **Figure 2**, a "Knockout-first" method is used to generate lines (Testa *et al.*, 2004). The strategy relies on targeting a critical exon of a gene which is common to all transcript variants. A *LacZ* reporter and neomycin selection marker (*neo*) are inserted upstream of the target exon along with flippase recognition target (FRT) and locus of X-over P1 (*loxP*) sites. The splice acceptor site of the *LacZ* reporter generates a fusion transcript with the endogenous upstream exon resulting in a truncated protein. To verify correct targeting, FLP recombinase (Flp) can be used to remove the *LacZ* and *neo* inserts by cleaving at flanking FRT sites. Removal should rescue the gene and allow for normal transcript variants. Cre recombinase driven by a promoter of choice can be used in addition or instead of Flp. Cre recombinase expression will excise the critical exon via cleaving at flanking *loxP* sites. Removal of this exon is designed to create a frame shift mutation which leads to absent expression of the protein. Consequently, the Knockout-first model can produce reporter KOs, conditional KOs and null alleles dependant on exposure to Cre and Flp (Testa *et al.*, 2004). However, as this approach requires the presence of a critical exon, the method may not be well suited for small genes with few exons.

For my screen, Sanger sent homozygous null mutant tissue along with controls. Where homozygosity was lethal, heterozygous tissue was sent. All lines generated at Sanger were screened blind to genotype and no attempt was made to influence which genes were targeted.

Figure 2: Sanger KO strategy

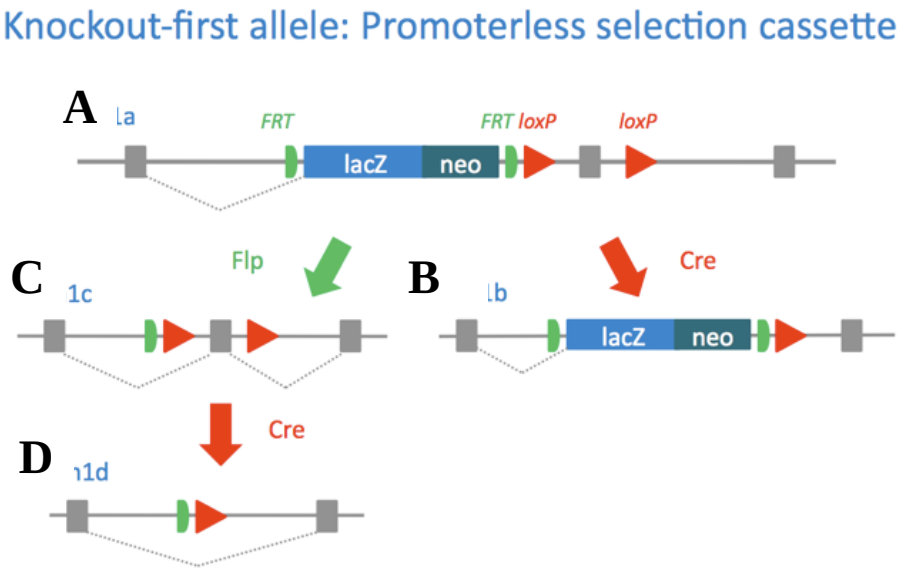


Figure 2.

KO first allele (reporter-tagged insertion allele) *(A)*

Post-Cre reporter-tagged null allele *(B)*

Post-Flp conditional allele *(C)*

Post-Flp and Cre null allele with no reporter *(D)*

Justification and explanation of my experimental design

Background to my screens

In my work I used ENU as a way to find genes involved in behaviour in mice. Historically this has been a difficult area, with few successes, even though one of the first successes of ENU was identifying a mutation that influences behaviour, namely variation in circadian activity (Vitaterna *et al.*, 1994).

Circadian rhythms are thought to be present in all known eukaryotic species and influence when animals eat, drink, move and sleep (Sollberger, 1965, Takahashi, 1995). These rhythms are driven by an internal molecular time-keeping system which is entrained by environmental stimuli such as light. The clock hypothesis proposes that circadian rhythms exist as transcription/translation negative feedback loops with expressed autoinhibitor proteins that limit their own transcription until they decay after a specific time period (King and Takahashi, 2000).

In "free-running" experiments, animals are placed under conditions which seek to minimise environmental entrainment of their molecular time-keeping system, typically constant darkness. Assuming a cycle period is not exactly 24 hours, the time of day in which an animal displays routine activity will gradually drift over the course of the experiment. The rate of this temporal drift in activity pattern reflects the magnitude of the difference between the free-running cycle period and 24 hours. Consequently, free-running experiments allow an animal's internal molecular time-keeping system to be assessed, aiding the identification of mutants that have cycle periods significantly different from the ~24 hour period of WT (Pittendrigh, 1993). As phenotyping for free-running abnormalities in circadian rhythm behaviour is straightforward, forward genetics resulted in significant progress identifying the genes which regulate the clock (Wager-Smith and Kay, 2000). For example, work in *Drosophila melanogaster* led to the generation of mutagenised lines and discovery of central

oscillator components, namely, the *timeless*, *period*, *cycle*, *double-time*, *cryptochrome* and *lark* genes (Sehgal *et al.*, 1994, Hardin *et al.*, 1990, Price *et al.*, 1998, Rutila *et al.*, 1998, Konopka and Benzer, 1971, Stanewsky *et al.*, 1998, Newby and Jackson, 1993).

Prior to the homologue being described in *Drosophila*, Vitaterna and colleagues were able to map and clone the *clock* mutation in ENU mutagenised mice by conducting an exercise wheel activity assay under free-running conditions (Vitaterna *et al.*, 1994, Allada *et al.*, 1998, King *et al.*, 1997). This was the first circadian rhythm mutation mapped in a mammal and, in conjunction with the ~20hr free-running cycle of the *tau* hamster mutant, demonstrated that gene mutations could influence circadian rhythms in vertebrates (Ralph and Menaker, 1988). As work from other organisms had suggested circadian rhythm mutations tended to be semi-dominant, Vitaterna *et al.* directly screened heterozygous G1 mutant animals (Hall, 1990, Dunlap, 1993). Variation in activity rhythm was low with the 304 animals screened having a mean free-running rhythm cycle of 23.7 hours with a standard deviation of just 0.17. As a result, the outlier *clock* mutant with its 24.8 hour free-running rhythm cycle was easy to identify.

From an evolutionary perspective, it is significant that the *Clock* gene is highly conserved among vertebrate species, including humans. Mice are often used as a tool in translational research as they have strong genomic and neuroanatomical similarities to humans, such as the importance of the suprachiasmatic nucleus in generating circadian rhythm (Akiyama *et al.*, 1999, Dunlap, 1999, Hastings, 1997, Venter *et al.*, 2001, Waterston *et al.*, 2002). As such, many researchers had hoped use dominant behavioural screening as a means of generating new genetic connections to phenotypes which are altered in both mouse and human disease states. However, in contrast to Vitaterna and colleagues' work, other screens for dominant mutations affecting behaviour have been limited in their effectiveness.

My first example is David Keays' screen of 864 G1 mice for aberrant anxiety phenotypes (Keays, 2005, Keays and Nolan, 2003). This screen was conducted at Harwell MRC and utilised established anxiogenic apparatus, namely, the open field maze, light-dark box and elevated plus maze (Crawley, 1985, Rodgers and Dalvi, 1997, Prut and Belzung, 2003). These tests were selected as they do not require the animal to be trained and could therefore be used for rapid screening.

In order to make the screens results meaningful, Keays put controls in place to limit unwanted sources of variation which may have compromised the screen. Firstly, as anxiety can be influenced by environmental factors, tests were carried out under stringent lighting and olfactory conditions at a fixed time of the day on naïve animals (Crabbe *et al.*, 1999, Kas and Van Ree, 2004, McIlwain *et al.*, 2001, Ohl and Keck, 2003, Ouagazzal *et al.*, 2003, Chesler *et al.*, 2002). Animals were age matched, housed in the same room and given 10 minutes to habituate to being isolated from littermates prior to testing.

Secondly, pilot tests were also done to see if the protocol and experimenter were able to replicate published findings showing behavioural differences between mouse inbred strains (Crabbe *et al.*, 1999, Mandillo *et al.*, 2008, Tarantino *et al.*, 2000). These tests proved successful and verified that the protocol and experimenter could detect differences in anxiety levels (Keays, 2005).

Despite these efforts to limit extraneous sources of variation, the 864 G1 mice screened yielded only one line with a heritable phenotype. The mutation was found to map to a mutation *Pde6b* gene. This gene is causal to retinal degeneration in the C3H/HeH mouse strain, the same strain which was used to generate animals for heritability testing (Keays, 2005, Nagy and Misanin, 1970). Altered visual ability, rather than a novel anxiety mutation, is therefore likely to underlie test performance.

My second example of a dominant ENU behavioural screen which yielded few findings was one which aimed to identify mutations leading to excessive alcohol consumption (Pawlak *et al.*, 2008). In this screen, Pawlak and colleagues individually housed 2,129 G1 animals for a test period of 5 weeks. During this time animals were given *ad libitum* access to two drinking bottles, the first containing water and second containing 10% ethanol v/v. Alcohol consumption was measured by weighting the drinking bottles twice weekly. G1 outliers were bred to test heritability, bringing the total number of screened mice to 3327. Despite the impressive scale of the screen, no stable high or low alcohol consuming lines were discovered. However, Pawlak and colleagues findings did support that factors other than mutations, namely sex and season, affect consumption rates (Pawlak *et al.*, 2008).

My final example of the difficulties of dominant ENU screens was conducted at Harwell MRC. This screen was more productive than the previous two examples as it screened for behavioural defects in conjunction with gross anatomical and physiological phenotypes. Building on the design of his 1997 pilot, Patrick Nolan and colleagues had generated 26,047 G1 animals for screening by the year 2000 (Nolan *et al.*, 1997, Nolan *et al.*, 2000). Over half of the G1 was tested using the SHIRPA protocol, a battery of up to 40 tests designed to semi-quantify aspects of behaviour and physiology (Rogers *et al.*, 1997). Additionally, 9,000 animals were tested in startle boxes, a test used for detecting defects in the acoustic startle response and prepulse inhibition. Eight thousand five hundred animals were also screened for locomotor activity defects.

By the publication of the 2000 paper, the screen had detected 1089 phenotypic outliers (Nolan *et al.*, 2000). About 50% of selected outlier animals failed to produce phenotypic offspring in heritability tests due, in part, to dominant pleiotropic mutations which caused infertility and premature death. Consequently, the screen had an overall successful mutation hit rate of less than 2%.

Furthermore, the screen showed some phenotypes were more penetrant than others. Sixty percent of lines which underwent preliminary mapping showed aberrant movement behaviours such as circling, tremor, ataxia or head bobbing. These included three peripheral neuropathy lines and the blind-drunk and robotic lines (Isaacs *et al.*, 2003, Jeans *et al.*, 2007, Oliver and Davies, 2005). The mutations underlying some of these lines are also pleiotropic. For example, the *Af4* mutation in the robotic mouse leads to cataracts in addition to cerebellar malfunction (Isaacs *et al.*, 2003).

Two conclusions can be drawn from this third example in addition to the low hit rate. First, ENU mutagenesis has been shown to create pleiotropic mutations which may complicate screening for complex behaviours (Godinho and Nolan, 2006). Second, mutations which affect activity and movement are disproportionately more likely to be detected under high throughput conditions than other behavioural phenotypes such as anxiety level or alcohol preference.

Taken together, these three examples suggest there are two main problems limiting the potential of dominant ENU behavioural screens. First, as argued by Pawlak *et al.*, the very low yields of the screens may suggest that more recessive alleles rather than dominant alleles may underlie certain behavioural defects (Pawlak *et al.*, 2008). Second, the effect size for a measured phenotype may be insufficient to generate a significant result (Flint and Mott, 2008). Whilst my example screens consumed huge numbers of mice, the population size analysed for any given mutation was limited to a single G1 animal. Consequently, the screens represent a plethora of low power tests. Thus, it is plausible that phenotypic animals are being generated but are not being detected.

Given these problems with dominant ENU behavioural screening, the next logical step would be to see if using a recessive breeding strategy would be sufficient to boost phenotypic yields. Previous publications would suggest the answer is “no”. For example,

Reijmers and colleagues used fear conditioning paradigms to screen 6,400 G3 animals from 260 pedigrees in an effort to find learning and memory deficient lines (Reijmers *et al.*, 2006). Two methodologies were used. Firstly, contextual conditioning, where mice were placed in an arena associated with a lemon odour and subsequently electrically shocked at intervals. Smell is the dominant sensory system in rodents and odour from coffee, cat fur and other sources has successfully been used in contextual fear conditioning by other authors (Kroon and Carobrez, 2009, Brennan and Keverne, 1997, Restrepo *et al.*, 2004, Munoz-Abellan *et al.*, 2009). Secondly, tonal conditioning, where mice would be placed in an arena where upon a noise would sound prior to the animal being repeatedly shocked. Subsequently, for both these paradigms, animals were re-exposed to the conditioned stimulus at a later date. Upon re-exposure, degree of freezing was measured in order to gauge if a memory association between the conditioned stimulus and electric shocking had been retained.

In addition to the large number of animals screened, the Reijmers *et al.* reported that their G1 mutagenesis rate was one mutation every 400,000 bases, a rate ~2.5 fold higher than in other major ENU mutagenesis projects (Nolan *et al.*, 2000, Quwailid *et al.*, 2004). At this mutation rate, they calculate that the 260 lines they screened should, as a whole, contain a functional mutation in ~25% of all genes in the genome (Reijmers *et al.*, 2006). Given ~35% of functional ENU mutations are non-sense or splice site, it can be extrapolated that Reijmers *et al.* are likely to have nullified or disrupted transcript expression in up to 8.75% of genes in the genome (Acevedo-Arozena *et al.*, 2008). This high gene coverage rate makes it all the more disappointing that, despite performing heritability tests in thirty candidate pedigrees, a phenotype was only shown to be heritable in three.

Additionally, Reijmers *et al.* state that these heritable lines are deficient in the odour based contextual fear conditioning paradigm but not tonal conditioning. Despite stating that deaf animals were removed from the screen, no mention is made of testing for olfactory

ability (Reijmers *et al.*, 2006). Consequently, it could be argued, that the findings do not exclude the possibility that a compromised ability to detect the olfactory cue, rather than a memory defect, influenced results of the contextual conditioned fear test in these lines.

Reijmers *et al.* acknowledge that their hit rate is lower than might have been expected and suggest two reasons for the low yield. First, there may be very few genes involved in the acquisition and retention of memories underlying fear conditioning. Second, it may be the case that mutations affecting memory are not readily observable as such lines may also feature neurodevelopmental abnormalities which, they imply, would be lethal and hence prevent behavioural assessment.

However, these arguments are unlikely to fully explain the paucity of phenotypic findings in the Reijmers *et al.* screen. Many viable mutant lines display gross anatomical or synaptic defects in addition to learning and memory impairments. Here are three examples.

Firstly, the mouse model of Down Syndrome, *Ts65Dn*, takes twice as long as WT mice to navigate to a hidden platform in the Morris water maze despite repeated trials (Reeves *et al.*, 1995). This suggests they are unable to adequately learn associations between the position of external cues and the location of the platform. Other tests show further impairments. *Ts65Dn* mice perform poorly at spontaneous alternation in a T maze suggesting a working memory defect (Faizi *et al.*, 2011). Similarly, a defect in memory retrieval in the line is suggested by mutants exhibiting significantly reduced freezing behaviour when re-exposed to a fear conditioned stimulus (Faizi *et al.*, 2011). In addition to behavioural defects, *Ts65Dn* mice feature a significantly reduced number of synapses, shorter and fewer dendritic spines, retarded hippocampal growth, defects in noradrenergic neurotransmission, and reduced embryonic neurogenesis (Faizi *et al.*, 2011, Popov *et al.*, 2011, Chakrabarti *et al.*, 2007).

My second example is the *LIS1*, also known as *PAFAH1b1*, which encodes for platelet-activating factor acetylhydrolase-1b subunit alpha (Hattori *et al.*, 1994). Unlike Lis1 null homozygote mice which are embryonic lethal, *Lis1* heterozygous animals are viable and show a defect in a Morris water maze spatial learning paradigm. (Hirotsune *et al.*, 1998, Paylor *et al.*, 1999). In conjunction with this behavioural defect, *Lis1* animals also feature aberrant neuronal migration. Neuroanatomical defects include poorly defined cortical layering, ventricle enlargement, cellular diffusion of the dentate gyrus, and heterotopia of the hippocampal pyramidal cell layer (Hirotsune *et al.*, 1998, Fleck *et al.*, 2000).

My final example is the *Reeler* mouse line which features a null mutation in the *Reelin* gene (D'Arcangelo *et al.*, 1995). *Reeler* mice have significantly increased social dominance and rarely retreat when exposed to a stranger mouse (Salinger *et al.*, 2003). Poor performance in nose poke and spontaneous alternation tests also indicate that homozygous *Reeler* mice have a significant impairment of working memory (Salinger *et al.*, 2003, Bliss and Errington, 1977). Mutants also have neuroanatomical abnormalities stemming from defective neuronal migration (Rice and Curran, 2001). Normally, the cerebral cortex is composed of six layers and is formed between E10 and E18 in an "inside-out" manner. The deepest layer contains the oldest neurons and progressively younger neurons migrate outwards to form the superficial layers (Angevine and Sidman, 1961). In *Reeler* mice, younger cells fail to migrate past older layers, resulting in an inversion of the layering structure and making Layer 1 indiscernible (Caviness and Sidman, 1973a, Caviness and Sidman, 1973b).

These three examples undermine Reijmers *et al.* argument that the presence of neuroanatomical defects would hinder the discovery of memory mutants. Whilst some neuroanatomically defective lines are embryonic lethal, this is not invariably the case. Consequently, an alternative theory is needed to explain the low yield of the Reijmers *et al.*

behavioural screen. I would argue that the problem of effect size and limited statistical power, which hinder the success of dominant ENU screens, also limit the effectiveness of recessive screening. For example, a fully penetrant recessive mutation would only affect an eighth of a pedigree's G3. Additionally as genotyping is impossible, data from these homozygous animals cannot be pooled and tested against heterozygous and WT littermates. Therefore, individual mice need to be compared against either a population of non-littermate WT animals or the whole G3 population which will be subject to contamination bias.

So, if effect size and statistical power are limiting factors, how can a screen overcome these difficulties and discover new genetic links to behaviour? The examples of *Ts65Dn*, *Lis1* and *Reeler* highlight that neuroanatomical defects can accompany behavioural abnormalities and have relatively large effect sizes on the anatomical phenotype, compared to the behaviour. Consequently, it may be possible to bypass the problem of small effect sizes in behaviour by screening for neuroanatomical defects.

Historically, ENU screens of general embryonic development have included analysis of the brain. One such screen, Herron *et al.* 2002, discovered 2 lines with exencephaly from simple histological screening of just 54 pedigrees (Herron *et al.*, 2002). Similarly, Kasarskis *et al.* 1998 identified 4 lines with neural tube defects by screening embryos from 86 lines (Kasarskis *et al.*, 1998). Although these early screens produced respectable yields of brain phenotypes, subsequent screens such as Mar *et al.* 2005 and Stottmann *et al.* 2011 have been met with even greater success as a result of refined experimental methodology.

Mar and colleagues used anti-neurofilament immunostaining to detect G3 embryos with abnormal cranial nerve development (Mar *et al.*, 2005). The screen was successful and 7 lines with neuroanatomical defects were detected from testing just 40 pedigrees (Mar *et al.*, 2005). This represents a hit rate of 17.5%. Hits included two lines with excessive proliferation of the anterior CNS, two mutants with abnormal telencephalic development, a

Pax3 mutant with defective neural tube closure, a line with defective axonal targeting and a line with defective axon fasciculation.

Stottmann and colleagues also enjoyed a similarly high phenotypic hit rate of 18.4% in their 2011 screen (Stottmann *et al.*, 2011). They report that 7 out of the 38 lines comprehensively analysed displayed a neuroanatomical phenotype and that a causal locus was identified in four of these. These include a novel allele of the Scrib gene associated with an open neural tube and a novel allele of caspase 3 associated with encephaloceles. Other detected phenotypes included cortical abnormalities, exencephaly and progressive hydrocephalus (Stottmann *et al.*, 2011). In order to detect these phenotypes, the screen contained three methodological components; an assiduous morphological and histological examination of the forebrain via paraffin embedded sectioning, use of a *lacZ* reporter transgene to highlight anatomical patterning and use of the *Lis1* genetically sensitising locus to predispose animals to defects. Subsequently, the *lacZ* reporter was found to be unreliable and the *Lis1* sensitising locus was found to be unnecessary (Stottmann *et al.*, 2011). Therefore, the primary reason for the screen's success was the detailed histological analysis of brain morphology.

Consequently, the rationale for my ENU neuroanatomical screen can be summarised with the following remarks. Small mutation effect sizes limit the potential of behavioural screens to make new gene-behaviour associations. As a result, previous screens have had poor phenotypic yields (Keays, 2005, Pawlak *et al.*, 2008, Reijmers *et al.*, 2006). In contrast, neuroanatomical screens using detailed histological analysis can be extremely powerful and produce yields in excess of 17% (Mar *et al.*, 2005, Stottmann *et al.*, 2011). In addition, lines with neuroanatomical abnormalities have shown to have behavioural defects (Keays *et al.*, 2007, Salinger *et al.*, 2003, Paylor *et al.*, 1999, Faizi *et al.*, 2011). Consequently, it was not unreasonable to expect a decent yield of phenotypic hits from my ENU neuroanatomical

screen that would be informative about developmental neurobiology and the biological basis of behaviour.

This logic also suggests that systematic neuroanatomical screening of KO lines may potentially be worth pursuing as a complimentary approach to ENU. Like ENU screening, systematic screening of KO animals blind to their genotype makes no *a priori* assumptions about which genes are important in neurodevelopment. Such screens have only recently become realistically feasible due to the mass production of KO lines by the IKMC. As a result, my screen was one of the first neuroanatomical KO screens to be undertaken.

Prior to the start of my KO screen, I expected phenotypic hit rates to be substantially less than those generated in my ENU screen. Of the 25-40 gene mutations typically carried by ENU G1 founder males, 8-12 mutations can be expected to result in null alleles or transcript disruption (Keays *et al.*, 2006, Acevedo-Arozena *et al.*, 2008). As ENU pedigrees were likely to feature multiple null alleles it seemed reasonably assume the phenotype hit rate would be many fold greater than the KO screen. However, the rate at which a genetic cause could be attributed to a phenotype would be substantially faster in the KO screen pipeline. Consequently, it was unclear which approach would ultimately be more efficient at making positive associations. Regardless, the KO screen had another important use. Unlike the ENU screen, the KO screen was also able to draw conclusions about which null alleles do not overtly affect gross neuroanatomical development. This would allow for the building of a negative results dataset that would to be informative, and potentially interesting, in its own right.

My experimental design

As my screens used adult mice, they had the potential to find both congenital and progressive abnormalities in structures not readily observable in embryos. Therefore, I designed a method for staining and anatomically quantifying several brain regions. To this end, I used Nissl staining as it is a fast, reliable and informative method suitable for mass production. The staining mixture is composed of cresyl violet acetate and stains cell bodies a deep purple by binding to ribosomes (Nievel and Cumings, 1967). Whilst it does not provide information on myelination, neurogenesis, ultrastructure or cell protein expression, the stain does reveal neuroanatomical structures. Unlike preparation for silver, immunohistological and electron microscopy stains, Nissl staining can be completed in hours and does not require tissue to be perfusion fixed (Bekesy *et al.*, 1961, Palay *et al.*, 1962, Pistorio *et al.*, 2006). Instead, tissue can be immersion fixed making the brain extraction process more rapid.

In addition, there is great flexibility in the timing of the Nissl staining process. Immunohistological stains can fail if epitopes are damaged due to overfixation and need to be processed within a rigid timeframe (Werner *et al.*, 2000). In contrast, brain tissue for Nissl staining can remain in fixative for an extended period with no drop in staining efficacy. Over and under staining can be easily corrected by further exposure to alcohol or cresyl violet acetate.

Nissl stained sections were analysed via microscope and subsequently scanned to computer so software could be used to take measurements designed to detect abnormal developmental mechanisms associated with disease. For example, cellular ectopias and structural abnormalities have previously been linked to disorders caused defects in neuronal migration (Keays *et al.*, 2007, Hong *et al.*, 2000, des Portes *et al.*, 1998, Reiner *et al.*, 1993). Reduced cortical thickness and brain section area measurements are associated with microcephaly and may be caused by aberrant cell proliferation, neuronal migration defects or

elevated cell death rates (Cooper, 2003, Garavelli *et al.*, 2009, Chakrabarti *et al.*, 2007, Boycott *et al.*, 2005, Francis *et al.*, 2006). Similarly, abnormal measurements of the corpus callosum may allude to disease affecting axon guidance or survival (Piluso *et al.*, 2009, Garavelli *et al.*, 2009, Schell-Apacik *et al.*, 2008). Furthermore, increases in lateral and dorsal 3rd ventricle areas suggest accumulation of cerebrospinal fluid (CSF) leading to hydrocephalus. Homologs of genes causal to hydrocephalus in mice have been linked to abnormal head size phenotypes and mental retardation in humans (Brunetti-Pierri *et al.*, 2008).

Overview of thesis

I detail the results of my ENU mutagenesis screen in **Chapter 3**. This chapter includes mapping and sequencing data identifying the likely causal mutations. For one line, I show complementation test results which validate a mutation's pathogenicity. For this line, I also show data suggesting the mutation compromises cilia function and impacts on the development of somatic tissues.

Chapter 4 details the results of my KO screen. Twenty seven lines in total were associated with an anatomical defect. Phenotypes were wide ranging and covered defects of the hippocampus, corpus callosum, cortex and ventricles. Hits included genes already linked to Mental Retardation as well as several candidate genes. I conducted further experiments in one KO line and verified an increased thickening of the stratum radiatum layer of the hippocampus occurred alongside exaggerated neurogenesis.

The Sanger institute, in a friendly yet utterly surreptitious fashion, incorporated ENU mutagenised lines with a deafness phenotype into the KO pipeline. The causal deafness mutations had been previously identified at the Sanger. These animals were screened blindly and their presence was only revealed after anatomical phenotyping had been completed. Two of the incorporated ENU lines featured neuroanatomical defects which were consistent with the aim of my thesis. These are described in **Chapter 5** along with follow up experiments which suggest the mutations are also causal to behavioural defects.

Chapter 6 details the results of additional developmental neurobiology assessment on *Jenna* mutants, an ENU line previously identified with having defective hippocampal anatomy. I explore the developmental basis of behaviour by examining the role progressive cell death and defective neuronal migration may play in an exaggerated acoustic startle response (ASR) phenotype.

Chapter 7 details the results of anatomical and behavioural analysis of *Sox1-Cre Cxcr4* conditional KO mice. Non-conditional cxcr4 -/- are embryonic lethal but have previously been associated with anatomical defects of the dentate gyrus and cerebellum (Lu *et al.*, 2002, Zou *et al.*, 1998). Additionally, cxcr4 has been found to promote oligodendrocyte progenitor cell differentiation and is required for remyelination of the corpus callosum (Patel *et al.*, 2010). By using a sox1 cre conditional KO, I was able to produce viable adult KO animals to study behaviour, myelination and cerebellar morphology.

Finally, **Chapter 8** discusses my results and their developmental and behavioural significance. I contrast the effectiveness of ENU mutagenesis and KO screening and consider the strengths and limitations of my approach in making novel gene-phenotype associations. Additionally, I use my results to suggest human gene homologs which may be worth screening in relevant human patient cohorts.

Chapter 2

Materials & Methods

How data was generated, assessed and utilised

Introduction

This chapter is divided into five sections. The first section, entitled "Neuroanatomical screening, gene mapping and assessment of phenotypic hits", covers methods which were used in **chapters 3 and 4**. The second section, "Behavioural methods", details the apparatus and methodology used in **chapter 5** to analyse the behaviour of the *Whirligig* and *Diminuendo* ENU mutagenised lines. This section also includes the methods used to behaviourally assess the cxcr4 conditional KO detailed in **chapter 7**. The third section, "Methods used for further analysis of the *Jenna* mouse", provides a description of techniques used in **chapter 6** to analyse the superior colliculus. The fourth section, "Histological methods used to assess the cxcr4 conditional knockout" relates to the study detailed in **chapter 7**. The final section of this chapter covers genotyping procedures for all animals used in my experiments.

Neuroanatomical screening, gene mapping and assessment of phenotypic hits

Sample collection and sectioning

For the ENU screen, G3 mice aged 6 weeks or over underwent cranial extraction and tail tipping at MRC Harwell laboratories. Brains were drop fixed in 4% paraformaldehyde (PFA) and taken in 15ml falcon tubes to the WTCHG for sectioning. Prior to sectioning brains were placed in 30% sucrose phosphate buffered saline (PBS) solution overnight until they reached osmotic equilibrium. Brains were subsequently sliced coronally into 40µm thick sections using a sliding microtome. Sections were collected throughout the extent of the hippocampus.

For the KO screen, 6 week old animals were perfusion fixed in 4% paraformaldehyde at the Wellcome Trust Sanger Institute. Brains were subsequently harvested by Sanger Staff and sent via courier to the WTCHG. For each KO line three homozygous samples were sent. Where a KO was homozygous lethal, heterozygous animals were sent instead. Control animals were also sent in each batch. Upon arrival, brains were placed in 30% sucrose and sectioned as detailed above.

All sections were stored in 96 well plates in antifreeze solution (50% PBS, 25% ethylene glycol, 25% glycerol) and stored at -20°C.

Nissl staining

Stereotaxically matched hippocampal sections were placed in a dish containing PBS and mounted onto electrostatically charged glass slides. Slides were then placed in a vertical slide holder to dry for at least 30 minutes. Slides were then dipped briefly in water to remove dust and placed in a 0.5%, 0.06% cresyl violet acetate/acetic acid solution for approximately 1 minute. Subsequently, slides were dipped in water to remove excess staining solution and taken through a 50%, 75%, 95% and 100% alcohol series in a timeframe determined by staining intensity. Sections were then placed in Histoclear (Fisher Scientific) for 5 minutes, coverslipped in DPX mounting medium and left to dry overnight.

Scanning and anatomical assessment

Slides were scanned to a computer at 6400dpi via an EPSON PERFECTION V750 PRO scanner. ImageJ freeware was used to quantify images using a scale of 0.251pixels/ µm. One section per brain was used for quantification. These sections were stereotaxically matched using thalamic anatomical markers. Measurements assessed the hippocampus, cortex, ventricles and corpus callosum (**Figure 3**). The total length of dentate gyrus and hippocampal area measurements were only introduced in the KO screen and were not used during the ENU screen. Sections which were heavily damaged or imperfectly cut were not assessed. For the ENU screen, only pedigrees with a minimum of 12 animals were quantified.

In addition to quantified measures, sections were assessed qualitatively. This involved examining sections under light microscopy for evidence of cellular ectopias.

Figure 3: Quantified neuroanatomical measurements

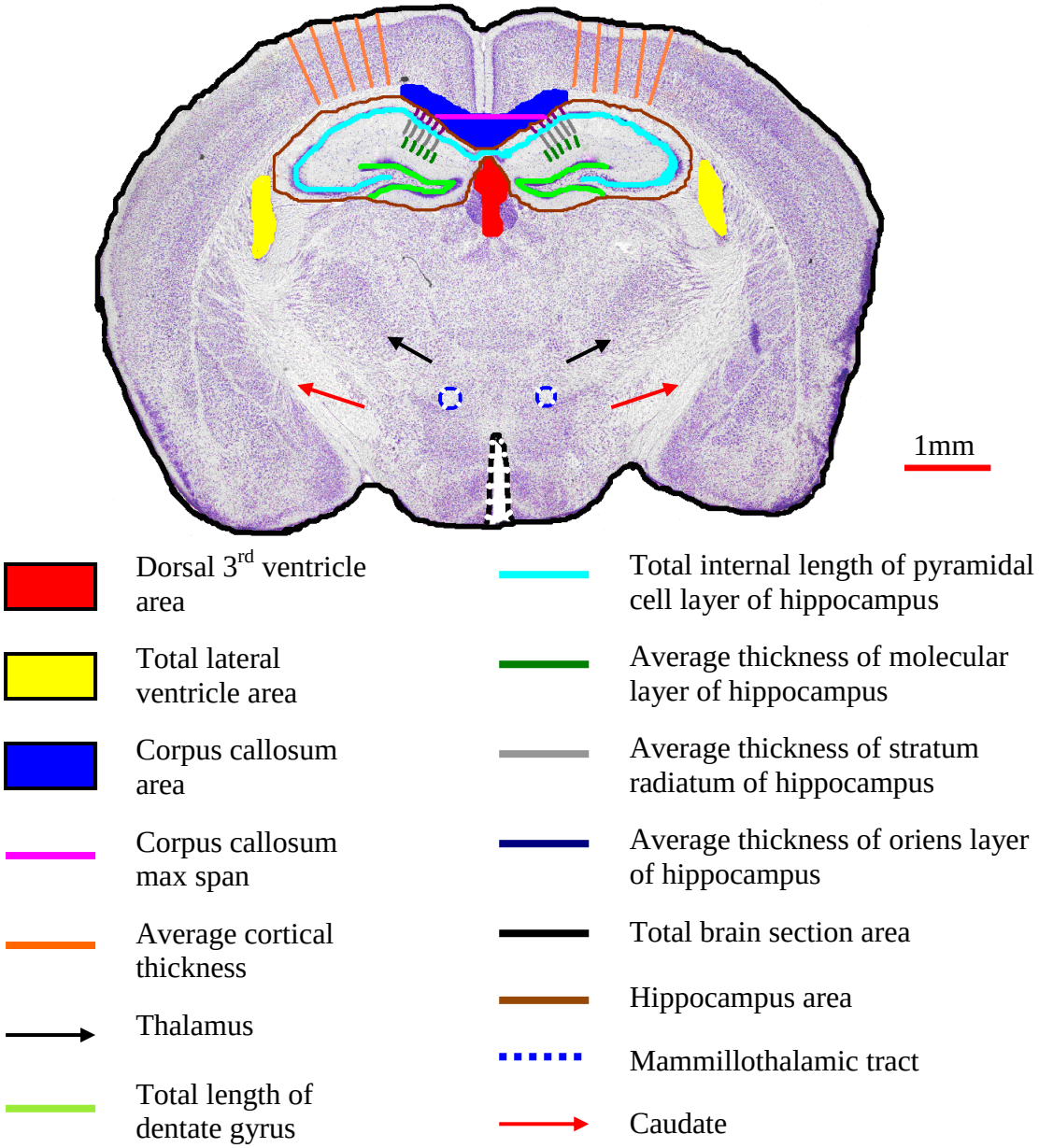


Figure 3. *Brain sections matching the above were selected using the mammillothalamic tracts, caudate and thalamic structures as markers. Only perfectly coronally cut sections were used for quantification of all the measurements shown in the key. All measurements were taken using ImageJ freeware. For cortical and hippocampal layer thickness measurements, measurements were taken 10 times throughout the structure and an average thickness calculated. Scale bar equals 1mm*

Statistics and identification of mutants in ENU screen

Individual anatomical measurements for animals were converted into Z-scores through the following calculation:

$$z = \frac{x - \mu}{\sigma}$$

Where: x = the raw score to be standardised,

μ = the mean of the population

σ = the standard deviation of the population

Z-scores were then ranked in order of magnitude. Scores of greater than z = + 3.29 or lower than z = -3.29 were considered to indicate phenotypically abnormal mice. A z < 3.29 or z > -3.29 is equivalent of being outside 99.9% of values covered by a normal distribution population curve. A pedigree was considered to be a possible carrier of a neuroanatomically disruptive mutation if it contained at least two animals with z-scores above or below ±3.29.

Z-scores formed from lateral ventricle volume measurements were skewed due to ~60% of the total population having lateral ventricle volume of 0μm^2. Consequently, the percentage of total brain section area occupied by the lateral ventricles was calculated and ranked in order of magnitude. Pedigrees featuring multiple animals with lateral ventricle measurements higher than the 98.8th centile were considered to be of interest.

Statistics and critical evaluation of lines in KO screen

R was used to perform t-tests on measurements collected in the KO screen. KO measurements were compared against background matched WT samples. -Log (10) was taken for all P values. Multiple test correction adjustments were used to filter out false positives (see chapter 4 for details). Critical evaluation consisted of ensuring that sections were undamaged, that measurements were accurate and that corpus callosum findings from 129 background lines were discounted. This was necessary as corpus callosum defects are prevalent in up to 70% of WT 129 animals (Livy and Wahlsten, 1997).

It was important to use background matched WT animals for performing comparisons as inbred lines vary in their neuroanatomy (Fredens, 1981, Wimer *et al.*, 1969, Chen *et al.*, 2006). This is due to inbred strains varying in their genetic profile which in turn influences their metabolism and growth (John B, 1967). Increased body weight correlates with increased brain size (Roderick *et al.*, 1973, John B, 1967). The relative position and volume of the subregions of the brain also differs between lines. This, in part, may be due to variations in skull morphology (Wahlsten *et al.*, 1975). Additionally, magnetic resonance imaging has been used to quantify differences in the 3D positioning of internal structures. The lateral ventricles of C57BL/6 animals are 73% larger than in 129Sv animals. This is likely to contribute towards the hippocampus being displaced by up to 400µm relative to the position in 129Sv (Chen *et al.*, 2006). Ventricle size has been shown to be a heritable trait and is influence by genes which affect cerebrospinal fluid dynamics such as *Tgf1* (transforming growth factor beta 1)**,** *Nf1a* (nuclear factor I a) and *Hydin* (Zygourakis and Rosen, 2003, Davy and Robinson, 2003, das Neves *et al.*, 1999, Moinuddin and Tada, 2000).

Genetic mapping of phenotypic mutants in ENU screen

DNA was extracted from tail tips of the analysed G3 mice with a Nucleon DNA Extraction Kit (Gen-Probe Life Sciences, UK). Extracted DNA, quantified on a spectrophotometer, and diluted to a concentration of 10ng/µl for use in subsequent PCR reactions. Contrasting length microsatellite markers between the mutation bearing C57BL/6 strain and C3H/HeH reference strain were amplified and used to map the mutations in phenotypic samples. Non-affected animals were also used in mapping where a mutation was considered fully penetrant. Once the mutation interval could no longer be narrowed using microsatellites, the interval was narrowed by amplifying and sequencing SNP differences between the C57BL/6 and C3H/HeH strains.

The following touchdown PCR program was used to amplify microsatellites with Qiagen hotstar taq:

1. 95°C for 10 minutes
2. 95°C for 30 seconds
3. 62°C for 30 seconds (-0.5°C per cycle)
4. 72°C for 1 minute (repeat steps 2-4 for 13 cycles)
5. 95°C for 30 seconds
6. 55°C for 30 seconds
7. 72°C for 1 minute (repeat steps 5-7 for 29 cycles)

The microsatellite markers used for mapping collectively covered the entire length of all the mouse autosomes and were spaced no more than 20 centimorgans (cM) apart. One centimorgan is a measurement of chromosomal length over which crossover events occur at a 1% frequency. However, as some areas of the genome are more predisposed to recombination events than others, the number of DNA bases covered by a centimorgan varies between chromosomal locations and between species (Dumont *et al.*, 2011). Across the mouse genome as a whole, the recombination rate is one centimorgan per 0.6 megabases (Mb) (Jensen-Seaman *et al.*, 2004). This contrasts with an average of 1.3cM/Mb across the human genome (Yu *et al.*, 2001). Smaller chromosomes are associated with a higher recombination rate. For example, chromosome 1, the largest chromosome in the mouse genome with a physical size of 196Mb, has a recombination rate of 0.6 cM/Mb. In contrast, chromosome 19 has a physical size of 61Mb and a recombination rate of 1.04 cM/Mb (Jensen-Seaman *et al.*, 2004). Additionally, over short genomic intervals, recombination rate can change rapidly due to the presence of recombination hotspots and recombination deserts (Shifman *et al.*, 2006, Yu *et al.*, 2001). Recombination hotspots are rich in CCTCCCT and CCNCCNTNNCCNC motifs (Shifman *et al.*, 2006, Myers *et al.*, 2008). Subsequent binding of Prdm9 protein to these motifs initiates recombination events (Baudat *et al.*, 2010, Grey *et al.*, 2011). In summary, it was important to map mutations using centimorgans rather than physical distance as recombination rate across the genome is subject to great variation.

Because of this regional variation in recombination rate, the number of mice required to narrow a mutation containing candidate interval to 1Mb will also vary. If local recombination rates were in line with the mouse average rate of 0.6 cM/Mb, 84 animals would be required to be bred in order to give a 50% probability of successfully generating a single recombination event in the 1Mb interval.

It is both unhelpful and unwanted to use a high number of animals to minimise the size of candidate intervals. Breeding large populations of animals takes considerable time, incurs high cage costs, and would be considered wasteful by the Home Office. Additionally, an interval can only be narrowed if it contains microsatellites and strain specific SNPs markers. Therefore, prior to sequencing, I narrowed candidate intervals to a size that sufficiently met any of the following criteria. One, the interval contained less than 10 genes (*Hydin* mouse mapping in chapter 3 yielded an interval containing only 2 genes). Two, the interval could be narrowed no further using reliable microsatellites or SNPs. Three, it was cheaper and more convenient to sequence the interval than to narrow it further (see *Pinky* and *Marble* sections in chapter 3). With the availability of next generation sequencing facilities, it was not difficult to locate candidate SNP mutations within large candidate intervals. If multiple candidates were found, then further breeding to narrow the interval may be justifiable.

Sanger sequencing ENU induced mutations

Sanger sequencing was used to locate the causal mutation in one phenotypic ENU pedigree and confirm the presence of a mutation in two other ENU lines. In preparation for sequencing, PCR products were purified using a 96 well Millipore PCR purification plate and resuspended in 20-50μl of H_2O. Sequencing reactions were conducted in 10μl volumes (7μl resuspended PCR product, 2μl BigDye® master mix (Applied Biosystems), 1μl primer (10pmol/μl)) and subject to the following amplification protocol: 95.0°C for 1 min (1 cycle), 95.0°C for 30 sec, 50.0°C for 30 sec, 60.0°C for 3.5 min (35 cycles). Products were precipitated by adding 50μl absolute ethanol and 2μl 3M sodium acetate and spun at 4°C at 3,000 rpm for 30 minutes. Following washing with 100μl of 70% ethanol, samples were resuspended in a 1:1 ratio of formamide to water and sequenced using a capillary electrophoresis ABI 3700 DNA sequencer (Perkin Elmer).

Next generation sequencing and SNP calling of ENU lines

The next generation sequencing carried out at the Sanger institute utilises technology developed by Illumina that is based on amplified single molecule arrays. Single molecules of DNA are placed on a glass chip and amplified to form a multitude of localised clusters of DNA. Sequencing-by-synthesis is then conducted simultaneously on these distinct DNA clusters through the use of fluorescent reversible terminator deoxyribonucleotides. Due to the terminator property of the deoxyribonucleotides, only one base is added to the growing DNA strand per cycle. Different fluorescent probes are attached to the A, T, G and C terminators, allowing the base added to the strand to be identified. At the end of a cycle, the florescent probe and termination property are removed from the added base, allowing the next terminator deoxyribonucleotide to be incorporated in the following cycle. As there are vast quantities of individual DNA clusters, and different genomic locations are being sequenced

per cluster, a plethora of DNA sequence "reads" are rapidly produced. Each read is approximately 35 bases in length (Bentley *et al.*, 2008). These reads are then overlapped and mapped to a reference sequence using SAM tools (Sequence Alignment/Map) freeware to produce a BAM file (Binary Alignment/Map). A BAM file contains the aligned sequence information for an entire exome and can be both visualised and navigated using Interactive Genome Viewer freeware.

For my project, I used next generation sequencing to decode the exome of two mouse lines; Pinky and Marble. For each line, DNA was extracted from a phenotypic animal tail tip. A minimum of 100µg of DNA was extracted per sample and suspended in 100µl TE buffer (10mM Tris-HCl, 1mM EDTA). Samples were then sent to Dr David Adams at the Wellcome Trust Sanger Institute for next generation exome sequencing. BAM files of the exomes were produced and C57BL/6 was used as the reference sequence. SNPs were filtered to remove all calls which were heterozygous, present in the C3H progenitor strain, poor quality and/or had a read depth less than 30.

A read depth of 30 was set as the quality threshold as the SNP calling had to be able to distinguish between heterozygous and homozygous SNPs. To confidently observe any heterozygous variant, the sample must be sequenced enough times to obtain a reasonable probability of observing both alleles (Bentley *et al.*, 2008). If sufficient observations are not made there is an increased risk that a SNP may inaccurately be called as homozygous. As mode of inheritance is important for assessing if a SNP correlates with phenotype, it is vital that heterozygous SNPs were not misidentified as homozygous. **Figure 4** shows work by Bentley *et al.* that highlights that a read depth of greater or equal to 30 is required to maximise SNP detection and reliably differentiate between heterozygous and homozygous genotypes.

Figure 4: SNP calls versus read depth

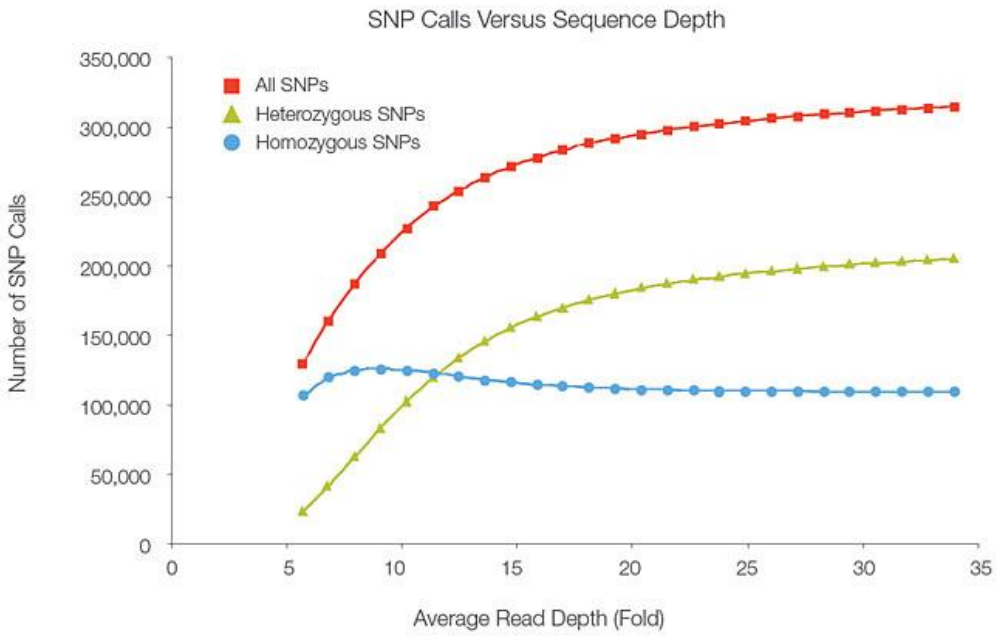


Figure 3. *A read depth equal or greater than 30 is required to maximise the identification of heterozygous SNPs. At low read depths there is an increased probability that heterozygous SNPs will be miscalled as homozygous. This figure is taken from Bentley et al., 2008.*

Scanning electron microscopy

Homozygous *Hydin* animals and WT littermates were perfused with a fixation solution pre heated to ~37˚C to ensure cilia were preserved in their normal physiological state. Fixation solution consisted of 2.5% gluteraldehyde, 2% paraformaldehyde and 0.1% picric acid in 100 mM phosphate buffer (pH 6.5). Testis and cilia were then harvested and stored in the fixative solution for one day. To complete processing, samples were then delivered to Dr Mike Shaw at the Dunn School of Pathology, University of Oxford. Samples were fine dissected, rinsed several times with distilled water and subsequently dehydrated through an ethanol series. After sputter-coating with gold, the samples were examined in a JOEL JSM 6390 scanning electron microscope. Images were subsequently collected by Dr Helen Dawe and me.

Neurogenesis immunostaining

Neurogenesis was measured by staining for doublecortin (DCX) on every sixteenth section through the entire rostrocaudal extent of the dentate gyrus. Free floating sections were incubated with goat anti-DCX antibody (1:400, Santa Cruz Labs) overnight at room temperature in 0.5% triton/PBS solution containing rabbit serum. Next day, a standard rabbit IgG ABC kit procedure was used and sections reacted with DAB. Sections were then mounted on electrostatically charged slides and dried on a vertical slide holder. Slides were then taken though a dehydrating alcohol series, cleared in histoclear and coverslipped in DPX mounting medium. DCX positive cells were counted manually on a standard light microscope using a 10x objective.

Git2 -/- Golgi staining and analysis

For *Git2 -/-* spine analysis, mutant and WT littermate brains were harvested and stained using an FD rapid Golgistain™ Kit in accordance with the manufacturer's instruction (FD Neuro Technologies). Brains were sectioned coronally at a thickness of 80µm using a microtome. Dendritic spines from CA1 of the hippocampus were used for analysis (**Figure 5**) and photographed using an Olympus BX-51 microscope equipped with a 100x objective.

Figure 5: Measuring dendritic spine density

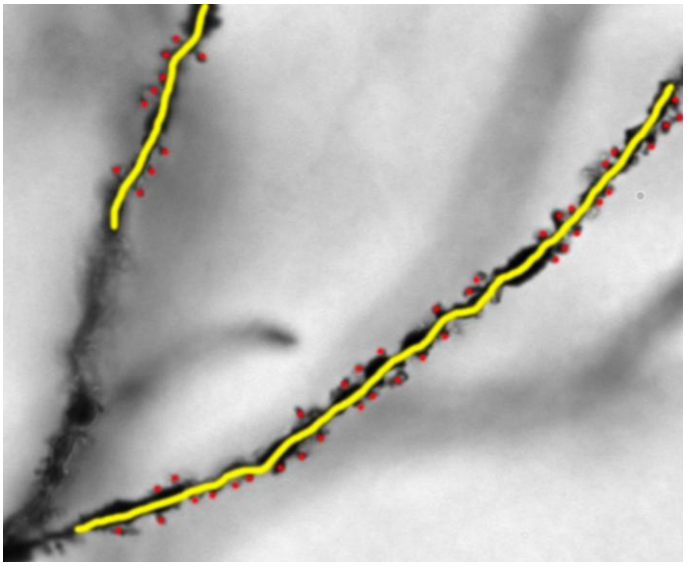


Figure 5: *ImageJ was used to calculate the length of in focus dendrites (yellows) at a scale of 15.725 pixels/µm. Spines (red dots) were then counted and density of spines per µm of dendrite calculated*

Behavioural methods

Order of tests and n numbers

Behavioural experiments were conducted at the Department of Experimental Psychology, University of Oxford. All mice tested were given a day of rest between experiments and were age matched.

Whirligig animals and controls were tested in the following experiments in the listed order: elevated plus maze, open field, Y maze, activity box, food neophobia and three chambered sociability box. A total of 12 *Whirligig* -/+ mutants (9 female, 3 male) and 25 WT littermates (10 female and 15 male) were used for testing.

Diminuendo and controls were tested in the following experiments in the listed order: open field, Y maze, activity box and complex labyrinth maze. A total of 8 homozygous mutants (4 female, 4 male), 16 heterozygous mutants (10 female, 6 male) and 9 WT littermates (5 female, 4 male) were used for testing.

Lastly, *Cxcr4-Sox1-Cre* conditional KO and controls were tested as follows: accelerating rotarod, activity box, running wheel and inverted mesh grid grip test. A total of 9 animals (5 male, 4 female) were used for testing in both the KO and WT littermate groups. However, the number of WT animals used in the running wheel and inverted mesh grid test dropped to 8 due to the death of one male animal.

Elevated plus maze

The elevated plus maze (EPM) was used to assess anxiety. As shown in **Figure 6**, mice were placed in the central zone of the maze (blue) facing a walled "closed arm" (orange) and tested for 300 seconds. The "open arms", which were unwalled, are shown in green. Ethovision tracking software was used to calculate the movements of the mouse and the duration spent in each zone. Data points were positioned on the nose, central body and posterior region of the mouse (sky blue, red and pink dots on yellow mouse in **Figure 6**). All three data points had to be in a given zone to contribute towards the time duration spent in that zone. If data points were between zones this was scored as interzonal time. An entry into a zone was counted when the nose data point entered that respective zone. A higher proportion of time spent in the closed arms and a lower open arm:closed arm entries ratio are considered indicative of increased anxiety (Rodgers and Dalvi, 1997, Pellow *et al.*, 1985).

Figure 6: Elevated plus maze protocol

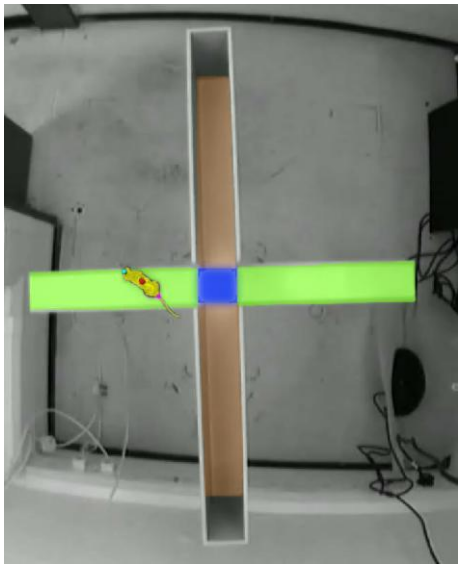


Figure 6: *The EPM in use with open arms, closed arms and central zone shown in green, orange and blue respectively.*

The open field maze

The open field was used to assess anxiety and locomotion behaviour. As shown in **Figure 7**, the OF is composed of a 15 box grid with the inner most three boxes being termed the "inner zone" (purple). The remaining boxes are the "outer zone" (blue). To be considered as having entered the inner zone the centre of the mouse had to be within the zone (red dot on yellow mouse in **Figure 7**). Ethovision software was used to track the movement of the mouse and make recordings from which instances of pausing, thigmotaxis loops and circling were manually quantified. Mice were tested for 300 seconds and initially placed in the upper left corner grid of the maze. Mice which spend less time in the inner zone of the maze are considered to be more anxious (Prut and Belzung, 2003).

Figure 7: Open field protocol

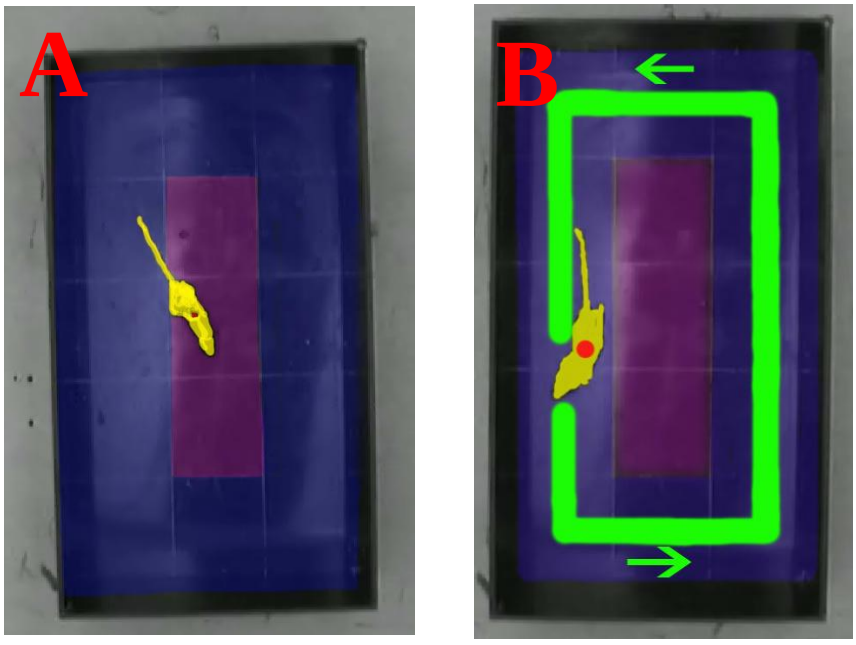


Figure 7. *The open field maze in use with the inner and outer zones shown in purple and blue respectively (A). The path of a mouse completing a thigmotaxis loop (also known as a homerun) (B).*

Y maze

The Y maze was used to assess spatial reference memory. As seen in **Figure 8**, a mouse was placed in a Y maze with one arm blocked off (blue). This blocked arm was termed the "novel" arm. The remaining arms, termed "start" and "other", were unblocked and the mouse had the opportunity to explore them for 5 minutes during the training phase. This allowed the mouse to become familiar with spatially fixed olfactory markers beyond the maze's boundary. The mouse was then removed for 1 minute and held in a holding cage whilst the barrier blocking the novel arm was removed. The mouse was subsequently re-placed back in the starting arm for testing. Once it exited the start arm (orange) the mouse was given two further minutes to explore the maze. The initial arm of exploration upon exiting the start arm was noted as the "first arm entry choice". The number of entries and duration spent in the start, other and novel arms (orange, red and blue) was also recorded. Typically, WT animals visit the novel arm first and spend a higher proportion there having become familiar with the other two arms during training (Sanderson *et al.*, 2007). Between mice, the novel, start and other arms were interchanged to limit bias.

Figure 8: Y maze protocol

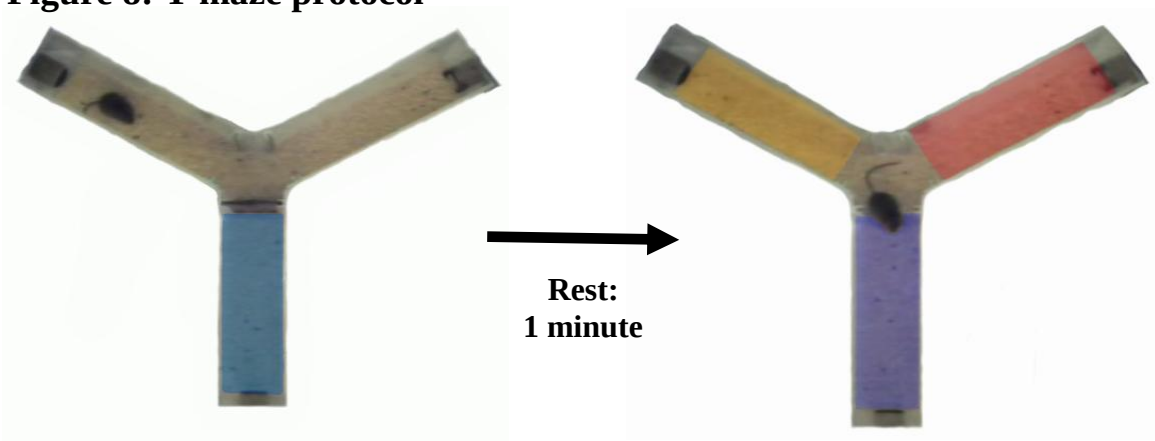


Figure 8. *The Y maze with the start, other and novel arms shown in orange, red and blue.*

Activity box

The activity box was used to measure activity rate over time. Mice were housed separately in transparent plastic cages for two hours. As shown in **Figure 9**, two low power laser beams were continuously fired across each box and targeted sensors on the opposite wall of the cage. If a mouse positioned itself between the beam emitter and sensor, a "beam break" would be automatically counted by a computer. When a mouse created a beam break at both lasers sequentially, this was counted as a "cross-over". As lasers are positioned at opposite ends of the box, the cross-over count reflects the number of times a mouse transverses the whole length of the cage. The counts for beam breaks and crossovers were measured over twenty four 5 minute intervals. As a control, the test period was always at a fixed time of day (10am till noon) and equal numbers of mutant and WT animals were tested per day.

Figure 9: Photonic locomotion activity box protocol

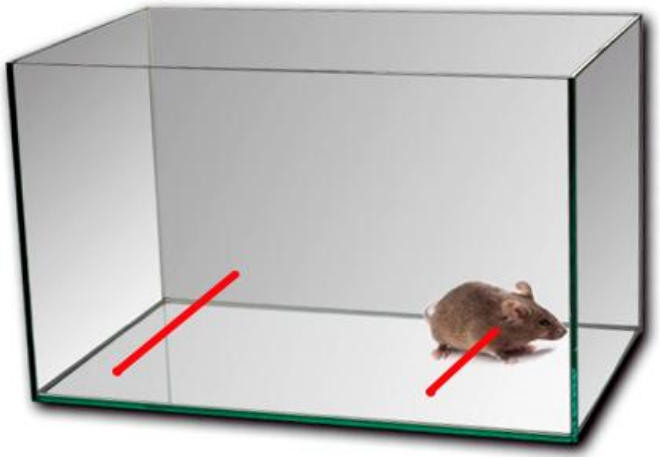


Figure 9. *Schematic of the activity boxes with laser beams shown in red. Pictured mouse is creating a beam break.*

Food neophobia

The food neophobia test was used to measure anxiety induced by food novelty in an unfamiliar environment. Mice were weighed and food deprived overnight. Subsequently, mice were reweighted the following morning so that percentage weight loss could be calculated. As shown in **Figure 10**, mice were then placed in an inverted plastic jug containing a thimble of condensed milk. The time taken for the mouse to start food consumption was then measured up to a maximum of 6 minutes. A longer latency in initiating food consumption can indicate elevated anxiety (Deacon, 2011).

Figure 10: Food neophobia protocol



Figure 10. *Food neophobia testing apparatus consists of an inverted jug with a thimble of condensed milk in the lip.*

Three chambered sociability box

The three chambered sociability box was used to assess sociability and preference for social novelty (Kaidanovich-Beilin *et al.*, 2011). This was done through detecting changes in locomotion behaviour and chamber preference upon the introduction of encaged stranger mice, or empty cage "objects", into the testing environment. As shown is **Figure 11**, mice were given time to explore the empty box in the habituation phase. This consisted of 5 minutes of the mouse exploring the central chamber (red) followed by a further 5 minutes where it had access to explore all three chambers (**Figure 11 A**). The test mouse was then enclosed back into the central chamber while the sociability phase was prepared. In this phase, an encaged stranger mouse was place in one side chamber (green) whilst an object was place in the opposite side chamber (blue) (**Figure 11 B**). After this phase, the test mouse was re-enclosed in the central chamber while a novel encaged stranger animal was swapped for the empty cage object. In the social novelty phase, the test mouse was once again allowed to access the side chambers and consequently react to both the novel and original stranger mice (**Figure 11 C**). Speed, circling rate, time spent in each zone and instances of freezing were recorded for each phase. All stranger mice were male CA1 animals of a comparable weight to the test animal.

Figure 11: Three chamber sociability box protocol

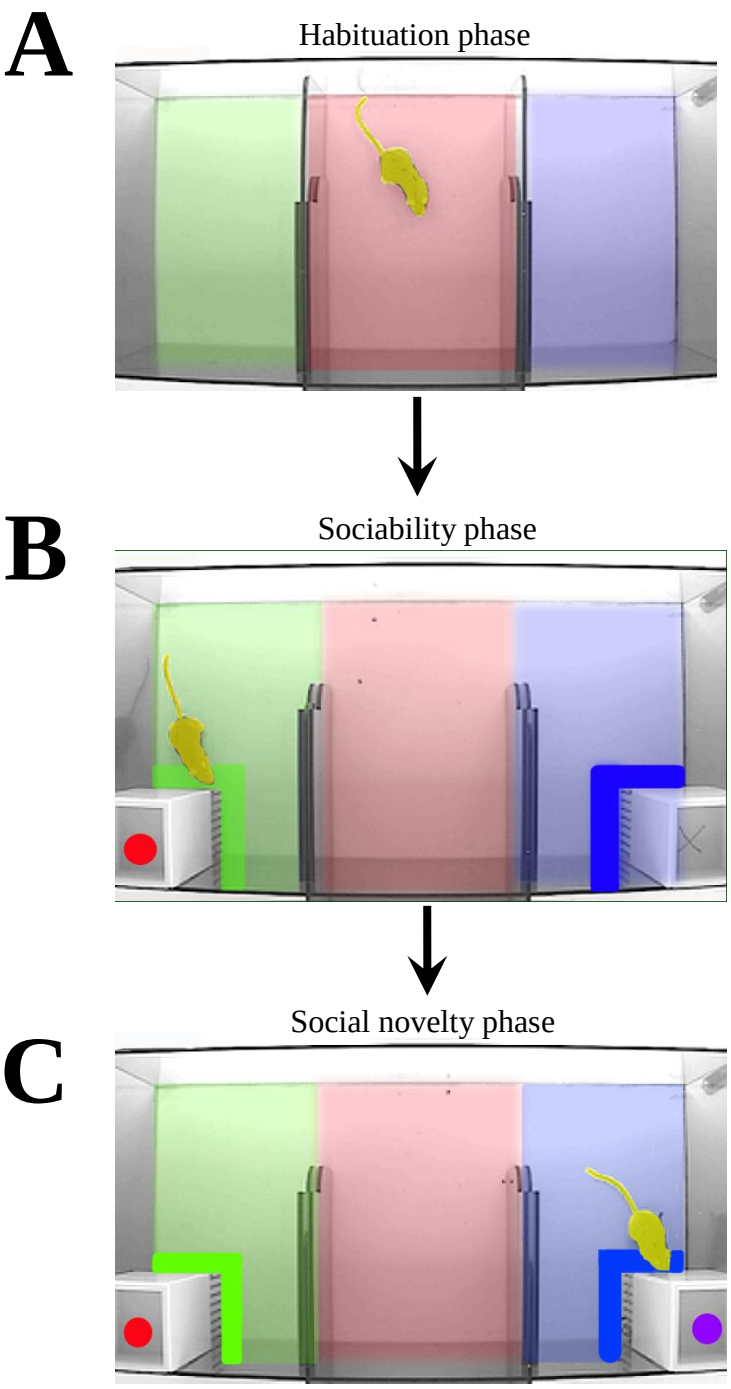


Figure 11. *A test animal is habituated to the central chamber (Red) for 5 minutes and then allowed an additional 5 minutes to explore the side chambers (green, blue) (A). An encaged stranger animal is then introduced to one side chamber (red dot) whilst and object is placed in the opposite side chamber (B). The object is then swapped for a novel encaged stranger animal (purple dot) (C).*

Complex labyrinth maze

The complex labyrinth maze was used to measure explorative behaviour and working memory. As seen in **Figure 12**, mice were introduced to the home zone of the maze (blue) and allowed 3 minutes to explore the various corridors, connecting passages and dead ends (green, orange and red). The time spent in the home zone, number of excursions from the home zone, time between excursions, largest excursion size, total dead end visits and total distinct dead end visits were measured.

Figure 12: Complex labyrinth maze protocol

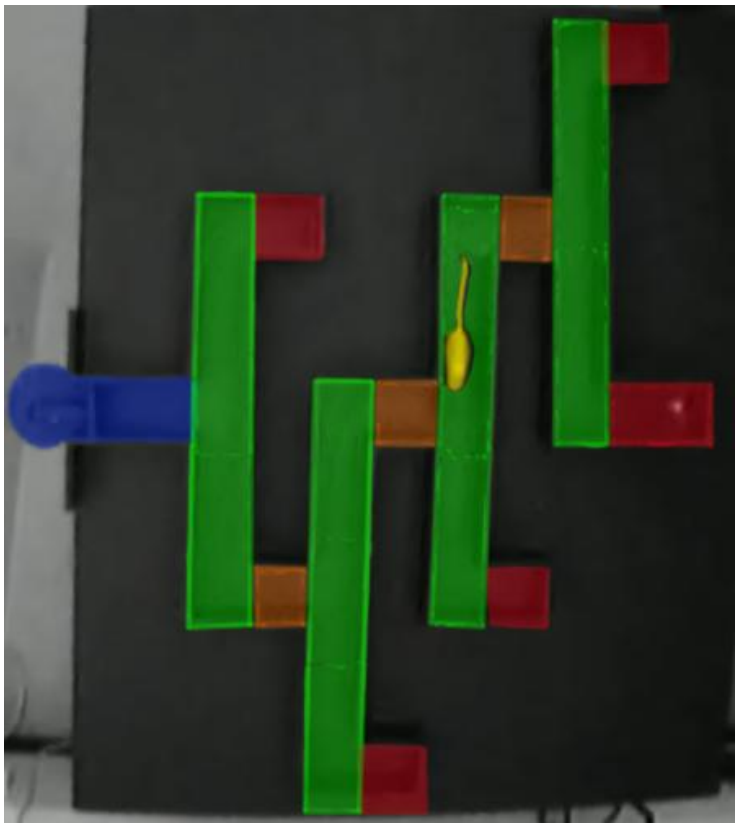


Figure 12. *Complex labyrinth maze in action showing the home zone, corridors, connecting passages and dead ends (blue, green, orange, red).*

Accelerating rotarod

The accelerating rotarod was used to test motor coordination ability (Jones and Roberts, 1968). Mice were held by the tail and placed on the rotarod, facing away from the direction of rotation so that they were required to walk forward in order to avoid falling. The rotarod moved at an initial speed of 4rpm. After 10 seconds, the rod speed was accelerated at a rate of 20rpm per minute. Once acceleration had been triggered, the time taken for mice to fall was noted.

Running wheel

The running wheel was used to over several days to measure changes in running ability and activity. Mice were separated from their littermates and individually housed in cages which contained a running wheel with a magnet positioned at the edge of the disc. With each rotation, the magnet relayed information to a pedometer positioned outside the cage. This allowed total distance travelled, average running speed and maximum running speed to be recorded. On day zero, mice were placed in the cages at 7pm and the pedometer readings recorded the following morning at 8am. The pedometer was then reset at 7pm and the new readings recorded at 8am the next day. This process was repeated for a total of 5 days.

Inverted mesh grid grip test

This test was used to detect defects in grip strength and compromised coordination of limbs. Mice were placed on the centre of a 43cm square wire mesh grid consisting of 12 mm squares of 1 mm diameter wire. The grid was surrounded by a 4cm thick wooden frame which prevented mice climbing to the inverse side. Once a mouse was positioned, the grid was turned upside down and elevated in order to force the mouse to grip the wire to avoid falling. The time taken for a mouse to fall was recorded. If an animal did not fall, the experiment was concluded after one minute. Additionally, the inverted grid was slowly tilted in order to encourage the mouse to move. This allowed any limb dragging and lack of clasping to be noted.

Methods used for further analysis of *Jenna* mouse

BrdU labelling

For birthdate labelling experiments, pregnant C3H females were injected with BrdU (50mg/g of body weight) 12 days after copulation with *Jenna* mutant males. All resultant P0 pups were sacrificed and genotyped. P0 brains were extracted and drop fixed in 4% paraformaldehyde for 4 hours before being placed in sucrose overnight. Brains (n=4) were then embedded in OCT, sectioned at 14mm on a cryostat, mounted onto electrostatic slides and stored at -20˚C. Prior to staining antigen retrieval was performed by placing slides in citrate buffer (0.01M, pH 6) at 90˚C for 1 hour. To quench natural peroxidase activity, slides were then placed in 3% H_2O_2 solution for 10 minutes and subsequently washed in PBS. Sections were then digested in trypsin (0.0125%) for 10 minutes at 37˚C, washed, and incubated for a further 20 minutes in 2M HCl. After washing, slides were incubated in a 0.3% triton/PBS with 2% rabbit serum (Rat Elite ABC Kit, Vector Labs) and 1:100 rat anti-human BrdU antibody (Accurate Chemical & Scientific) in a humidity chamber overnight. Slides were then washed and stained as directed in the Elite ABC Kit, using DAB permanent staining.

Gallyas staining

Twelve week old *Jenna* mutant mice and WT littermates were perfused with 0.9% saline and 10% formalin solution. Brains were extracted and left in 10% formalin solution for 4 weeks. Subsequently brains were dehydrated in 30% sucrose PBS and sectioned at a thickness of 20µm on a sliding microtome. Sections were matched, mounted on electrostatically charged slides, and stained using a Gallyas silver staining method based on Pistorio *et al.*, 2006 (Pistorio *et al.*, 2006).

The staining process involved the following steps. Sections were washed and subsequently placed in a freshly made two part pyridine: one part acetic anhydride solution for 70 minutes. Slides were then taken through 50% EtOH, 30% EtOH, and a 0.05%, 0.1%, 0.5% acetic acid

series for 5, 5, 3, 3 and 10 minutes respectively. Sections were then placed in freshly made silver nitrate solution for 60 minutes in the dark (Recipe: 0.77g ammonium nitrate, 0.8g silver nitrate, 2.4ml 4% sodium hydroxide solution, dissolved in a darkened bottle containing 400ml of distilled water). Sections were then washed in 0.5% acetic acid three times for five minutes before being placed in freshly made ABC developer solution for 4 minutes in the dark. ABC developer solution is composed of the stock solutions mixed at the ratios detailed in **Figure 13**. The constituents of the ABC developer were mixed slowly in order to avoid the formation of a detrimental white precipitate. After exposure to the ABC developer, sections were briefly washed in 0.5% acetic acid and placed in 0.2% potassium ferricyanide solution for 55 minutes followed by a further 4 minutes in 0.5% sodium thiosulphate. Sections were then retaken three times through a cycle of 0.5% acetic acid washes, ABC developer, 0.5% acetic acid, 0.2% potassium ferricyanide and 0.5% sodium thiosulphate. The time in 0.2% potassium ferricyanide was reduced by 5 minutes per cycle. After the last cycle, sections were taken through a dehydration alcohol series and mounted in DPX.

Figure 13: ABC developer solution composition and stock chemicals

A

Stock solution	Chemicals used and notes
A	40g sodium carbonate dissolved in 800ml of distilled water
B	1g ammonium nitrate, 1g silver nitrate and 5g silicotungstic acid dissolved, in that order, into 500ml distilled water (KEEP IN DARK)
C	1g ammonium nitrate, 1g silver nitrate, 5g silicotungstic acid and 2.55ml 37.5% formaldehyde solution, dissolved, in that order, into 500ml distilled water (KEEP IN DARK)

B

Ambient temperature (◦C)	Quantities mixed to make ABC developer (ml)		
	Solution A	Solution B	Solution C
15	10	0	10
20	10	3	7
22	10	4	6
25	10	5	5
30	10	7	3

Figure 13: *Stock solutions, required to make ABC developer, which can be stored for many months (A) Composition of the ABC developer is determined by ambient temperature (B)*

In situ hybridisation

In situ hybridisation on 12 week old *Jenna* mutant and WT littermate tissue was performed with help from Dr David Keays and Dr Peter Oliver. A 429 base pair probe targeting the *Tumour Protein D52-like-1* (*Tpd52l1*) gene was amplified by PCR, using primers designed by the Allen Brain Atlas resource, and ligated into the pCRII-TOPO vector (Invitrogen). This vector was transformed into competent DH5α *E.Coli* cells in accordance with the manufacturer's specifications (TOPO® Cloning Kit). Cells were then spread onto plates containing 100μg/ml ampicillin and 40mg/ml X-gal. Recombinants were selected by blue/white screening and cultured overnight in broth containing 100μg/ml ampicillin at 37°C. Plasmid DNA was isolated utilising a Qiagen Mini Prep kit (Qiagen) and linearised using Not1 endonuclease.

Linearised DNA was visualised on an agarose gel and extracted with a Qiagen gel purification kit (Qiagen). An *in vitro* transcription reaction was utilised to create the riboprobe. This reaction, in a total volume of 20μl, contained: 250-500ng of linearised plasmid DNA; 2μl of DIG labelling mix (10 mM ATP, CTP, GTP (each), 6.5 mM UTP, 3.5 mM DIG-11-UTP, Roche); 2μl of polymerase buffer ("10x" concentration as supplied by Roche); 1μl of RNasin (20-40U/μl, Promega); and 2μl of RNA polymerase (≥20 U/μl, Roche). Following an incubation of 2hrs at 37°C the probe was ethanol precipitated and air dried. The pellet was then resuspended in 50μl TE (10mM Tris-HCl, 1mM EDTA).

Whole mouse brains were frozen in OCT (Merck, Darmstadt, Germany) on dry ice, and 14 μm coronal sections were cut and mounted on electrostatically charged slides. Sections were fixed in 4% PFA in PBS solution for 10 minutes at room temperature, followed by three washes (3mins) in PBS. Slides were placed in an acetylation mix (0.25% acetic

anhydrate in 250ml 0.1M RNAse-free triethanolamine-HCl, pH8). The acetylation mix was made at time of use, with the acetic anhydride being slowly added to the 0.1M RNAse-free triethanolamine over a period of 4 minutes. Following a further incubation of 6 minutes, slides were washed three times (3 minutes per wash) in PBS. Sections were then incubated in 200µl 50% formamide in 2x saline-sodium citrate buffer (SSC) for 1hr at room temperature. 2x SSC (300mM NaCl, 30 mM trisodium citrate) was made fresh from 20x SSC stock (3M NaCl, 300 mM trisodium citrate) diluted in RNAse-free water. Slides were drained and placed in 200µl of 0.5µg/ml riboprobe containing hybridisation solution (50% formamide, 0.2 mg/ml *E. coli* tRNA, 1 × Denhardt's solution, 10% dextran sulfate, 0.6 M NaCl, 0.25% SDS, 1 mM EDTA, and 10 mM Tris-HCl, pH 7.6). Sections were then incubated for 16-20 hours at 60-70°C in a chamber containing 20ml 5 X SSC, 50% formamide. Following hybridisation slides were washed in 0.2 x SSC in a shaking water bath for 1 hr and then blocked for 1hr in B1 solution (150mM NaCl, 100mM Tris-HCl ph 7.6) with 1% blocking powder (Roche). Samples were incubated with 500µl of Anti-DIG antibody (1:5000, Roche) diluted in B1 solution at 4°C overnight, and washed three times for 5mins in B1 solution the following morning. Slides were equilibrated in B2 solution (100mM NaCl, 100mM Tris-HCl ph 9.5, 50mM $MgCl_2$) for 5mins before detection using a NBT/BCIP mix (Pierce)**.** Following an incubation of 12-48 hours, slides were mounted in 90% glycerol: 10% PBS mixture and coverslipped.

Juvenile and adult immunohistochemistry

Cohorts of P21 and 12 week old *Jenna* mutant and WT littermate mice (n=4) were perfused with 0.9% NaCl and 4% paraformaldehyde and brains post-fixed for 6 hours followed by dehydration in 30% sucrose solution. Sections (40mm) were prepared on a freezing microtome and stored in antifreeze solution at -20˚C. For each P21 and 12 week brain, three

matched SC sections were selected for staining. Sections were incubated with the primary antibody overnight in 0.3% triton/PBS, containing 2% of the serum, at the following concentrations: NeuN (1:500, Chemicon); Calbindin (1:500, Chemicon); Er81 (1:4000, gift from Dr. Thomas Jessel). Following three five minute washes in PBS, sections were incubated with biotinylated secondary antibody (1:500, Vector lab Elite ABC kit) in 0.3% triton/PBS for 2 hours. After a series of washes in PBS, sections were incubated for one hour with fluorescein-conjugated streptavidin (1:500, Vector Labs). Sections were then mounted onto electrostatic slides and coverslipped with DAPI containing mounting media (Vector Labs).

Apoptosis study

Seven week old mice *Jenna* mutant and WT littermate mice were perfused and sectioned (n=5). Every 8th section from the beginning of the superior colliculus through to the start of the inferior colliculus was mounted on electrostatic slides. Prior to staining, slides underwent antigen retrieval, peroxidase quenching and PBS washing. Sections were incubated with the caspase 3 primary antibody (1:400, Cell Signaling Technology) overnight in 0.3% triton/PBS with 2% goat serum. Slides were then washed and stained as directed in the Elite ABC Kit, using DAB permanent staining. Total cell counts were then obtained by multiplying the number of positive cells observed by a factor of 8.

Quantification and statistics

The superior colliculus was analysed using 10, 250µm wide, zonal analysis boxes in which cells were counted (**Figure 14**). Boxes were drawn on images of the superior colliculus using ImageJ freeware, positioned 100µm from the midline. The boxes were of equal height within an image, with the height of each box being a tenth of the distance between the surface of the zonal layer of the superior colliculus to a depth in the periaqueductal grey level with the

cerebellar aqueduct. Once analysis boxes were formatted, labelled cells within each box were counted manually. The percentage of neurons within each box was calculated from the number of NeuN staining cells as a proportion of DAPI cells. Statistics were performed in Graphpad Prism. A one-way ANOVA with a Bonferroni correction for multiple comparisons was used for the analysis of measurements for NeuN, BrdU and DAPI cell density zonal measurements. T-tests were used for analysis of superior colliculus thickness measurements and caspase 3 positive cell counts.

Figure 14: Superior colliculus analysis box plotting protocol

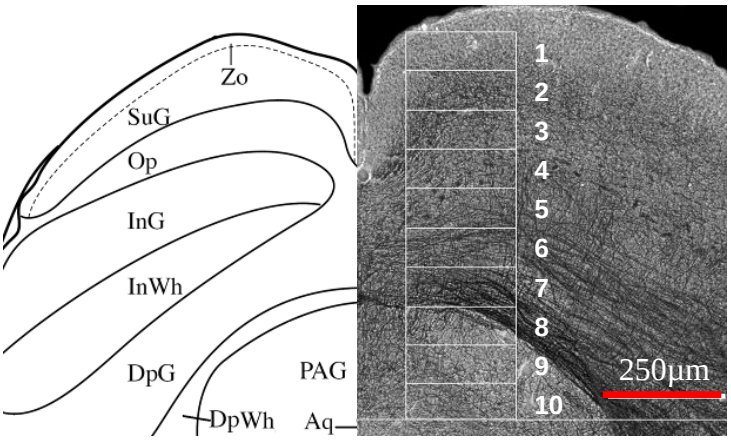


Figure 14. *Diagram showing the layers of the SC aligned with Gallyas stained WT and mutant sections. Equally proportioned analysis boxes (shown in white) were drawn from the aqueduct to the dorsal surface of the zonal layer. Scale bar equals 250µm*

Histological methods used to assess the *Cxcr4* conditional knockout

Cerebellar Gallyas staining

Four, thirteen week old *Sox1-Cre Cxcr4* -/- conditional KOs and WT littermates were culled, fixed and processed as detailed on pages 48-50. However, brains were sectioned sagittally. Images of the whole sections were taken at 6400dpi using a EPSON PERFECTION V750 PRO scanner. A series of images across the cerebellum was taken at 4x magnification using a light microscope for each brain. Image series were then photomerged in Adobe Photoshop Creative Suite 5 to generate high resolution images showing the whole cerebellum.

Golgi staining, dendritic spine analysis and Purkinje cell imaging

Five, thirteen week old *Sox1-Cre Cxcr4* -/- conditional KOs and WT littermates were culled and processed as detailed on pages 36. However, one brain hemisphere was cut sagittally while the other was cut coronally. Dendritic spines were imaged from the molecular layer of hippocampus as, according to the Allen Brain Atlas, *Cxcr4* is expressed in this area in WT development at P4. For each brain, 10 images of spines were taken on an Olympus BX-51 microscope equipped with a 100x objective. This microscope was also used to take an image series of Purkinje cells. As Purkinje cells are large, this image series was required to create a merged image where all the dendritic branches were in focus. This focused image was created using the create High Dynamic Range Image feature in Adobe Photoshop Creative Suite 5.

Genotyping

All mice used in my experiments were genotyped as described in **Figure 15**. Except where specified otherwise, the following "TD1" touchdown PCR program was used to make a 10µl reaction mix (1µl of primers (10pM); 2µl DNA (10ng/µl); 1µl HotStar taq buffer (Qiagen); 1µl dNTPs (10mM each); 0.6µl $MgCl_2$ (25 mM); 0.05ml HotStar taq (5 U/ µl, Qiagen); 4.35 µl H_2O):

TD1 touchdown program:

1. 95°C for 10 minutes
2. 95°C for 30 seconds
3. 62°C for 30 seconds (-0.5°C per cycle)
4. 72°C for 1 minute (repeat steps 2-4 for 13 cycles)
5. 95°C for 30 seconds
6. 55°C for 30 seconds
7. 72°C for 1 minute (repeat steps 5-7 for 29 cycles)

Endonuclease digestion of PCR product is required for *Hydin*, *Jenna* and *Whirligig* genotyping. The specific endonucleases required for each line is given in **Figure 15**. Digestion reactions are comprised of the following reagents and are incubated at 37◦C for 4 hours before being electrophoresed on a 1% agarose gel: 8µl PCR product; 1µl NEBuffer (concentration as supplied by New England Biolabs), 1µl endonuclease (1000U/ µl, New England Biolabs).

Where applicable, animal genotypes were cross referenced with phenotyping information as several lines featured overt somatic phenotypes. This included the *Jenna*, *Hydin*, *Diminuendo*, and *Whirligig* lines which featured reduced body weight, hydrocephalus, lack of pinnae reflex and circling respectively.

Figure 15: Genotyping protocols

Mouse line	PCR primers	PCR program, notes and further steps	Product sizes
Diminuendo	WT Forward = TTGGCACTAGCACATTTTTGC Mutant Forward = TTGGCTCTAGCACATTTTTGC Common Reverse = GAAGGCTAGACCCCAAAGACG	1. 95°C - 10 min 2. 95°C - 35 secs 3. 65°C - 35 secs 4. 72°C - 1 min 5. Go to "2" X 42 6. 72°C - 7 mins Run on separate gels. Use low $MgCl_2$ ($1/6^{th}$ of the specified amount for TD1)	Both bands = 370bp Forward primers over the SNP, designed to fail if does not perfectly match template.
Sox1-Cre Cxcr4 -/-	*Cxcr4* Forward = GACCTGGGTATGATGGGCAACGGTG *Cxcr4* Reverse = CTGGGACGTTAGAGTCACACTGTCC *Sox1-cre* Forward = GCATAACCAGTGAAACAGCATTGCTG *Sox1-cre* Reverse = GGACATGTTCAGGGATCGCCAGGCG	*Cxcr4*: 7. 95°C - 10 min 8. 95°C - 35 secs 9. 57°C - 35 secs 10. 72°C - 1 min 11. Go to "2" X 35 12. 72°C - 7 mins *Sox-1 cre*: 1. 94°C - 3 min 2. 94°C - 30 secs 3. 58°C - 30 secs 4. 72°C - 1 min 5. Go to "2" X 35 6. 72°C - 7 mins	WT band = 210bp Flox band = 310bp
Git 2	WT Forward = GCATGAATCAACTTTGGAGACA Mutant Forward = CACAAACGAAGGGACCAGAG Common Reverse = CATTTCAGAGTCTGCTGCCTTA	1. 94°C - 10 min 2. 93°C - 30 secs 3. 56°C - 30 secs 4. 65°C - 3 mins 5. Go to "2" X 39 6. 65°C - 10 mins	WT band = 690bp Mutant band = 860bp
Hydin	Forward = AGACTAACCTCTGCTCTCCC Reverse = GGTAGAAGCCTCTGTCATAGC	TD1 Program Follow with DdeI digest	Post-digest WT bands = 205, 74 and 58bp Mutant bands = 109, 96, 74, 58bp Heterozygous bands = 205 ,109 ,96 ,74 and 58bp
Hy3	WT Forward = CTTCCAGGATTTCCCCAT Mutant Forward = CTTCCAGGATTTCCCATA	1. 94°C - 10 min 2. 94°C - 40 secs 3. 58°C - 45 secs	Both bands = 410bp Forward primers over

	Common Reverse = TGTGATCTCAGAGGCTTAGT	4. 72°C – 1 min 5. Go to "2" X 42 6. 72°C - 7 mins Run on separate gels. Use low $MgCl_2$. ($1/6^{th}$ of the specified amount for TD1)	the SNP, designed to fail if does not perfectly match template.
Mdb2	WT Forward = AAGAACAAGCAGAGACTCCG WT Reverse = ACGCTGGCCTAGTGCCGTGC Mutant Forward = TTGTGGTTGTGCTCAGTTC Mutant Reverse = TCCGCAAACTCCTATTTCTG	TD1 program Use all primers together	WT band = 250bp Mutant band = 150bp
Jenna	*Tuba1* Forward = AGGGTGTCTTGGTATCTGTC *Tuba1* Reverse = AGGGTCACATTTCACCATC T7 Forward = GCCGCTAATACGACTCACTA T7 Reverse = TCCCAAGACTCTACCACAAC	1. 94 - 10 mns 2. 94 - 1 min 3. 94 - 30 secs 4. 65 - 30 secs 5. 68 - 1 min 6. Go to "2" X 35 7. 68 - 3 mins Use titanium taq (clontech) Follow with BceAI digest	T7 = 270bp Tuba1 = 680bp Mutant product is cleaved in digest.
Whirligig	Forward = ACTCAGGGAATACCAATTGGAG Reverse = CAAAGAAAAGTTCCCAGCAAAC	TD1 program followed by MfeI digest.	Post-digest WT band = 204bp Mutant band = 233bp

Chapter 3

ENU Mutagenesis Screen Results

Anatomical phenotyping and gene identification

Introduction

In this chapter I present the results of my ENU mutagenesis screen. A total of 1,912 animals were harvested and sectioned. All slides generated from these G3 ENU mutagenised animals were inspected microscopically for evidence of ectopias and cellular disruption. G3 pedigrees comprising of more than 12 individuals were anatomically quantified as described in **Chapter 2**. This totalled 703 mice from 38 pedigrees. The median age of screened mice was sixteen weeks.

I conducted experiments to identify the causal mutation in three pedigrees: *Marble*, *Pinky* (PEDV76) and *Hydin* (PEDV50). For *Marble* and *Pinky*, I present candidate gene mutations from exome sequencing data. There was not sufficient time to fully evaluate whether these candidate mutations were causal to neuroanatomical defects. For the *Hydin* line, I verified that the V4858E mutation was causal by performing a complementation test. I subsequently evaluated the impact of the V4858E hydin mutation on the development of somatic tissues. I show that homozygous mutants feature accumulation of debris in the trachea and produce tailless sperm.

Detection and rederivation of phenotypic pedigrees

For the quantitative screen, pedigrees were considered abnormal if the G3 contained two or more mice that shared an extreme morphological abnormality resulting in a Z score beyond ±3.29. A Z score beyond ±3.29 represents less than 0.001% of instances in a normal population. This conservative threshold was used in order to limit false positives.

As only half the backcrossed G2 daughters in a pedigree were likely to be heterozygous carriers, only 1 in 8 G3 pups were expected to be affected in lines bearing fully penetrant autosomal recessive mutations. In instances where all backcrossed G2 daughters were carriers, 1 in 4 G3 pups would be affected. The number of affected pups from six G3 pedigrees were consistent with these ratios (**Figure 16**). No lines displayed ratios consistent with dominant or sex linked modes of inheritance. **Figure 16** is refined from Z-score plots produced for each of the ten measurements detailed in the materials and methods. These plots are shown in **appendix 1**. The total hit rate for the quantificational ENU screen was six lines out of thirty eight, equivalent to 15.8%. This is comparable to the 17% hit rate of embryo focused ENU neuroanatomical screens (Mar *et al.*, 2005, Stottmann *et al.*, 2011).

Figure 16: Phenotypic ENU pedigrees

Pedigree	Affected animals/ Analysed population	Phenotype	Fate and progress
PEDV25	2/13 (15%)	Reduced length of pyramidal cell layer	Sperm Frozen
PEDV41	3/28 (11%)	Hydrocephalus	Sperm Frozen
PEDV50* **(Later renamed "*Hydin*")**	7/26 (27%)	Severe hydrocephalus	Mutation Identified
PEDV52	8/41 (20%)	Increased thickening of the molecular layer of the hippocampus	Sperm Frozen
PEDV64	3/14 (21%)	Corpus callosum agenesis	Line extinct due to poor breeding
PEDV76* (Later renamed "*Pinky*")	4/18 (22%)	3 animals with corpus callosum agenesis, one animal with CA1 ectopia	Exome sequenced

Figure 16. *Table lists all mouse pedigrees containing multiple extreme phenodeviants.*

* *Pedigrees in which a causal mutation has been identified or a heritable anatomical phenotype has been proven.*

Due to the number of hits, it was only possible to select a subset of lines for mapping. The PEDV64 line went extinct at Harwell as the G1 founder was a poor breeder and was culled without sperm freezing. Compared with the other phenotypic lines, PEDV25 and PEDV52 displayed subtle abnormalities which may have been harder to map. Consequently, I selected PEDV41, PEDV50 and PEDV76 for rederivation and further testing due to the availability of the mice and striking nature of their phenotype. Hydrocephalus in several PEDV50 samples was so pronounced that the lateral ventricles dominated more than 10% of the total section area (**Figure 17**). Histological sections of the lines featuring the most overt phenotypes are shown in **Figure 18**.

Figure 17: ENU pedigrees featuring enlarged lateral ventricles

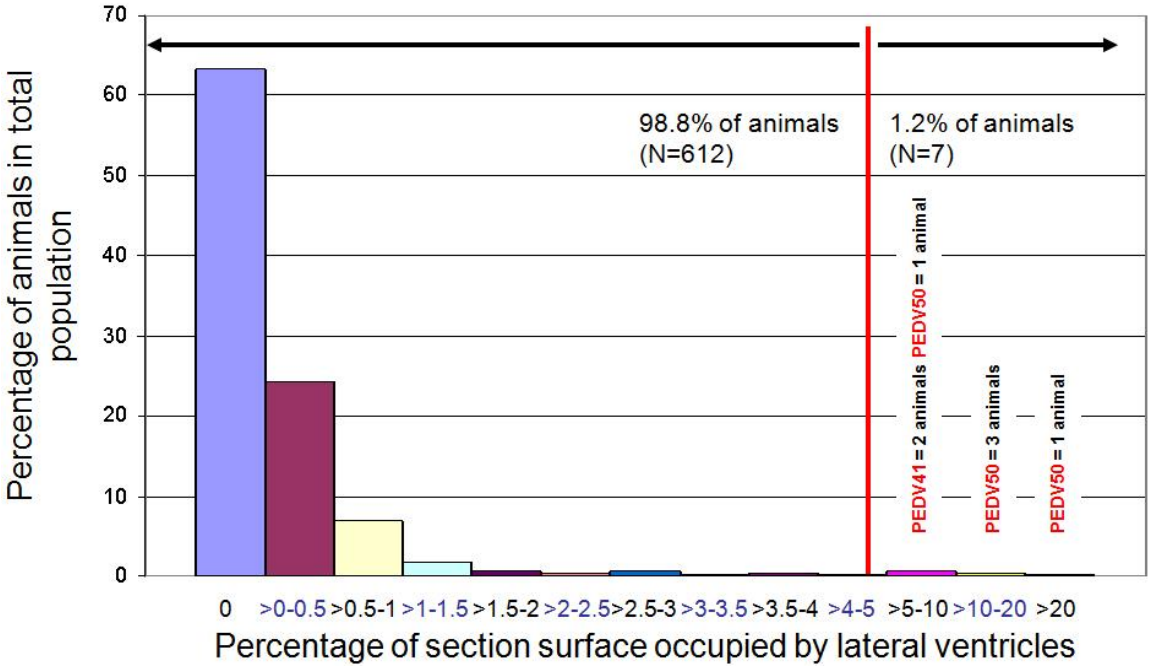


Figure 17. *High proportion of brain section area is dominated by lateral ventricles in the PEDV41 and PEDV50 pedigrees.*

Figure 18: Affected ENU pedigree histology from quantitative screen

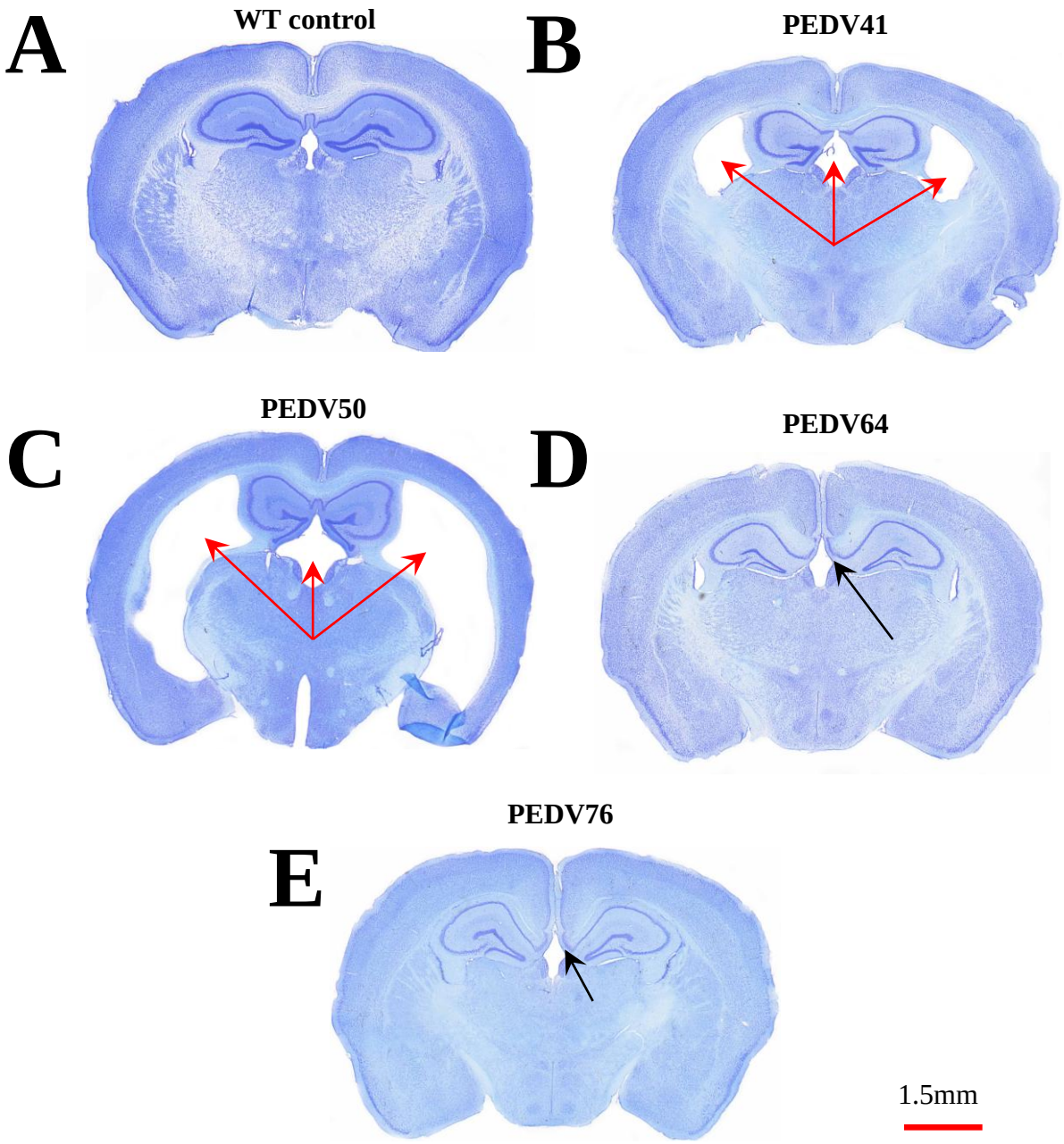


Figure 18. *Control mouse (A). PEDV41 and PEDV50 with red arrows showing ventricle swelling (B and C). PEDV64 and PEDV76 with black arrows showing corpus callosum agenesis (D and E). Scale bar equals 1.5mm*

A qualitative screen searching for ectopias was conducted on all 1,912 mice harvested. This covered 125 pedigrees in total, 87 of which were not included in the quantitative screen due to having a G3 of less than 12 animals. Out of all 125 pedigrees, only one line featured ectopia. This represents an ectopia phenotype hit rate of 0.8%, far less than the 15.8% hit rate for all phenotypes covered in the quantitative screen. This ectopia line was renamed *Marble* (originally named PEDM23) and was rederived to the WTCHG. The original *Marble* G3 consisted of fewer than 12 animals and was not included in the quantificational screen. From qualitative assessment, three phenotypes were initially identified in the pedigree: hydrocephalus, partial corpus callosum agenesis and CA1 pyramidal cell layer ectopia (**Figure 19**).

I managed to stabilise the ectopia phenotype through breeding and discovered that the mutation was recessively inherited. Gradually purifying the line onto a C3H background resulted in the ectopia phenotype becoming more strongly pronounced with warping of the pyramidal cell layer (**Figure 20**). Successive breeding led to the loss of the hydrocephalus and corpus callosum phenotypes suggesting they were caused by unlinked mutations. Tail clasping and hepatomegaly mutation phenotypes were also purged from the line.

Figure 19: *Marble* line phenotypes prior to rederivation

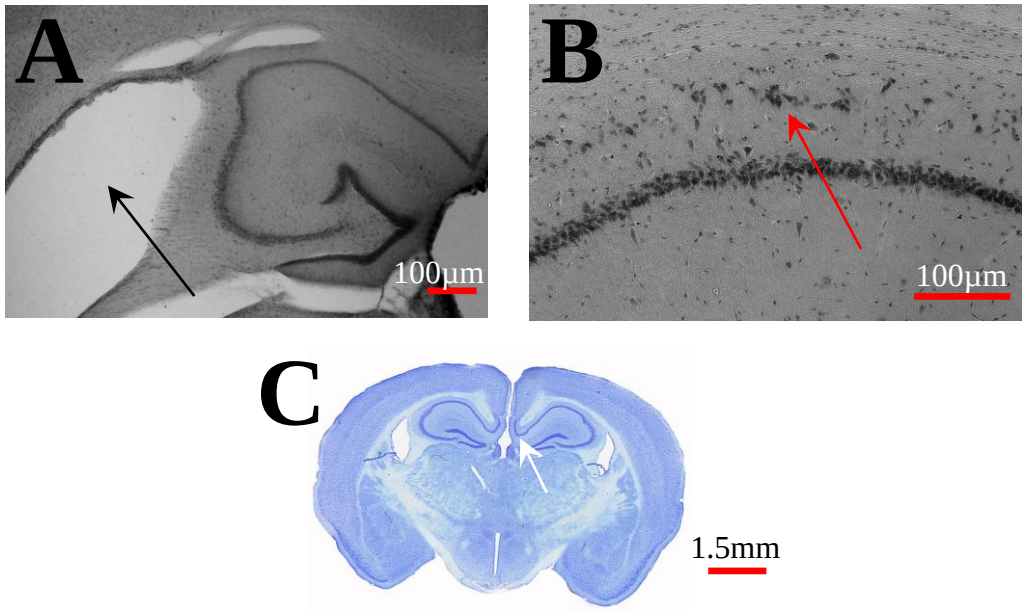


Figure 19. *Marble mouse displaying: hydrocephalus (black arrow shows enlarged lateral ventricle) (A), CA1 pyramidal cell layer ectopia (red arrow) (B), Corpus callosum agenesis (white arrow) (C). Images A and B were originally produced by Dr David Keays. Scale bars equals 250µm (A, B) and 1.5mm (C)*

Figure 20: *Marble* ectopia phenotype after rederivation

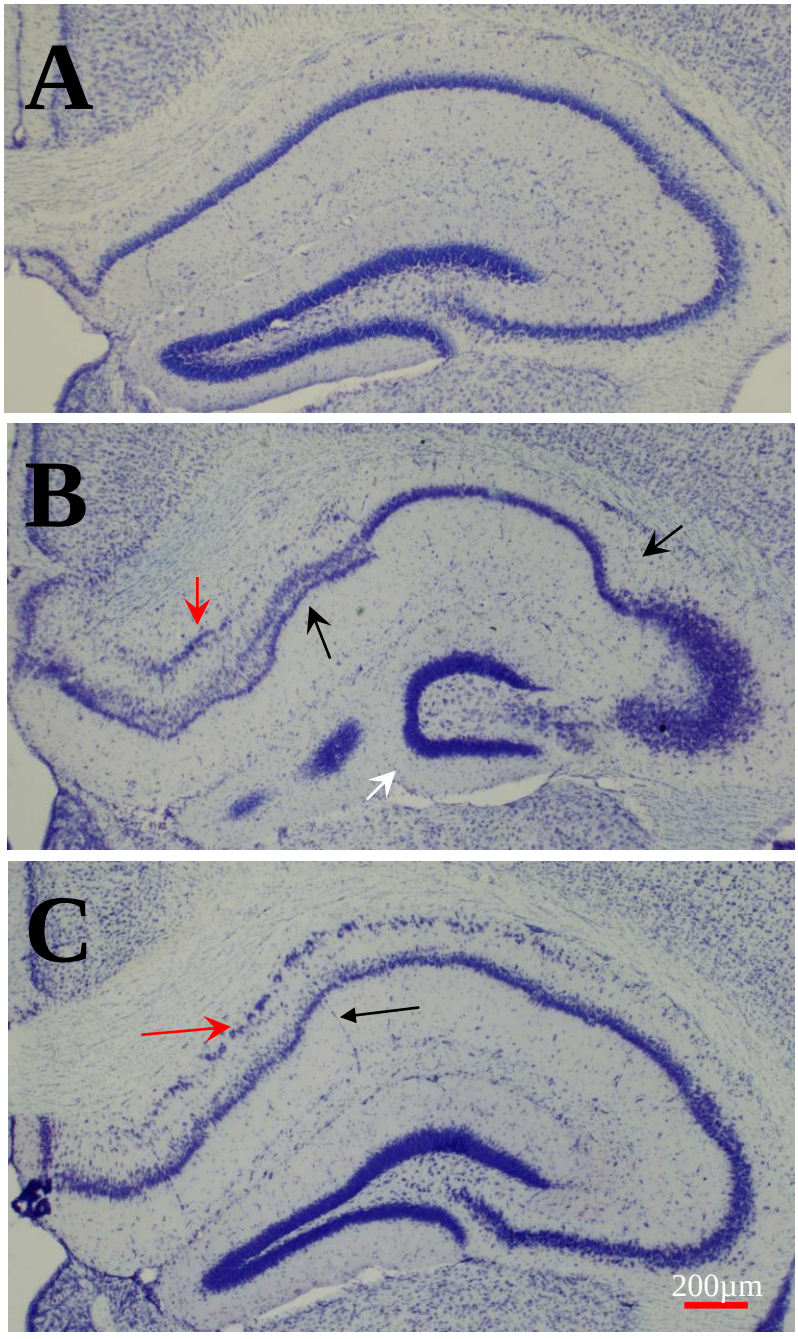


Figure 20. *Control mouse (A). Atypical Marble mutant with extreme cortical warping, ectopia and dentate gyrus disruption (B). Typical Marble phenotype with CA1 ectopia and warping of pyramidal cell layer curvature (C). Layer warping (black arrows) Ectopia (red arrows) Disrupted dentate gyrus (white arrow). Scale bar equals 200µm.*

Mapping and analysis

The quantitative screen generated three lines for mapping, PEDV41, PEDV50 and PEDV76. Mapping in PEDV41 was abandoned as the phenotype was not replicated in subsequent generations. Additionally, the qualitative screen generated the *Marble* line for mapping.

PEDV50: The *Hydin* mouse

Using strain specific polymorphisms, the PEDV50 hydrocephalus inducing mutation was mapped to 112824822-113202462bp on chromosome 8 (**Figure 21**). This interval contained only two genes: *Vac14* and *Hydin*.

Figure 21: PEDV50 mutation interval

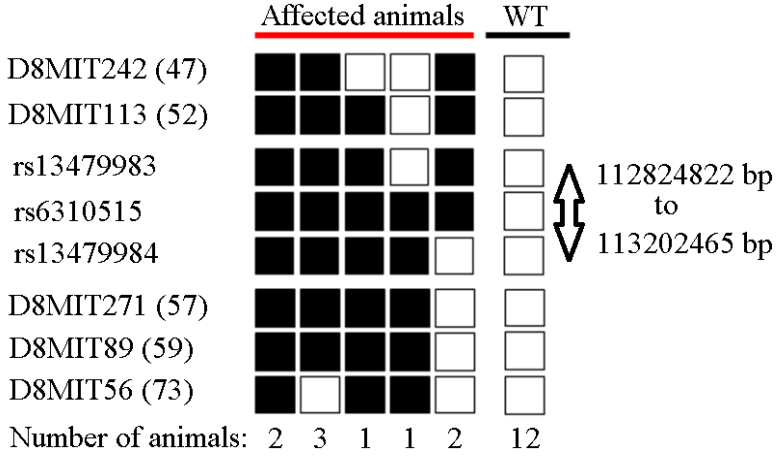


Figure 21. *For a given polymorphic marker, a black box denotes that a mouse is homozygous for the mutation bearing C57BL/6 strain. A white box denotes that an animal is heterozygous or homozygous for the reference C3H strain.*

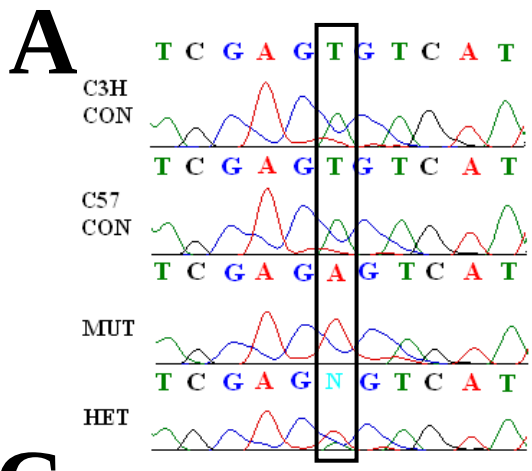
All exons within the affected PEDV50 interval were sequenced. This led to the discovery of a T>A transversion in the 47th nucleotide of exon 85 in the *Hydin* gene resulting in a V4858E mutation in the protein sequence (**Figure 22, A, B**). The affected residue and several surrounding residues are highly conserved suggesting they are crucial to protein function (**Figure 22, C**).

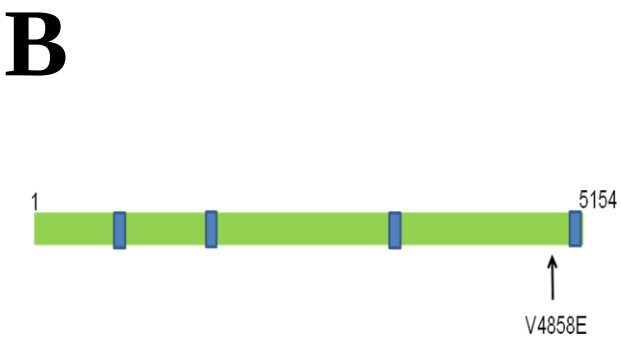
The *Hydin* gene had previously been linked to hydrocephalus in the hy3 line (Davy and Robinson, 2003, Robinson *et al.*, 2002). *Hy3* mutants feature a single base-pair deletion in exon 15 which creates a premature stop codon and leads to loss of 89% of the full-length gene product. I used the hy3 line to perform a complementation test to verify pathogenicity of the PEDV50 mutation. Mating between PEDV50 and hy3 heterozygous animals generated compound mutants which developed hydrocephalus (**Figure 23**).

Hydrocephalus in the hy3 mutant has been attributed to the protein's role in cilia central pair microtubules. Homozygous hy3 cilia beat at a lower frequency in an uncoordinated and irregular fashion (Lechtreck *et al.*, 2008). This leads to disrupted CSF flow and the development of rapidly progressing hydrocephalus after birth. Mutants typically die at 4-6 weeks of age and seldom survive beyond 7 weeks (Gruneberg, 1943, Davy and Robinson, 2003). In contrast, affected PEDV50 animals were over 12 weeks of age at screening.

The prolonged survival of PEDV50 mutants allowed examination of adult ciliated somatic tissue. In 1943, Hans Gruneberg speculated that homozygous hy3 animals maybe infertile as, rarely, mutants survived into adulthood yet failed to produce pups (Gruneberg, 1943). Consequently, I assessed fertility in PEDV50 homozygotes.

Figure 22: PEDV50 mutation is in hydin at V4858





C

Species	Protein Sequence
Hydin mutant	YKEGLYTAKVIFRNEVTNEFLYYTESFRVTPSGIIKTIQMTSPVRQSVS
Mus musculus	YKEGLYTAKVIFRNEVTNEFLYYTVSFRVTPSGIIKTIQMTSPVRQSVS
Rattus norvegicus	YKEGLYTAKVIFRNEVTNEFLYYTVSFRVTPSGIIKSIQMTSPVRQSVS
Homo sapiens	HKEGTYAAKVIFRNEVTNEFLYYNVSFRVIPSGIIKTIEMVTPVRQVAS
Pan troglodytes	HKEGTYTAKVIFRNEETNEFLYYNVSFRVIPSGINKTIEMVTPVRQVAS
Pongo pygmaeus	HKEGTYTAKVIFRNEVTNEFLYYNVSFRVIPSGIIKTIEMVTPVRQVVS
Equus caballus	HKEGLYTAKVIFRNEVTSEFLFFTVSFRVIPSGAIKTIEMVSPVRQSTS
Canis familiaris	HKEGLYSAKVIFRNEVTSEFLYYMVSFRVIPSGVIRTIEMVSPVRQSTS
Felis catus	XXXXXXXXXVIFRNEVTNEFLYYMVGFRVIPSGVIKTIEMVSPVRQSTS
Gallus gallus	YKEGVFSTMVTFLNEVTEEYLFYMVTFKATASGPIGTVEVSAAVRQNVS
Xenopus tropicalis	YKEGTFSVKVTFRNEATQEYLFYFVTFKATPPGIITTIEMVTPVRQSTV
Ciona intestinalis	HKEGNFGAKVIFRNERSGEYIFYYVTLRATSAGVMSTIELETPVRRSAV

Please turn page for remainder of figure

Figure 22. *Sequence analysis revealed a T47A transversion mutation at exon 85 of Hydin in affected PEDV50 animals (A). This translates into a V4858E mutation in the amino acid sequence. This mutation is not located in an ASH domain (Blue) (B). V4858 is highly conserved across species down to ciona intestinalis, the sea squirt: red text shows mutated V4858 hydin residue; blue column shows cross species conservation at the mutated hydin residue; grey shows surrounding conserved residues; Orange highlights variation across species (C).*

Figure 23: Hydrocephalus in PEDV50/hy3 compound mutants

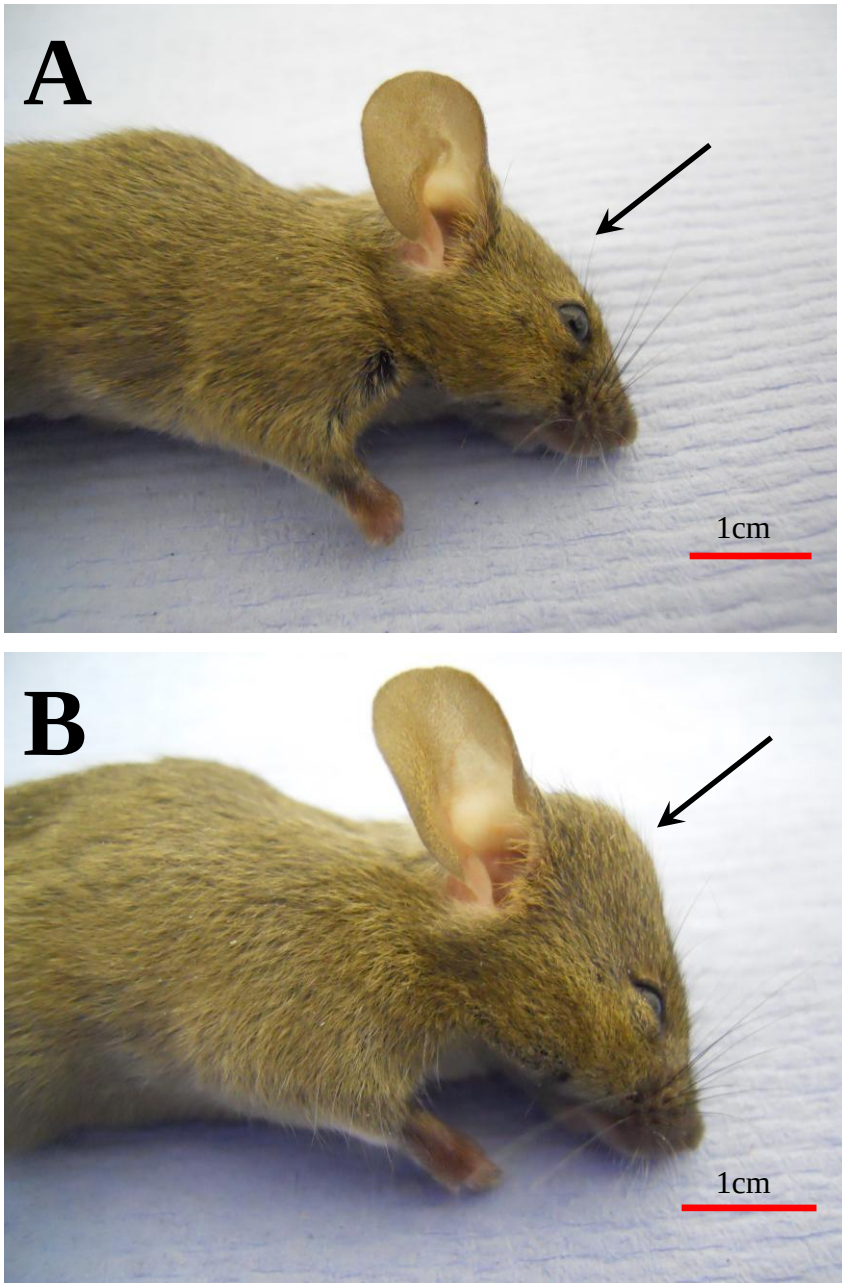


Figure 23. *WT mouse (A). PEDV50 x hy3 compound mutant with hydrocephalus (B). Scale bar equals 1cm*

Mating between WT and homozygous V4858E hydin mutants yielded no pups suggesting both male and female homozygous animals are infertile (**Figure 24, A**). Testicular weight was significantly lower in homozygous mutants than WT (P<0.01). The rate of testicle weight growth between 4-10 weeks of age is comparable between mutants and WT (**Figure 24, B**). SEM of 7wk old testis tissue revealed that homozygous mutant sperm are either tailless or exhibit extremely stunted tails (**Figure 25**). Live extracted mutant sperm also showed no motility under light microscopy (data not shown).

Figure 24: Infertility and reduced testicle weight in V4858E hydin mutants

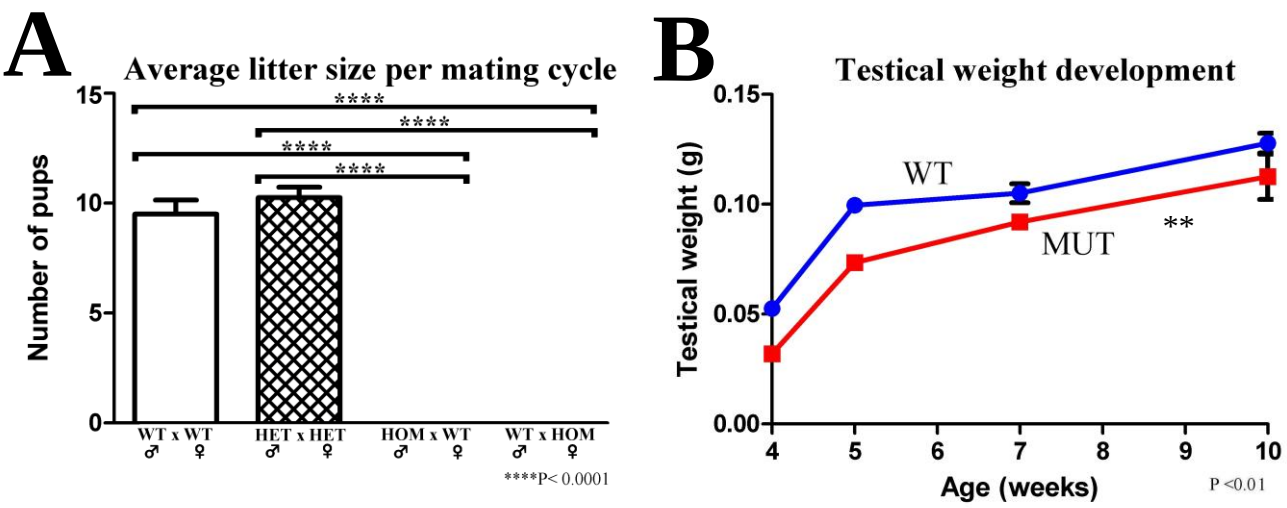


Figure 24. *Homozygous V4858E hydin mutants produced no litters (A). Testicle weight is significantly lower in mutant over 4 to 10 weeks of age (B). Error bars show SEM. Histogram summary: **P<0.01 ****P<0.0001*

Figure 25: V4858E hydin mutant sperm are tailless

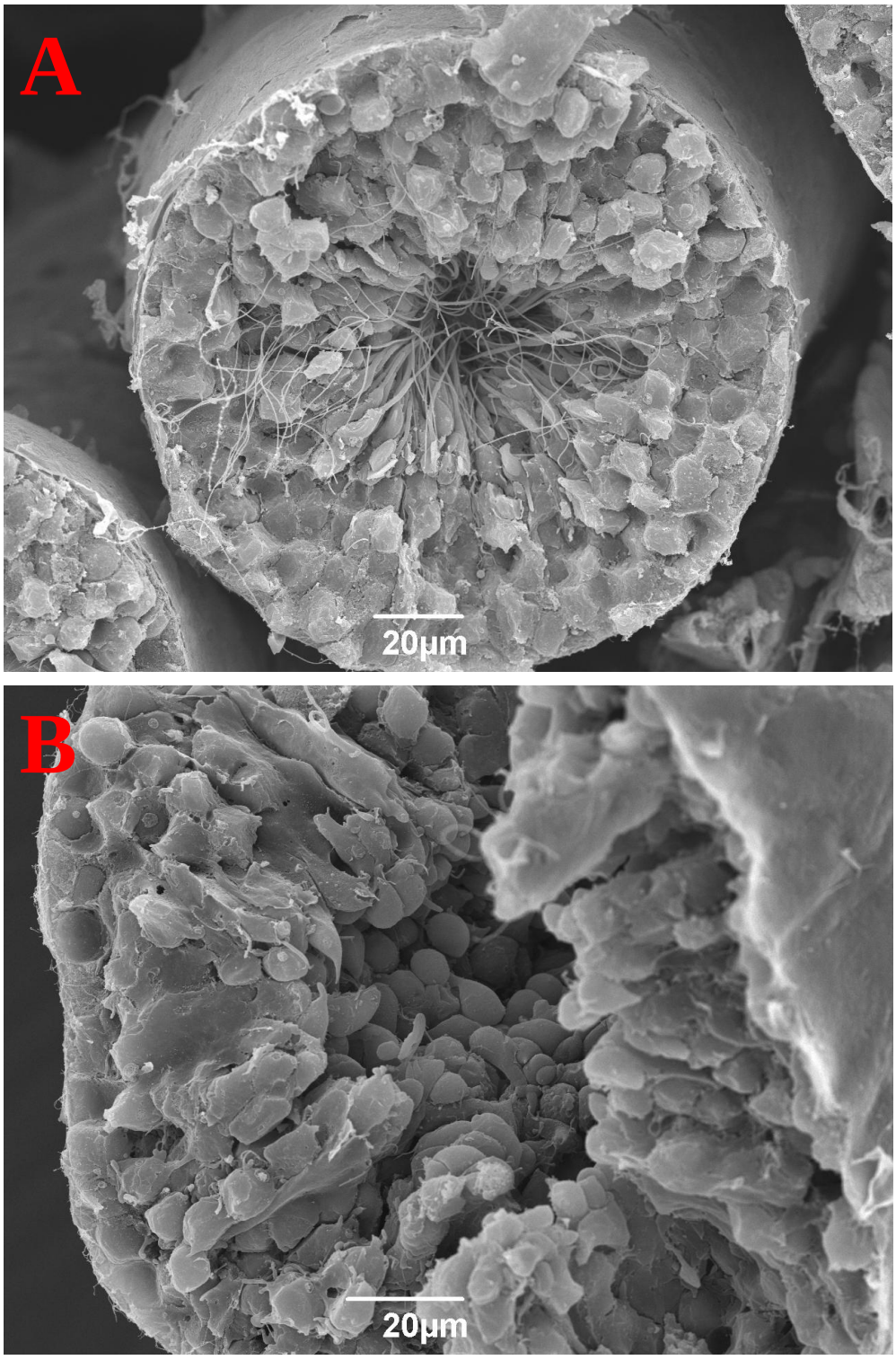


Figure 25. *SEM image showing WT seminiferous tubule containing fully formed sperm (A). V4858 homozygote seminiferous tubule contain only tailless sperm (B). Dr Mike Shaw prepared the transmission elector microscopy. Dr Helen Dawe helped to capture the images. Scale bars equal 20µm.*

Lastly, I examined trachea tissue. In 1943 Gruneberg observed that hy3 animals displayed a heavy discharge of mucus from the nose (Gruneberg, 1943). SEM on V4858E mutant trachea tissue showed an abundance of globular detritus on cilia (**Figure 26**). This suggests that cilia beat is inadequate to slough off an accumulation of mucus.

Figure 26: Build up of globular debris in V4858E hydin mutant trachea

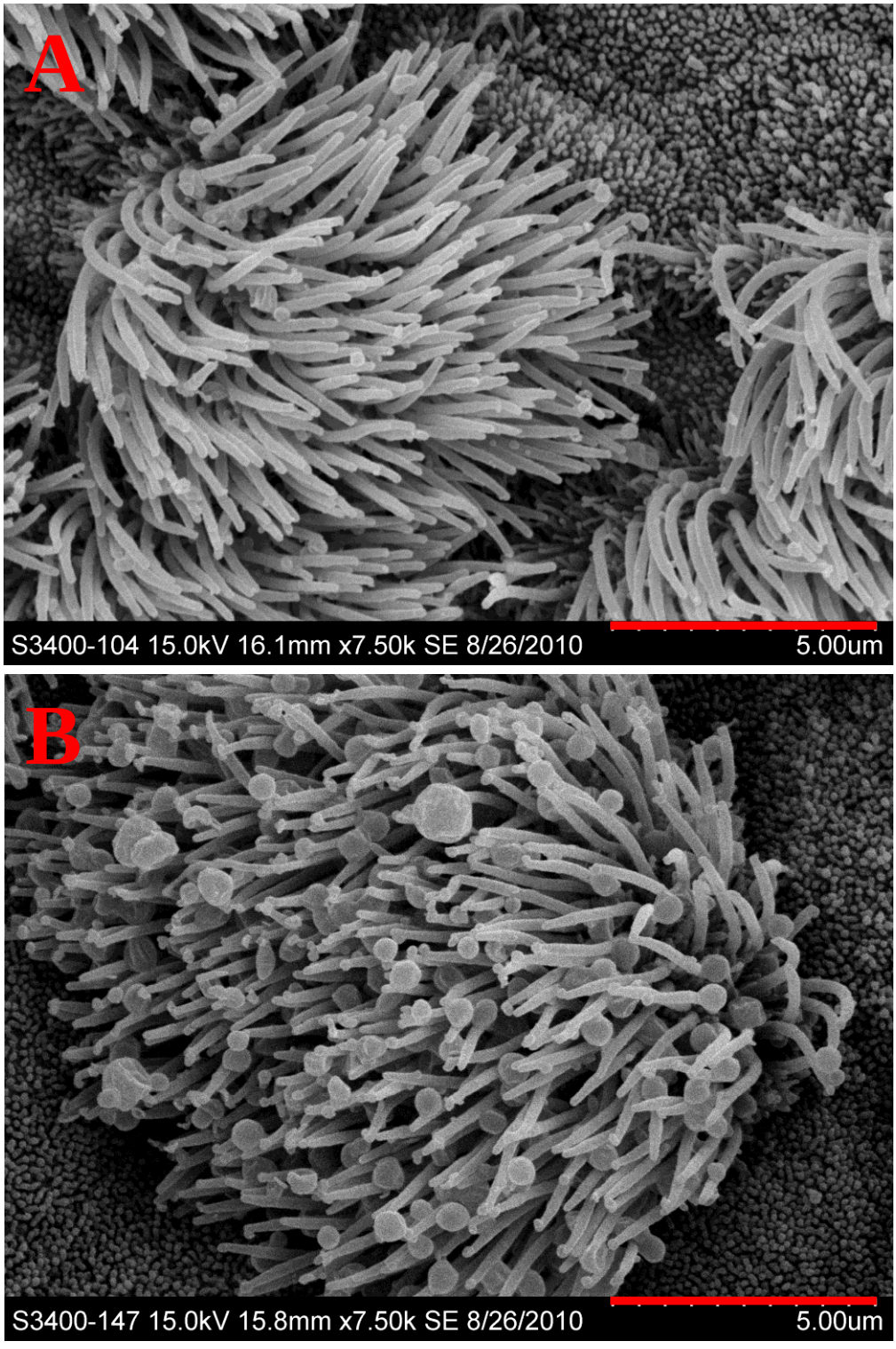


Figure 26. *WT ciliated cell in trachea (A). V4858E homozygote ciliated cell covered with globular debris (B). Dr Mike Shaw prepared the transmission elector microscopy. Dr Helen Dawe helped to capture the images. Scale bars equal 5µm.*

PEDV76: The *Pinky* mouse

Microsatellite markers were used to map the *Pinky* mutation to 100779519-111841382bp on chromosome 3 (**Figure 27**). This region contained 185 genes.

Figure 27: *Pinky* mutation interval

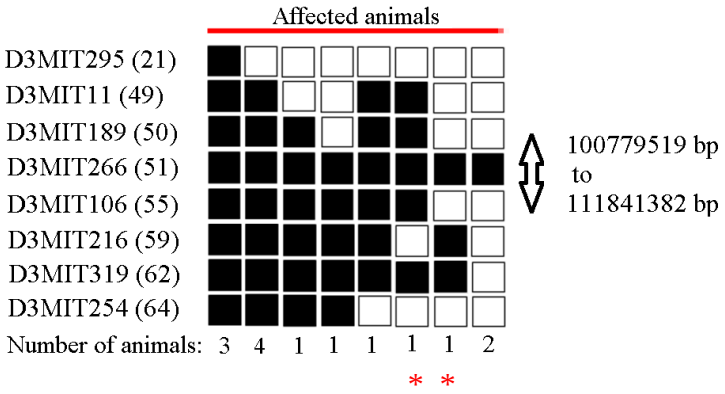


Figure 27. *For a given polymorphic marker, a black box denotes that a mouse is homozygous for the mutation bearing C57BL/6 strain. A white box denotes that an animal is heterozygous or homozygous for the reference C3H strain. Red asterisk shows animals featuring double recombination events between D3MIT266 and D3MIT319.*

As there were no reliable microsatellite markers contained within the 100779519-111841382bp candidate interval, the decision was taken to send a phenotypic sample for next generation sequencing rather than attempt to narrow the interval further. SNP calling on exome sequencing data failed to find a polymorphism with a read depth greater than 30 in the 100779519-111841382bp interval. As two affected animals featured in **Figure 27** had double recombination events between D3MIT266 and D3MIT319 (see red asterisks), it was possible that a recombination hotspot occurred prior to D3MIT319. Double recombination events occurring between MIT markers could mask the location of the causative mutation. Consequently, I broadened the candidate region to include up to D3MIT319 making the expanded interval cover 10779519-128042686bp. Calling SNPs in this expanded interval revealed 2 polymorphisms with a read depth greater than 30 that were not present in the progenitor strains (**Figure 28**). These SNPs result in the following mutations: Y205X in Fnbp1l and S394P in Ndst3.

It is unclear whether Fnbp1L Y205X and/or Ndst3 S394P underlie the corpus callosum agenesis phenotype in *Pinky*. As the mutations are only ~1Mb apart, segregating the SNPs may prove difficult due to linkage. Chromosome 3 has an average recombination rate of 0.44 cM/Mb (Jensen-Seaman *et al.,* 2004). Therefore, 114 animals would be required to give a 50% probability of successfully segregating the two SNPs. According to the Allen Brain Atlas, both genes are expressed in the cortex and hippocampal pyramidal cell layer. Fnbp1L (formin binding protein 1-like, also known as Toca1) interacts with N-WASP (Neuronal Wiskott–Aldrich Syndrome Protein) to induce remodelling of the actin cytoskeleton, membrane tubulation and the formation of motile vesicles (Bu *et al.*, 2010, Fricke *et al.*, 2009).

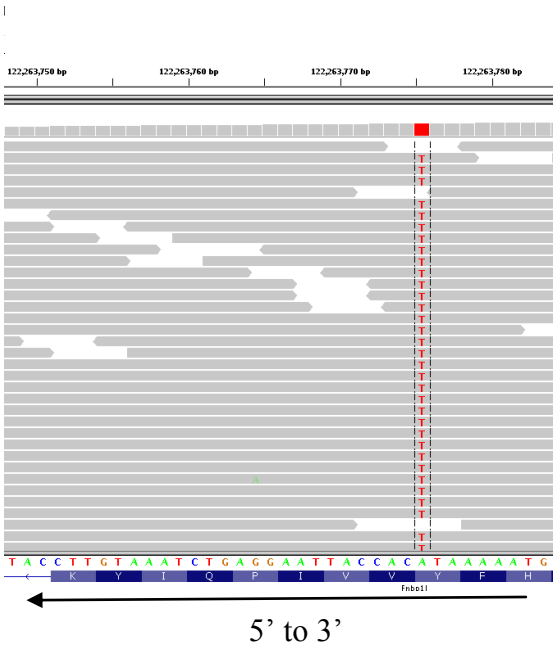
Ndst3 (N-deacetylase/N-sulfotransferase (heparan glucosaminyl) 3) is a Golgi membrane protein which modifies N-acetylglucosamine residues in heparan sulphate. Adult Ndst3 -/- brains are reported to be anatomically normal by Pallerla *et al.*, however, the group present no figures to support this negative result (Pallerla *et al.*, 2008). Perturbed CNS development and elevated apoptosis are reported in *Ndst1/Ndst3* -/- compound mutant embryos (Pallerla *et al.*, 2008). Pallerla *et al.* also report that *Ndst3* -/- mice are significantly less anxious on the elevated plus maze.

Figure 28: High quality SNPs in *Pinky* mutation interval

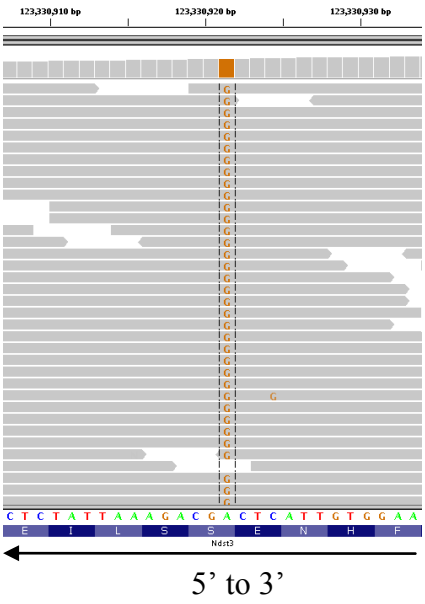
A

SNP location	Read depth	Quality*	Sense strand base change	Comments
Chr3: 122263775	247	282	T to A	Creates TAA stop codon in exon 7 of Fnbp1l (gene has 16 exons in total). Mutation is Y205X.
Chr3: 123330921	303	282	T to C	Would create a mutation in exon 3 of Ndst3 leading to a serine to proline change at S394. This residue is highly conserved.

B



C



Please turn page for remainder of figure

D

Species	Protein Sequence
Pinky mutant	GSVDEFWWFPHMWSHMQPHLFHNE**P**SLIEQMILNKKFALEHGIPTDMGY
Mus musculus	GSVDEFWWFPHMWSHMQPHLFHNE**S**SLIEQMILNKKFALEHGIPTDMGY
Rattus norvegicus	GSVDEFWWFPHMWSHMQPHLFHNE**S**SLIEQMILNKKFALEHGIPTDMGY
Homo sapiens	GSVDEFWWFPHMWSHMQPHLFHNE**S**SLVEQMILNKKFALEHGIPTDMGY
Pan troglodytes	GSVDEFWWFPHMWSHMQPHLFHNE**S**SLVEQMILNKKFALEHGIPTDMGY
Pongo pygmaeus	GSVDEFWWFPHMWSHMQPHLFHNE**S**SLVEQMILNKKFALEHGIPTDMGY
Equus caballus	GSVDEFWWFPHMWSHMQPHLFHNE**S**SLVEQMILNKKFALEHGIPTDMGY
Canis familiaris	GSVDEFWWFPHMWSHMQPHLFHNE**S**SLVEQMILNKKFALEHGIPTDMGY
Felis catus	GSVDEFWWFPHMWSHMQPHLFHNE**S**SLVEQMILNKKFALEHGIPTDMGY
Gallus gallus	RSVDEFWWFPHMWSHMQPHLFHNE**S**SLVEQMILNKKFALEHGIPTDMGY
Xenopus tropicalis	GSVDEFWWFPHMWSHMQPHLFHNE**S**SLVEQMMLNKKFALEHGIPTDMGY
Danio rerio	KYVDEFWWFPHMWSHMQPHLFHNE**S**SLMEQMILNKDFALEHGIPVDLGY

Figure 28. *Table homozygous SNPs in expanded Pinky interval with more than 30 reads (A). Interactive genome viewer screenshots of SNPs (B and C). Ndst3 S394 is highly conserved across species down to Danio rerio, the Zebra fish: red text shows mutated Ndst3 S394 residue; blue column shows cross species conservation at the mutated residue; grey shows surrounding conserved residues; Orange highlights variation across species (D). * Quality denotes -log10 of the probability that call is wrong. Dr Wei Yuan helped to call the SNPs. The Sanger institute was responsible for the production of the BAM file.*

PEDM23: The *Marble* mouse

Microsatellite markers were used to map the *Marble* mouse ectopia mutation to between 86133527-114675923bp on chromosome 9 (**Figure 29**). This region contained 439 genes.

Figure 29: *Marble* mutation interval

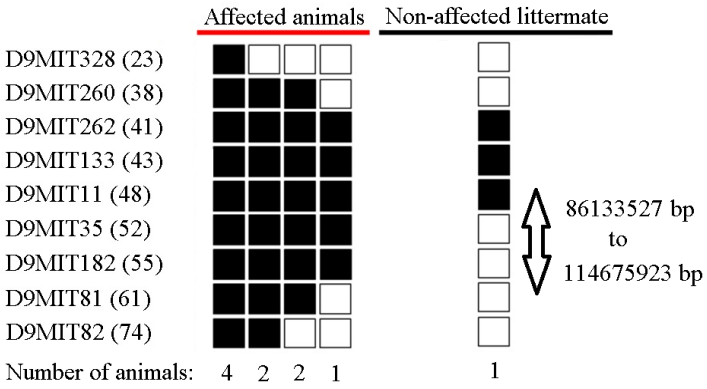


Figure 29. *For a se is homozygous for the mutation bearing C57BL/6 strain. A white box denotes that an animal is heterozygous or homozygous for the reference C3H strain.*

The exome of an affected animal was subsequently sequenced using next generation sequencing. Automated SNP calling was then performed against a progenitor strain reference. Heterozygous SNPs and inbred strain specific SNPs were discounted. Only one SNP with a read depth greater than 30 was located in the mapped interval (**Figure 30**).

Figure 30: High quality SNP in *Marble* mutation interval

A

SNP location	Read depth	Quality*	Sense strand base change	Comments
chr9:105552642	41	198	T to A	Intron-exon border

B

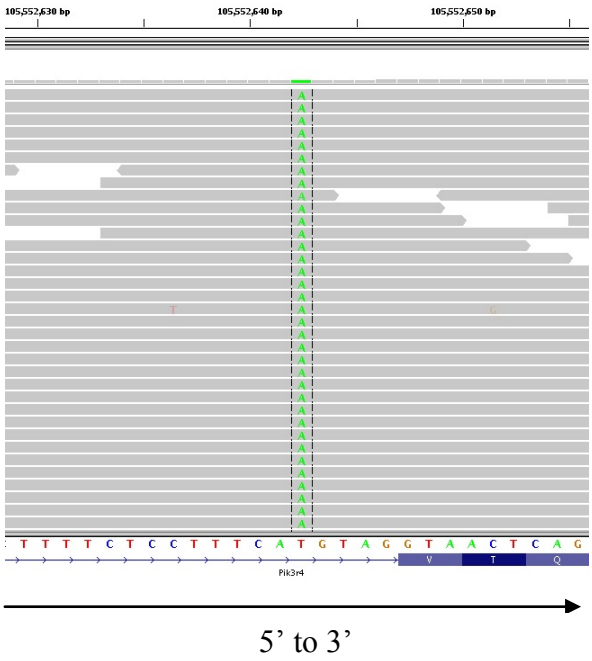


Figure 30. *Table of homozygous SNPs in mapped interval with more than 30 reads (A). Interactive genome viewer screenshots of SNP in Pik3r4 (B).* Quality denotes -log10 of the probability that call is wrong. Dr Wei Yuan helped to call the SNP. The Sanger institute was responsible for the production of the BAM file.*

The chr9:105552642 SNP occurs at the intron 3-4 boundary of exon 4 of *Pik3r4* (phosphatidylinositol 3 kinase, regulatory subunit, polypeptide 4). The mutation is likely to be pathogenic for the following reasons. First, the anatomical disruption in the *Marble* line suggests that the causal gene is expressed in CA1 pyramidal cells during development. The expression pattern of *Pik3r4* at P4 is consistent with this (**Figure 32**). Second, the mutation creates a new splice acceptor site three bases upstream of the WT splice acceptor site. This results in the generation of an immediately following in-frame TAG stop codon (**Figure 31**). As *Pik3r4* has 20 exons, the premature stop codon is far from the 3' poly-A tail. As no alternative splice variants of *Pik3r4* have been described, nonsense mediated degradation is likely to nullify the expression of all Pik3r4 protein in the mutant. In order to verify this, reverse transcriptase PCR (RT-PCR) assays should be conducted so that mutant *Pik3r4* mRNA can be converted into cDNA and subsequently sequenced (see "Future work plans for *Pinky*, *Hydin* and *Marble*" section for details).

Literature evidence also supports a role of *Pik3r4* in CNS development. Pik3r4 regulates Pik3 (phosphoinositide 3-kinase) activity. *In vitro* cultures of neurons from FMRP (Fragile X Mental Retardation Protein) -/- mice feature excessive Pik3 activity. Treating these cultures with Pik3 inhibitors counters the development of Fragile X associated traits such as deregulated synaptic protein synthesis and increased spine density (Gross *et al.*, 2010).

Figure 31: *Marble Pik3r4* mutation creates premature stop codon

Species	25th → 1st nucleotide upstream of exon 4
Marble mutant	TGGACCCTTTTCTCCTTTCAAGTAG
C57BL/6 (Mouse)	TGGACCCTTTTCTCCTTTCATGTAG
Rattus norvegicus	TGTACCCTTTTCTCCTTTCACGCAG
Cavia porcellus	TAACCCTCATTTTCTTTCTTACAG
Monodelphis domestica	TTTGATTCATTCATGCTTGGTGCAG
Pteropus vampyrus	ATTACAGTTTTTCTTCCTTTTATAG
Homo sapiens	AATTCCTTTTCTTCCCTTGGTATAG
Pan troglodytes	AATTCCTTTTCTTCCCTTGGTATAG
Gorila gorila	AATTCCTTTTCTTCCCTTGGTATAG
Bos taurus	TACTCCCATTCTCCCCTTGGTGTAG
Danio rerio	TTTAATTTTACTCCACTTTTTGTAG
Takifugu rubripes	ACCCTTGGTTTCATTCCTCTTCCAG

Figure 31. *Blue highlights bases which are conserved as pyrimidines (C or T). This is the polypyrimidine track which lies upstream of AG splice acceptor sites (grey). Pik3r4 mutation (red) creates new splice acceptor site (solid box). New splice acceptor site is followed immediately by a newly generated TAG stop codon (dotted box).*

Figure 32: *Pik3r4* is expressed in CA1 of hippocampus

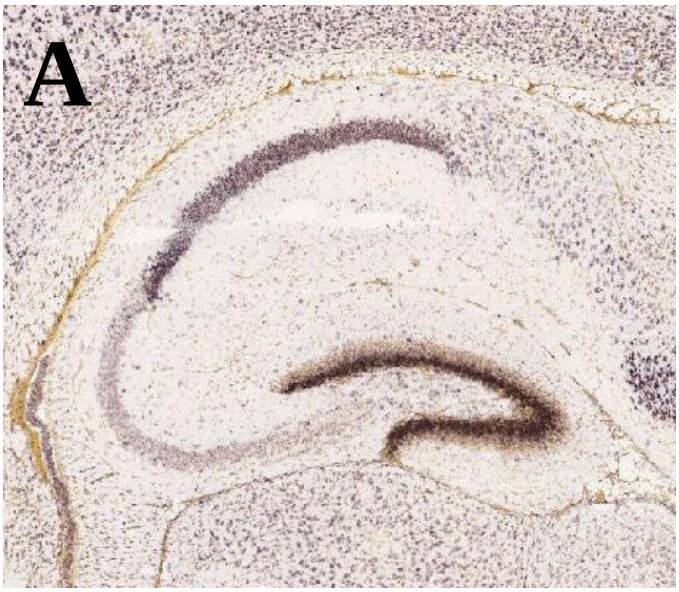


Figure 32. *Allen developing mouse brain atlas images for P14 animals. Pik3r4 is expressed in CA1 of hippocampus and dentate gyrus (A).*

Future work plans for Pinky, Hydin and Marble

For the Pinky line, it is important to establish whether the *Fnbp1L* mutation or the *Ndst3* mutation is causal to the corpus callosum agenesis phenotype. The Chr3:122263775 SNP in exon 7 of *Fnbp1L* is predicted to result in a premature stop codon. At time of writing, EUCOMM have developed a *Fnbp1L* -/- line. It would be prudent to screen these KO animals to see if they also feature corpus callosum agenesis. If that is the case, it would strongly suggest the Chr3:122263775 SNP in Pinky is responsible for the phenotype.

The Chr3:123330921 SNP in *Ndst3* is predicted to result in a S394P mutation in the protein. S394 and surrounding residues are highly conserved. The exchanging of serine residue for a proline may disrupt protein structure and function. Proline residues are associated with ridged structural kinks (Ceruso and Weinstein, 2002). *Ndst3-/-* mice are also available (Pallerla *et al.*, 2008).These mice should be screened to verify if corpus callosum agenesis is present. If it is not, it implies one of two possibilities regarding the Chr3:123330921 SNP. One, it is not responsible for the *Pinky* mouse phenotype. Two, if it is responsible for the *Pinky* mouse phenotype it must act as a gain-of-function mutation. Conversely, if *Ndst3-/-* mice are found to feature corpus callosum agenesis it implies that the Chr3:123330921 SNP in *Ndst3* is causal to the *Pinky* phenotype.

Attempting to genetically rescue the *Pinky* mouse phenotype would also help ascertain whether the *Fnbp1L* mutation or the *Ndst3* mutation was causal. This would involve testing whether adding WT copies of the respective genes to the *Pinky* mouse genome would be sufficient to reverse (or alleviate) the phenotype. To do this I would use a method based on the work of Vadolas and colleagues (Vadolas *et al.*, 2005). This would involve sourcing a Bacterial Artificial Chromosome (BAC) containing *Fnbp1L* or *Ndst3* from the BACPAC Resources Center (http://www.chori.org/bacpac/). These would be used to attempt two separate rescue attempts. Using the method detailed by Vadolas *et al.* 2005, the genetic

inserts containing the respective genes would be purified and microinjected into the pronucleus of C3H embryos. These embryos would then be transferred into the oviducts of 0.5 day pseudo pregnant surrogate mice. The resultant pups would be ear clipped and the presence of a transgene assessed by quantitative PCR (in order to assess copy number). Upon maturation, transgenic animals would then be mated to C3H in order to confirm germ line transmission. The neuroanatomy of the resultant pups should be assessed to verify if any neuroanatomical defects are correlated with an increase *Fnbp1L* or *Ndst3* copy number. The germline transgenic animals should then be mated with *Pinky* mice that are positive for the mutant Chr3:122263775 and Chr3:123330921 SNPs. Pups that bear the transgene and are heterozygous for the SNPs would then be backcrossed to their *Pinky* parent. This would lead to the creation of mice that are homozygous for the Chr3:122263775 and Chr3:123330921 SNPs and also bear either the *Fnbp1L* or *Ndst3* transgene. These animals should then be neuroanatomically assessed to verify if the *Pinky* phenotype has been rescued. If the *Fnbp1L* transgene rescues the phenotype it demonstrates that the Chr3:122263775 SNP is causal to *Pinky* mouse pathology. Conversely, if the *Ndst3* transgene rescues the phenotype it implicates the Chr3:123330921 SNP.

Once the causal gene had been identified I would do the following. One, I would behaviourally test the animals using the same battery of tests used for the analysis of *Whirligig* animals (detailed in chapter 5). This is due to both lines featuring corpus callosum agenesis. Two, I would conduct a Gallyas stain to reveal the Pinky mouse myeloarchitecture. This would allow for assessing whether or not the corpus callosum agenesis was associated with defective axonal guidance elsewhere in the brain.

For the *Hydin* line, it is important to address how the mutation leads to cilia dysfunction. Lechtreck and colleagues have previously demonstrated that hydin in not required for the assembly of cilia in mice but is required for ciliary motility (Lechtreck *et al.*,

2008). Hydin is speculated to be the component of the ciliary central pair that regulates the activity of the axonemal Dynein arms allowing switching between effective and recovery strokes (Lechtreck *et al.*, 2008). WT hydin has been shown to interact with the central pair proteins CPC1 (central pair complex 1) and KLP1 (kinesin-like protein1) in *chlamydomonas reinhardtii* (Lechtreck and Witman, 2007).

In order to investigate the hydin mutation I would do the following experiments. One, I would assess if V4858E hydin localised to extruded ciliary central pair complexes. To do this I would conduct a double labelling immunofluorescence assay using anti-hydin and anti-acetylated tubulin immunoglobulins. This approach was used to show WT hydin colocalisation with extruded ciliary central pair complexes in Lechtreck and Witman, 2007. If V4858E hydin is does not localise to the central pair this would explain the impaired cilia function in the *Hydin* mouse.

Two, I would assess how the V4858E mutation in hydin affected the ultrastructure of the central pair. To do this I would use anti-hydin immunogold labelled transmission electron microscopy. This would allow me to determine if V4858E hydin was, like WT hydin, associated with the C2 microtubule of the central pair (Lechtreck and Witman, 2007). *Hydin* mutations resulting in a truncated protein are associated with an absence of C2b and C2c microtubule projections.

Three, I would assess if the V4858E mutation disrupted interactions between hydin and its binding partners. To do this I would perform a co-immunoprecipitation assay using the method detailed by Antrobus and Borner (Antrobus and Borner, 2011). Brain tissue from the ventricular lining would be isolated and solubilised in detergents. This solution would then be incubated in the presence of anti-hydin immunoglobulin, forming an anti-body protein complex. This anti-body protein complex would then be recovered using sepharose beads. Hydin, and the bound proteins which interact with it, would then be eluted from the

beads. Subsequently, the eluted proteins would be separated using SDS-PAGE (sodium dodecyl sulphate polyacrylamide gel electrophoresis) and identified (and semi-quantified) via western blotting. Hydin binding partners are likely to include proteins present in the cilia central pair. Consequently, immunoglobulins targeting these proteins should be used in the western blot analysis.

For the Marble line, RT-PCR should be used to verify the absence of any alternative splicing in *Pik3r4* and to ascertain if chr9:105552642 SNP affects the mRNA transcript. Theoretically, the SNP would generate an in-frame stop codon at the start of exon 4. To test this, whole brain mRNA should be extracted from littermate animals that are homozygous, heterozygous and WT for the SNP. Reverse transcriptase and oligo (dT) primers (which hybridise to poly (A) tails) should then be used to generate full-length cDNA. Next, as shown in **Figure 33**, a pair of forward and reverse PCR primers can be designed to flank a region containing exon 4. If amplification leads to the generation of multiple products of differing size, it implies that exon 4 is skipped in some alternative spliced *Pik3r4* transcripts. Conversely, if only a single band is produced, it implies exon 4 is present in all transcripts. To confirm any finding, it is important to test multiple sets of primer pairs in separate reactions, all designed to amplify a region of varying size containing exon 4. This is due to the possibility that a hypothetical splice variant may skip exon 4 in addition to the binding sites for a specific pair of primers (this would result in no amplified product and the splice variant would not be detected).

All transcripts should then be purified and sequenced to determine whether, as hypothesised, a premature stop codon is present in the mutant mRNA transcripts at exon 4. If this codon is present, and there are no alternative splice variants, it implies that all isoforms of Pik3r4 protein will be compromised. If an antibody targeting the N-terminus region of Pikr4 were generated, a western blot could be performed to further test whether the SNP

results in truncated or absent Pik3r4 protein (Burnette, 1981). This approach of using RT-PCR and Western blots to evaluate the effect of genetic mutations on mRNA and protein has been used previously by other authors (Drogemuller *et al.*, 2011, Thongnoppakhun *et al.*, 2000, Kubo *et al.*, 2005, Magnusson *et al.*, 2000, Carothers *et al.*, 1989).

I would also assess if the anatomical CA1 defect in the Marble line was associated with behavioural abnormalities. Work by other authors has shown that morphological and biochemical abnormalities in CA1 correlate with alterations in depression-like behaviour (Bedrosian *et al.*, 2011, Zheng *et al.*, 2011, Garcia-Fuster *et al.*, 2011, Fonken *et al.*, 2011). For example, Bedrosian *et al.* induced depression-like behaviour in hamsters by housing them in light/dim light conditions, depriving them of a dark cycle. (Bedrosian *et al.*, 2011). They found that mice housed under these conditions had significantly increased CA1 dendritic spine densities. They also showed that CA1 spine density correlated with tests of depression-like behaviour: the greater spine density, the greater sucrose intake; the greater the spine density, the lesser the float time in a forced swim test. Additionally, Zheng *et al* have shown that neonatal exposure to the antidepressant drug fluoxetine significantly increased CA1 spine density in adult (P90) mice (Zheng *et al.*, 2011).

Figure 33: RT-PCR method

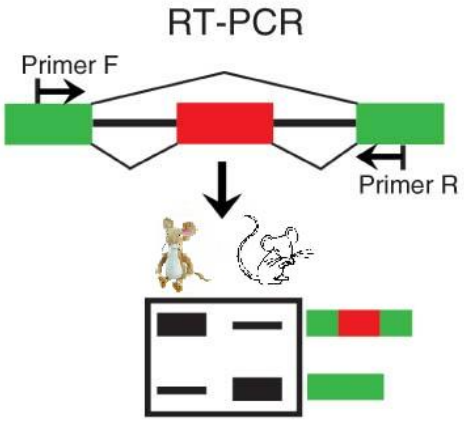


Figure 33. *Primers are used to amplify a region. Multiple bands of differing size will be produced if alternative transcripts exist as these vary in the exon content positioned between the two primers. Figure adapted from Lu et al. 2011(Lu et al., 2011).*

Summary

The quantitative ENU screen had a hit rate of 15.8% and yielded two mapped lines: *Pinky* and *Hydin*. For *Pinky*, the genetic mutations potentially responsible for the lines corpus callosum agenesis phenotype were not verified. These include Y205X in Fnbp1l and S394P in Ndst3. These SNPs are located ~1Mb apart making segregation challenging.

A V4858E mutation in hydin was verified to cause hydrocephalus via a complementation test. Unlike hy3, the previously discovered truncated hydin mutant, V4858E homozygous animals typically survive into adulthood. SEM analysis revealed ciliary defects in V4858E mutant somatic tissues: sperm are tailless and trachea cells are covered in an excess of mucus.

The qualitative screen for ectopias had a hit rate of 0.8% and lead to the discovery of the *Marble* mouse. Exome sequencing and mapping results suggest the causative mutation is a premature stop codon immediately upstream of exon 4 of *Pik3r4*.

Chapter 4

Sanger Transgenic Knock Out Screen Results

Neuroanatomical assessment and characterisation

Introduction

In this chapter I present the results of my KO screen. All hits are from quantitative analysis. Mr Jon Krohn helped design the R script which was used to perform these analyses. Although 1352 animals were qualitatively assessed for ectopias, no ectopias were found. A total of 247 distinct genes were quantitatively screened giving rise to 27 phenotypic hits across 6 week old and 16 week old cohorts. Detected anatomical phenotypes were wide ranging and included corpus callosum defects, alterations to cortical thickness, microcephaly, ventricle enlargement and aberrant hippocampal size and/or layering structure. Hits include genes which have already been implicated in human central nervous system disorders. These include *AP4E1*, *MCPH1* and *SLX4*. Other hits are related to genes which are involved in brain development or are reported in candidate microdeletion/duplication intervals where no monogenic cause of pathology has yet been established. These include *Ncaph2*, *Prkcz*, *Sptbn2*, *Ube2b* and *Wdr47*.

I conducted further tests on one line which neared significance; *Git2*. I contrast data from the *Git2* KO line with an *Mbd2* KO line to show an association between neurogenesis level and stratum radiatum thickness. I also show an increase in CA1 synaptic spine density in *Git2* -/- animals.

Determining level of significance

A total of 788 mice were neuroanatomically quantified for the twelve distinct measurements detailed in **chapter 2**. Due to the number of t-test comparisons made (3199 in total), it was important to determine a significance threshold that would balance the relative risks of false positives versus false negatives. A threshold corrected for the number tests (Bonferroni correction) would be:

p value required for significance = (target p value) / (number of comparisons)

However many of the measures I used are correlated, so that a strictly applied Bonferroni test would be over conservative.

Therefore, the following adjustment was used:

p value required for significance = (target p)/ (number of correlated measurements)

The twelve anatomical measurements collected fall into four distinct categories; corpus callosum, ventricle, cortex or hippocampal formation. Therefore, the adjustment involves the target p being divided by four. This equates to an adjusted threshold of $p < 0.0125$ (equivalent to $-\log p > 1.9$) for a target p of 0.05. This threshold reflects the point where values deviate from a linear distribution line on Q-Q plots for each cohort (**figure 34**).

Figure 34: Q-Q plots for KO cohorts

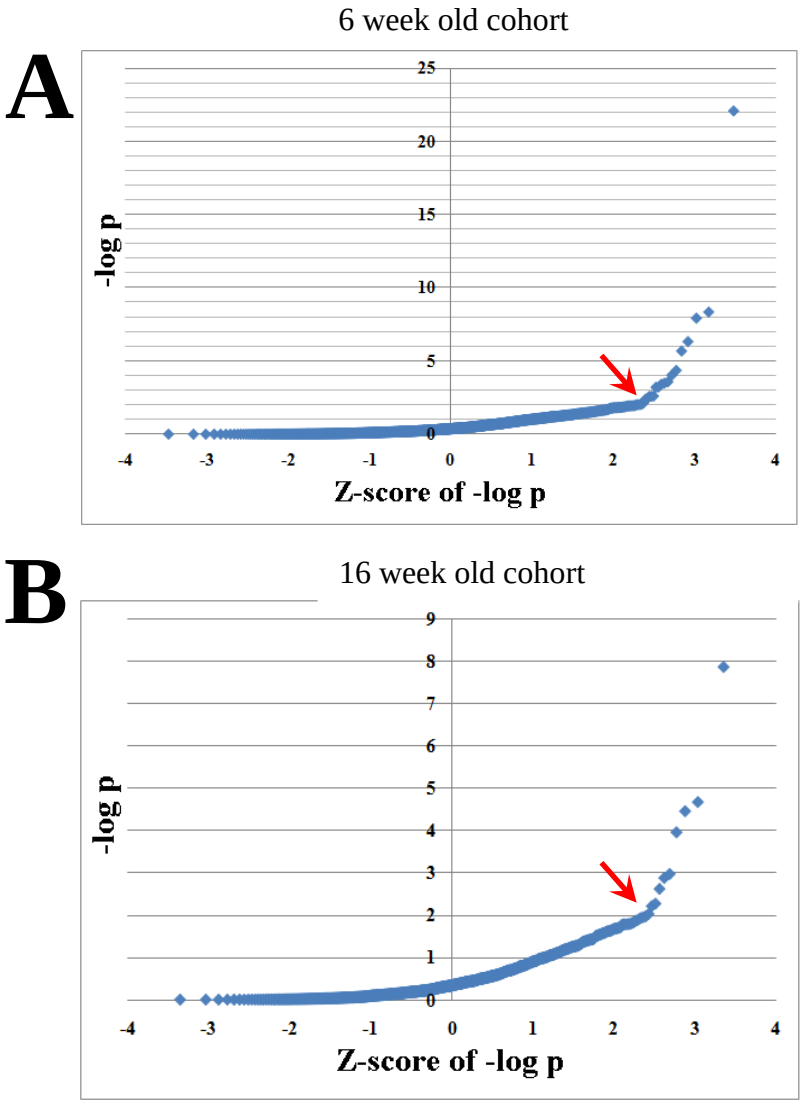


Figure 34. *Q-Q plot of p values from the 6 week cohort (A) and the 16 week cohort (B).*

Neuroanatomical screen: 6 week KO cohort

All 158 genes screened in the 6 week old KO cohort are listed in **Figure 35**. The figure uses a colour coding system to denote the background strain of each KO line. All mutant lines were contrasted against their respective background matched WT pools. The majority of KO alleles were on a BL/6 background (~89%). 70% of the entire WT mouse population analysed were BL/6.

The remaining ~11% of KO alleles were split across seven different background populations. Six of these populations were mixed background animals descended from 129 substrains. As 129 substrains are known to display neuroanatomical defects with varying penetrance, the reliability of using these populations for screening is compromised (Balogh *et al.*, 1999). The WT pools for these populations are also substantially smaller than the BL/6 WT pool (non-BL/6 WT pool sizes = 1 to 10 animals, BL/6 WT pool = 91 animals).

Due to this difference in background strain power and reliability, I have presented my hits from BL/6 lines separately from the non-BL/6 lines. I have also detailed whether or not each hit gene has links in the literature to CNS pathology or development.

Figure 35: All genes screened in 6 week old KO cohort

# to Cn	Co to Ld	Lk to Pn	Po to Sn	Sn to Z
1100001H23Rik	*Cog2*	*Lrf1*	*Polr1e*	*Snip1*
2010003O18Rik	*Crlf3*	*Lrrc16*	*Ppp5c*	*Snx5*
2310046K01Rik	*Ctnnal1*	*Magi2* ✗	*Prdx6*	*Socs7*
3110001A13Rik	*Cx3cl1*	*Man1c1*	*Prkcz* ✗	*Sparc*
4933425L06Rik	*D11Wsu99e*	*Mapk1*	*Prmt3*	*Sptbn1* ✗
5031439G07Rik	*Dctn5*	*Matn1*	*Prmt5*	*Spns2*
Acot6	*Ddx27*	*Matn3*	*Prmt8*	*Stard5*
Adam17	*Dhcr24*	*Mbtd1*	*Prpsap2*	*Stx8*
Agpat3	*Dotl1*	*Mcph1*	*Psmb2* ✗	*Supv3l1*
Akt2	*Dusp3* ✗	*Mdn1*	*Rarsl*	*Sympk*
Amfr	*Efna1*	*Mecr*	*Rhobtb3*	*Sytl1*
Ampd3 ✗	*Epc1* ✗	*Mgst3* ✗	*Rnaseh2b*	*Tbc1d10a*
Ankrd13a	*Epc2* ✗	*Mier1*	*Rpap2*	*Tcf712*
Anks4b	*Fabp5*	*Mks1*	*Rpn2*	*Tpd52l2*
Anxa6	*Farp2* ✗	*Mta1* ✗	*Rtf1*	*Tpi1*
ApoE	*Fto*	*Mta3*	*S100b*	*Trafd1*
Appl2	*Gap43*	*Mtrf1l*	*Sae2*	*Trim45*
Arpc4	*Gif*	*Myo7a*	*Sec24a*	*Trim66*
Asxl1	*Git2*	*Mysm1* ✗	*Setdb1*	*Trpc4ap*
Baz1b	*Gmnn*	*Ncaph2* ✗	*Sh2d1b2*	*Trrap*
Bbx	*Grin2a*	*Necab2*	*Sirt2*	*Ttll3*
Brd7 ✗	*Hdac3*	*Nf1*	*Slc22a21*	*Ubap1*
Brd8	*Herc3*	*Nfkb1*	*Slc25a21*	*Ube3b* ✗
Brpf3	*Hmx3*	*Nipa1*	*Slc35f1*	*Wdr3*
C79407	*Ikbkap*	*Nploc4*	*Slc41a3*	*Wdr47* ✗
C9orf54	*Impad1*	*Obl*	*Slc9a8*	*Yipf1*
Cadm1	*Inpp1*	*Ogfod1*	*Slx4*‡ ✗	*Zfp184*
Capzb	*Ints12*	*Otud6b*	*Smyd2* ✗	*Zfp367*
Cbx7	*Jarid2*	*Pfkl*	*Smyd3*	*Zranb2*
Cc2d1b	*Kctd10* ✗	*Phf20*	*Smyd5*	*Zzz3*
Cds2	*Ldha*	*Pld5*	*Snapc4*	
Cntfr	*Lkbkb*	*Pnpt1*	*Snf8*	
Background strain colour code (number of background matched WTs used in computations)				
129P2:129S5 (3)	**129P2:B6 (2)**	**129P2:CBA (10)**	**129S4:B6 (1)**	**129S5:B6 (7)**
129S5 (8)	**C3Heb/FeJ (8)**	**B6 (91)**		
Screen summary				
Total genes screened = 158		Total mice screened = 453		
Total genetic phenotypic hits = 19		Total WT mice = 130		

Figure 35. *Genes screened at 6 weeks of age. ✗= Phenotypic hit with adjusted – log p >1.3.*

BL/6 background lines

A total of 12 out of 141 genes on BL/6 background lines met the adjusted – log p value required for significance (**Figure 36**). This represents a hit rate of 8.5%.

Figure 36: Hit genes on BL/6 KO lines (6 week cohort)

KO Gene (number of mutant samples)	Phenotype	Adjusted -log p (unadjusted -log p)	F (df1,df2)	95% CI
Dusp3 (-/-) n = 3	Hippocampus area is increased Total brain section area is increased Length of pyramidal cell layer is increased Corpus callosum area is increased	3.54 (4.14) 2.19 (2.79) 1.68 (2.28) 1.53 (2.13)	17.3 (1, 92) 10.5 (1, 92) 8.2 (1, 92) 7.5 (1, 91)	+823679 to +2292884 µm^2 +3546610 to +14348006 µm^2 +376 to +2015 µm +46842 to +281630 µm^2
Epc2 (+/-) n = 1	Total lateral ventricle area is increased	1.32 (1.92)	6.6 (1, 90)	+753963 to +5594839 µm^2
Farp2 (-/-) n = 3	Average cortical thickness is increased	2.03 (2.63)	9.8 (1, 92)	+59 to +255 µm
Mgst3 (-/-) n = 3	Oriens layer thickness is decreased	1.34 (1.94)	6.7 (1, 91)	-4 to -26 µm
Mysm1 (-/-) n = 3	Average cortical thickness is decreased Total brain section area is decreased Length of the dentate gyrus is decreased	4.34 (4.94) 3.3 (3.9) 1.74 (2.34)	21.5 (1, 92) 16 (1, 92) 8.4 (1, 92)	-135 to -333 µm -5637481 to -16443268 µm^2 -274 to -1409 µm
Ncaph2 (+/-) n = 3	Corpus callosum area is increased	1.44 (2.04)	7.1 (1, 91)	+278452 to +42348 µm^2
Prkcz (-/-) n = 2	Corpus callosum span is decreased Stratum radiatum thickness is decreased	1.73 (2.33) 1.37 (1.97)	8.4 (1, 90) 6.8 (1, 90)	-83 to -427 µm -7 to -50 µm
Psmb2 (+/-) n = 3	Oriens layer thickness is decreased Total brain section area is decreased	1.51 (2.11) 1.47 (2.07)	7.4 (1, 91) 7.2 (1, 92)	-4 to -27 µm -2006370 to -12826526 µm^2
Slx4 (-/-) n = 3	Average cortical thickness is decreased Total brain section area is decreased Stratum radiatum thickness is decreased	3.82 (4.42) 2.96 (3.56) 1.39 (1.99)	18.7 (1, 92) 14.3 (1, 92) 6.9 (1, 91)	-119 to -316 µm -5017941 to -15794701 µm^2 -6 to -41 µm
Sptbn1 (+/-) n = 3	Hippocampus area is decreased Oriens layer thickness is decreased	1.42 (2.02) 1.37 (1.97)	7 (1, 92) 6.8 (1, 91)	-255538 to -1721385 µm^2 -4 to -27 µm
Smyd2 (-/-) n = 3	Average cortical thickness is decreased	1.35 (1.95)	6.7 (1, 92)	-31 to -228 µm
Wdr47 (-/-) n = 2	Corpus callosum span is decreased (agenesis) Corpus callosum area is decreased (agenesis)	23.69 (24.29) 7.07 (7.67)	206.4 (1, 90) 37.8 (1, 90)	-1087 to -1430 µm -305276 to -591100 µm^2

Figure 36: *Table of data. In order to calculate the number of WT mice used in a comparison use the following equation: (df2+1) – n (number of knockout samples)*

Non-BL/6 background lines

A total of 7 out of 17 genes on non-BL/6 background lines met the adjusted – log p value required for significance (**Figure 37**). This represents a hit rate of 41%, nearly quintuple the hit rate of the BL/6 lines. This suggests a strong likelihood of false positives in non-BL/6 lines due to mixed 129 background effects.

Figure 37: Hit genes on non-BL/6 KO lines (6 week cohort)

KO Gene (number of mutant samples)	Phenotype	Adjusted –log p (unadjusted –log p)	F (df1,df2)	95% CI
Ampd3 (-/-) n = 3	Dorsal 3rd ventricle area is increased Stratum radiatum thickness is decreased	2.83 (3.43) 1.43 (2.03)	28.5 (1, 10) 10.9 (1, 9)	+158960 to +343488 µm^2 -12 to -45 µm
Brd7 (+/-) n = 3	Total lateral ventricle area is increased	1.42 (2.02)	10.8 (1, 9)	+82995 to +328952 µm^2
Epc1 (+/-) n = 1	Length of the dentate gyrus is decreased	1.78 (2.38)	17.4 (1, 7)	-516 to -1431 µm
Kctd10 (+/-) n = 1	Length of the dentate gyrus is decreased	1.35 (1.95)	10.1 (1, 9)	-387 to -1637 µm
Magi2 (+/-) n = 3	Total lateral ventricle area is increased	1.4 (2)	21.2 (1, 4)	+84357 to +209172 µm^2
Mta1 (-/-) n = 3	Length of the dentate gyrus is decreased	2.97 (3.57)	33.3 (1, 9)	-582 to -1179 µm
Ube3b (-/-) n = 2	Length of the pyramidal cell layer is decreased Hippocampus area is decreased Stratum radiatum thickness is decreased Length of the dentate gyrus is decreased Total brain section area is decreased	2.81 (3.41) 1.46 (2.06) 1.34 (1.94) 1.32 (192) 1.1 (1.7)	27.3 (1, 10) 10.6 (1, 10) 10.6 (1, 8) 9.3 (1, 10) 7.7 (1, 10)	-943 to -2075 µm -408070 to -1648568 µm^2 -14 to -58 µm -265 to -1211 µm -2460695 to -14348207 µm^2

Figure 37: *Table of data. In order to calculate the number of WT mice used in a comparison use the following equation: (df2+1) – n (number of knockout samples)*

Hits with evidence in the literature supporting a role in CNS

Of the twelve hit genes on a BL/6 background, seven (58%) have literature evidence supporting a role in CNS development or function. Only two of the seven non-BL/6 hit lines have similar evidence (28%). BL/6 lines with supporting literature evidence include: *Epc2, Farp2, Ncaph2, Prkcz, Slx4, Sptbn1* and *Wdr47*. Non-CNS phenotypes associated with these KO lines are given in Appendix 2. Brain expression data is given in Appendix 3.

Epc2 (Enhancer of polycomb homolog 2) deletions have been reported in a majority of patients with 2q23.1 deletion syndrome. Patients feature mental retardation with severe speech impairments often presenting with microcephaly, behavioural defects and seizures. Whilst haploinsufficiency of *MBD5* is considered the principle cause of 2q23.1 deletion syndrome, *Epc2* deletions have been suggested to influence the variability and severity of the phenotype (Williams *et al.*, 2010b, van Bon *et al.*, 2010).

Farp2 (FERM, RhoGEF and pleckstrin domain protein 2), also known as FIR**,** has been shown to associate with the plexin-A1–neuropilin-1 complex which is involved in neuronal outgrowth. Knocking down *Farp2* nearly eliminates Sema3a-mediated repulsion of neuronal growth cones *in vitro* (Toyofuku *et al.*, 2005). Ectopic expression of *Farp2* induces shortened neuritis and an excess of growth cones (Kubo *et al.*, 2002). *FARP2* has also been reported to be significantly downregulated in a patient with autism and 2q37.3 deletion syndrome (Felder *et al.*, 2009).

Ncaph2 **(**non-SMC condensin II complex, subunit H2, also known as Kleisin-*β*) is deleted in a 7.9 Mb interval in a patient featuring mental retardation, autism, epilepsy, immature myelination and low T-cell counts (Chen *et al.*, 2010). However, it is currently unclear how, if at all, haploinsufficiency of *Ncaph2* contributes towards the neurological phenotype.

Prkcz **(**protein kinase C, zeta) is involved in mediating Wnt induced axon differentiation (Zhang *et al.*, 2007). Clinical and molecular characterisation of small interstitial deletions by Rosenfeld *et al.* suggested that *Prkcz* mutations underlie the neurological symptoms associated with monosomy 1p36 syndrome. Symptoms include the following, with the percentage of patients affected given in brackets: mental retardation (98%), neuroanatomical defects (88%) and microcephaly (63%) (Rosenfeld *et al.*, 2010).

SLX4 **(**SLX4 structure specific endo-nuclease subunit homolog, also known as *Btbd12***)** has been reported to cause Fanconi anaemia in humans. Patients feature similar phenotypes to the KO mice: microcephaly, shortened stature, bone abnormalities, small eyes, hypopigmentation and reduced platelet counts (Stoepker *et al.*, 2011). *Slx4* is expressed in the pyramidal cell layer and dentate gyrus in adult mice (Appendix 3). The dentate gyrus is a major site of neurogenesis throughout development and impairments to neurogenesis have been associated with microcephally (Schlessinger *et al.*, 1975, Chakrabarti *et al.*, 2007).

Sptbn1 (spectrin, beta, non-erythrocytic 1**,** also known as *Spnb2***)** encodes for a beta subunit of spectrin. Spectrins are scaffolding proteins that integrate into the cytoskeleton and consist of α and β subunit heterodimers. *Sptan1* and *Sptbn1* encode for α-II and β-II respectively. *SPTAN1* (spectrin alpha, non-erythrocytic 1) mutations have been implicated in West syndrome (Saitsu *et al.*, 2010). The condition is associated with mental retardation, cortical and cerebellar atrophy, corpus callosum malformation, hypomyelination, poor visual attention and epilepsy. West syndrome patients with heterozygous *de novo* mutations in *SPTAN1* feature reduced stability of α-II/β-II subunit heterodimers (Saitsu *et al.*, 2010). As *SPTAN1* mutations have been linked to CNS pathology, *SPTBN1* mutations that disrupt heterodimer formation may, perhaps, also underlie brain defects in humans. In mice, *Sptbn1* is widely expressed in the brain. Areas with the strongest expression include the pyramidal cell layer, dentate gyrus and cerebellum (Appendix 3). Given the expression of *Sptbn1* in the

cerebellum and the cerebellar atrophy described in patients with *SPTAN1* mutations, it may be of interest to histologically analyse the cerebellums of *Sptbn1* -/- mice for defects (See the "Future work plans for the KO screen" section).

Wdr47 (WD repeat domain 47) is a member of a family of proteins which feature tryptophan-aspartic acid (WD) repeats resulting in a propeller like domain structure. Genes of the WD family have been associated with mental retardation including: *LIS1* (Miller-Dieker syndrome) and *CSA* (Cockayne syndrome) (Li and Roberts, 2001). *WDR62* mutations have also been associated with microcephaly, cortical malformations and corpus callosum hypoplasia (Bilguvar *et al.*, 2010). Additionally, Wdr47 is reported to be a putative ligand for the N-terminal *Reeler* domain of Reelin (McGillewie, 2009).

Magi2 and *Ube3b*, both found on 129 mixed backgrounds have supporting literature evidence for a role in CNS development. Both genes are strongly expressed throughout the adult mouse brain (Appendix 3). *MAGI2* **(**membrane associated guanylate kinase, WW and PDZ domain containing 2), has previously been implicated in infantile spasm pathology, an early onset form of severe epilepsy which predominantly presents alongside Williams-Beuren syndrome (Marshall *et al.*, 2008). However, *MAGI2* is not be deleted all infantile spasm patients and it has been argued that nearby genes, *FZD9* and/or *STX1A*, are more likely to underlie the phenotype (Paciorkowski *et al.*, 2011).

Finally, *UBE3b* (ubiquitin protein ligase E3B) has been reported to be included in a 12q22-q24 deletion interval in a patient with autosomal dominant deafness, mental retardation and motor defects (Petek *et al.*, 2003). Disruption of the maternal allele of a related gene, *UBE3a*, is causal to Angelman syndrome. Angelman syndrome is associated with profound mental retardation, microcephaly, motor defects and increased sensitivity to heat (Williams *et al.*, 2010a). Defects in heat sensitivity and skull morphology have been

reported for *Ube3b* -/- mice in the Sanger mouse portal. My data for this gene is shown in **Figure 37**.

Figure 38: *Ube3b* -/- mouse brains feature microcephaly

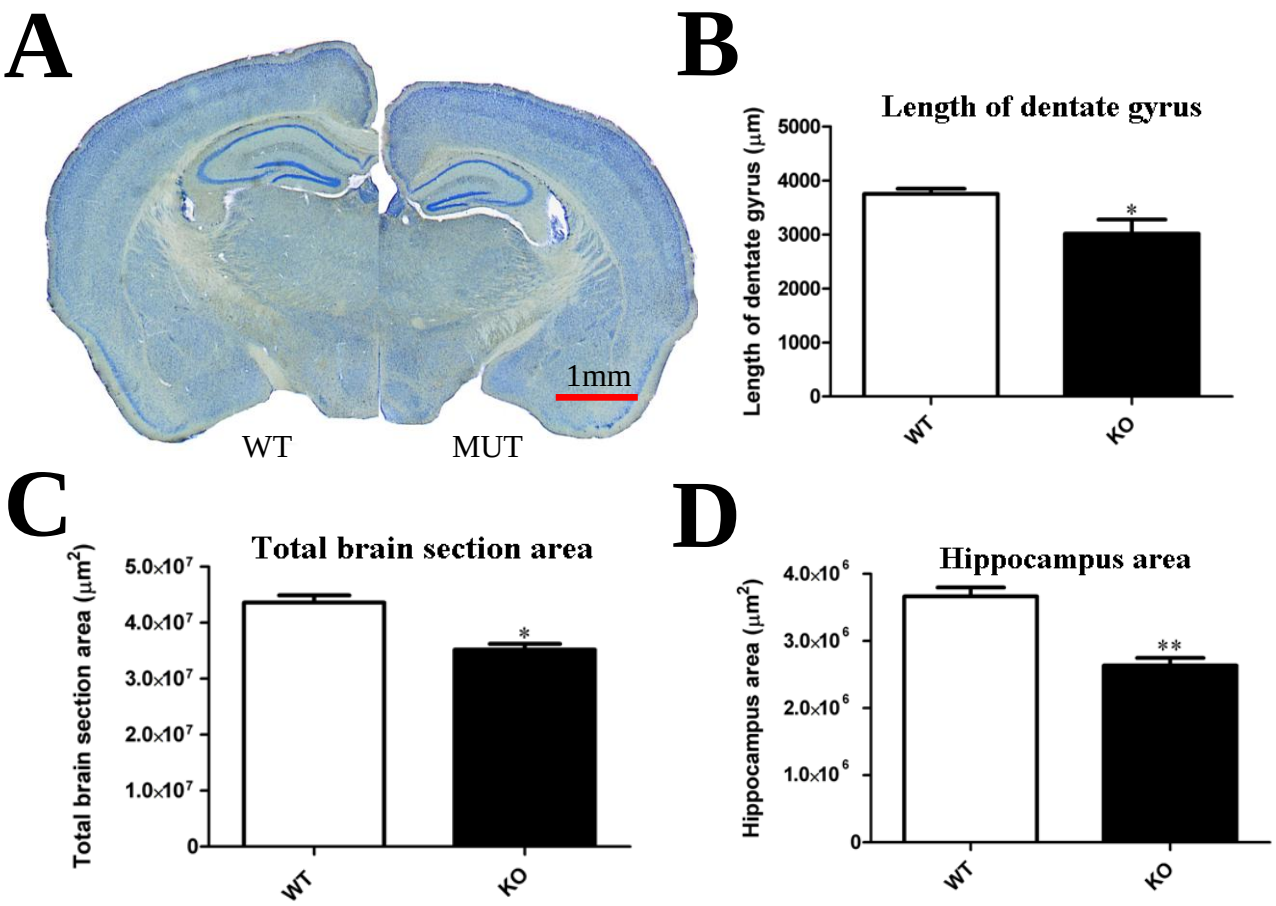


Figure 38. *Nissl stained sections of WT and Ube3b -/- mice showing microcephaly (A). Histograms of t-tests showing selected significant anatomical changes: reduction in length dentate gyrus, P<0.05, t = 3.06, df =10, n = 9 WT, 2 Hom (B); reduction in total brain section area, P<0.05, t = 2.77, df =10, n = 9 WT, 2 Hom (C); and reduction in hippocampus area, P<0.01, t = 3.24, df =10, n = 9 WT, 2 Hom (D). Scale bar equals 1mm. Error bars show SEM. Histogram summary: *P<0.05, **P<0.01*

Hits with no current literature links to CNS development

Several genes were not supported by literature evidence of a CNS role. These include six BL/6 lines (*Dusp3, Mysm1*, *Mgsm1*, *Mgst3, Psmb2* and *Symd2*) and five non-BL/6 lines (*Ampd3*, *Brd7*, *Epc1*, *Kctd10*, and *Mta1*). Non-CNS phenotypes associated with these KO lines are given in Appendix 2. Brain expression data is given in Appendix 3.

Several of these genes relate to cancer. *Brd7* (Bromodomain containing 7) is a tumour suppressor gene required for p53 pathway induced senescence (Drost *et al.*, 2010). *Dusp3* (Dual specificity phosphatase 3, also known as *VHR***)** has been shown to be down regulated in non-small cell lung tumours and its expression can limit cancer cell proliferation *in vitro* (Wang *et al.,* 2011). Down regulation of *Kctd10* **(**potassium channel tetramerisation domain containing 10) in cancer cells *in vitro* inhibits proliferation rate (Wang *et al.*, 2009). Over expression of *Epc1* (Enhancer of polycomb homolog 1), *Mta1* **(**Metastasis-associated protein 1) and *Smyd2* (SET and MYND domain containing 2) have been shown to increase tumour proliferation (Komatsu *et al.*, 2009, Li *et al.*, 2011, Nakahata *et al.*, 2009). It is unclear if neuroanatomical abnormalities in these lines are due to aberrant cell division rates or are false positives. The high yield of cancer genes may be reflective of a cancer gene targeting bias. *Ampd3*, *Epc1* and *Kctd10* are not strongly expressed in the brain (Appendix 3). Findings from these lines are therefore more likely to be false positives. In contrast, *Brd7* and *Mta1* are strongly expressed in the pyramidal cell layer and dentate gyrus. *Mta1* is also strongly expressed in the cortex and cerebellum.

The remaining genes which are not related to cancer include *Ampd3, Mgst2*, *Mysm1* and *Psmb2*. *Ampd3* (adenosine monophosphate deaminase 3) deficiency in humans is considered clinically asymptomatic (Yamada *et al.*, 2001)**.** Similarly, *Mgst3* (microsomal glutathione S-transferase 3) and *Psmb2* (proteasome subunit, beta type, 2) mutations are not known to be associated with disease and -/- mice are phenotypically somatically normal. In

contrast, *Mysm1* **(**Myb-like, SWIRM and MPN domains, also known as 2ADUB) coordinates histone acetylation and deubiquitination and -/- mice feature malformed tail and limbs, reduced weight, abnormal coat colour, reduced bone mineralisation and blood irregularities (Zhu *et al.*, 2007).

Borderline hit genes

Four genes (*Akt2*, *Cadm1*, *Git2* and *Hmx3*) from the non-BL/6 dataset neared the adjusted –log p required for significance (**Figure 39**). With only 1 to 2 mutant animals and fewer than 7 WT animals contributing to their respective data pools, these genes were potentially underpowered. All of these genes have supporting literature evidence of a role in CNS development or function. They are also all expressed in the adult mouse brain. See Appendices 2 and 3 for data on non-CNS phenotypes and the specific pattern of gene expression.

Figure 39: Borderline non-Bl/6 hit genes in 6 week old

KO Gene (number of mutant samples)	Phenotype	Adjusted –log p (unadjusted –log p)	F (df1,df2)	95% CI
Akt2 (-/-) n = 2	Length of the dentate gyrus is decreased	1.22 (1.82)	9.5 (1, 8)	-358 to -1612 µm
Cadm1 (+/-) n = 2	Stratum radiatum thickness is decreased	1.23 (1.83)	11.5 (1, 6)	-15 to -56 µm
Git2 (-/-) n = 1	Stratum radiatum thickness is increased	0.99 (1.59)	7.9 (1, 7)	+13 to +71 µm
Hmx3 (-/-) n = 2	Hippocampus area is decreased	0.95 (1.55)	508.7 (1, 2)	-150333 to -178948 μm^2

Figure 39: *Table of data. In order to calculate the number of WT mice used in a comparison use the following equation: (df2+1) – n (number of knockout samples)*

Akt2 (v-akt murine thymoma viral oncogene homolog 2) was found to be duplicated in a small supernumerary chromosome in a human patient with corpus callosum agenesis (Davidsson *et al.*, 2010). A related gene, *Akt3*, has been implicated in microcephaly and corpus callosum agenesis in humans (Boland *et al.*, 2007). It was not possible to assess if knocking out *Akt2* induced corpus callosum abnormalities as any phenotype would be masked by a 129 background effect. However, the near statistically significant reduction in the length of the dentate gyrus suggests that a genetic effect on neuroanatomical development may be present. Consistent with this, *Akt2* is expressed in the dentate gyrus of adult mice (Appendix 3).

CADM1 **(**cell adhesion molecule 1) mutations, H246N and Y251S, have been reported in autistic spectrum disorder patients (Fujita *et al.*, 2010). Transfection of H246N and Y251S mutant *CADM1* into cultured neurons harvested at E16 led to a shortened or absent dendritic branching relative to WT. It is unclear whether such changes in branching would occur *in vivo,* although behavioural abnormalities in *Cadm1* +/- have been reported. *Cadm1* +/- mice are aggressive, displaying both a reduced latency to initiate an attack and increased attack duration in an intruder test (Takayanagi *et al.*, 2010).*Cadm1* is expressed throughout the adult mouse brain. Expression is greatest in the pyramidal cell layer, dentate gyrus and cortex (Appendix 3).

Git2 (G protein-coupled receptor kinase interactor 2) -/- mice are reported to feature an elevated anxiety phenotype and visit the lightened chamber of a light/dark box significantly less (Schmalzigaug *et al.*, 2009). They also spend significantly less time per visit in the open areas of a zero maze, suggesting they are hesitant to remain in a exposed area for an extended period. Morphological abnormalities have been noted in KO animals for the related gene, *Git1*. *Git1* -/- mice feature a reduction in hippocampal dendritic spine density and length relative to WT (Menon *et al.*, 2010). *Git2* is highly expressed in the subventricular

zone of the lateral ventricles, olfactory bulbs, dentate gyrus and cerebellum in adult mice. These areas are associated with neurogenesis or the migration of newly formed cells (Ponti *et al.*, 2008, Schlessinger *et al.*, 1975, Bovetti *et al.*, 2011)

Lastly, *Hmx3* (H6 family homeobox 3) is deleted in overlapping hemizygous intervals covering 10q25.3 to 10qter in four patients with mental retardation, microcephaly, craniofacial abnormalities, hearing loss and vestibular dysfunction (Miller *et al.*, 2009). In addition to *Hmx3*, the overlapping region contains 20 genes including *Hmx2*. *Hmx2* and *Hmx3* are both expressed in the developing neural tube (Wang *et al.*, 2001). ENU derived *Dumbo -/-* mice bear a mutation in a related gene, *Hmx1*, and exhibit a 40% embryonic death rate due to exencephaly (Munroe *et al.*, 2009). In adult mice, *Hmx3* is expressed throughout the brain. Staining is most intense in the cerebellum, thalamus, brainstem and layers 3 & 4 of the cerebral cortex (Appendix 3).

Neuroanatomical screen: 16 week KO cohort

A list of all 99 genes screened in the 16 week KO cohort is given in **Figure 40**. Hits for BL/6 background lines are given in **Figure 41**. Eight out of ninety seven KO alleles displayed a significant phenotype. This represents a hit rate of 8.2%, similar to the 8.5% hit rate for BL/6 lines in the 6 week old cohort. Only two KO alleles were not on a BL/6 background. One of these, *Mta1*, was also analysed in the 6 week old cohort. In both cohorts *Mta1* -/- mice exhibited a significant reduction in the length of the dentate gyrus suggesting the finding is genuine (**Figure 42**).

Figure 40: All genes screened in 16 week old KO cohort

KO genes				
# to A	**B to Gm**	**Gm to N**	**O to Se**	**Sf to Z**
1700058C13Rik	*BC013712*	*Gm1040*	*Osbpl9*	*Sfrs4* ✗
1810073N04Rik	*Brpf3*	*Gsk3a*	*Pik3cb*	*Sgol1*
2310007B0Rik	*C9orf54*	*Gtf3c5*	*Plekhm2*	*Slc25a21*
3010026O09Rik	*Cbx1*	*Gys2*	*Prmt1*	*Slc25a29*
3110001I22Rik	*Cenpj*	*Hdac1*	*Prmt3*	*Slc5a2*
Abcd1	*Cish*	*Hira*	*Prmt7*	*Slc9a8*
Acpl2	*Cldn16*	*Kptn*	*Psat1*	*Smarcal1*
Adar	*Csrp2bp*	*Krt76*	*PSD93*	*Smyd4*
Agtr2	*Cyb561*	*Lmnb2*	*PSD95*	*Snap29*
Akap9	*Dip2b*	*Lrig1*	*Ptges2*	*Sqstm1*
Ap4e1 ✗	*Dnase1l2*	*Mcph1* ✗	*Pus7l*	*Src* ✗
Appl2	*Ehd1*	*Mta1* ✗	*Rbbp7*	*Stard13*
Aprin	*Eps15*	*Myh9*	*Rdh16*	*Supt7l*
Arhgap18	*F730047E07Rik*	*Myl12b*	*Rg9mtd2*	*Suv420h1*
Arid2	*Farp2*	*Myo5a*	*Rhd*	*Tcf7l1*
Arl4d ✗	*Fkbp7*	*Nap1*	*Rhot*	*Traf3ip3*
Asxl1	*Fundc1*	*Ncaph2*	*Rhou*	*Ttll3*
Atp5a1 ✗	*Gbe1*	*Ndufs3*	*Sco1*	*Twf1*
Atpaf2	*Gm134*	*Ninl*	*Sepn1*	*Wbp2*
Atpif1 ✗	*Gm468* ✗	*Nkiras2*	*Setmar*	
Background strain colour code (number of background matched WTs used in computations)				
129SvEv (2)	**129P2:B6JIco (3)**	**B6 (115)**		
Screen summary				
Total mice screened = 335		Total WT mice = 120		
Total genes screened = 99		Total genetic phenotypic hits = 9		

Figure 40. *Genes screened at 16 weeks of age.* ✗ = *Phenotypic hit with adjusted – log p >1.3.*

Figure 41: Hit genes on BL/6 lines (16 week cohort)

KO Gene (number of mutant samples)	Phenotype	Adjusted –log p (unadjusted -log p)	F (df1,df2)	95% CI
Gm468 (-/-) n = 1	Dorsal 3rd ventricle area is decreased	1.5 (2.1)	7.3 (1, 114)	-54514 to -341248 μm^2
Ap4e1 (-/-) n = 3	Total lateral ventricle area is increased Corpus callosum span is decreased	3.21 (3.81) 1.39 (1.99)	15.3 (1, 113) 6.8 (1, 106)	+232420 to +697804 μm^2 -51 to -357 µm
Arl4d (-/-) n = 3	Hippocampus area is decreased Total brain section area is decreased Dorsal 3rd ventricle area is decreased	3.74 (4.34) 3.22 (3.82) 2.59 (3.19)	18 (1, 115) 15.3 (1, 115) 12.3 (1, 116)	-728727 to -1983390 μm^2 -3399697 to -10211308 μm^2 -65355 to -230938 μm^2
Atp5a1 (+/-) n = 3	Molecular layer thickness is decreased	1.31 (1.91)	6.5 (1, 113)	-5 to -35 µm
Atpif1 (-/-) n = 3	Molecular layer thickness is decreased Length of dentate gyrus is decreased	7.51 (8.11) 5.48 (6.08)	39 (1, 113) 27.2 (1, 116)	-33 to -63 µm -954 to -2104 µm
Mcph1 (-/-) n = 4	Average cortical thickness is decreased	1.54 (2.14)	7.5 (1, 116)	-25 to -153 µm
Sfrs4 (+/-) n = 1	Dorsal 3rd ventricle area is increased	1.34 (1.94)	6.6 (1, 114)	+44381 to +331115 μm^2
Src (+/-) n = 2	Hippocampus area is decreased	1.34 (1.94)	6.6 (1, 114)	-239927 to -1780587 μm^2

Figure 41: *Table of data. In order to calculate the number of WT mice used in a comparison use the following equation: (df2+1) – n (number of knockout samples)*

Figure 42: Hit genes on non-BL/6 lines (16 week cohort)

KO Gene (number of mutant samples)	Phenotype	Adjusted –log p (unadjusted –log p)	F (df1,df2)	95% CI
Mta1 (-/-) n = 2	Length of dentate gyrus is decreased	1.19 (1.79)	59.5 (1,3)	-776 to -1305 µm

Figure 42: *Table of data. In order to calculate the number of WT mice used in a comparison use the following equation: (df2+1) – n (number of knockout samples)*

Hits with evidence in the literature supporting a role in CNS

Of the eight hit genes on a BL/6 background, six (75%) have literature evidence supporting a role in CNS development or function; *Ap4e1, Arl4d, Atp5a1, Atpif1, Mcph1* and *Src*. Non-CNS phenotypes associated with these KO lines are given in Appendix 4. Brain expression data is given in Appendix 5.

During my screen, *AP4E1* (Adaptor related protein complex 4, epsilon 1 subunit) was implicated in autosomal recessive human mental retardation by other labs. Patients feature shy character, absent speech, microcephaly, retarded growth, stereotypic laughter, decreased muscle mass and inability to walk (Abou Jamra *et al.*, 2011, Moreno-De-Luca *et al.*, 2011). *MCPH1* (microcephalin) mutations are associated with mental retardation and are a major cause of primary autosomal recessive microcephaly in humans (Jackson *et al.*, 2002). This is consistent with my finding that the cortical thickness is significantly reduced in the *Mcph1* -/- mice. *SRC* (Schmidt-Ruppin A-2 viral oncogene homolog, also known and *pp60*) has also been linked to human mental retardation with disruption of SRC kinase activity by ethanol being a potential mechanism underlying foetal alcohol syndrome (Yeaney *et al.*, 2009).

No current evidence links *Arl4d, Atp1f1* or *Atp5a1* to human pathology. However, mouse work by other authors is consistent with these genes having a role in the CNS. Transfection of GFP-tagged WT *Arl4d* (ADP-ribosylation factor-like protein 4D) into mouse neuroblastoma cells induces neuronal outgrowth whilst knocking down Arl4d by siRNA inhibits the neuronal outgrowth induced by valproic acid by 70% (Yamauchi *et al.*, 2009). Arl4d has been shown to recruit cytohesin-2/ARF to modulate actin remodelling, a possible mechanism for influencing neuronal outgrowth (Li *et al.*, 2007).

Evidence for a CNS role for *Atpif1* (ATPase inhibitory factor 1) and *Atp5a1* (ATP synthase, H+ transporting, mitochondrial F1 complex, alpha subunit 1) is more circumstantial. *Atpif1* and *Atp5a1* are downregulated in the cortex of mice subchronically

dosed with arsenic via their drinking water (Hong *et al.*, 2009). Higher exposure to arsenic has been linked to poor performance in cognitive tests both in mice and humans (Hong *et al.*, 2009, Martinez-Finley *et al.*, 2009, O'Bryant *et al.*, 2011). Both genes play a role in limiting the depletion of cellular ATP and KO from both lines share a common phenotype; reduced molecular layer thickness.

Comparing the KO cohorts

Ten genes were assessed at both 6 weeks and 16 weeks. Results were constant across both cohorts for seven of these genes. This left three phenotypic hit genes with inconsistent levels of significance between cohorts; *Ncaph1*, *Mcph1* and *Farp2*.

Ncaph1 was significant in the 6 week cohort but not in the 16 week cohort. Three *Ncaph1* +/- animals were analysed in the 6 week cohort whilst only one was analysed in the 16 week cohort. This suggests the inconsistency in Ncaph1 significance is due to a lack of power.

The inconsistency in *Mcph1* and *Farp2* results can be explained by morphological changes to the cortex with age. A t-test on all WT BL/6 animals analysed shows that cortical thickness is significantly reduced between 6 and 16 weeks of age (**Figure 43. A**). This finding was also supported by data from the non-phenotypic ENU pedigrees analysed in **chapter three,** with a Pearson correlation test showing that cortical thickness negatively correlated with age (**Figure 43. B**). Therefore, *Mcph1* and *Farp2* null mutations may influence how age related changes to cortical thickness manifest relative to WT.

Figure 43: Cortical thickness is affected by age

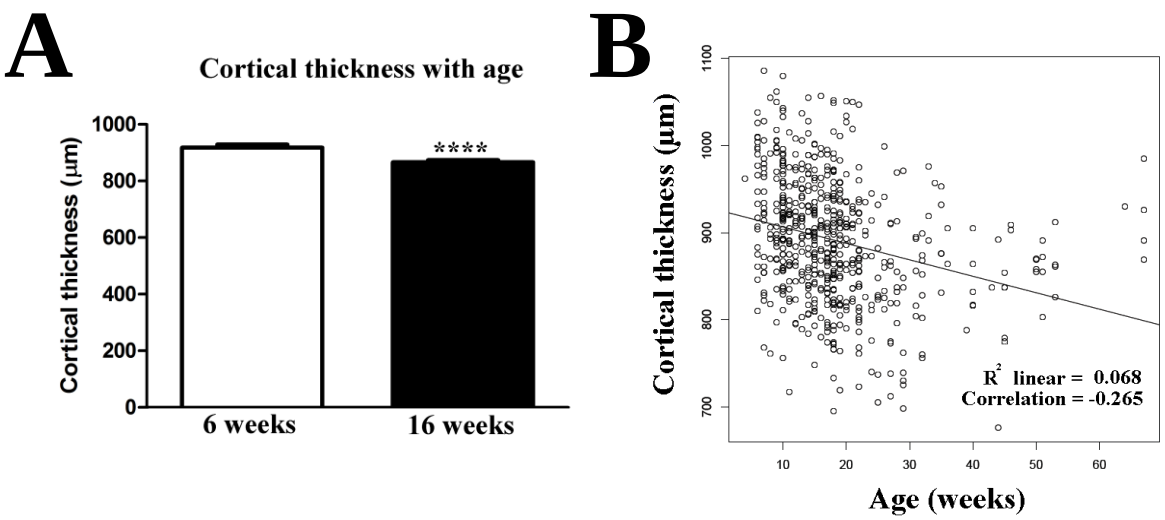


Figure 43. *T test of cortical thickness for all WT BL/6 mice used in KO screen showing thickness is significantly reduced at 16 weeks (P<0.0001, t = 5.8, df = 203, 95% CI = -40.64 to -82.05µm. Total n=204 (89 aged 6 weeks, 115 aged 16 weeks*) *(A). Pearson correlation plot, generated from the ENU cohort used in chapter 3, showing cortical thickness is reduce with age (P<0.0001, F = 44.9 (1, 592), Correlation = -0.265, R^2 linear = 0.068, N= 593) (B).*

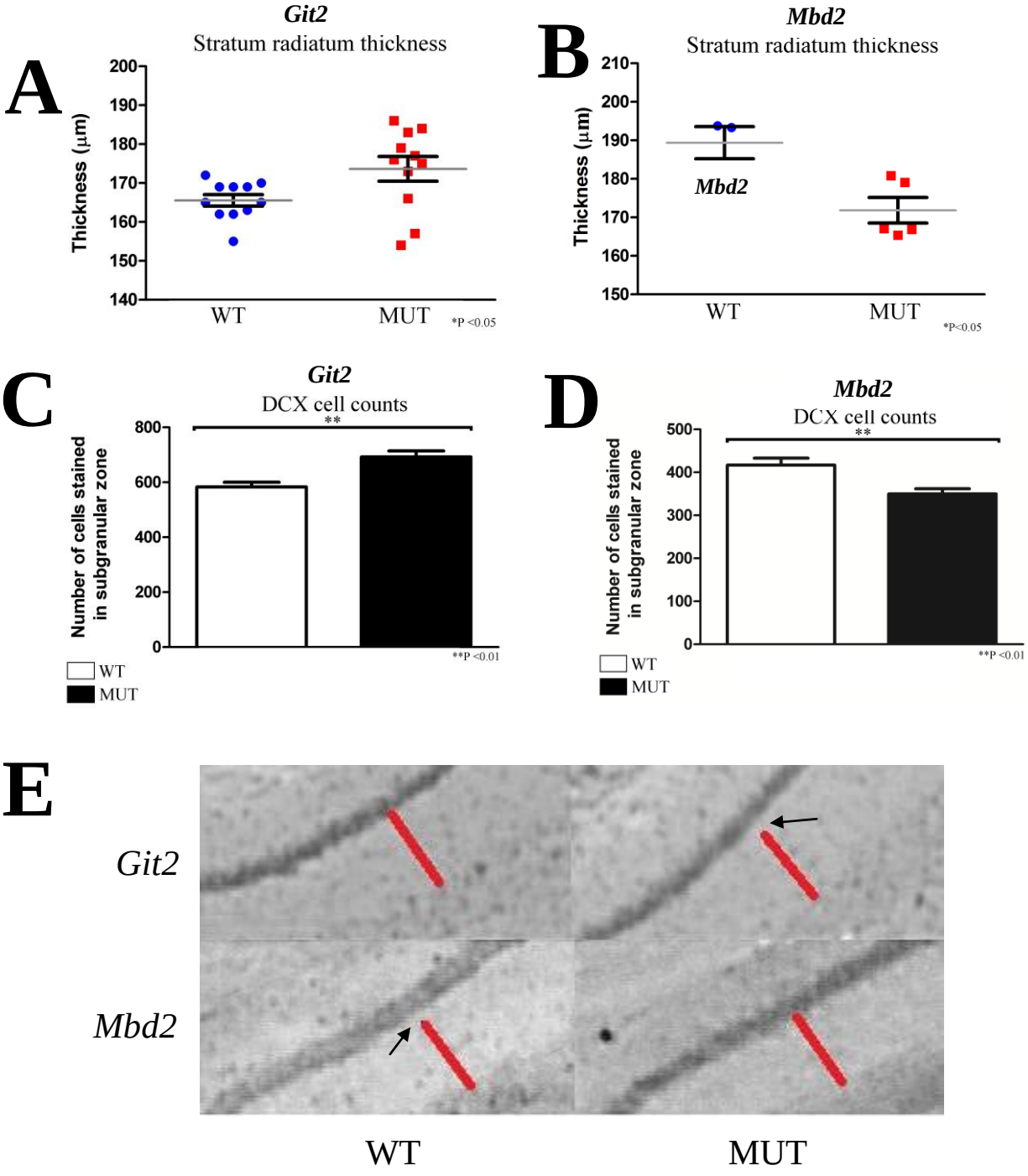
Further analysis of *Git2* KO mice

Git2 was selected for further analysis due to the near significant reduction in stratum radiatum thickness and literature evidence supporting an elevated anxiety phenotype (Schmalzigaug *et al.*, 2009). Rather than sourcing mixed background animals from Sanger, *Git2* KO animals on a pure BL/6 background were sent from Duke university.

Neurogenesis and cortical thickness are elevated in *Git2* -/-

My colleague, Dr Guo-Jen Huang, was interested in quantifying neurogenesis levels in *Git2* and *Mbd2* (methyl-CpG binding domain protein 2) mutants as part of a candidate gene study. Together, we verified that the thickness of the stratum radiatum, and neurogenesis, is increased in *Git2* -/- animals (**Figure 44. A, C, E**). The converse is true in *Mbd2* -/- animals; stratum radiatum thickness is decreased and neurogenesis is reduced (**Figure 44. B, D, E**). This implies that stratum radium thickness may be influenced by neurogenesis level.

Figure 44: Neurogenesis and radiatum thickness in *Git2* and *Mbd2*



Please turn page for remainder of figure

F

Statistics

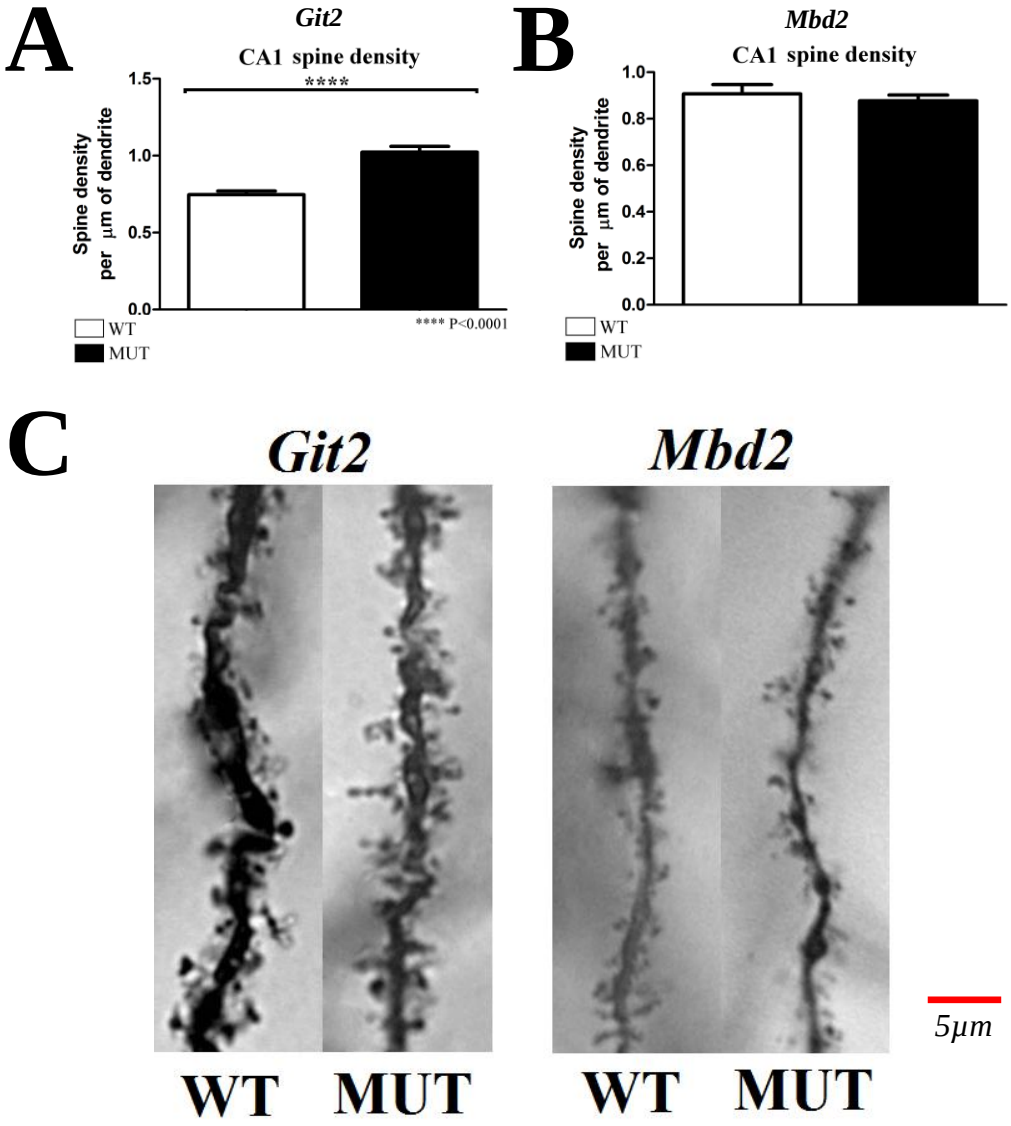
Stratum radiatum thickness, T-test				
Comparison	**P**	**t**	**Df**	**95% CI (µm)**
***Git2*, Hom vs. WT**	<0.05	2.3	20	+0.76 to +15.42
***Mbd2*, Hom vs. WT**	<0.05	3.25	6	-4.34 to -30.725
DCX counts in dentate gyrus, T-test				
Comparison	**P**	**t**	**Df**	**95% CI (cells)**
***Git2*, Hom vs. WT**	<0.01	3.82	19	+49.54 to +169.42
***Mbd2*, Hom vs. WT**	<0.01	3.19	13	-21.64 to -112.1

Figure 44. *Scatter charts showing stratum radiatum thickness is significantly increase in Git2 -/- (n =11 WT, 11 Hom) and significantly decreased in Mbd2 -/- (n = 3 WT, 5 Hom) (A, B). DCX positive cells in the dentate gyrus, an indicator of neurogenesis, is significantly increased in Git2 -/- (n =11 WT, 11 Hom) and significantly decreased in Mbd2 -/- (n =7 WT, 7 Hom) (C, D). Thickness of stratum radiatum measurements. Red lines are 170µm in length. Black arrows highlight that the stratum radiatum thickness is greater than the 170µm line for Git2 -/- and Mdb2 WT (E). Statistical results table (F). No image of DCX histology is shown as positive cells were counted directly on a microscope and not imaged. Error bars show SEM. Histogram summary: *P<0.05 **P<0.01 ***P<0.001*

Synaptic spine density is increased in *Git2* -/-

As *Git1* -/- animals are reported to exhibit a decrease in CA1 synaptic spine density, I measured spine density in the *Git2* line (Menon *et al.*, 2010). I also measured spine density in the *Mbd2* line, although no change in density was to be expected from the literature. In contrast to *Git1* KOs, *Git2* -/- animals displayed a significant increase in CA1 spine density. This further supports that *Git2* is involved in hippocampal anatomy. *Mbd2* -/- spine density is comparable to WT (**Figure 45**).

Figure 45: CA1 spine density in *Git2* and *Mbd2*



D

Statistics

CA1 dendritic spine density, T-test				
Comparison	**P**	**T**	**Df**	**95% CI (spines/µm)**
***Git2*, Hom vs. WT**	<0.0001	6.3	108	+0.19 to +0.36
***Mbd2*, Hom vs. WT**	=0.51	0.66	72	+0.06 to -0.12

Figure 45. *CA1 dendritic spine density is significantly increased in Git2 KOs (N =4 WT, 4 Hom) (A). Spine density in Mbd2 KO is not significantly different to controls (N =3 WT, 4 Hom) (B). Golgi stain image showing WT and KO CA1 spine densities for the respective Git2 and Mdb2 groups (C). Statistical results table (D). Scale bar equals 5µm. Error bars show SEM. Histogram summary: ****P<0.0001*

Future work for plans the KO screening project

How could the reliability of the screen be improved? To increase reliability I would make the following two changes. One, all lines would be generated on BL/6 background. Standardisation of the background would eliminate variance caused by mixed background strain effects. It would also ensure KO measurements could be contrasted against a large pool of background matched WT samples. In the current dataset, non-BL/6 lines could only be compared with a background matched WT pool of less than 7 animals. In comparison, BL/6 lines are contrasted with a WT pool of ~90 animals. As a result, non-BL/6 comparisons were underpowered and subject to greater variance. Due to this, all genes analysed in non-BL/6 KO lines should also be knocked out in BL/6 and reassessed.

Two, a minimum of 3 KO samples per line should be quantified. Occasionally due to processing difficulties, some KO samples were destroyed and the analysed KO pool was reduced less than this threshold. Low n numbers increases the risk that data will be skewed by an atypical sample. Consequently, where the number of KO animal analysed per line fell below 3, replacement samples should be sent to boost the n number.

How could the screen be adapted to collect more scientifically useful data? Assuming money was no barrier, I would also make the following improvements to increase the usefulness of the screen. One, prior to cranial extraction, brains would be scanned on a magnetic resonance imaging machine using the method described by Chen and colleagues (Chen *et al.*, 2006). This would allow for 3D assessment of the internal neuroanatomy and provide information on brain areas beyond that which is was measured in my screen.

Two, markers of neurogenesis and cell death would be quantified for each KO line using immunocytochemistry. In order to achieve this, all samples would need to be perfusion fixed. I could then test whether the level of neurogenesis and cell death correlate with hippocampal layer thickness.

Three, I would also quantify the anatomy of the cerebellum in the KO lines using nissl stained sections. This would require additional staff to help manage the additional workload. During my screen, the cerebellum is discarded during processing. This represented a significant waste of tissue resources and failure to screen the cerebellum may have lead to lines featuring cerebellar abnormalities not being detected.

Four, I would upload my histological data to an online resource similar to the Allen Brain Atlas. This would allow the scientific community to search for genes associated with a specified neuroanatomical abnormality (or see which neuroanatomical abnormalities are associated with a specified gene KO). Sanger is currently in the process of developing such a resource.

Even without these improvements, my screen has generated a large amount of data. So what is the most significant finding to date? The microcephally and reduced hippocampus size of the *Ube3b* line is arguably the most interesting finding. This is due to the human homolog of gene being present in a deletion interval of a patient with mental retardation (Petek *et al.*, 2003). Additionally, the gene is related to *UBE3A*; the gene defective in Angelman syndrome (Williams *et al.*, 2010a).

To validate the significance of the finding I would generate a brain specific *Ube3b* KO. As all Sanger KOs are generated using the Knockout-first approach, a critical exon of *Ube3b* is already floxed (Testa *et al.*, 2004). Consequently, a brain specific KO can be made in two breeding cycles. First, *Ube3b -/-* animals should be mated with a *Sox1-cre* line in order to generate *Sox1-cre Ube3b +/-* offspring. These offspring should then be intercrossed to generate the brain specific KOs, *Sox1-cre Ube3b -/-*, as well as *Sox1-cre Ube3b +/+* littermate controls. The advantages of generating a brain specific KO is that somatic tissues should develop normally and the mice will have a body weight comparable to WT. If nissl staining revealed the anatomical defects were still present in the brain specific KO, it would

counter any argument that the original *Ube3b-/-* findings were entirely due to a reduced body weight.

Assuming the *Sox1-cre Ube3b -/-* mice did feature microcephally and a significant reduction in hippocampal area, I would then try to ascertain the causal pathogenic mechanisms. This would include BrdU injections during embryogenesis followed by sacrifice at P0. The method for this approach is detailed in Edwards *et al.* 2011. By counting the number of BrdU cells the neurogenesis level can be assessed. Additionally, the localisation of the BrdU cells can be measured in order to evaluate if a neuronal migration defect is present (I have used this approach in **chapter 6**). I would also immunostain brain sections for caspase-3, a marker for apoptotic cell death, in order to verify if elevated cell death contributed towards the phenotype.

Summary

The hit rate of my KO screen was 8.7% for BL/6 background lines when data from both the 6 week and 16 week cohorts is combined (20 hits out of 229 unique genes). In non-BL/6 lines the total hit rate was 38.8% (7 out of 18 unique genes), although these animals were at risk of being false positives due to a mixed 129 genetic background.

Collectively, 13 out of the total 27 hit genes had literature evidence supporting a role in the CNS. Three of the thirteen genes are directly associated with a human brain disorder. These include: *AP4E1* in autosomal recessive cerebral palsy; *MCPH1* in microcephaly and *SLX4* in microcephaly associated Fanconi anaemia. The remaining eight genes include: *Arl4d*, *Atpif1*, *Epc2*, *Magi2*, *Ncaph2*, *Prkcz*, *Sptbn2*, *Src*, *Ube2b* and *Wdr47*. The significance of these findings is discussed in **chapter 8**.

In addition, I conducted further analysis on one of the lines which neared significance; *Git2*. An alternatively sourced *Git2* KO line on a BL/6 background, showed a significant thickening of the stratum radiatum and increased neurogenesis in -/- animals. Additionally, *Git2* -/- animals featured an increase in CA1 synaptic spine density.

Chapter 5

Anatomical and Behavioural Assessment of Sanger ENU Mice

Characterisation of ENU mice added to KO pipeline

Introduction

The Sanger institute incorporated several known ENU mutant lines into the KO pipeline. Two of the screened ENU mutant lines displayed neuroanatomical defects; *Whirligig* and *Diminuendo*. Both of these lines were discovered by Karen Steel's lab at Cambridge and feature a deafness phenotype.

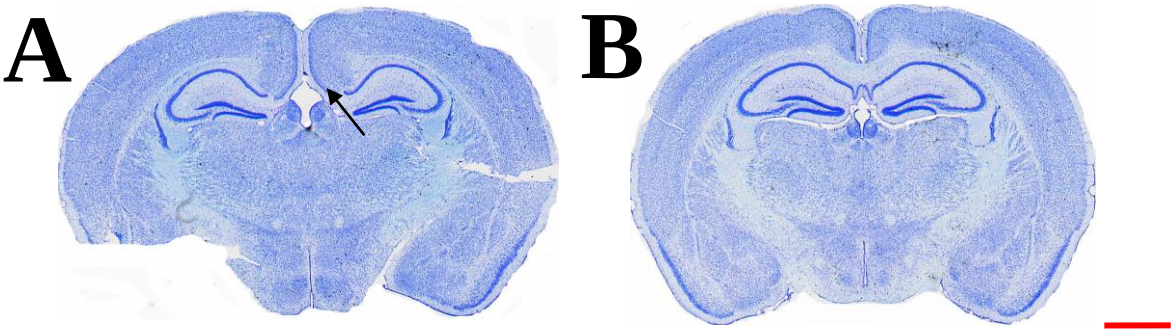
The *Whirligig* mice are heterozygous for a W973X mutation in Chromodomain Helicase DNA-binding protein 7 (CHD7), the homolog of the gene responsible for human CHARGE syndrome (Vissers *et al.*, 2004, Bosman *et al.*, 2005). Many aspects of CHARGE syndrome are present in the *Whirligig* +/- mutant such as choanal atresia and defects of the semicircular canal, heart, eye, palate, and gonads (Bosman *et al.*, 2005, Bergman *et al.*, 2010). Human CHARGE patients also display anatomical and behavioural abnormalities including corpus callosum agenesis, autism and MR (Fernell *et al.*, 1999). Here I report the discovery that *Whirligig* +/- mice also mirror these abnormalities.

I also present the discovery of hippocampal abnormalities and aberrant behaviours in the *Diminuendo* line. *Diminuendo* mice feature an A>T mutation in the seed region of microRNAs 96 (miR-96) (Lewis *et al.*, 2009). MicroRNAs are small noncoding RNAs that bind to specific sites in the 3' UTR of target mRNAs, inducing transcript destabilization and translational inhibition.

Whirligig and *Diminuendo* neuroanatomy and physical phenotype

Whirligig heterozygous mutants were discovered to feature corpus callosum agenesis (**Figure 46**). Mutants feature an overt circling phenotype, reduced weight and coloboma of the eyes (Bosman *et al.*, 2005). These eye defects are unlikely to influence behavioural results as all animals, including WT littermate controls, are on the C3H background and consequently blind from retinal degeneration from 6 weeks of age (Nagy and Misanin, 1970).

Figure 46: Corpus callosum agenesis in *Whirligig* +/- mutant



C

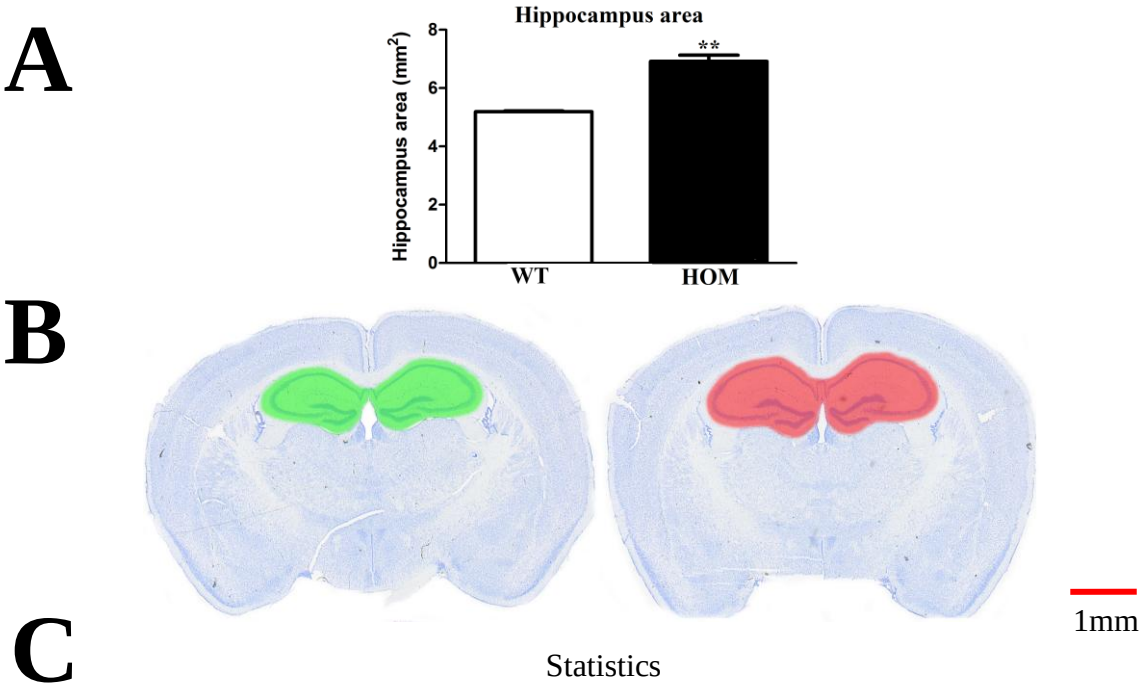
Statistics

Phenotype	F (df1, df2)	Adjusted –log p (unadjusted –logp)	95% CI
Corpus callosum span is decreased (agenesis)	468.1 (1, 9)	7.74 (8.34)	-1236 to -1483 µm
Corpus callosum area is decreased (agenesis)	161.1 (1, 9)	5.72 (6.32)	-425773 to -581270 μm^2

Figure 46. *Nissl stained brain sections from chd7 Whirligig +/- mutant (A) and WT (B) (black arrow shows corpus callosum agenesis). ANOVA table of statistics generated from contrasting mutants with WT controls in KO pipeline (N =7 WT,3 MUT) (C) Scale bar equals 1mm.*

Homozygous, but not heterozygous, *Diminuendo* mutants were discovered to feature an enlarged hippocampus (**Figure 47**). Homozygous animals also feature a head thrashing phenotype and occasionally exhibit circling behaviour.

Figure 47: Increased hippocampus area in *Diminuendo* homozygotes



Statistics

Comparison	Phenotype	F (df1, df2)	Adjusted –log p (unadjusted –logp)	95% CI
Hom vs. WT	Length of pyramidal cell layer	147.9 (1, 3)	2.32 (2.92)	+1230 to +1703 µm
	Hippocampus area	113 (1, 3)	2.15 (2.75)	+1405704 to +2041273 µm^2
Het vs. WT	Length of pyramidal cell layer	0 (1, 4)	-0.53 (0.07)	+337 to -414 µm
	Hippocampus area	2 (1, 4)	0.03 (0.63)	+49060 to -295426 µm^2

Figure 47. *Histogram of hippocampus area showing enlargement in homozygous mutants (N =2 WT,3 Het, 2 Hom) (A). Area of hippocampus for WT (green) and homozygous Diminuendo animals (red) on matched sections (B). ANOVA table of statistics generated from contrasting mutants with WT controls in KO pipeline (C) Scale bar equals 1mm. Error bars show SEM. Histogram summary: **P<0.01*

Whirligig behaviour

Choice of behavioural tests

As *Whirligig* +/- mutants bear a mutation in Chd7 it seemed appropriate to test them for behaviours which are aberrant in human CHARGE syndrome. CHARGE syndrome is an acronym:

C: Coloboma of the eye, central nervous system abnormalities

H: Heart defects

A: Atresia of the choanae

R: Retardation of growth and development

G: Genital or urinary abnormalities

E: Ear abnormalities and/or deafness

As *Whirligig* +/- mutants share these somatic defects, my tests could not rely on visual or auditory stimuli. Behavioural phenotypes prevalent in CHARGE syndrome patients include cognitive impairment, hyperactivity, autistic spectrum disorder, obsessive compulsive disorder and impulsiveness (Nicholas, 2005, Graham *et al.*, 2005, Bernstein and Denno, 2005). When contrasted with patients with other forms of mental retardation, CHARGE patients are described as less anxious (Graham *et al.*, 2005). In order to assess these aspects of behaviour I used the following tests:

Anxiety and impulsiveness: EPM, OF and food neophobia

Activity level and locomotion: Activity box and OF

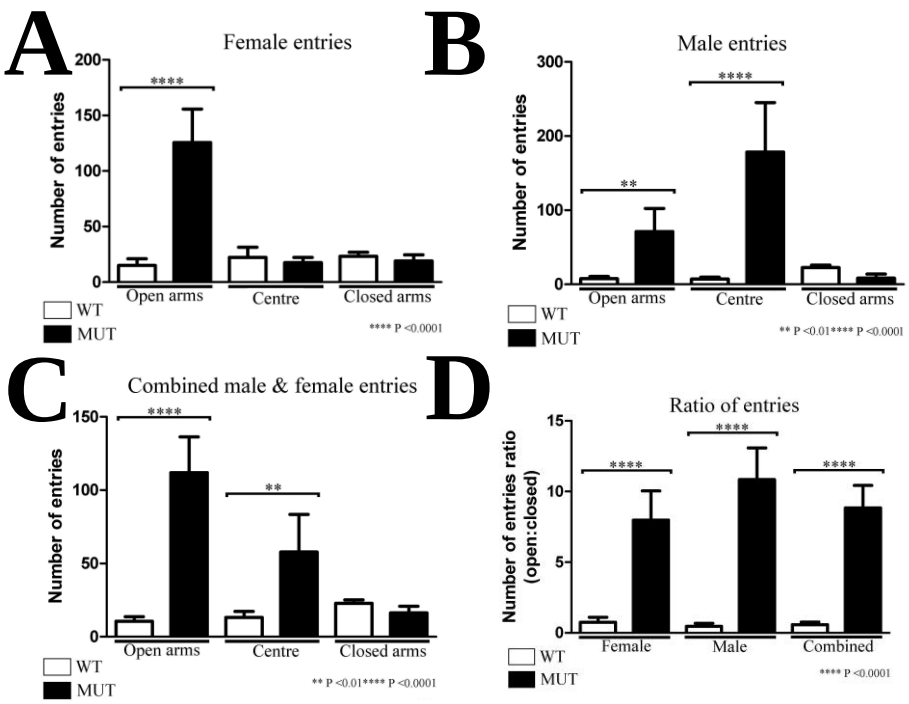
Reference memory: Y maze

Social behaviour: Sociability box

Elevated plus maze

Whirligig +/- behaviour on the EPM suggests lessened anxiety and elevated activity levels in comparison to their WT littermates. Mutant mice have significantly increased entries to open arms (**Figure 47. A, B, C, E**). Entries to the open arms in mutant animals are particularly high for two reasons. First, very low anxiety mutant mice were regularly observed to move their head beyond the open arm ledge in order to sniff beyond the maze. Each time the head re-entered the maze an entry was automatically counted on the Ethovision motion detection software. This was particularly pronounced in female mutants and is apparent from their high open arm entries score not being complimented with a high entry score to the maze centre (**Figure 48. A, E**). Second, mutant animals displayed hyperactive circling behaviour on the open arms and were observed to rapidly circle from one open arm directly to the other open arm. This circling behaviour was tightly co-ordinated as mice did not fall off the arm ledge. In contrast, the closed arms were too narrow to engage in circling behaviour and an entry would have required a mouse to slow down, modulate its motion and negotiate a 90° turn. Using an open:closed arm ratio, it was observed that the mutants display a strong preference for the open arm versus the closed arm (**Figure 48. D, E**). The open arms are considered more anxiogenic as any mouse exploring the arm would be more visible and unsheltered from hypothetical predators. Several mutant animals were observed exploring the entire length of the open arms suggesting very low levels of anxiety or a lack of hypothetical danger awareness.

Figure 48: *Whirligig* +/- make more Elevated plus maze arm entries



E

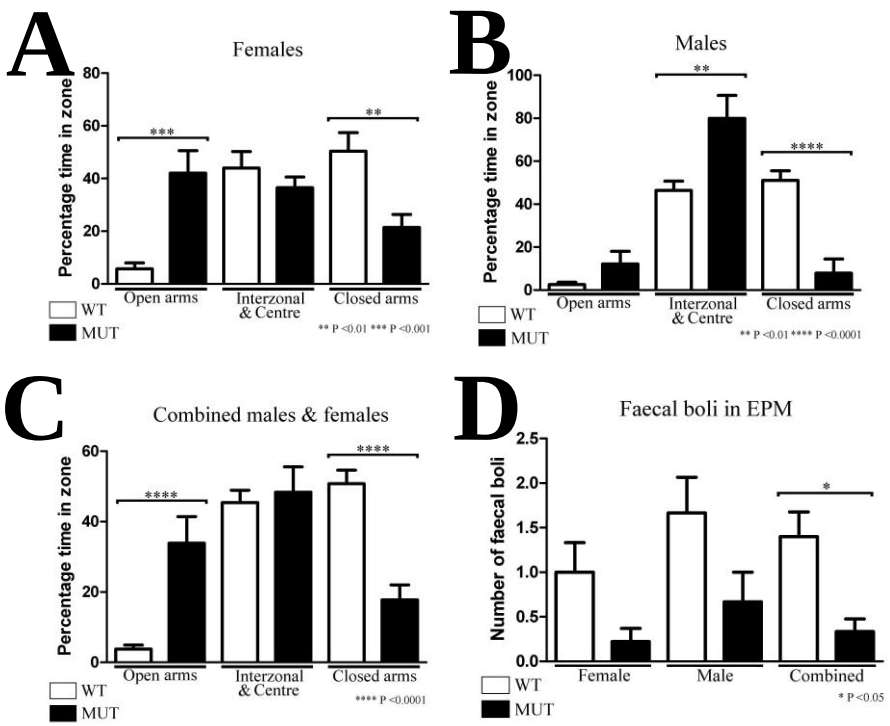
Statistics

Entries open arms, mutant vs. WT (ANOVA with Bonferroni MCT)			
Comparison	**F (df1, df2)**	**Adjusted P {unadjusted P}**	**95% CI**
Female	F (1, 18) = 36	P<0.0001 {P<0.000033}	+65.08 to +156
Male	F (1, 17) = 12.6	P<0.01 {P<0.0033}	+19.09 to +107.7
Combined	F (1, 36) = 46.8	P<0.0001 {P<0.000033}	+65.34 to +137.4
Entries to centre, mutant vs. WT (ANOVA with Bonferroni MCT)			
Comparison	**F (df1, df2)**	**Adjusted P {unadjusted P}**	**95% CI**
Female	F (1, 18) = 0.06	P>0.05 = NS {P = 0.81}	+40.84 to -50.11
Male	F (1, 17) = 91.9	P<0.0001 {P<0.000033}	+126.9 to +215.5
Combined	F (1, 36) = 9.1	P<0.01 {P<0.0033}	+8.619 to +80.65
Ratio of entries (open:closed), mutant vs. WT (ANOVA with Bonferroni MCT)			
Comparison	**F (df1, df2)**	**Adjusted P {unadjusted P}**	**95% CI**
Female	F (1, 16) = 28.7	P<0.0001 {P<0.000033}	+3.91 to +10.53
Male	F (1, 17) = 36	P<0.0001 {P<0.000033}	+6.13 to +14.64
Combined	F (1, 34) = 68.3	P<0.0001 {P<0.000033}	+5.74 to +10.77

Figure 48. *ANOVAs with Bonferroni MCT. Entry results for females, males and combined sexes respectively (A, B, C). Open:closed arm entries ratio (D). Statistical results table (E).* Total male n= 18 (3 *Whirligig* +/-, 15 WT); total female n= 19 (9 *Whirligig* +/-, 10 WT). *Error bars show SEM. Histogram summary: **P<0.01 ****P<0.0001*

The percentage of time spent in each of the arms further suggests that *Whirligig* +/- mutants exhibit a lesser degree of anxiety than WT. Mutant animals spend significantly more time in the open arms and significantly less in the closed (**Figure 49. A, B, C, E**). The low anxiety hypothesis is further supported by the mutant animals having a significantly lower defecation rate during the experiment (**Figure 49. D, E**). The discrepancy in results between males and females is likely due to the low number of mutant males available for testing (total male n= 18 (3 *Whirligig* +/-, 15 WT); total female n= 19 (9 *Whirligig* +/-, 10 WT)). This n of only 3 mice reduces the reliability of the male *Whirligig* +/- dataset as individual variation and outlier mice have greater potential to skew the data for the group as a whole. Please see the "Future work plans for *Diminuendo* and *Whirligig*" section of this chapter for a description of how behavioural tests could be improved.

Figure 49: Elevated plus maze suggests reduced anxiety in *Whirligig* +/-



E

Statistics

Percentage time in open arms, mutant vs. WT (ANOVA with Bonferroni MCT)			
Comparison	**F (df1, df2)**	**Adjusted P {unadjusted P}**	**95% CI**
Female	F (1, 18) = 18.9	P<0.001 {P<0.00033}	+15.59 to +57.09
Male	F (1, 17) =1.2	P>0.05 = NS {P =0.29}	-12.47 to +31.72
Combined	F (1, 36) = 22.7	P<0.0001 {P<0.000033}	+14.73 to +45.44
Percentage interzonal and centre time, mutant vs. WT (ANOVA with Bonferroni MCT)			
Comparison	**F (df1, df2)**	**Adjusted P {unadjusted P}**	**95% CI**
Female	F (1, 18) = 0.8	P>0.05 = NS {P = 0.34}	+13.32 to -28.18
Male	F (1, 17) =14.2	P<0.01{P<0.0033}	-12.47 to +31.72
Combined	F (1, 36) =0.2	P>0.05 = NS {P = 0.66}	-12.41 to +18.30
Percentage time in closed arms, mutant vs. WT (ANOVA with Bonferroni MCT)			
Comparison	**F (df1, df2)**	**Adjusted P {unadjusted P}**	**95% CI**
Female	F (1, 18) = 11.9	P<0.001 {P<0.00033}	-8.16 to -49.66
Male	F (1, 17) = 23.5	P<0.0001 {P<0.000033}	-21.11 to -65.29
Combined	F (1, 36) = 27.4	P<0.0001 {P<0.000033}	-17.68 to -48.39
Number of faecal boli, mutant vs. WT (ANOVA with Bonferroni MCT)			
Comparison	**F (df1, df2)**	**Adjusted P {unadjusted P}**	**95% CI**
Female	F (1, 18) = 2.1	P>0.05 =NS {P = 0.16}	+0.55 to -2.11
Male	F (1, 17) = 1.8	P>0.05 =NS {P = 0.19}	+0.83 to -2.83
Combined	F (1, 36) = 6.7	P<0.05 {P<0.016}	-0.05 to -2.08

Please turn page for remainder of figure ⟶

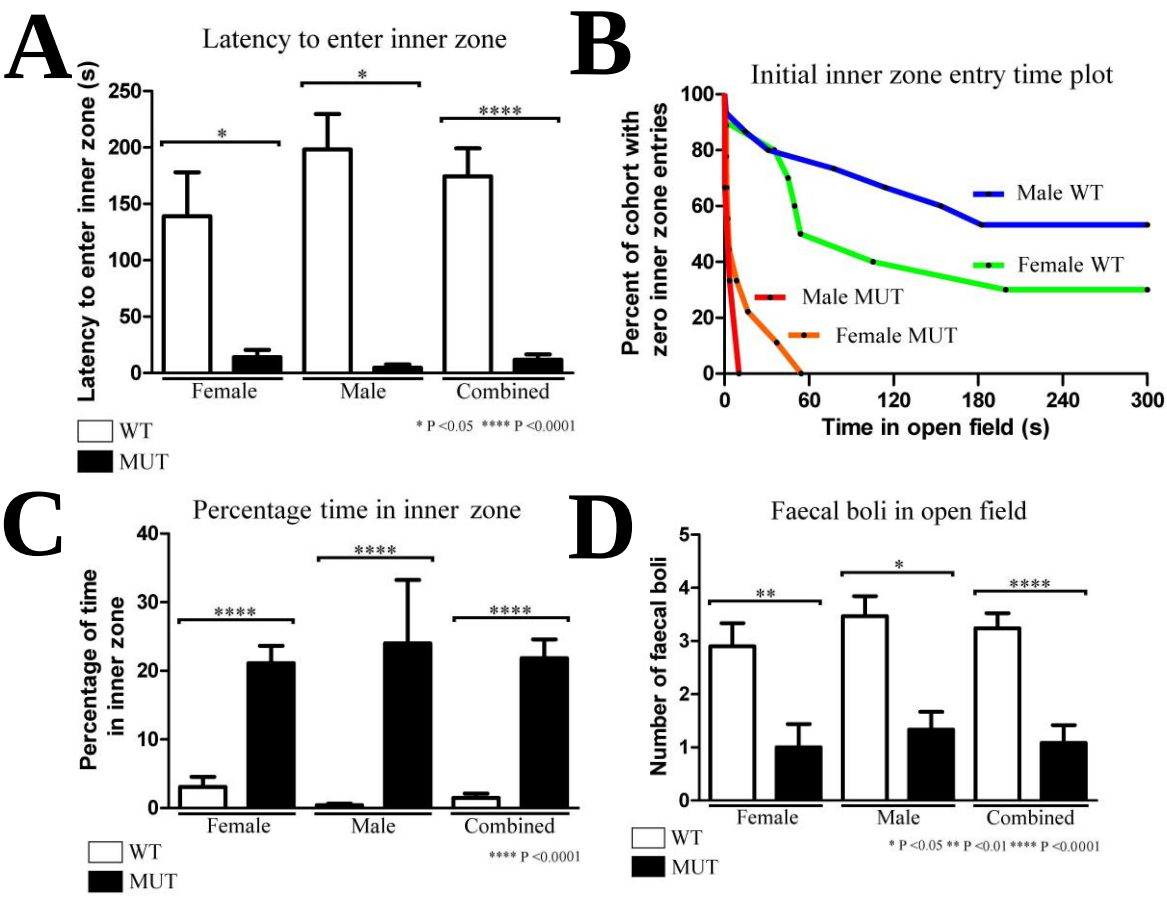
Figure 49. *ANOVAs with Bonferroni MCT. Percentage in open, centre and closed arm zones for females, males and combined sexes respectively (A, B, C). Defecation rate during experiment (D). Statistical results table (E).* Total male n= 18 (3 *Whirligig* +/-, 15 WT); total female n= 19 (9 *Whirligig* +/-, 10 WT). *Error bars show SEM. Histogram summary: *P<0.05 **P<0.01 ****P<0.0001*

Open field

The OF also supports that *Whirligig* +/- mutants are less anxious than WT littermates. Similar to the open arms of the EPM, the inner zone of the OF is considered more anxiogenic as it is more exposed. WT animals typically took more than fifty percent of the overall test duration to initially enter the inner zone. In contrast, mutant animals entered significantly sooner (**Figure 50. A, E**). Approximately 40% of WT animals failed to enter the maze centre prior to the conclusion of the test. In contrast, all mutant animals tested entered the inner zone in under a minute resulting in a significantly different "survival plot" of latency to enter (Survival with Mantel-Cox test: df = 3, chi square = 24.96, P<0.0001) (**Figure 50. B**).

A motion defect could result in the mutant briefly stumbling into the inner zone by accident. To account for this, the percentage of time spent in the inner zone was calculated. Mutant animals spend significantly more time in the inner zone than WT (**Figure 50. C, E**). Mutants spend ~20% of the test duration in the inner zone, mirroring the percentage of floor space dedicated to the zone. This suggests that whilst WT animals actively avoid the inner zone, mutant animals display no aversion and explore it to the same degree as the outer zone. Additionally, the mutants have a lesser rate of defecation during testing further supporting a reduced anxiety phenotype (**Figure 50. D, E**).

Figure 50: Open field suggests reduced anxiety in *Whirligig* +/-



E

Statistics

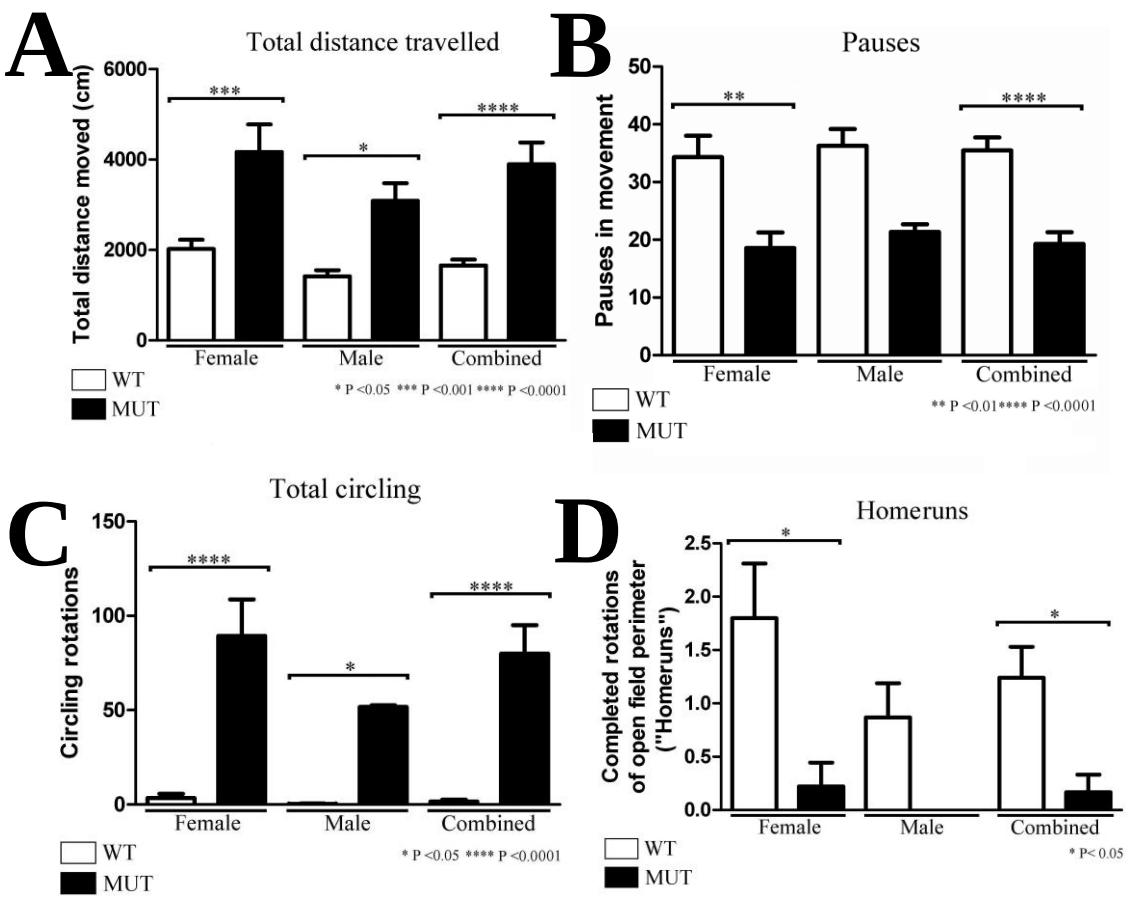
Latency to enter inner zone, mutant vs. WT (ANOVA with Bonferroni MCT)			
Comparison	**F (df1, df2)**	**Adjusted P {unadjusted P}**	**95% CI (s)**
Female	F (1, 18) = 7	P<0.05 {P<0.00166}	-9.34 to -240.6
Male	F (1, 17) = 8.9	P<0.05 {P<0.00166}	-34.45 to -352.7
Combined	F (1, 36) = 20.5	P<0.0001 {P<0.000033}	-74.49 to -251.2
Percentage of time in inner zone, mutant vs. WT (ANOVA with Bonferroni MCT)			
Comparison	**F (df1, df2)**	**Adjusted P {unadjusted P}**	**95% CI**
Female	F (1, 18) = 43.4	P<0.0001 {P<0.000033}	+11.30 to +24.72
Male	F (1, 17) = 39.3	P<0.0001 {P<0.000033}	+14.36 to +32.84
Combined	F (1, 36) = 94.8	P<0.0001 {P<0.000033}	+15.22 to +25.48
Number of faecal boli, mutant vs. WT (ANOVA with Bonferroni MCT)			
Comparison	**F (df1, df2)**	**Adjusted P {unadjusted P}**	**95% CI**
Female	F (1, 18) = 9.3	P<0.01 {P<0.0033}	-0.372 to -3.43
Male	F (1, 17) = 6.2	P<0.05 {P<0.0166}	-0.03 to -4.24
Combined	F (1, 36) = 20.5	P<0.001 {P<0.00033}	-0.99 to -3.32

Please turn page for remainder of figure ⟶

Figure 50. ANOVA with Bonferroni MCT (A, B, D)**.** *Latency to enter inner zone (A). Survival plot of latency to enter inner zone (B). Percentage time spent in inner zone (C). Defecation rate during experiment (D). Statistical results table (E). Error bars show SEM. Histogram summary: *P<0.05 **P<0.01 ****P<0.0001*

The OF was also used to measure locomotory behaviour in addition to anxiety. Locomotion analysis suggests that mutant animals are hyperactive, travelling over twice the total distance covered by WT (**Figure 51. A, E**). This will in part be due to mutant animals pausing significantly less in their movement (**Figure 51. B, E**). Mutant animals also exhibit pronounced circling behaviour (**Figure 51. C, E**). Furthermore, WT animals often engage in thigmotaxis and systematically explore the walls of the maze. Despite allowing for circling, mutant animals fail to explore the box systematically (**Figure 51. D, E**).

Figure 51: Open field shows abnormal locomotion in *Whirligig* +/-



Please turn page for remainder of figure

E

Statistics

Total distance travelled, mutant vs. WT (ANOVA with Bonferroni MCT)			
Comparison	**F (df1, df2)**	**Adjusted P {unadjusted P}**	**95% CI (cm)**
Female	F (1, 18) = 19.5	P<0.001{P<0.00033}	+952.4 to +3333
Male	F (1, 17) = 6.3	P<0.05 {P<0.0166}	+35.04 to +3312
Combined	F (1, 36) = 36.5	P<0.0001 {P<0.000033}	+1329 to +3148
Pauses in movement, mutant vs. WT (ANOVA with Bonferroni MCT)			
Comparison	**F (df1, df2)**	**Adjusted P {unadjusted P}**	**95% CI**
Female	F (1, 18) = 11.1	P<0.01 {P<0.0033}	-4.12 to -27.37
Male	F (1, 17) = 5.2	P>0.05 = NS {P = 0.035}	+1.06 to -31
Combined	F (1, 36) = 20.1	P<0.0001 {P<0.000033}	-7.35 to -25.11
Total circling, mutant vs. WT (ANOVA with Bonferroni MCT)			
Comparison	**F (df1, df2)**	**Adjusted P {unadjusted P}**	**95% CI**
Female	F (1, 18) = 40.8	P<0.0001 {P<0.000033}	+35.16 to +136.7
Male	F (1, 17) = 7.7	P<0.05 {P<0.0166}	-18.55 to +121.21
Combined	F (1, 36) = 58.2	P<0.0001 {P<0.000033}	+39.55 to +117.16
Number of homeruns, mutant vs. WT (ANOVA with Bonferroni MCT)			
Comparison	**F (df1, df2)**	**Adjusted P {unadjusted P}**	**95% CI**
Female	F (1, 18) = 7.8	P<0.05 {P<0.00166}	-0.19 to -2.97
Male	F (1, 17) = 1.2	P>0.05 = NS {P = 0.29}	+1.05 to -2.78
Combined	F (1, 36) = 6.2	P<0.05 {P<0.00166}	-0.01 to -2.14

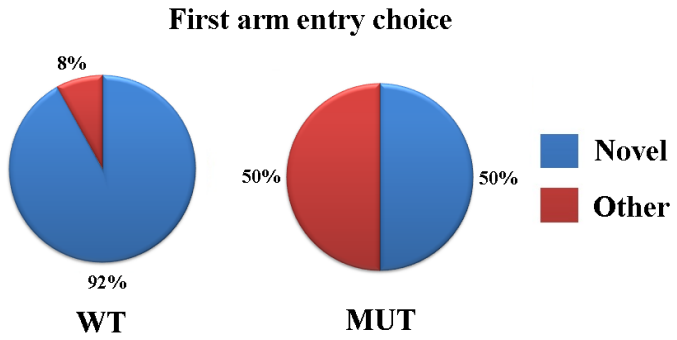
Figure 51. ANOVAs with Bonferroni MCT. *Total distance travelled by mice during experiment (A). Number of pauses in movement lasting more than 1 second (B). Total circling exhibited (C). Number of systematic complete loops of maze periphery (D). Statistical results table (E).* Total male n= 18 (3 *Whirligig* +/-, 15 WT); total female n= 19 (9 *Whirligig* +/-, 10 WT). *Error bars show SEM. Histogram summary: *P<0.05 **P<0.01 ***P<0.001 ****P<0.0001*

Y maze

The Y maze suggests that *Whirligig* +/- mutants have a defective spatial reference memory. WT animals display a strong novelty preference, opting to explore novel areas instead of areas recollected as familiar. Of the WT animals tested, 92% chose the novel arm as their first choice for exploration upon being returned to the maze after habituation. This contrasts with only 50% of mutant animals (chi-square= 8.44, df = 1, P<0.05) (**Figure 51. A, B**). This 50% selection rate for the novel arm is equivalent to the expected rate should the mouse have selected randomly. This suggests that the mutants were unable to differentiate between the previously explored arm and the novel arm.

Figure 52: *Whirligig* +/- show lack of novelty preference in Y maze

A



B

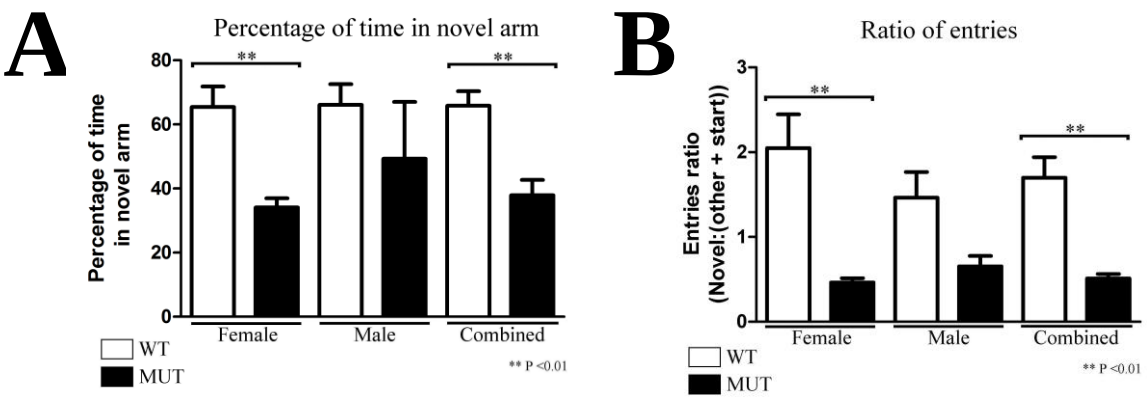
Genotype	First arm entry choice		Total
	Novel	Other	
WT*	23	2	**25**
MUT**	6	6	**12**
Total	**29**	**8**	**37**
Statistical analysis			
Chi-square =8.44			**P <0.01**

* WT female/male: 10/10 and 13/15 choose novel ** Mut female/male: 4/9 and 2/3 choose novel

Figure 52. *Pie chart of first choice of exploration for Novel versus Other arm (A). Chi-square table showing significant difference (B).* Total male n= 18 (3 *Whirligig* +/-, 15 WT); total female n= 19 (9 *Whirligig* +/-, 10 WT)

The percentage of total test time dedicated to exploring the novel arm further suggests a reference memory defect in the *Whirligig* +/- mutant. WT mice spend approximately two thirds of their time exploring the novel arm. As the arm only occupies a third of the total maze area, the amount of time WT mice spend exploring it is disproportionate. This suggests the WT mice focus their efforts searching the novel arm at the expense of the familiar arms. In contrast, the mutants spend approximately one third of their time exploring the novel arm, in line with the proportions of the maze (**Figure 53. A, C**). This further suggests that mutants may not be able to differentiate between the familiar and novel areas. Additionally, the ratio of entries shows that mutants visit each arm in an approximately equal fashion unlike WT animals which display a strong preference for the novel arm (**Figure 53. B, C**).

Figure 53: Reduced exploration of Y maze novel arm by *Whirligig* +/-



C

Statistics

Percentage of time exploring novel arm, mutant vs. WT (ANOVA with Bonferroni MCT)			
Comparison	**F (df1, df2)**	**Adjusted P {unadjusted P}**	**95% CI**
Female	F (1, 18) = 10.7	P<0.01{P<0.0033}	-7.51 to -55.06
Male	F (1, 17) = 1.6	P>0.05 = NS {P = 0.22}	+15.93 to -49.53
Combined	F (1, 36) = 14.2	P<0.01 {P<0.0033}	-9.75 to -46.1
Entries ratio, Novel: (Other + start), mutant vs. WT (ANOVA with Bonferroni MCT)			
Comparison	**F (df1, df2)**	**Adjusted P {unadjusted P}**	**95% CI**
Female	F (1, 18) = 11.7	P<0.01{P<0.0033}	-0.45 to -2.73
Male	F (1, 17) = 1.6	P>0.05 = NS {P = 0.22}	+0.76 to -2.38
Combined	F (1, 36) = 11.2	P<0.01 {P<0.0033}	-0.32 to -2.06

Figure 53. *ANOVAs with Bonferroni MCT. Percentage time in novel arm(A). Novel:(Start + Other) arm entries ratio (B). Statistical results table (C).* Total male n= 18 (3 *Whirligig* +/-, 15 WT); total female n= 19 (9 *Whirligig* +/-, 10 WT). *Error bars show SEM. Histogram summary: **P<0.01 ***P<0.001*

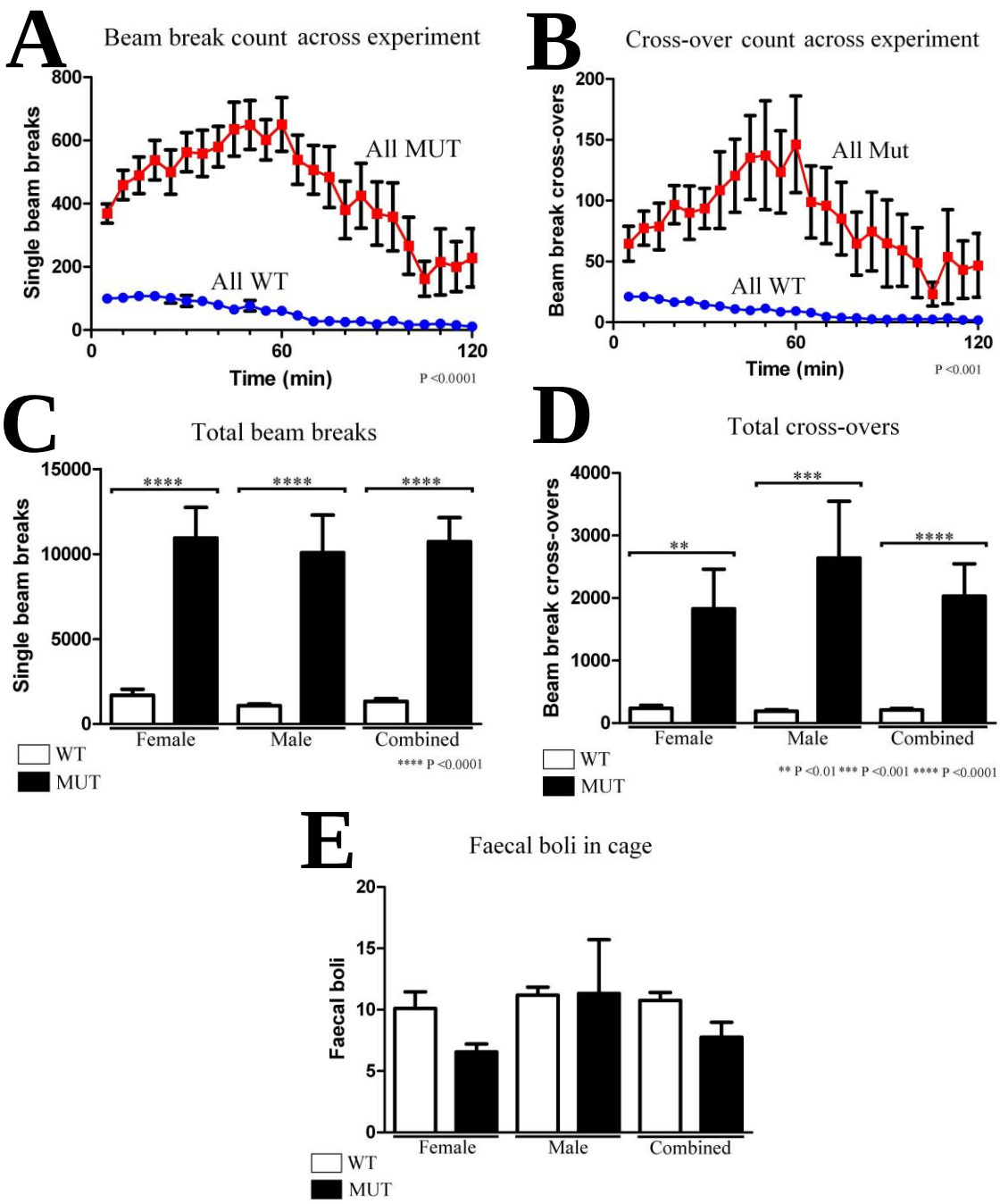
Activity box

The photonic locomotion activity box test suggests that *Whirligig* +/- mutants are hyperactive and display an abnormal pattern of activity with time. WT animals display peak activity at the beginning of the two hour long experiment, with activity declining gradually. In contrast, activity in the mutants steadily increased during the first hour of testing. This is true for both single beam breaks and cross-overs (**Figure 54. A, B, F**). After the initial sixty minutes of testing, mutant activity decreases until the last twenty minutes of testing where there is another rise in activity.

The magnitude of hyperactivity is extremely pronounced with the lowest levels of activity in the mutant exceeding peak activity in WT. The total number of beam breaks and cross-overs counted over the experiment is approximately ten fold higher in the mutant (**Figure 54. C, D, F**).

Additionally, the opportunity was taken to count faecal boli in order to gauge basal defecation rate in a pseudo-home cage environment. This produced a borderline, but nevertheless non-significant, difference between mutant and WT (**Figure 54. E, F**). This borderline result may reflect subtly differing levels of anxiety in response to isolation, differing need for defecation due to activity level, or a combination of these factors. Regardless, the result suggests that the faecal boli data collected from the EPM and OF is not due to a constipation phenotype.

Figure 54: Activity box results show *Whirligig* +/- are hyperactive



Please turn page for remainder of figure

F

Statistics

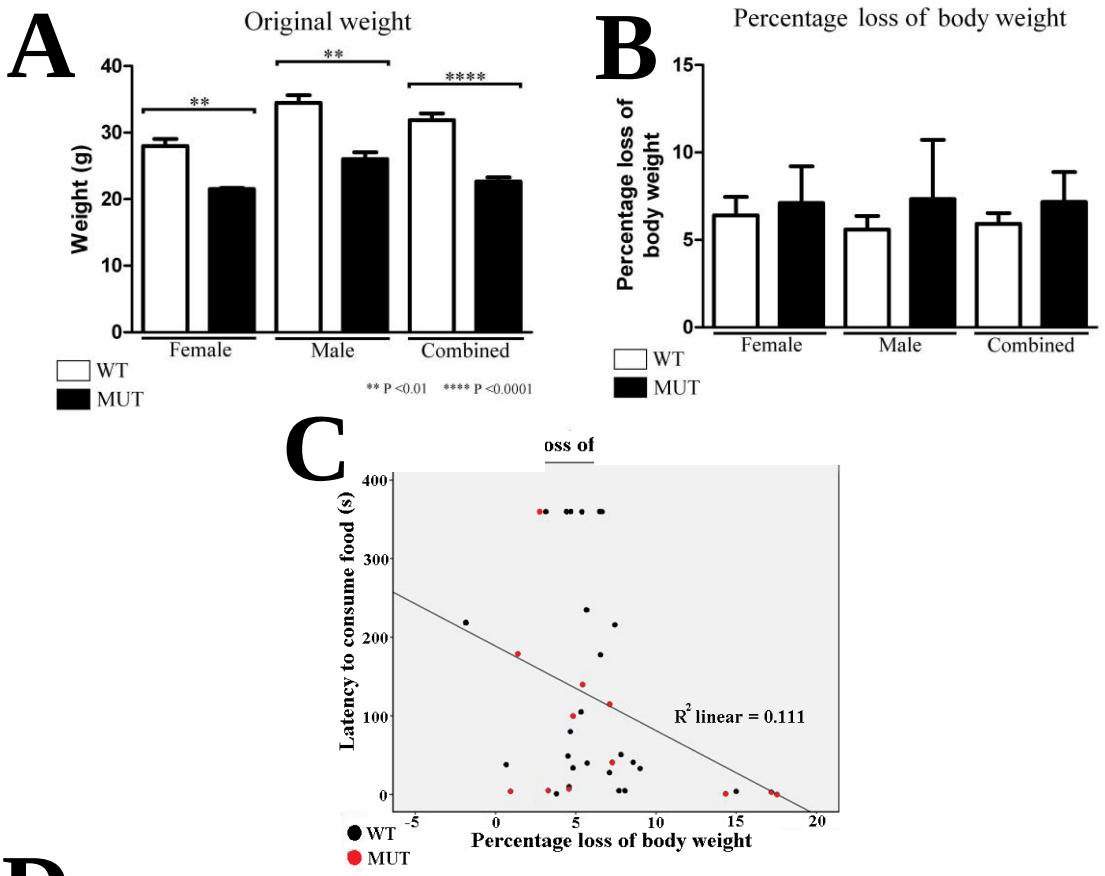
Beam breaks across experiment, mutant vs. WT (Paired T test)			
Comparison	**t (df)**	**P value**	**95% CI**
Combined	14.7 (23)	P<0.0001	+336.8 to +446.7
Cross-overs across experiment, mutant vs. WT (Paired T test)			
Comparison	**t (df)**	**P value**	**95% CI**
Combined	12.1 (23)	P<0.0001	+62.88 to +88.72
Total beam breaks, mutant vs. WT (ANOVA with Bonferroni MCT)			
Comparison	**F (df1, df2)**	**Adjusted P {unadjusted P}**	**95% CI**
Females	F (1, 18) = 50	P<0.0001 {P<0.000033}	+6041 to +12465
Males	F (1, 17) = 24.9	P<0.0001{P<0.000033}	+4570 to +13413
Combined	F (1, 36) = 88.3	P<0.0001{P<0.000033}	+6946 to +11856
Total cross-overs, mutant vs. WT (ANOVA with Bonferroni MCT)			
Comparison	**F (df1, df2)**	**Adjusted P {unadjusted P}**	**95% CI**
Female	F (1, 18) = 11.7	P<0.01 {P<0.0033}	+451 to +2730
Male	F (1, 17) = 14.7	P<0.001 {P<0.00033}	+882 to +4019
Combined	F (1, 36) = 26.4	P<0.0001 {P<0.000033}	+951 to +2693
Number of faecal boli, mutant vs. WT (ANOVA with Bonferroni MCT)			
Comparison	**F (df1, df2)**	**Adjusted P {unadjusted P}**	**95% CI**
Female	F (1, 18) = 4.8	P>0.05 = NS {P = 0.042}	+0.44 to -7.5
Male	F (1, 17) = 0	P>0.05 = NS {P = 0.98}	-5.346 to +5.612
Combined	F (1, 36) = 5.9	P>0.05 = NS {P = 0.02}	-0.03 to -6

Figure 54. *Paired T tests of beam breaks and cross-over rate across experiment (A, B). ANOVAs with Bonferroni MCT. Total number of beam breaks and cross-overs (C, D). Basal defecation rate (E). Statistical results table (F).* Total male n= 18 (3 *Whirligig* +/-, 15 WT); total female n= 19 (9 *Whirligig* +/-, 10 WT). *Error bars show SEM. Histogram summary: **P<0.01, ***P<0.001 ****P<0.0001*

Food neophobia

Whilst the EPM and OF use a sense of openness to induce anxiety, the food neophobia test measures the reluctance of a mouse to consume a novel food source in a novel environment (Deacon, 2011). Testing occurs after mice have been food deprived overnight. Consequently, the latency for a mouse to consume food reflects a balance between the incentive of hunger versus the disincentive of food novelty anxiety. The test was complicated by the fact that mutant mice are hyperactive and, as a result, substantially leaner than WT animals (**Figure 55. A, D**). Whilst the difference in proportion of body weight lost during overnight food deprivation was not significantly different between WT and mutant animals, the trend was of increased loss in the mutant (**Figure 55. B, D**). A higher latency to consume was found to correlate with a lower percentage loss of body weight (**Figure 55. C, D**). However, an ANCOVA found no significant difference in latency to consume between mutant (M = 122 s, SD = 37 s) and WT (M = 151 s, SD = 26 s) when percentage weight loss was taken as a covariant (P = 0.53).

Figure 55: No significant difference in food neophobia in *Whirligig* +/-



D

Statistics

Original weight, mutant vs. WT (ANOVA with Bonferroni MCT)			
Comparison	**F (df1, df2)**	**Adjusted P {unadjusted P}**	**95% CI**
Female	F (1, 18) = 12.5	P<0.01{P<0.0033}	+1.979 to -10.92
Male	F (1, 17) = 11.3	P<0.01 {P<0.0033}	-2.282 to -14.58
Combined	F (1, 36) = 43.9	P<0.0001 {P<0.000033}	-5.8 to -12.63
Percentage weight loss, mutant vs. WT (ANOVA with Bonferroni MCT)			
Comparison	**F (df1, df2)**	**Adjusted P {unadjusted P}**	**95% CI**
Female	F (1, 18) = 0.13	P>0.05 = NS {P = 0.72}	-4.07 to +5.49
Male	F (1, 17) = 0.41	P>0.05 = NS {P = 0.52}	-4.85 to +8.32
Combined	F (1, 36) = 0.71	P>0.05 = NS {P = 0.41}	-2.40 to +4.90
Latency to consume vs. percentage weight loss correlation (Pearson's correlation)			
Comparison	**R^2**	**P value**	**N**
All animals	0.111	0.05	37

Figure 55. *ANOVAs with Bonferroni MCT (A, B, C). Weight prior to food deprivation (A). Percentage weight loss from overnight food deprivation (B). XY scatter plot showing correlation (C). Statistical results table (D).* Total male n= 18 (3 *Whirligig* +/-, 15 WT); total female n= 19 (9 *Whirligig* +/-, 10 WT). *Error bars show SEM. Histogram summary: **P<0.01 ****P<0.0001*

Three chambered sociability box

The pattern of how mutant animals modulate their locomotory behaviour over the three test phases of the sociability box experiment differs from WT. As the basal activity rate and motion behaviour is significantly different between mutant and WT, it is not informative to make a direct comparison between the groups for any one phase of testing. However, modulation of activity between phases illustrates how mutants and WT response to changing social stimuli.

The three phases of the test differ in the number of objects and encaged stranger mice to which the test animal is exposed (**Figure 56. A**). Progressing from the habituation to the sociability phase, mutant animals display a significant reduction in average speed whilst WT animals displayed a near significant reduction (**Figure 56. B, C, H**). Additionally, the number of rotations in movement falls for both groups between the habituation and sociability phase. During the social novelty phase, the number of rotations returns to basal habituation levels for mutants but remains suppressed for WT (**Figure 56. D, E, H**).There is also a significant increase in freezing behaviour in WT animals between test phases which is not mirrored by a significant result in the mutant (**Figure 56. F, G**).

The results suggest that both groups modulate aspects of their motion behaviour when they first encounter a stranger mouse during the sociability phase. Unlike WT animals, the locomotory behaviour of the mutant animals during the social novelty phase is not significantly different to the habituation phase. This may suggest that the reaction elicited by mutant animals to social stimuli is more fleeting than in WT.

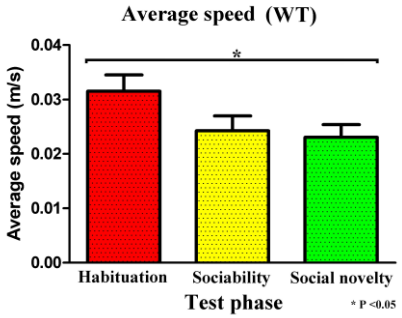
Figure 56: *Whirligig* and WT animals respond differently to social cues

A

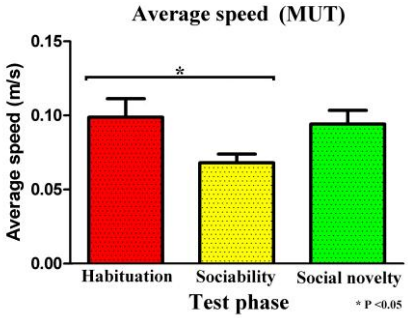
Test phases

Contents	1: Habituation	2: Sociability	3: Social novelty
Side A	Nothing	Caged mouse	Original caged mouse
Side B	Nothing	Empty cage	Novel caged mouse

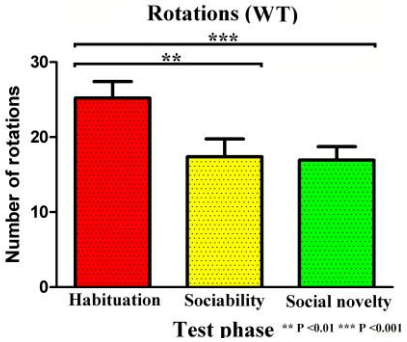
B



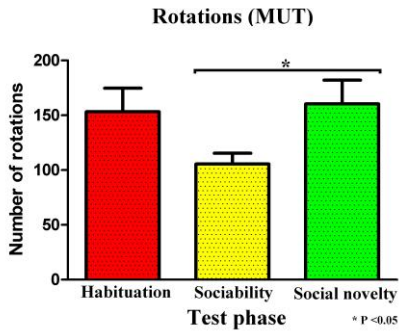
C



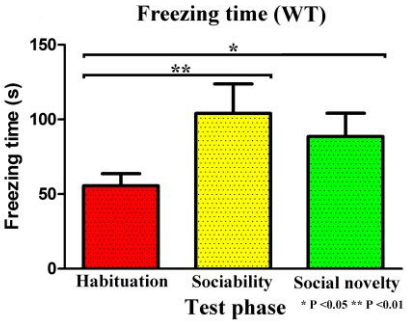
D



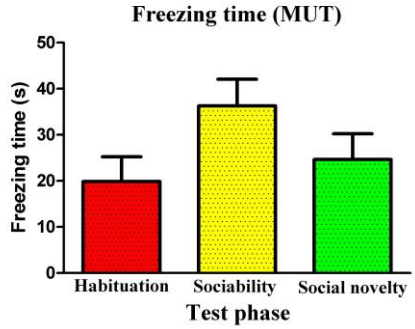
E



F



G



Please turn page for remainder of figure

H

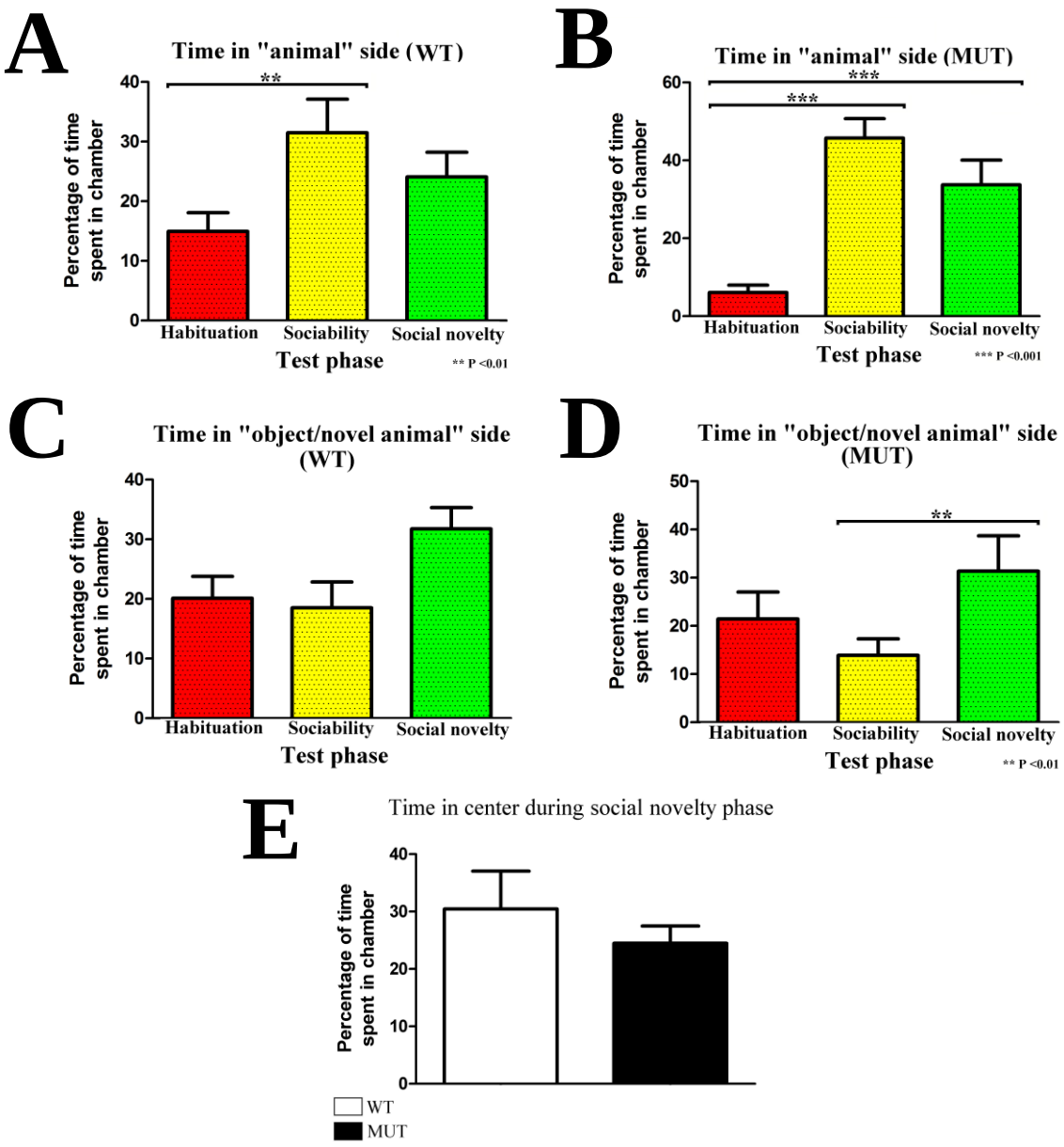
Statistics

Average speed (Repeated measures ANOVA with Tukey MCT)				
Group	**F (df1, df2)**	**q**	**Adjusted P {unadjusted P}**	**95% CI (m/s)**
Sociability vs. habituation phase				
WT	F (1, 14) = 4.9	3.14	P>0.05 = NS {P = 0.042}	+0.001 to -0.015
Mutant	F (1, 10) = 6.7	3.64	P<0.05 {P = 0.025}	-0.00058 to -0.061
Social novelty vs. habituation phase				
WT	F (1, 14) = 6.7	3.66	P<0.05 {P = 0.021}	-0.0004 to -0.0166
Mutant	F (1, 10) = 0.1	0.55	P>0.05 = NS {P = 0.76}	+0.026 to -0.035
Social novelty vs. sociability phase				
WT	F (1, 14) = 0.1	0.52	P>0.05 = NS {P = 0.76}	+0.007 to -0.009
Mutant	F (1, 10) = 4.8	3.1	P>0.05 = NS {P = 0.05}	+0.056 to -0.004
Number of rotations (Repeated measures ANOVA with Tukey MCT)				
Group	**F (df1, df2)**	**q**	**Adjusted P {unadjusted P}**	**95% CI**
Sociability vs. habituation phase				
WT	F (1, 14) = 15	5.48	P<0.01 {P = 0.0002}	-2.82 to -12.78
Mutant	F (1, 10) = 6.2	3.51	P>0.05 = NS {P = 0.031}	+0.88 to -96.15
Social novelty vs. habituation phase				
WT	F (1, 14) =16.9	5.81	P<0.001 {P = 0.001}	-3.28 to -13.25
Mutant	F (1, 10) = 0.1	0.53	P>0.05 = NS {P = 0.76}	-41.3 to +55.7
Social novelty vs. sociability phase				
WT	F (1, 14) = 0.1	0.33	P>0.05 = NS {P = 0.76}	+4.52 to -5.45
Mutant	F (1, 10) = 8.2	4.04	P<0.05 {P = 0.016}	+6.30 to +103.33
Time freezing (Repeated measures ANOVA with Tukey MCT)				
Group	**F (df1, df2)**	**q**	**Adjusted P {unadjusted P}**	**95% CI (s)**
Sociability vs. habituation phase				
WT	F (1, 14) =14.5	5.38	P<0.01 {P =0.002}	+16.93 to +80.12
Mutant	F (1, 10) = 2.1	2.97	P>0.05 = NS {P = 0.18}	+36.19 to -3.33
Social novelty vs. habituation phase				
WT	F (1, 14) = 6.7	3.66	P<0.05 {P = 0.022}	+1.39 to +64.58
Mutant	F (1, 10) = 0.4	0.87	P>0.05 = NS {P = 0.54}	-14.94 to +24.58
Social novelty vs. sociability phase				
WT	F (1, 14) = 1.5	1.72	P>0.05 = NS {P = 0.24}	+16.05 to -47.13
Mutant	F (1, 10) = 2.2	2.1	P>0.05 = NS {P =0.17}	+8.15 to -31.37

Figure 56. *Repeated measures ANOVAs with Tukey MCT. Summary of objects and mice to which test animal is exposed per phase (A). WT and mutant average speed per test phase (B, C). WT and mutant number of rotations per test phase (D, E). WT and mutant freezing time per test phase (F, G). Statistical results table (H).* Total male n= 18 (3 *Whirligig* +/-, 15 WT); total female n= 19 (9 *Whirligig* +/-, 10 WT). *Error bars show SEM. Histogram summary: *P<0.05 **P<0.01 ***P<0.001*

Over the different test phases, WT and mutant animals display a similar pattern in the time dedicated to exploring the central and side zones of the sociability box. During habituation, both WT and mutant animals spend the majority of their time in the central chamber. When the initial stranger animal is introduced during the sociability phase, animals exhibit a significant increase in exploring the "animal" side (**Figure 57. A, B**). In conjunction, both WT and mutants display a non significant increase in exploring the "object/novel animal side" when the second stranger mouse is introduced during the social novelty phase (**Figure 57. C, D**). Additionally, there is no significant difference in time spent in the central chamber during the social novelty phase between WT and mutants (**Figure 57. E**). This implies that neither group were actively avoiding entering the side chambers containing stranger mice.

Figure 57: Neither *Whirligig* +/- or WT animals avoid stranger mice



Please turn page for remainder of figure

F

Statistics

Percentage time in "animal" side (Repeated measures ANOVA with Tukey MCT)				
Group	**F (df1, df2)**	**q**	**Adjusted P {unadjusted P}**	**95% CI (s)**
Sociability vs. habituation phase				
WT	F (1, 14) =15.1	5.5	P<0.01 {P =0.001}	+6.01 to +27.06
Mutant	F (1, 10) =58.8	10.84	P<0.001 {P =0.00001}	+26.56 to +52.71
Social novelty vs. habituation phase				
WT	F (1, 14) = 4.6	3.04	P>0.05 = NS {P = 0.05}	-1.39 to +19.66
Mutant	F (1, 10) =28.6	7.56	P<0.001 {P = 0.0002}	+14.56 to +40.71
Social novelty vs. sociability phase				
WT	F (1, 14) = 3	2.46	P>0.05 = NS {P = 0.1}	+3.12 to -17.92
Mutant	F (1, 10) = 5.4	3.28	P>0.05 = NS {P = 0.04}	+1.08 to -25.08
Percentage time in "object/novel animal" side (Repeated measures ANOVA with Tukey MCT)				
Group	**F (df1, df2)**	**q**	**Adjusted P {unadjusted P}**	**95% CI (s)**
Sociability vs. habituation phase				
WT	F (1, 14) = 0.1	0.42	P>0.05 = NS {P = 0.76}	+11.64 to -14.84
Mutant	F (1, 10) = 2.1	2.04	P>0.05 = NS {P = 0.18}	+5.69 to -20.78
Social novelty vs. habituation phase				
WT	F (1, 14) = 4.7	3.07	P>0.05 = NS {P = 0.05}	-1.64 to +24.84
Mutant	F (1, 10) = 3.6	2.68	P>0.05 = NS {P = 0.08 }	-3.33 to +23.14
Social novelty vs. sociability phase				
WT	F (1, 14) = 6.1	3.49	P>0.05 = NS {P = 0.026}	-0.036 to +26.44
Mutant	F (1, 10) =11.1	4.72	P<0.01 {P =0.006}	+4.22 to +30.69
Percentage time in central chamber, mutant vs. WT (T test)				
t (df)		**P value**		**95% CI**
0.72 (25)		P>0.05 = NS		+10.90 to -22.86

Figure 57. *Percentage time spent in "animal" side per phase by WT and mutant respectively (A, B). Percentage time spent in "object/novel animal" side per phase by WT and mutant respectively (C, D). Time in central chamber during social novelty phase (E). Statistical results table (F). Total male n= 18 (3 Whirligig +/-, 15 WT); total female n= 19 (9 Whirligig +/-, 10 WT). Histogram summary: **P<0.01 ****P<0.0001*

Diminuendo behaviour

Choice of behavioural tests

Use of the OF and activity box was justified due to the overtly abnormal locomotion displayed by the homozygous mutant animals. Data from the OF was also used to assess anxiety levels. There was no histological basis for suspecting an anxiety defect would be present. However, as the data required for anxiety assessment was automatically collected by Ethovision software during locomotory assessment, an analysis of anxiety levels represented no additional effort.

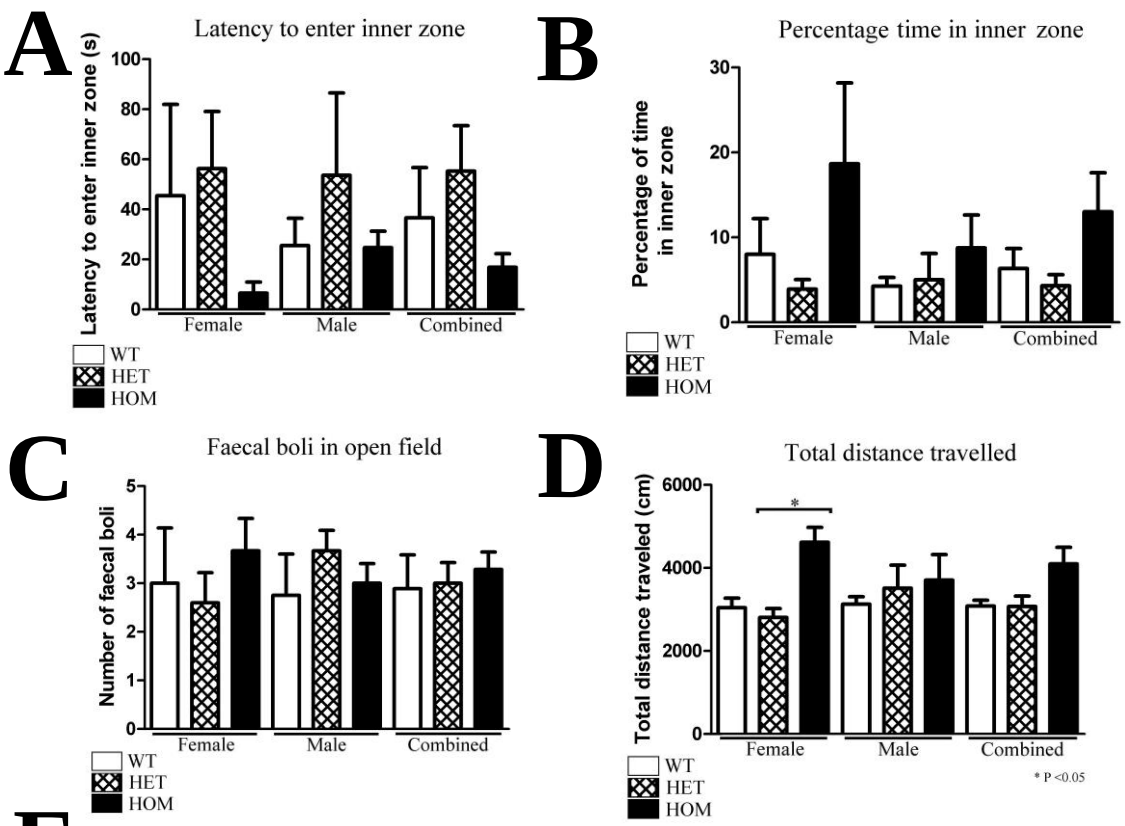
Additionally, as *Diminuendo* homozygotes feature an enlarged hippocampus, I selected tests that related to hippocampal function. Lesion studies have shown that the hippocampus is a critical structure involved in spatial reference memory (Morris, Garrud *et al.* 1982). Therefore, mice were tested in a Y maze paradigm designed to reveal reference memory defects (Sanderson *et al.*, 2007). The complex labyrinth maze was then used to determine if positive findings from the Y maze could be explained by a loss of explorative drive.

Open field

OF testing in the *Diminuendo* line suggest no significant difference in anxiety levels between WT, heterozygous and homozygous mutant animals. No significant difference was found for latency to enter inner zone, percentage time spent in inner zone or in defecation rate ($F<1$, unadjusted $P>0.05$) (**Figure 58. A, B, C**).

There was a significant difference in total distance travelled in the OF maze by homozygous females relative to heterozygous animals ($P<0.01$) but this signal was borderline significant when data from both sexes was combined (**Figure 58. D, E**). Total distance travelled between homozygous and WT groups were also borderline significantly different (**Figure 58. E**)

Figure 58: Open field suggest WT anxiety levels in *Diminuendo*



E

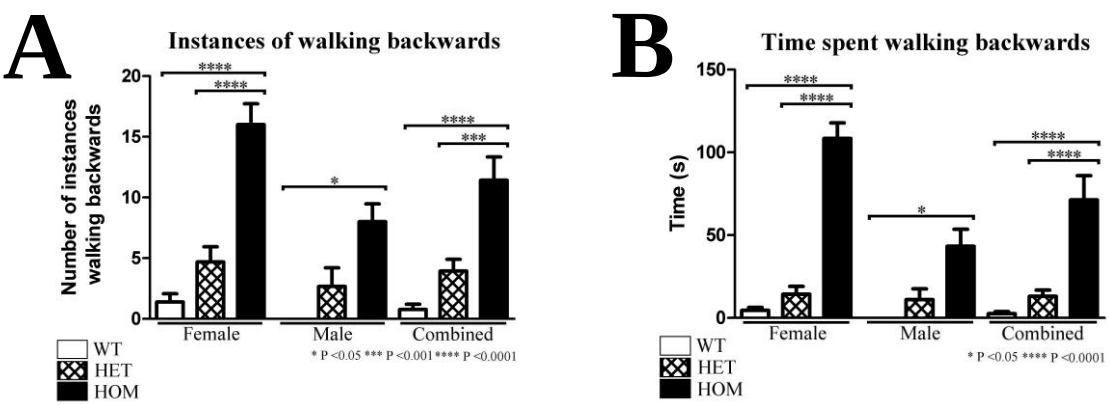
Total distance travelled statistics

Total distance travelled (ANOVA with Bonferroni MCT)			
Hom vs. WT			
Comparison	**F (df1, df2)**	**Adjusted P {unadjusted P}**	**95% CI (cm)**
Females	F (1, 7) = 5.9	P>0.05 = NS {P = 0.045}	-297 to +3446
Males	F (1, 7) = 0.85	P>0.05 = NS {P = 0.38}	-1233 to +2391
Combined	F (1, 24) = 5.16	P>0.05 = NS {P = 0.032}	-275 to +2308
Het vs. WT			
Comparison	**F (df1, df2)**	**Adjusted P {unadjusted P}**	**95% CI (cm)**
Females	F (1, 12) = 9.57	P<0.01 {P<0.0011}	+121.7 to +3496
Males	F (1, 11) = 0.45	P>0.05 = NS {P = 0.53}	-1269 to +2040
Combined	F (1, 24) =6.48	P>0.05 = NS {P = 0.0177}	-137 to +2186
Hom vs. Het			
Comparison	**F (df1, df2)**	**Adjusted P {unadjusted P}**	**95% CI (cm)**
Females	F (1, 12) = 9.57	P<0.01 {P<0.0011}	+121.7 to +3496
Males	F (1, 11) = 0.11	P>0.05 = NS {P = 0.75}	-1461 to +1847
Combined	F (1, 24) = 6.48	P>0.05 = NS {P = 0.0177}	-137 to +2186

Figure 58. *ANOVA with Bonferroni MCT. Latency to enter inner zone (A). Percentage time spent in inner zone (B). Defecation rate during experiment (C). Total distance travelled by mice during experiment (D). Travelled distance statistical results table (E). Total n = 32 (WT =9 (4M, 5F); Het =16 (6M, 10F); Hom = 7 (4M, 3F). Error bars show SEM. Histogram summary: *P<0.05*

Homozygous animals also exhibit a characteristic backwards walk. The number of instances of backwards walking is significantly higher than in WT (**Figure 59. A, C).** Total time spent walking backwards is also significantly higher (**Figure 59. B, C**). When data for both sexes is pooled, the homozygous animals spend ~1 minute, twenty percent of test time, walking backwards. There is also a possible intermediate phenotype in heterozygous animals, although there is insufficient power to drive a significant result (Het vs. WT, Instances of walking backwards, P =0.039 before adjusting for multiple comparisons) (**Figure 59. C)**.

Figure 59: *Diminuendo* homozygotes display backwards walking motion



C

Statistics

Instances of walking backwards (ANOVA with Bonferroni MCT)			
Hom vs. WT			
Comparison	**F (df1, df2)**	**Adjusted P {unadjusted P}**	**95% CI**
Female	F (1, 7) = 33.36	P<0.0001 {P<0.000011}	+7.3 to +21.9
Male	F (1, 7) = 10.69	P<0.05 {P<0.0056}	+0.94 to +15.06
Combined	F (1, 15) =37.21	P<0.0001 {P<0.000011}	+5.6 to +15.69
Het vs. WT			
Comparison	**F (df1, df2)**	**Adjusted P {unadjusted P}**	**95% CI**
Female	F (1, 14) = 3	P>0.05 =NS {P = 0.11}	-2.17 to +8.77
Male	F (1, 9) = 1.4	P>0.05 =NS {P = 0.27}	-3.78 to +9.12
Combined	F (1, 22) = 4.8	P>0.05 =NS {P = 0.039}	-1 to +7.3
Hom vs. Het			
Comparison	**F (df1, df2)**	**Adjusted P {unadjusted P}**	**95% CI**
Female	F (1, 12) = 24.6	P<0.0001 {P<0.000011}	+4.72 to +17.88
Male	F (1, 9) = 5.7	P>0.05 =NS {P = 0.04}	-1.12 to +11.78
Combined	F (1, 22) = 22.8	P<0.001 {P<0.00011}	+2.963709 to +12.01843
Time spent walking backwards (ANOVA with Bonferroni MCT)			
Hom vs. WT			
Comparison	**F (df1, df2)**	**Adjusted P {unadjusted P}**	**95% CI (s)**
Female	F (1, 7) = 62	P<0.0001 {P<0.000011}	+66 to +142
Male	F (1, 7) = 11.6	P<0.05 {P<0.0055}	+6.6 to +80.1
Combined	F (1, 15) =57.5	P<0.0001 {P<0.000011}	+42.55 to +94.92
Het vs. WT			
Comparison	**F (df1, df2)**	**Adjusted P {unadjusted P}**	**95% CI (s)**
Female	F (1, 14) = 1	P>0.05 = NS {P = 0.33}	-18.77 to +38.16
Male	F (1, 9) = 0.9	P>0.05 = NS {P = 0.37}	-22.48 to +44.61
Combined	F (1, 22) = 2	P>0.05 = NS {P = 0.17}	-11.13 to +32.18
Hom vs. Het			
Comparison	**F (df1, df2)**	**Adjusted P {unadjusted P}**	**95% CI (s)**
Female	F (1, 12) = 63.2	P<0.0001 {P<0.000011}	+60.02 to +128.44
Male	F (1, 9) = 7.2	P>0.05 = NS {P = 0.025}	-1.26 to +65.83
Combined	F (1, 22) = 50.9	P<0.0001 {P<0.000011}	+34.65879 to +81.75424

Please turn page for remainder of figure ⟶

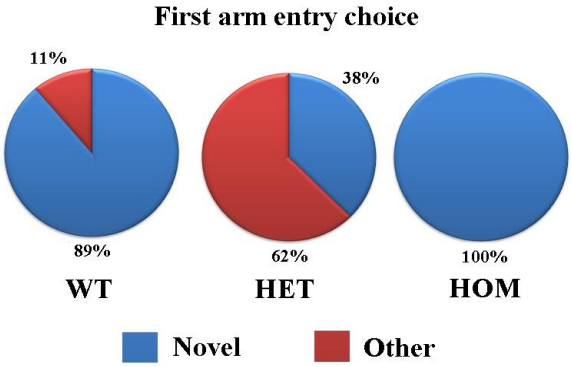
Figure 59. *ANOVAs with Bonferroni MCT. Instances of backwards walking (A). Total time spent walking backwards during experiment (B). Statistical results table (C). Total n = 32 (WT =9 (4M, 5F); Het =16 (6M, 10F); Hom = 7 (4M, 3F). Error bars show SEM. Histogram summary: *P<0.05 ***P<0.001 ****P<0.0001*

Y maze

The Y maze suggests that heterozygous *Diminuendo* mutants have a defective spatial reference memory. WT animals display a strong novelty preference and explore novel areas over other areas recollected as familiar. Of the WT animals tested, 89% chose the novel arm as their first choice for exploration upon being returned to the maze after habituation. Similarly, this value was 100% in the homozygous animals. This contrasts with only 38% of heterozygous animals (chi-square= 12.1, df = 2, $P<0.01$) (**Figure 60**). Consequently, heterozygous animals may be unable to differentiate between the previously explored arm versus the novel arm.

Figure 60: *Diminuendo* hets display no first entry novelty preference

A



B

Genotype	First arm entry choice		Total
	Novel	Other	
WT*	8	1	**9**
HET**	6	10	**16**
HOM***	**8**	**0**	**8**
Total	**24**	**11**	**33**
Statistical analysis			
Chi-square			**P <0.01**

* WT female/male: 4/5 and 4/4 choose novel ** HET female/male: 4/10 and 2/6 choose novel
*** HOM female/male: 4/4 and 4/4 choose novel

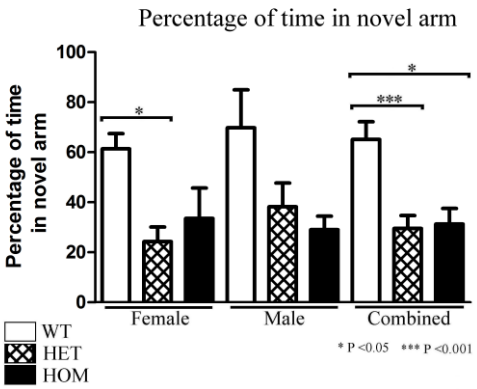
Figure 60. *Pie chart of first choice (A). Chi-square table shows significant difference (B).*

Total n = 33 (WT =9 (4M, 5F); Het =16 (6M, 10F); Hom = 7 (4M, 4F).

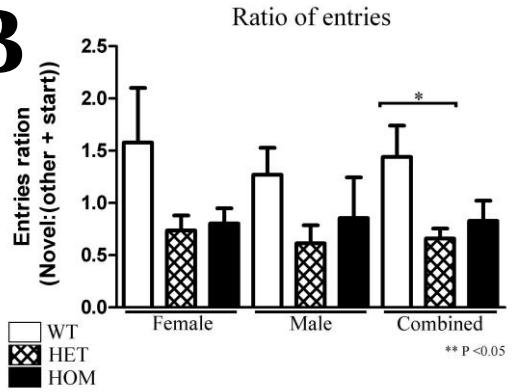
WT mice spend approximately two thirds of their time exploring the novel arm suggesting efforts are focused on searching the novel arm at the expense of the familiar arms. In contrast, both heterozygous and homozygous mutants spend only one third of their time exploring the novel arm (**Figure 61. A, C**). This is in line with the proportion of the total maze area taken up by the arm. The ratio of entries also shows that WT animals preferentially visit the novel arm whilst both heterozygous and homozygous mutants visit each arm in an approximately equal fashion (**Figure 61. B, C**). This data further supports a reference memory defect in the heterozygotes. As all homozygous animals preferentially entered the novel arm first upon reintroduction to the maze, the subsequent lack of exploration of the arm may suggest a rapid loss of explorative drive or a lesser degree of memory impairment. I have suggested additional tests in the future work section of this chapter that are designed to clarify why the difference in Y maze first preference behaviour between homozygous and heterozygous animals may occur.

Figure 61: Reduced exploration of Y maze novel arm by *Diminuendo*

A



B



C

Statistics

Percentage time in novel arm (ANOVA with Bonferroni MCT)			
Hom vs. WT			
Comparison	**F (df1, df2)**	**Adjusted P {unadjusted P}**	**95% CI**
Female	F (1, 14) = 4.1	P>0.05 = NS {P = 0.062}	+11.67 to -67.47
Male	F (1, 9) = 7.9	P>0.05 = NS {P = 0.02}	+0.96 to -82.46
Combined	F (1, 24) = 11.6	P<0.05 {P<0.0055}	-5.2 to -62.52
Het vs. WT			
Comparison	**F (df1, df2)**	**Adjusted P {unadjusted P}**	**95% CI**
Female	F (1, 14) = 10.9	P<0.05 {P<0.0055}	-4.79 to -69.41
Male	F (1, 9) = 5.7	P>0.05 = NS {P = 0.04}	+6.49 to -69.66
Combined	F (1, 24) = 17.4	P<0.001 {P<0.00011}	-11.03 to -60.19
Hom vs. Het			
Comparison	**F (df1, df2)**	**Adjusted P {unadjusted P}**	**95% CI**
Female	F (1, 14) = 0.6	P>0.05 = NS {P = 0.45}	-25.7 to +44.1
Male	F (1, 9) = 0.5	P>0.05 = NS {P = 0.5}	-47.24 to +28.91
Combined	F (1, 24) = 0.04	P>0.05 = NS {P = 0.84}	-23.79 to +27.29
Ratio of entries (Novel:(Start + Other)) (ANOVA with Bonferroni MCT)			
Hom vs. WT			
Comparison	**F (df1, df2)**	**Adjusted P {unadjusted P}**	**95% CI (s)**
Female	F (1, 14) = 3.5	P>0.05 = NS {P = 0.082}	+0.42 to -1.97
Male	F (1, 9) = 0.9	P>0.05 = NS {P = 0.37}	+0.85 to -1.68
Combined	F (1, 24) = 4.1	P>0.05 = NS {P =0.054}	+0.25 to -1.48
Het vs. WT			
Comparison	**F (df1, df2)**	**Adjusted P {unadjusted P}**	**95% CI (s)**
Female	F (1, 14) = 6.2	P>0.05 = NS {P = 0.026}	+0.14 to -1.82
Male	F (1, 9) = 2.7	P>0.05 = NS {P = 0.13}	+0.49 to -1.8
Combined	F (1, 24) = 9.2	P<0.05 {P<0.0055}	-0.04 to -1.53
Hom vs. Het			
Comparison	**F (df1, df2)**	**Adjusted P {unadjusted P}**	**95% CI (s)**
Female	F (1, 14) = 0.03	P>0.05 = NS {P = 0.86}	-0.9899 to +1.121
Male	F (1, 9) = 0.4	P>0.05 = NS {P = 0.54}	-0.9099 to +1.393
Combined	F (1, 24) = 0.4	P>0.05 = NS {P = 0.53}	-0.6031 to +0.9419

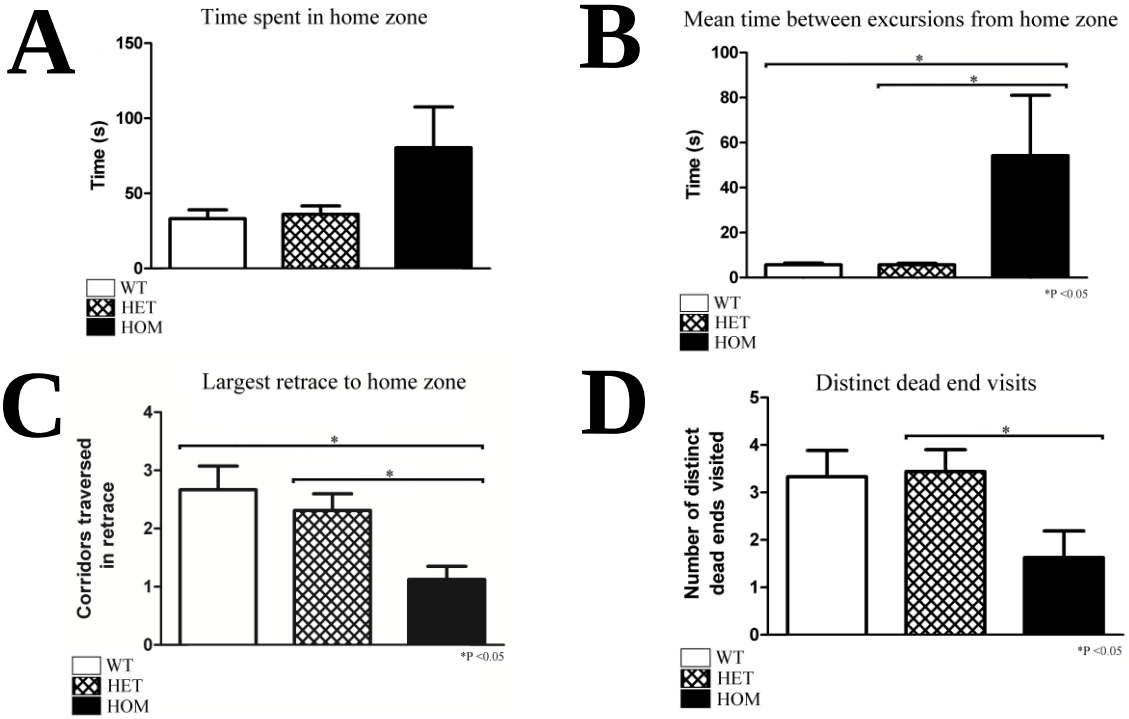
Please turn page for remainder of figure

Figure 61. *ANOVAs with Bonferroni MCT. Percentage time in arm results for females, males and combined sexes respectively (A). Novel:(Start + Other) arm entries ratio (B). Statistical results table (C). Total n = 32 (WT =9 (4M, 5F); Het =16 (6M, 10F); Hom = 7 (4M, 3F). Error bars show SEM. Histogram summary: *P<0.05 **P<0.01 ***P<0.001*

Complex labyrinth maze

The complex labyrinth maze was used to assess explorative behaviour in order to aid interpretation of the Y maze results. The results suggest no significant difference between WT and heterozygous animals. In contrast, homozygous *Diminuendo* mutants are less eager to actively explore the maze. Homozygous mutants spend more time in the home zone where they were initially introduced, although this does not reach significance after MCT adjustment (**Figure 62. A, E**). The homozygous mutants also spend a significantly longer time in the home zone between excursions ($P<0.05$) (**Figure 62. B, E**). They also travel a significantly shorter distance before returning to the home zone ($P<0.05$) (**Figure 62. C, E**). As a consequence, homozygous animals visit significantly less distinct dead ends within the maze than heterozygous animals (**Figure 62. D, E**). The difference versus WT is nears significance but lacks power.

Figure 62: Exploration reduced in *Diminuendo* homozygotes



E

Statistics

Time spent in home zone (ANOVA with Bonferroni MCT)			
Comparison	**F (df1, df2)**	**Adjusted P {unadjusted P}**	**95% CI (s)**
Hom vs. WT	F (1, 16) = 5.5	P>0.05 = NS {P = 0.032}	-3.655 to +98.12
Het vs. WT	F (1, 24) = 0.03	P>0.05 = NS {P = 0.86}	-40.74 to +46.54
Hom vs. Het	F (1, 23) = 6.1	P>0.05 = NS {P = 0.021}	-1.012 to +89.69
Mean time between excursions from home zone (ANOVA with Bonferroni MCT)			
Comparison	**F (df1, df2)**	**Adjusted P {unadjusted P}**	**95% CI (s)**
Hom vs. WT	F (1, 16) = 7.38	P<0.05 {P<0.016}	+3.23 to +93.74
Het vs. WT	F (1, 24) = 0.01	P>0.05 = NS {P = 0.98}	-38.77 to +38.84
Hom vs. Het	F (1, 23) = 9.3	P<0.05 {P<0.016}	+8.12 to +88.78
Largest retrace to home zone (ANOVA with Bonferroni MCT)			
Comparison	**F (df1, df2)**	**Adjusted P {unadjusted P}**	**95% CI (corridors traversed)**
Hom vs. WT	F (1, 16) = 6.6	P<0.05 {P<0.016}	-0.22 to -2.86
Het vs. WT	F (1, 24) = 0.6	P>0.05 = NS {P = 0.44}	+0.78 to -1.48
Hom vs. Het	F (1, 23) = 8.8	P<0.05 {P<0.016}	-0.01 to -2.36
Number of distinct dead ends visited (ANOVA with Bonferroni MCT)			
Comparison	**F (df1, df2)**	**Adjusted P {unadjusted P}**	**95% CI (dead ends)**
Hom vs. WT	F (1, 16) = 4.04	P>0.05 = NS {P = 0.062}	+0.45 to -3.86
Het vs. WT	F (1, 24) = 0.02	P>0.05 = NS {P = 0.88}	+1.95 to -1.74
Hom vs. Het	F (1, 23) = 5.7	P>0.05 = NS {P = 0.026}	+0.11 to -3.73

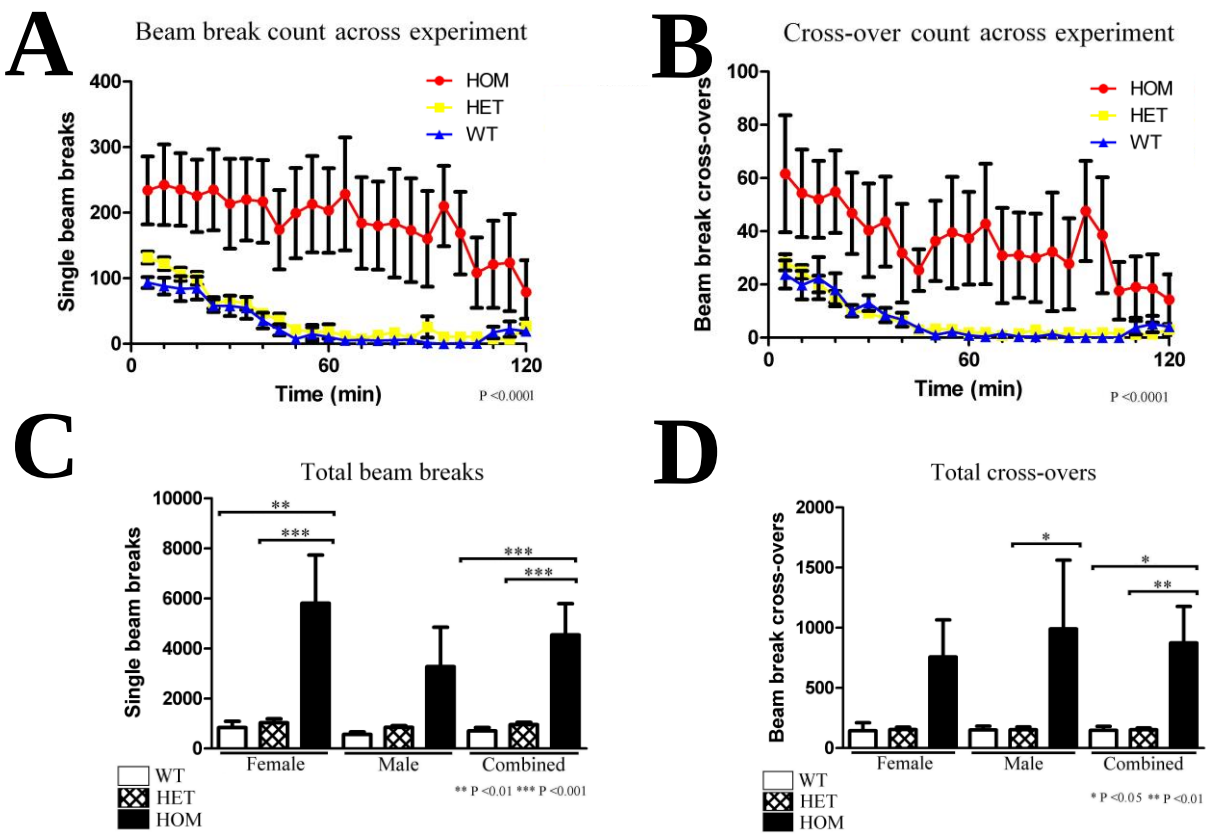
Please turn page for remainder of figure →

Figure 62. *ANOVAs with Bonferroni MCT. Time spent in home zone (A). Time between excursions from home zone (B). Largest retrace to home (C). Total number of distinct dead end (D). Statistical results table (E). Total n = 32 (WT =9 (4M, 5F); Het =16 (6M, 10F); Hom = 7 (4M, 3F). Error bars show SEM. Histogram summary: *P<0.05*

Activity box

The photonic locomotion activity box suggests homozygous animals are significantly more active than WT and heterozygous animals. For all groups, activity is typically highest at the beginning of the experiment and subsequently falls as mice become more familiar with the test cage environment. However, unlike WT and heterozygous animals, homozygous animals do not become sedentary at any point during testing (**Figure 63. A, B**). As a consequence, homozygous animals have significantly higher counts for total beam breaks (Females, $P<0.01$; Combined, $P<0.001$) and total cross-overs (Combined, $P<0.05$) (**Figure 63. C, D, E**).

Figure 63: Activity box shows *Diminuendo* homozygotes are hyperactive



Please turn page for remainder of figure

E

Statistics

Beam break count per 5 minute interval (Repeated measures ANOVA with Bonferroni)			
Comparison	**F (df1, df2)**	**Adjusted P {unadjusted P}**	**95% CI**
Hom vs. WT	F (1, 23) = 543	P<0.0001 {P<0.000033}	+143.8 to +175.7
Het vs. WT	F (1, 23) = 2.6	P>0.05 = NS	+5.55 to -26.29
Hom vs. Het	F (1, 23) = 541	P<0.0001 {P<0.000033}	+133 to +165
Cross over count per 5 minute interval (Repeated measures ANOVA with Bonferroni)			
Comparison	**F (df1, df2)**	**Adjusted P {unadjusted P}**	**95% CI**
Hom vs. WT	F (1, 23) = 399	P<0.0001 {P<0.000033}	+26.53 to +34.06
Het vs. WT	F (1, 23) = 0.03	P>0.05 = NS	+3.50 to -4.02
Hom vs. Het	F (1, 23) = 393	P<0.0001 {P<0.000033}	+27 to +34
Total beam breaks (Hom vs. WT) (ANOVA with Bonferroni MCT)			
Comparison	**F (df1, df2)**	**Adjusted P {unadjusted P}**	**95% CI**
Hom vs. WT			
Female	F (1, 7) = 15.6	P<0.01 {P<0.0011}	+1330.77 to +8600.73
Male	F (1, 7) = 4.6	P>0.05 = NS {P = 0.069}	-933.22 to +6336
Combined	F (1, 15) = 18.6	P<0.001 {P<0.0011}	+1263.43 to +6404.07
Het vs. WT			
Female	F (1, 12) = 0.03	P>0.05 = NS {P = 0.87}	-2894.58 to +3283.69
Male	F (1, 9) = 0.06	P>0.05 = NS {P = 0.81}	-3036.68 to +3599.85
Combined	F (1, 22) = 0.1	P>0.05 = NS {P = 0.75}	-2001.58 to +2499.53
Hom vs. Het			
Female	F (1, 12) = 19.9	P<0.001 {P<0.00011}	+1682.06 to +7860.33
Male	F (1, 9) = 4.1	P>0.05 = NS {P = 0.073}	-898.1 to +5738.43
Combined	F (1, 22) = 21.1	P<0.001 {P<0.00011}	+1334.22 to +5835.33
Total cross-overs (Hom vs. WT) (ANOVA with Bonferroni MCT)			
Comparison	**F (df1, df2)**	**Adjusted P {unadjusted P}**	**95% CI**
Hom vs. WT			
Female	F (1, 7) = 3.8	P>0.05 = NS {P = 0.09}	-294.41 to +1522.41
Male	F (1, 7) = 7.1	P>0.05 = NS {P = 0.03}	-68.4 to +1748.41
Combined	F (1, 15) = 10.7	P<0.05 {P<0.0056}	+84.66 to +1369.34
Het vs. WT			
Female	F (1, 12) = 0.01	P>0.05 = NS {P = 0.92}	-761.61 to +782.39
Male	F (1, 9) = 0.01	P>0.05 = NS {P = 0.92}	-827.59 to +830.93
Combined	F (1, 22) = 0.01	P>0.05 = NS {P = 0.92}	-556.23 to +568.63
Hom vs. Het			
Female	F (1, 12) = 5.1	P>0.05 = NS {P = 0.058}	-168.39 to +1375.61
Male	F (1, 9) = 8.5	P<0.05{P<0.0056}	+9.07 to +1667.59
Combined	F (1, 22) = 13.7	P<0.01 {P<0.0011}	+158.37 to +1283.23

Figure 63. *Repeated measures ANOVA of beam breaks and cross-over rate across experiment (A, B). ANOVAs with Bonferroni MTC for total number of beam breaks and cross-overs (C,D). Statistical results table (E). Total n = 32 (WT =9 (4M, 5F); Het =16 (6M, 10F); Hom = 7 (4M, 3F). Error bars show SEM. Histogram summary: *P<0.05 **P<0.01, ***P<0.001 ****P<0.0001*

Future work plans for *Diminuendo* and *Whirligig*

In order to strengthen reliability, the experiments should be repeated using a minimum of ten animals per genotype per sex. This would allow for a more robust assessment of the extent to which sex influences the behavioural manifestations of the *Whirligig* and *Diminuendo* mutations.

Additionally, I would conduct two further behavioural tests to gain greater insight into the putative memory/navigation defects present in both lines. First, I would perform a modified Morris water maze experiment to test for spatial learning in a paradigm reliant on extra-maze olfactory cues (Vorhees and Williams, 2006). For each mouse tested, the protocol involves the following. A circular tank filled with 3cm of water. This shallow depth is required to negate the risk of *Whirligig* and *Diminuendo* mice drowning due to their respective locomotory defects. Within the maze there is a platform hidden just above water level. This platform can be mounted allowing mice to escape the water. Distinctive olfactory cues are placed around the perimeter of the maze in fixed positions. These serve as landmarks and allow the mouse to learn the relative position of the hidden platform. Olfactory cues must be used as mice are blind due to their C3H background (Nagy and Misanin, 1970). Sound cues are also not suitable as *Whirligig* and *Diminuendo* mice are deaf (Lewis *et al.*, 2009, Bosman *et al.*, 2005). A previous study by Bergman and colleagues suggest *Whirligig* mutants feature a weakened sense of smell (Bergman *et al.*, 2010). However, the severity of this suggested impairment was mild. Consequently, olfactory cues of sufficiently strong aroma should suffice as landmarks.

Mice should be tested in the maze in two phases. The first phase represents a series of trials in which the mouse is placed in the maze and the time taken to navigate to the platform measured. If mice are able to learn the position of the platform relative to the olfactory landmarks, then the time taken to reach the platform will decline over repeated trials

(Vorhees and Williams, 2006). The rate at which platform discovery time improves between successive trials reflects a mouse's learning ability. If the trend in the reduction of platform discovery time is delayed or weakened between trials it suggests a degree of learning impairment. The second phase of the experiment involves retesting the mouse with the platform removed. The time taken futilely searching for the platform in its former location should then be measured. Mice that have learned the former position of the platform will focus their search efforts in that quadrant of the maze. Mice with poorer recollections of the position of the platform will search a larger, more imprecise, area.

This water maze test paradigm has major advantages over the Y maze test. The unpleasant nature of the water incentivises mice to navigate to the best of their ability in order to escape. This avoids the problem of low explorative drive that could lead to a mouse performing abnormally in the Y maze despite having a functioning memory. The trend in platform discovery time in the water maze is also more informative about the dynamics of memory impairment allowing more questions to be addressed: are mutant mice able to learn the location of the platform but at a slower rate?; if the interval between trails is extended does this negate improvements in platform discovery time?

Second, I would also perform a modified version of the passive avoidance test described by Moriarty and colleagues (Moriarty *et al.,* 2012). The passive avoidance test is a classical fear conditioning paradigm that assesses learning and memory resulting from an adverse experience. My modified method would involve placing a mouse in a chamber containing zones of smooth floor surface and rough textured floor surface. These rough floor surface zones would be enriched with lemon odour in order to make them particularly distinct. If a mouse remains on a rough textured zone for more than a second it would be shot from below with an air puff. Consequently, the test would assess if *Whirligig* and *Diminuendo* mice featured a delay in learning to associate the rough textured zones with

punishment. After a rest period of one week, the animals could also be returned to the test chamber. If mice continued to avoid the rough zones it would suggest the association with air puffs was retained in memory. If the rough zones were not avoided it would suggest long term memory impairment.

Additionally, I would conduct further histological tests in *Whirligig* and *Diminuendo* with the aim of providing an underlying biological basis for their respective aberrant behaviours. For Whirligig, I would perform a Gallyas stain (using the protocol described in **chapter 2**). The presence of corpus callosum agenesis in Whirligig is suggestive of an axonal guidance defect and it would be prudent to stain myelinated fibre tracts throughout the brain so irregularities could be detected. Gallyas staining would achieve this. For both *Whirligig* and *Diminuendo,* I would perform a Golgi stain and a transmission electron microscopy investigation of the hippocampal ultrastructure. The Golgi stain would allow for the morphology and density of synaptic spines to be quantified. Electron microscopy of the hippocampus would further highlight any alterations to synapse bouton morphology, vesicle trafficking or axonal myelination. Increased understanding of the neuropathology in *Whirligig* may provide insight into the potential mechanisms underlying CHARGE syndrome associated mental retardation. Additionally, it is important to assess why the homozygous *Diminuendo* hippocampus is enlarged. Does it reflect an increase in neurogenesis or a decrease in cell death? To assess these, I would immunostain *Diminuendo* brain sections for Ki67 (a neurogenesis marker) and Caspase-3 (an apoptosis marker).

Summary

In this chapter, I have shown that *Whirligig* +/- mutants feature corpus callosum agenesis. Corpus callosum agenesis has been reported in human CHARGE syndrome patients although its incidence is unclear (Fernell *et al.*, 1999). My behavioural test results suggest that *Whirligig* +/- mice exhibit phenotypes associated with CHARGE syndrome; reduced anxiety, hyperactivity, repetitive behaviour, cognitive impairment and abnormal sociability.

I have also shown that the *Diminuendo* line display anatomical and behavioural abnormalities. Homozygous mutants feature a significantly enlarged hippocampus, display a backwards walking phenotype, and are hyperactive. Y maze testing suggests that both homozygous and heterozygous mutants have impaired spatial reference memory. However, results from the complex labyrinth maze suggest that homozygous mutants also feature a weak explorative drive which may potentially have influenced the Y maze results. Consequently, further tests are required to assess memory and navigation ability in the diminuendo mutants. A summary of all behavioural tests shown in this chapter is given in **Figure 64**.

Figure 64: Summary of behavioural tests and findings

Whirligig	
Test	**Finding**
Elevated plus maze	*Whirligig* animals are significantly less anxious; they spend more time in the open arms and defecate significantly less than WT.
Open field	*Whirligig* animals are significantly less anxious; the spend significantly more time in the centre of the open field maze and defecate significantly less than WT.
Y maze	*Whirligig* animals have a memory defect; unlike WT, they do not preferentially explore the novel arm of the maze.
Activity box	*Whirligig* mice are significantly more active.
Food neophobia	*Whirligig* mice are not significantly different to WT.
Three chamber sociability box	*Whirligig* mice motion behaviour returns to basal levels before WT. This suggests that *Whirligig* mutants become disinterested in stranger mice at a faster rate.
Diminuendo	
Test	**Finding**
Open field	*Diminuendo* mutants have an anxiety level comparable to WT. Homozygous *Diminuendo* mutants feature a backwards walking phenotype.
Y maze	Unlike WT, both homozygous and heterozygous *Diminendo* mutants do not preferentially spend more time exploring the novel arm. This is consistent with a memory defect. Additionally, only 38% of the heterozygous mice visit the novel arm as their first exploration choice upon being returned to the maze. This further supports the presence of a memory defect in the heterozygous mutants. However, homozygous animals always visited the novel arm as their first exploration choice, suggesting their memory is not impaired. Consequently, more experiments are required to verify if homozygous mice feature a memory defect or if the results are due to another factor such as explorative drive or navigation ability.
Complex labyrinth maze	Homozygous *Diminuendo* mutants have a significantly reduced explorative drive.
Activity Box	*Diminuendo* mutants are significantly more active than WT.

Figure 64. *Summary table of tests and findings.*

Chapter 6

Additional Anatomical Assessment of The ENU Derived *Jenna* Mouse

An analysis of the superior colliculus

Introduction

In this chapter, I present neuroanatomical findings consistent with an aberrant behavioural phenotype in the *Jenna* mouse. *Jenna* mutants are heterozygous for an ENU induced S140G mutation in *Tuba1* which leads to disrupted hippocampal neuronal migration and architecture. The line was discovered during a previous ENU screen which focused on behavioural phenotyping (Keays *et al.*, 2007). In addition to hyperactivity, low anxiety and poor working memory, *Jenna* mutants feature an exaggerated acoustic startle response (ASR) (Keays, 2005, Keays *et al.*, 2007). I conducted an anatomical analysis of the superior colliculus, an area previously linked to the ASR (Meloni and Davis, 2000, Koch, 1999, Davis *et al.*, 1982). For example, infusion of bicuculline, a $GABA_a$ antagonist, into the deep layers of the superior colliculus has previously been shown to enhance the ASR (Meloni and Davis, 2000). My findings report abnormalities in gross morphology, myeloarchitecture and neuronal migration in the *Jenna* mouse superior colliculus. I also present evidence of progressive cell death which is especially pronounced in the deep layers.

Structural defects in *Jenna* mouse superior colliculus

Gross structure

The superior colliculus of *Jenna* mutants is less enveloped by cortex than control animals making it appear more exposed on the brain surface (**Figure 65. A**). Sagittal Nissl stained sections reveal that it is elongated in the rostral-caudal plane (**Figure 65. B, C**). Additionally, coronal sections demonstrates that it is significantly thinner that WT littermates both at P0 and 12 weeks of age (P<0.0001) (**Figure 66.**).

Figure 65: Increased superior colliculus exposure and length in *Jenna*

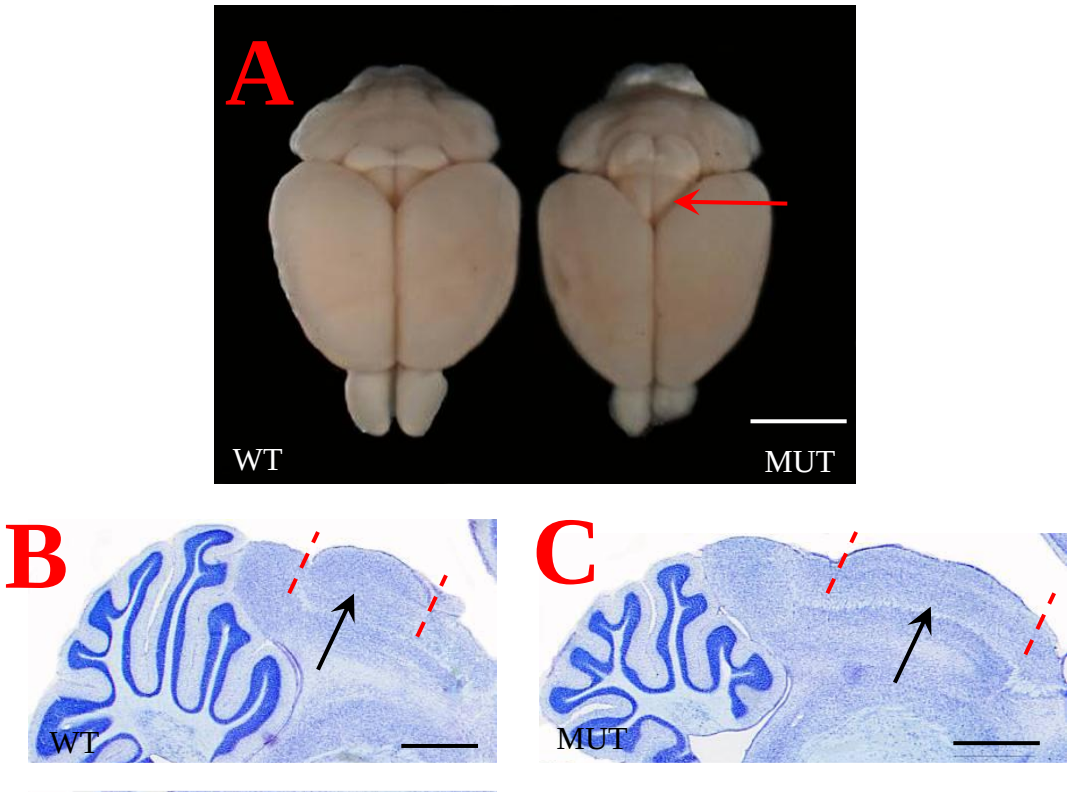
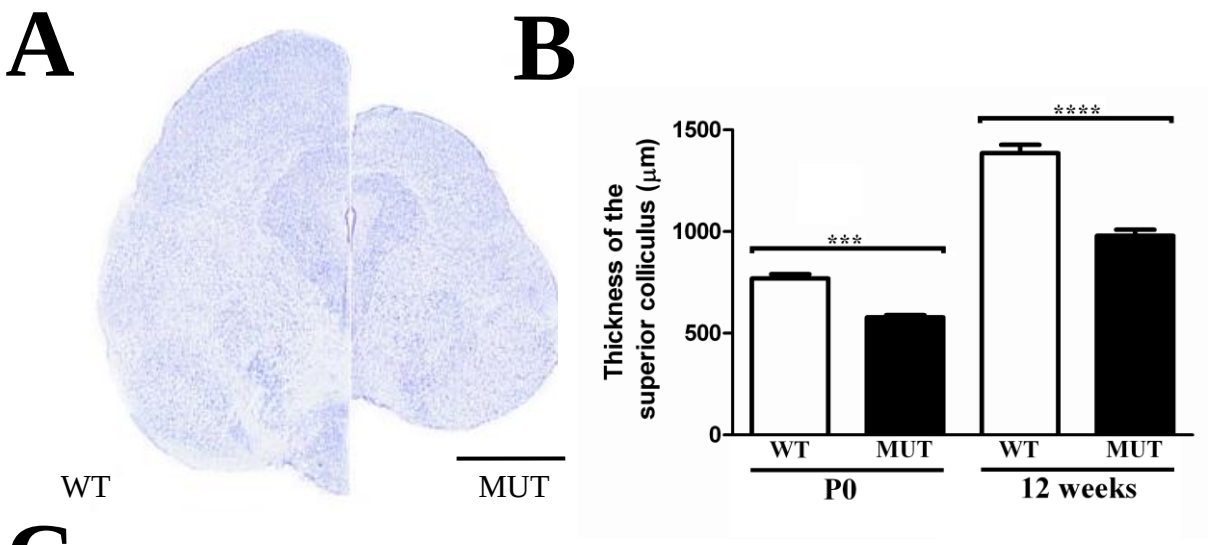


Figure 65. *WT and Jenna brains with red arrow highlighting exposed SC in the mutant (A). Sagittal sections with black arrow between redlines showing SC in WT and mutant littermates (B,C). Note that the SC is elongated in the mutant. Scale bars equal 5mm (A), 1mm (B, C).*

Figure 66: Reduced thickness of superior colliculus in *Jenna* +/-



C

Statistics

Superior colliculus thickness, *Jenna* +/- vs. WT (ANOVA with Bonferroni MCT)			
Comparison	**F (df1, df2)**	**Adjusted P {unadjusted P}**	**95% CI (μm)**
P0	F (1, 27) = 58.3	P < 0.0001{P<0.00005}	-261 to -490
12 weeks	F (1, 40) = 116	P < 0.0001{P<0.00005}	-351 to -541

Figure 66. *Coronal nissl stain of WT and mutant superior colliculi illustrating the reduced dorsal-ventral thickness in Jenna mutants (A). ANOVA with Bonferroni MCT of superior colliculus thickness in WT and mutant animals at P0 and 12 weeks (n = 4 WT, 4 MUT) (B). Statistical results table (C). Scale bar equals 1mm. Histogram summary: ***P<0.001 ****P<0.0001*

Laminar structure

The SC consists of seven layers: the zonal layer (Zo); the superficial grey layer (SuG); the optic layer (Op); the intermediate grey layer (InG); the intermediate white layer (InWh); the deep grey layer (DpG) and the deep white (DpWh) layer. In order to study the laminar structure, I searched the Allen Brain Atlas for genes that showed layer specific expression (Lein *et al.*, 2007). I found that: calretinin, which labels GABAnergic interneurons in layers 2/3 of the mouse cortex, labelled the superficial Op layers (Park *et al.*, 2002); tumour protein D52-like (Tpd52l1), a cell cycle-regulated protein, labelled cells in the proximity of the InG (Boutros and Byrne, 2005); and Er81, a transcription factor present in layer V neurons in the cortex, labelled the InG/InWh (Watakabe *et al.*, 2007). Immunohistochemistry (Er81 and calretinin) and *in situ* hybridisation (*Tpd52l1*) revealed that, despite some dispersion of labelled cells, the laminar structure of the superior colliculus in *Jenna* mutants is intact (**Figure 67**).

I also employed a Gallyas silver stain to investigate the myeloarchitecture of the colliculus. In WT animals a clear distinction could be made between the various grey and white layers with the dark silver stain highlighting the myelin rich Op, InWh and DpWh (**Figure 68. A**). In mutants the definition between superficial and intermediate layers was less defined, exemplified by the fusion of the InG layer with the InWh layers (**Figure 68. B**). The collicular commissure that is observable in the DpW was observed to cross the midline in both WT controls and *Jenna* mutants.

Figure 67: Cell marker laminar structure is intact in *Jenna* +/-

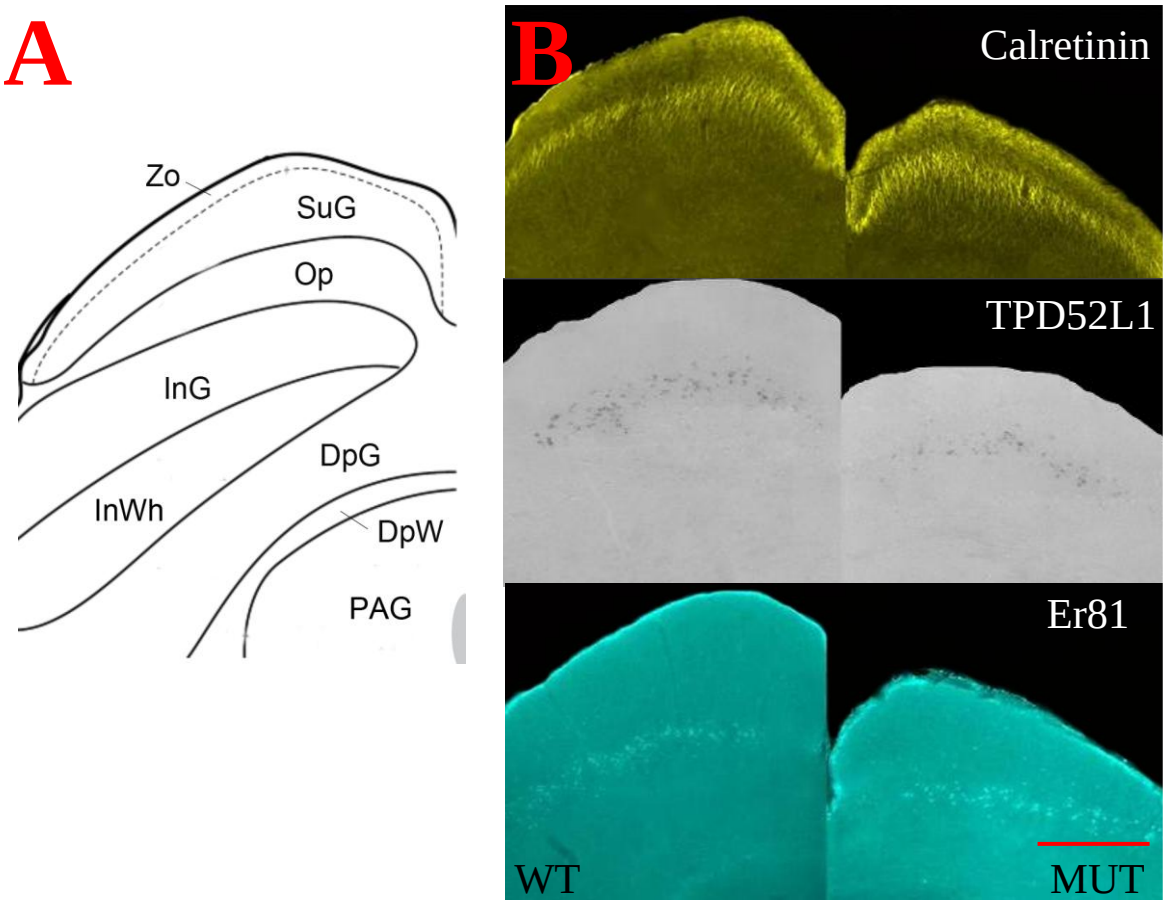


Figure 67. *Diagram illustrating the laminar structure of the SC adapted from Paxinos and Watson's Brain Atlas (Paxinos, 2007) (A). Calretinin, Tpd52l1 and Er81 staining show the laminar structure of the superior colliculus is intact in Jenna mutants. (B). Scale bar equals 250µm.The Tpd52l1 in situ was produced by Dr Peter Oliver.*

Figure 68: Defects in *Jenna* +/- laminar myeloarchitecture

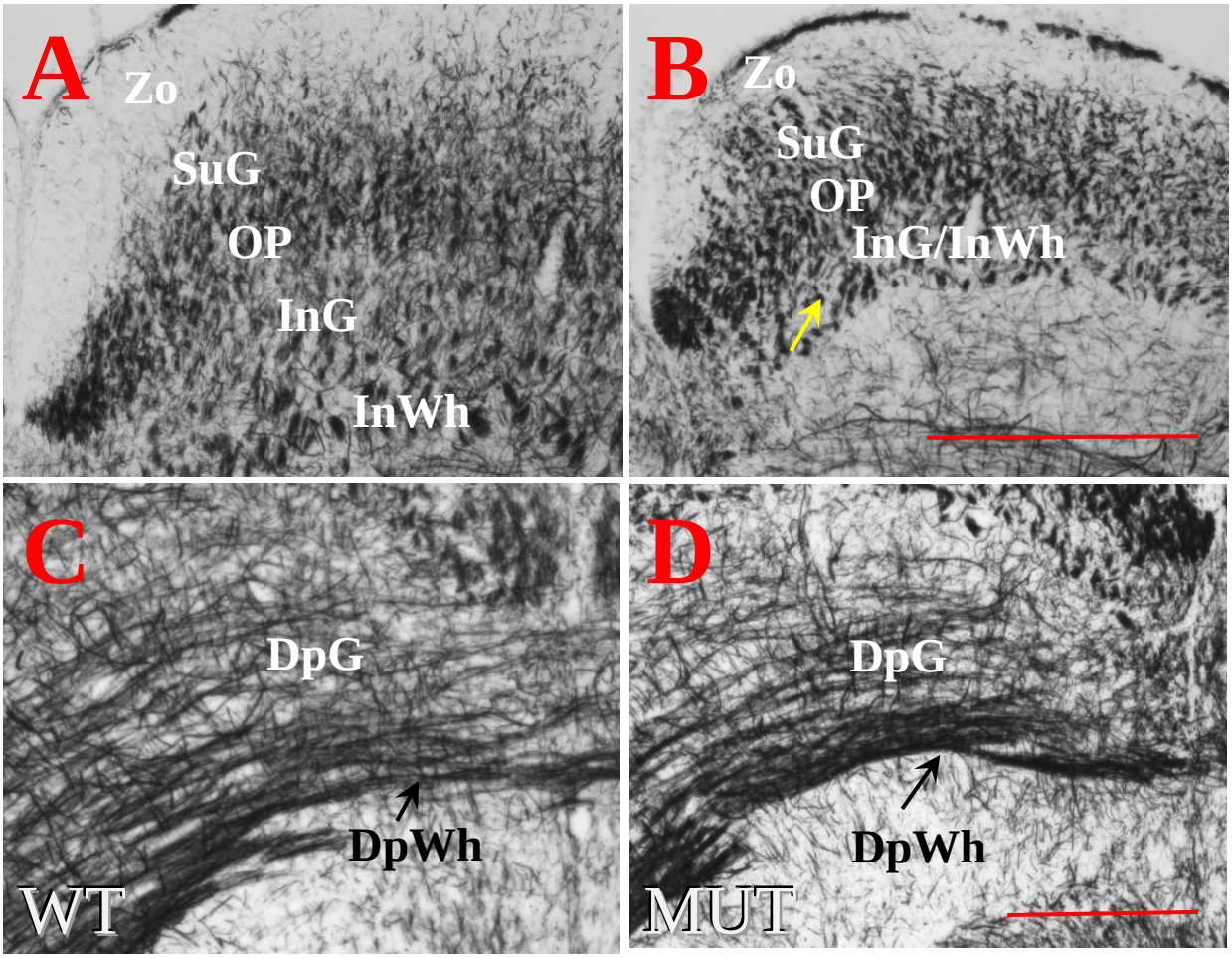


Figure 68. *The superficial and intermediate layers of Gallyas stained WT and Jenna mutant animals (A, B). The superficial superior colliculus appears compacted and less defined in the mutant with a fusion of the InG and InWh (yellow arrow). Deep layers (DpG and DpWh) of Gallyas stained sections in WT and mutant animals (C, D). Sections appear similar, with crossing of the collicular commissure observed in both groups. Scale bars equal 250µm*

Defective neuronal migration in *Jenna* superior colliculus

The laminar structure of the superior colliculus is a product of an inside-out migration of neurons. However, unlike the neocortex, GABAergic interneurons in the SC migrate radially and there is a temporal overlap in neurogenesis between deep and superficial layer neurons (Tsunekawa *et al.*, 2005). Tangential migration, as occurs in cortical GABAergic interneurons, describes migration which is parallel to the surface of the brain. In contrast, radial migration describes migration which is perpendicular to the surface of the brain. Radial migration, but not tangential migration, is reliant on radial glia (Keays, 2007).

As previously reported by Keays *et al.*, *Jenna* mice feature a S140G mutation in the T4 (tubulin 4) loop motif of α-tubulin (Keays *et al.*, 2007). The T1-T6 loops form the non-exchangable site (N-site) on α-tubulin and are required for GTP binding (Lowe *et al.*, 2001, Spiegelman *et al.*, 1977). Unlike the GTP at the exchangeable site of α-tubulin, GTP bound to the N-site is not hydrolysed and acts to stabilise αβ-tubulin heterodimers (Spiegelman *et al.*, 1977). Polymerisation of αβ-tubulin heterodimers is required for the formation of microtubules (Luduena *et al.*, 1977). As a consequence of the S140G mutation in the N-site, there is an 80% reduction in GTP binding efficiency (Keays *et al.*, 2007). This results in reduced formation of polymerisation-competent heterodimers and perturbs microtubule function (Keays *et al.*, 2007). Microtubules are critical for radial glial morphology (Li *et al.*, 2003). In WT, radial glia are orientated perpendicularly to the superficial surface of the brain and act as scaffolds that guide radially migrating neurons (Gadisseux *et al.*, 1990). Genetic mutations which disrupt microtubule function result in disorganisation of the radial glial processes and consequently lead to aberrant neuronal migration (Jaglin and Chelly, 2009). As GABAergic interneurons in the SC migrate radially, and thus rely on radial glia, I hypothesised that a neuronal migration defect would present in the superior colliculus of *Jenna* mice. Additionally, as microtubules are important in the formation of the mitotic

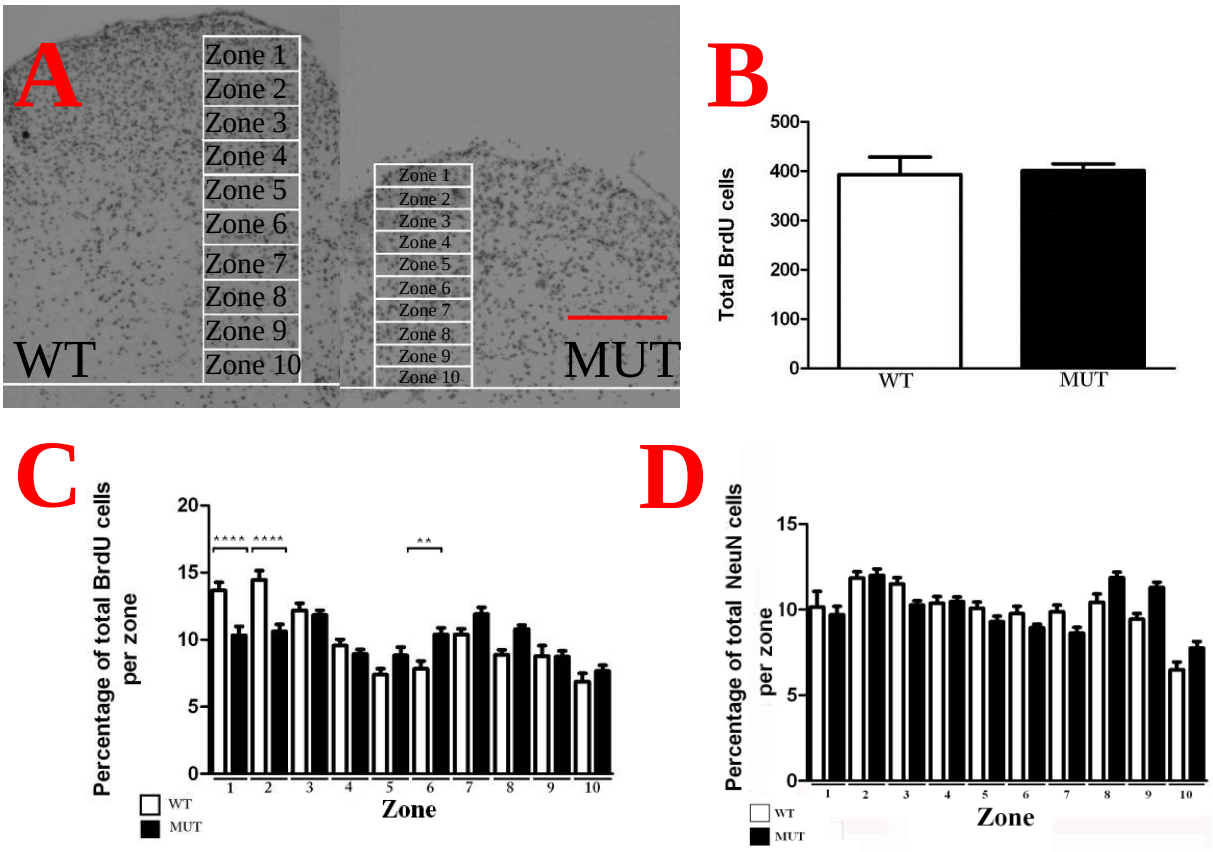
spindle, it was important to assess if the neurogenesis rate was compromised (Gambino *et al.*, 1984).

To test neurogenesis level and migration I labelled newly born cells with BrdU. The peak generation time for deep layer neurons is E11 to E13, and for superficial layer neurons E12 to E13 (Edwards *et al.*, 1986). Consequently, I injected BrdU at E12.5.

BrdU positive cells were counted by dividing the SC into ten equal zones extending from the cerebellar aqueduct to the surface of the SC (**Figure 69. A**). I observed no significant difference in the average number of BrdU cells between WT and *Jenna* mutants suggesting that the generation of neurons is not affected by the S140G mutation (T test, $t = 0.23$, $df = 32$, $P>0.05$ =NS) (**Figure 69. B**). I then tested for an interaction between genotype and the mean percentage of cells in each zone. I found that the percentage of labelled cells present in the two most superficial analysis boxes was significantly reduced in *Jenna* mutants indicative of a defect in the radial migration of neurons ($P<0.0001$). This is complimented by a significantly higher percentage of BrdU cells in *Jenna* mutants being present in zone 6, a region inclusive of the DpG ($P<0.01$) (**Figure 69. C, E**).

I then tested to see if neurons completed their migration postnatally. To do this, I stained serial sections with the post mitotic marker NeuN at P21. While I observed a higher percentage of neurons in the deep layers in mutant animals, this difference was not significant, indicating that most of the neurons delayed during development eventually compete their migration between P0 and P21 (**Figure 69. D**).

Figure 69: Defective neuronal migration in *Jenna* +/- superior colliculus



E

Significant results:

Percentage of total BrdU cells per zone (ANOVA with Bonferroni MCT)			
Zone	**F (df1, df2)**	**Adjusted P {unadjusted P}**	**95% CI (%)**
1	F (1, 33) = 20.3	P<0.0001{ P<0.00001}	-0.8 to -5.8
2	F (1, 33) = 26.9	P<0.0001{P<0.00001}	-1.39 to -6.32
6	F (1, 33) = 11.8	P<0.01 { P<0.0001}	+0.08 to +5.01

Please turn page for remainder of figure

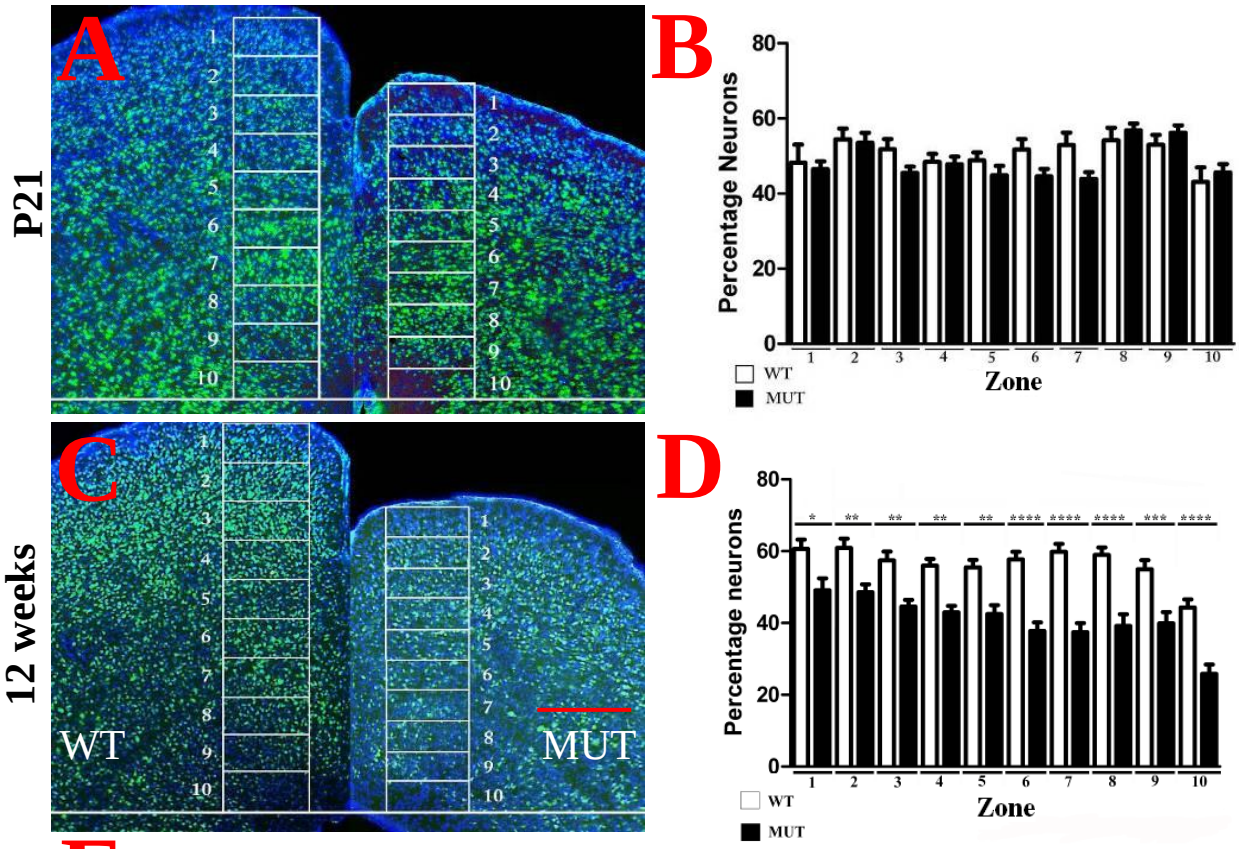
Figure 69: *Staining for BrdU in the SC of littermate controls and Jenna mutants harvested at P0 following injection of BrdU at E12.5 (n=4) (A). The SC was divided into ten equal bins (shown in white) extending from the aqueduct to the dorsal surface of the zonal layer and BrdU positive cells counted. There was no significant difference in the number of cells labelled per section between WT and mutant littermates (B). The percentage of BrdU cells in the upper two zones was significantly reduced in Jenna mutants indicative of a migratory defect during the formation of the SC (C). Staining of post-mitotic neurons at P21 with the marker NeuN, reveals that those most neurons delayed in utero catch up postnatally, although some remain in the deeper layers (D). Significant results table (E). Scale bar equals 250µm. Histogram summary: **P<0.01 ****P<0.0001*

Neuron cell death in adult *Jenna* mutants

I then assessed how the S140G mutation affected the survival of neurons within SC layers at P21 and 12 weeks of age. To do this, I divided the colliculus into ten equal bins extending from the cerebellar aqueduct to the surface, and counted the number of NeuN positive and DAPI labelled cells (**Figure 70. A, C**).

At P21 both mutant and littermate control animals had similar percentages of neurons (50%) in each zone (**Figure 70. B**). This contrasts with observations at 12 weeks of age, where I found a large reduction in the percentage of neurons in all zones in mutant animals (**Figure 70. D, E**). The greatest loss of neurons occurred in zones 6 and 7, equating with the intermediate and deep layers ($P<0.0001$). Additionally, zones 8-10 which cover the periaqueductal grey (PAG) showed a significant drop in the percentage of neurons (Zones 8, 10 = $P<0.0001$, Zone 9 = $P<0.001$).

Figure 70: Loss of neurons in the SC of *Jenna* +/-



E

Significant results:

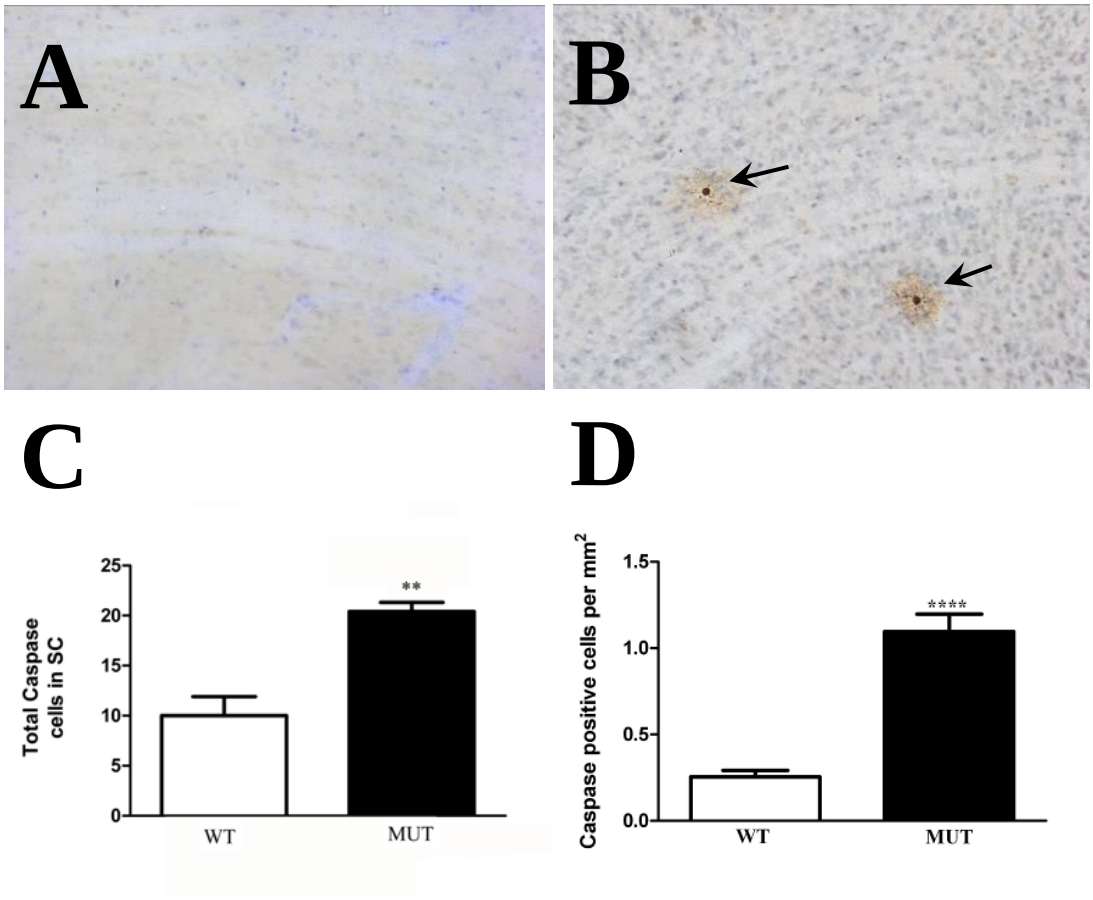
Percentage neurons in zone, 12 weeks, *Jenna* +/- vs. WT (ANOVA with Bonferroni MCT)			
Zone	**F (df1, df2)**	**Adjusted P {unadjusted P}**	**95% CI (%)**
1	F (1, 40) = 10.99	P<0.05 {P<0.005}	-1.7 to -21.29
2	F (1, 40) = 12.65	P<0.01 {P<0.001}	-2.54 to -22.12
3	F (1, 40) = 13.82	P<0.01 {P<0.001}	-3.1 to -22.68
4	F (1, 40) = 14.08	P<0.01 {P<0.001}	-3.22 to -22.8
5	F (1, 40) = 14.05	P<0.01 {P<0.001}	-3.208 to -22.79
6	F (1, 40) = 33.07	P<0.0001 {P<0.00001}	-10.15 to -29.74
7	F (1, 40) = 41.58	P<0.0001 {P<0.00001}	-12.57 to -32.15
8	F (1, 40) = 32.58	P<0.0001 {P<0.00001}	-10.00 to -29.59
9	F (1, 40) = 18.87	P<0.001 {P<0.0001}	-5.274 to -24.86
10	F (1, 40) = 28.21	P<0.0001 {P<0.00001}	-8.627 to -28.21

Please turn page for remainder of figure

Figure 70: *The SC was divided into ten equal bins for Jenna mutants and WT littermates and DAPI (blue) and NeuN (green) labelled cells were counted at P21 and 12 weeks of age (n=4) (A,C). This enabled the percentage of neurons to be calculated for each zone at each time point (B,D). There was no significant difference between genotypes for any zone in the P21 cohort (B). In contrast, there was a reduction in the percentage of neurons throughout the SC in 12 week old Jenna mutants (D). The loss of neurons reached significance in all zonal boxes, particularly zones 6 and 7 which map to the DpG/DpWh layers. Significant results table (E). Scale bars equals 250µm. Histogram summary: *P<0.05 **P<0.01 ***P<0.001 ****P<0.0001*

To demonstrate that this loss of neurons is due to cell death I stained the SC for caspase-3, an activated protease that labels apoptotic cells (Porter and Janicke, 1999). This experiment was performed on mice aged 7 weeks of age, a time point mid-way between P21 and 12 weeks (**Figure 71. A, B**). Staining of serial sections revealed that there was a significant increase in both the number ($P < 0.01$) and density ($P < 0.0001$) of caspase 3 positive cells in *Jenna* mutants (**Figure 71. C, D, E**).

Figure 71: Increase in caspase staining in 7wk old *Jenna* +/-



E

Statistics

Total caspase cells in superior colliculus, mutant vs. WT (T test)			
T	**df**	**P value**	**95% CI**
4.6	9	P<0.01	+5.29 to +15.51
Caspase positive cells per mm^2, mutant vs. WT (T test)			
T	**df**	**P value**	**95% CI**
8.5	9	P<0.001	+0.62 to +1.07

Figure 71: *Caspase 3 immunostaining of the SC of 7 week old WT and Jenna mutant animals (black arrows highlight positive cells) (A, B). Staining shows a significant increase in the total number and density of caspase positive cells in Jenna mutants (n=5) (C, D).Statistical results table (E). Histogram summary: **P<0.01 ****P<0.0001*

Future work plans for *Jenna*

One important question arising from the *Jenna* mouse data is thus: is the elevated cell death phenotype independent of the migratory defect or due to it? In order to answer this question, a heterozygous *Tuba1* KO mouse needs to be developed. At time of writing, EUCOMM is in the process of generating these KOs and have confirmed targeting in embryonic stem cells. Once generated, neuroanatomical assessment of heterozygous *Tuba1* KOs will answer a simple question: is haploinsufficiency of *Tuba1* responsible for the defect in the *Jenna* mouse? Assuming heterozygous KO mice mirror *Jenna* neuropathology, an inducible heterozygous *Tuba1* KO should subsequently be developed. To develop these mice, I would use a modified version of the cre-ERT2 method described by Vallier and colleagues (Vallier *et al.*, 2001). This modified method would involve the following: 1) creating a line featuring a floxed *Tuba1* allele (Tuba1$^{+/floxed}$); 2) creating a *sox1-creERT2* line; 3) crossing these lines to generate *Sox1-creERT2 Tuba1*$^{+/floxed}$ and *Sox1-creERT2 Tuba1*$^{+/+}$ mice. The brain specific *Sox1* promoter would drive the expression of the cre-ERT2 fusion protein (Pevny *et al.*, 1998). After exposure tamoxifen, cre-ERT2 would enter the nucleus compartment and delete the floxed *Tuba1* allele via recombination.

For the experiment, *Sox1-creERT2 Tuba1*$^{+/floxed}$ mice and their *Sox1-creERT2 Tuba1*$^{+/+}$ littermates should be matured. This is to allow for neurons to migrate and form an anatomically normal superior colliculus. After this period of normal development, I would knock out the floxed *Tuba1* allele by injecting the mice with tamoxifen (resulting in the floxed animals adopting a *Sox1-creERT2 Tuba1*$^{+/-}$ genotype). If *Sox1-creERT2 Tuba1*$^{+/-}$ also feature increased cell death relative to their littermates, it would suggest that haploinsufficiency of *Tuba1* is causal to a cell death phenotype independent of a neuronal migration defect. If this were the case, the induced KO mice should be tested on the same

array of behavioural test that were used to assess the *Jenna* line (Keays *et al.*, 2007). This would establish if the cell death phenotype contributed towards behavioural defects. Ascertaining the impact of the cell death phenotype would help address the following questions: to what extent does cell death contribute to the *Jenna* mouse behavioural profile relative to the migratory defect?; would countering the elevated rate of cell death help attenuate the severity of the behavioural abnormalities?

To address this latter question, I would crossbreed *Jenna* mice with the *Wld*^{S} (Wallerian degeneration slow) mouse line. Wld^{S} is a fusion protein where the N-terminal fragment of Ube4b (ubiquitination factor E4B) is fused to Nmnat (nicotinamide mononucleotide adenylyltransferase) (Mack *et al.*, 2001). The fusion protein conveys a dose-dependent neuroprotective effect and has been shown to be protective in cortical lesioning, MPP+ induced Parkinsonism and neurodegenerative disease models (Mack *et al.*, 2001, Gillingwater *et al.*, 2006, Antenor-Dorsey and O'Malley, 2012, Wishart *et al.*, 2006). The neuroprotective effect of Wld^{s} is due to increased mitochondrial motility and increased mitochondrial Ca2+ buffering capacity (Avery *et al.*, 2012). I would assess, via caspase staining, if crossbreeding *Jenna* with *Wld*^{s} resulted in reduced cell death. I would then assess the effect of Wld^{s} on *Jenna* mouse behaviour.

Finally, I would examine the *Jenna* mouse superior colliculus ultrastructure via transmission electron microscope using the method described by Koch and colleagues (Koch *et al.*, 2011). This would allow for hallmarks of cell death pathology to be quantified. For example, is there a significant loss of synapses or axonal degeneration preceeding cell death? Is there a higher proportion of anatomically abnormal synapses in Jenna? Are the vesicle pools at the synapses altered? These questions are relevant as microtubules play a role in synapse formation and in vesicular cargo trafficking (van den Berg and Hoogenraad, 2012).

Summary

In this chapter, I have shown the superior colliculus of *Jenna* mice is anatomically abnormal. The superior colliculus is thinned in the dorsal-ventral plane and elongated in the rostral-caudal plane. Whilst cell layering structure is preserved, myeloarchitecture is disrupted and the InG/InWh layers are fused. My BrdU cell labelling experiments at E12.5 support that defective neuronal migration underlies the anatomical abnormalities, consistent with previous studies in the hippocampus (Keays *et al.*, 2007). Additionally, my results implicate postnatal cell death in *Jenna* mouse pathophysiology. NeuN/DAPI cell labelling shows that neurons are lost between P21 and 12 weeks of age, with a greatest lost occurring in the deep layers. Caspase3 positive cell counts are increased in 7 week old *Jenna* mutants versus controls illustrating elevated apoptosis. The loss of neurons in the deep layers of the superior colliculus is likely to disrupt its role in modulating sensorimotor gating (Davis, Gendelman *et al.* 1982; Meloni and Davis 2000). Consequently, my findings are consistent with the exaggerated acoustic startle response behaviour observed in the *Jenna* mutant (Keays, 2005, Davis *et al.*, 1982, Meloni and Davis, 2000).

Chapter 7

Analysis of *Sox1-Cre Cxcr4* Conditional Knock Out Mice

Histology and behaviour

Introduction

Sanger's KO lines are generated using the knockout-first technique allowing them to be converted into conditional mutants via the cre-lox system (Testa *et al.*, 2004). Lines that are embryonically lethal due to somatic defects can potentially be made into brain specific KOs in order to evaluate adult neuroanatomy and behaviour. In this chapter, I evaluate one such conditional mutant; *Sox1-Cre* (SRY-related HMG-box gene 1) *Cxcr4* (chemokine, C-X-C motif, receptor 4). Although the line was not made by Sanger, it was generated using similar conditional knockout technology. This chapter demonstrates how a floxed line, such as those generated by Sanger, could be converted into a brain specific KO and studied.

Non-conditional *Cxcr4* -/- mice feature fatal embryonically haematopoietic and cardiac defects (Zou *et al.*, 1998). Embryos also feature neuroanatomical abnormalities including cerebellar granule cell ectopia, reduced neurogenesis, and failure of the dente gyrus to form distinct inner and outer blades (Zou *et al.*, 1998, Lu *et al.*, 2002).

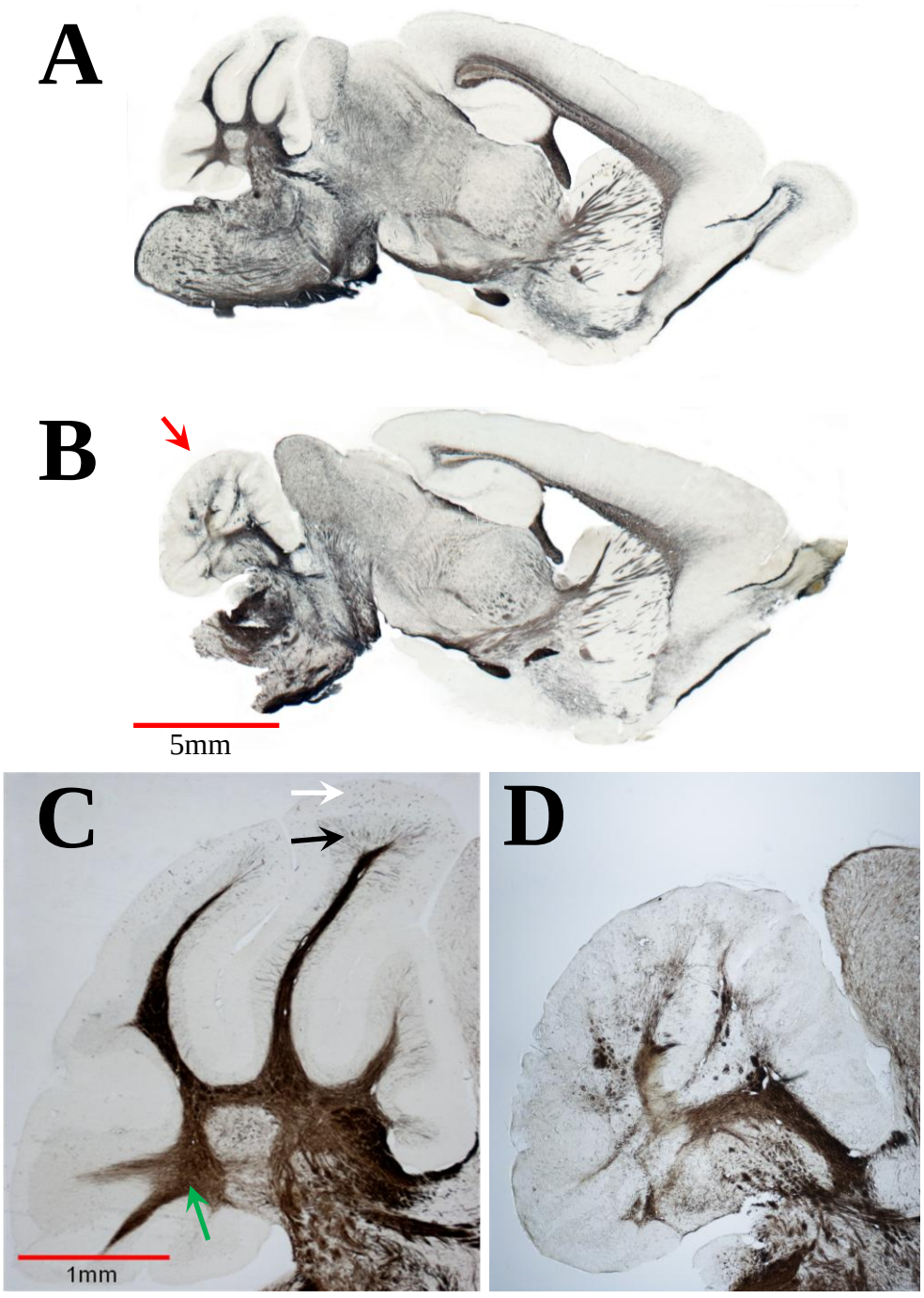
In adults, Cxcr4 has been shown to be required for the maturation of oligodendrocyte precursor cells after chemically induced damage. Mice fed a diet enriched with cuprizone leads to apoptosis of oligodendrocytes. Knocking down *Cxcr4* with $_{sh}$RNA, or use of the antagonist AMD3100, inhibits remyelination after cuprizone treatment is withdrawn (Patel *et al.*, 2010). My data shows *Sox1-Cre Cxcr4* -/- mice feature developmental defects in myelination, cerebellar patterning, Purkinje cell morphology and locomotory behaviour.

Anatomical abnormalities

Sox1 expression defines the neuronal precursors of the embryonic central nervous system (Pevny *et al.*, 1998, Li *et al.*, 1998). Therefore, the *Sox1-Cre Cxcr4* -/- mouse is a brain specific KO. *Sox1* is expressed in the adult mouse at sites of neurogenesis; the subventricular zone, subgranular zone of the dentate gyrus and the Bergmann glia cells of cerebellum (Alcock and Sottile, 2009). Bergmann glia cells are radial glia and serve two major known functions. First, they are involved in the migration of granule cell precursors (Dahmane and Ruiz i Altaba, 1999). Second, they serve as scaffolding for Purkinje cell dendrites (Yamada and Watanabe, 2002, Lordkipanidze and Dunaevsky, 2005). We speculated that disruption of the Bergmann glia may cause defects in cerebellar and Purkinje cell morphology.

I performed a Gallyas stain and observed that the gross morphology of the brain is preserved in *Sox1-Cre Cxcr4* -/- mice with the exception of the cerebellum (**Figure 72. A, B**). A clear distinction is observable between the cerebellar molecular and granule layers and lobules in WT but not in -/- (**Figure 72. C, D**). This suggests a migration defect leading to fusion of the molecular and granule layers, consistent with the role of Bergmann glia as radial glia. The overall degree of myelination is also reduced, suggesting Cxcr4 influences maturation of oligodendrocyte precursors during development.

Figure 72: Myeloarchitecture defects in *Sox1-Cre Cxcr4* -/-



Please turn page for remainder of figure

Figure 72: *Sagittal gallyas stained sections of WT and Sox1-Cre Cxcr4 -/- brains (A,B). Red arrow highlights abnormal cerebellum in mutant (B). Cerebellum of WT mouse showing molecular layer (white arrow), granular layer (black arrow) and myelinated fibre tracts (green arrow) (C). These structures are poorly defined in the mutant; there is hypomyelination and the molecular and granular layers are fused (D). Scale bars equal 5mm (A, B) and 1mm (C,D).*

Golgi staining revealed that the dendritic branching network of *Sox1-Cre Cxcr4* -/- Purkinje cell is simplified and reduced in sprawl size (**Figure 73**). This suggests a failure of the Bergmann glia to function as scaffolding cells. Additionally, as hippocampal defects have been reported in the embryonically lethal *Cxcr4* -/- mutant, I examined CA1 hippocampal spine density (Lu *et al.*, 2002). I found no significant difference between WT and mutant (**Figure 73**).

Figure 73: Purkinje cell arborisation simplified in *Sox1-Cre Cxcr4* -/-

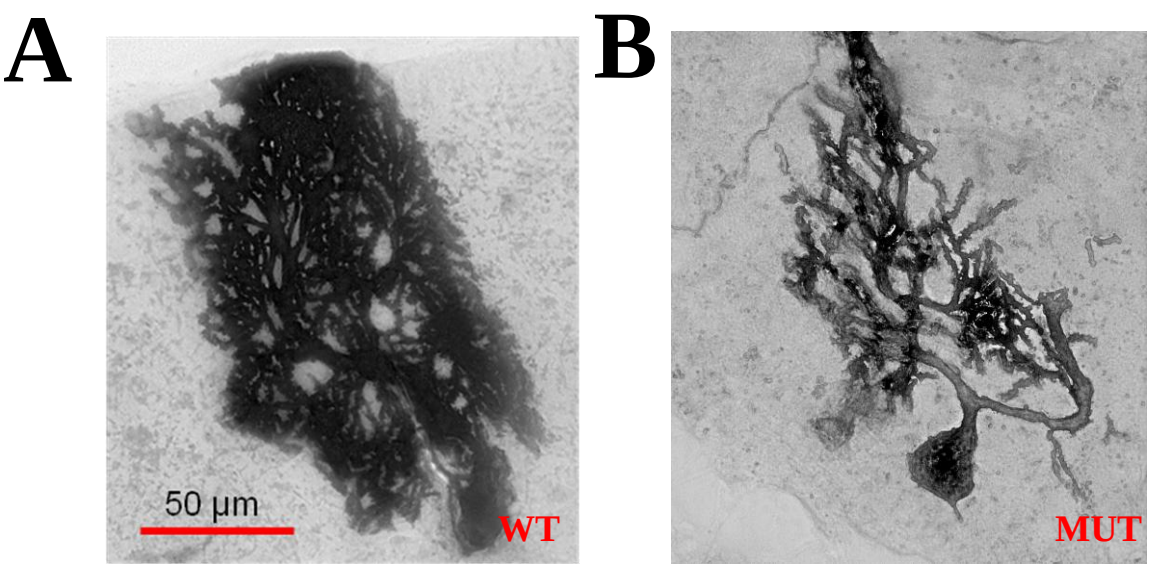


Figure 73: *WT and Sox1-Cre Cxcr4 -/- Purkinje cells (A and B). Branching is simplified in mutant. Scale bar equals 50µm.*

Figure 74: CA1 spine density in *Sox1-CreCxcr4* -/- mirrors WT

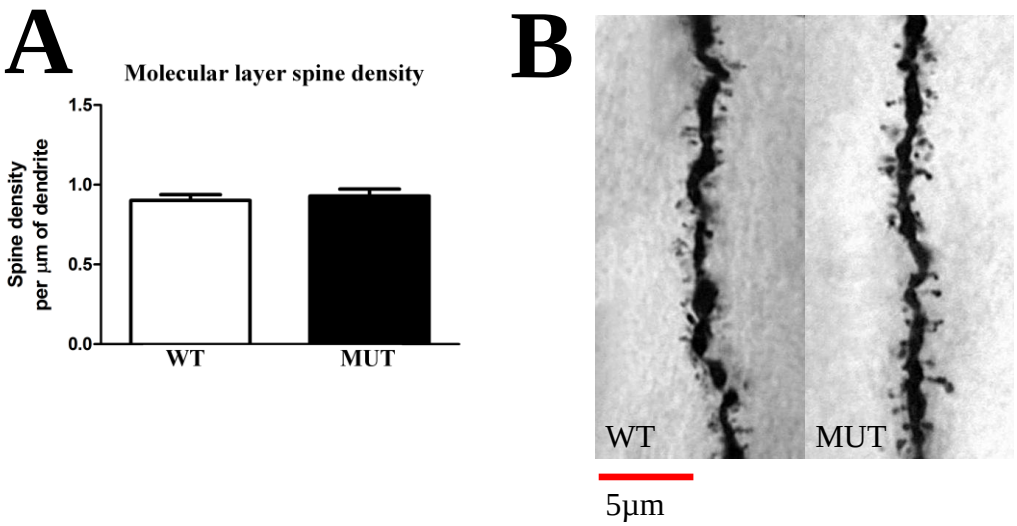


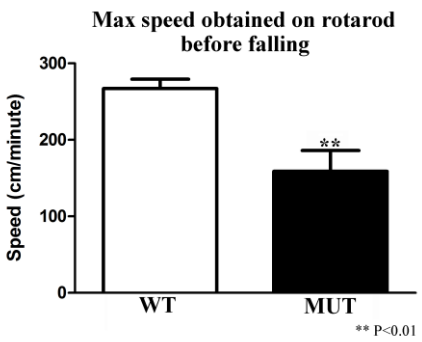
Figure 74: *Histogram and image showing CA1 spine density in WT and Sox1-CreCxcr4 -/- mice (A,B). There is no significant difference in density with genotype. n = 4 WT, 4 MUT. Scale bar equals 5µm.*

Behavioural defects

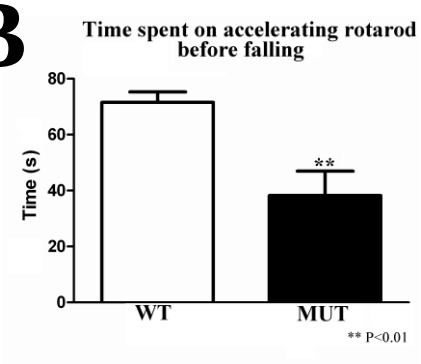
Damage and malformation of the cerebellum is associated with ataxia and hind limb weakness (Fine *et al.*, 2002, Lock *et al.*, 2001). Consequently, I used an accelerating rotarod, running wheel and inverted mesh grid to test for defects in motor coordination and hind limb strength. *Sox1-CreCxcr4* -/- mice fall from the rotarod at a lower speed than WT mice (**Figure 75**). Mutant mice also perform poorly in a five day running wheel trial; they cover less distance and run at a significantly reduced average and maximum speed (**Figure 76**). The inverted mesh grid test suggests mutants also display limb weakness and fail to optimally use their hind limbs for clasping (**Figure 76**). These results support that the anatomical defects in *Sox1-CreCxcr4* -/- mice compromise cerebellar function.

Figure 75: *Sox1-CreCxcr4* -/- mice perform poorly on rotarod

A



B



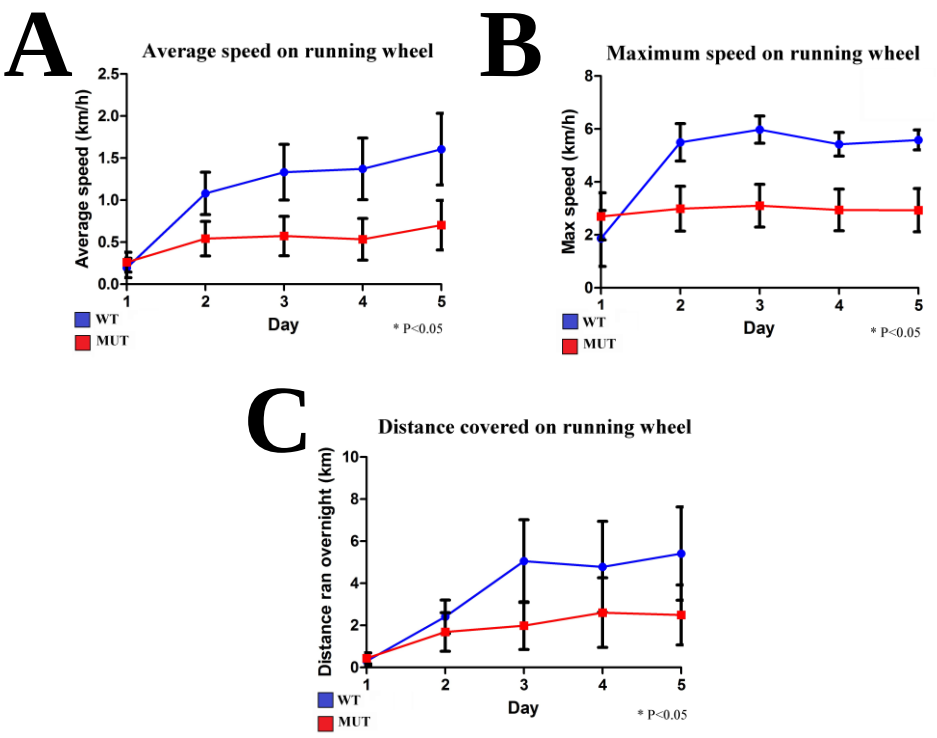
C

Statistics

Mutant vs. WT (t-test)			
Comparison	**t (df)**	**P value**	**95% CI**
Max speed	3.62 (16)	<0.01	-4.47 to -17.15 (cm/min)
Time on rod	3.5 (16)	<0.01	-13.12 to -53.54 (s)

Figure 75: *Sox1-CreCxcr4 -/- mice achieve a smaller maximum speed, and fall from the accelerating rotarod significantly sooner, than WT (A, B). Table of statistics (C). n = 10 WT (5M, 5F), 10 MUT (5M, 5F).*

Figure 76: *Sox1-CreCxcr4* -/- mice are impaired on running wheel



D

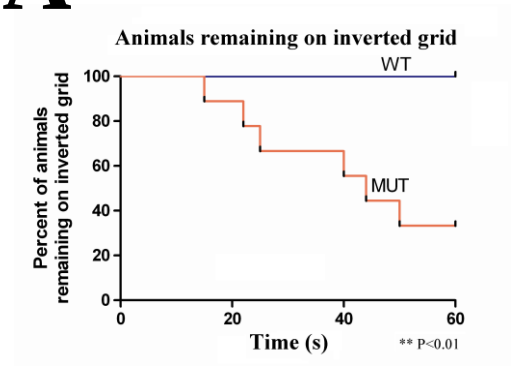
Statistics

Mutant vs. WT (Paired T test)			
Comparison	**t (df)**	**P value**	**95% CI**
Average speed	3.36 (4)	<0.05	-0.26 to -2.7 km/h
Max speed	2.79 (4)	<0.05	-0.02 to -9.7 km/h
Distance	2.78 (4)	<0.05	-0.01 to -8.7 (km/night)

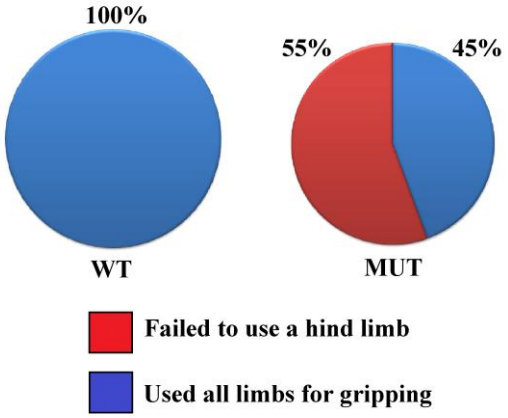
Figure 76: *Sox1-CreCxcr4 -/- mice achieve a smaller average speed, maximum speed and cover less distance on the running wheel than WT (A, B, C). Table of statistics (D). n = 10 WT (5M, 5F), 10 MUT (5M, 5F).*

Figure 77: *Sox1-CreCxcr4* -/- mice fail inverted mesh grip test

A



B



C

Statistics

Remaining on grid, Mutant vs. WT (Survival with Mantel-Cox test)			
Comparison	**Chi square (df)**	**P value**	**95% CI (Hazard ratio)**
Percentage of animals remaining on grid	7.76 (1)	<0.01	0.01946 to 0.5037

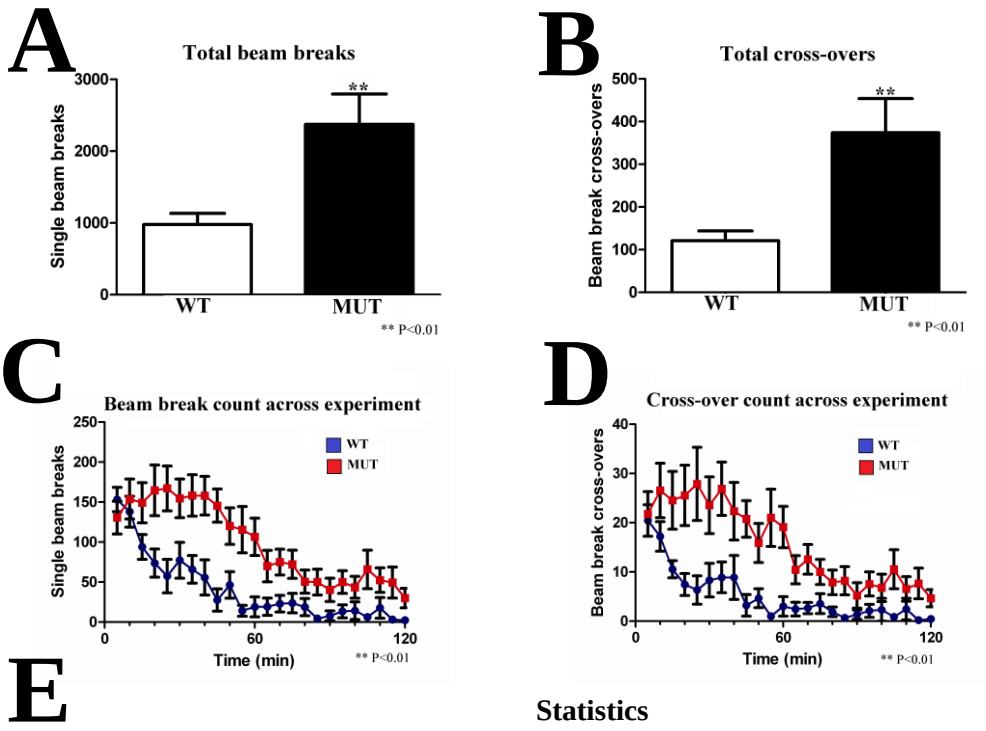
Hind limb use, Mutant vs. WT (Chi square)				
Genotype	**Used all limbs**	**Failed to use a hind limb**	**Total mice**	**Chi square (P value)**
WT	8	0	8	6.3 (<0.05)
Mutant	4	5	9	
All	12	5	17	

Figure 77: *While all WT remain on inverted mesh grid after one minute, 66 % of Sox1-CreCxcr4 -/- animals fall (A). All WT animals successfully used all their limbs for clasping while 55% of mutant animals failed to use at least one of their hind limbs (B). Table of statistics (C). n = 10 WT (5M, 5F), 10 MUT (5M, 5F).*

I also performed non-balance related tests. First, the activity box tests to establish if impaired performance on the running wheel was reflective of an overall decrease in activity. *Sox1-CreCxcr4* -/- produced significantly more beam breaks and crossovers than WT mice (**Figure 78**). This suggests that the running wheel results are reflective of poor balance rather than reduced activity. The significant increase in beam breaks and cross overs may be due to a stumbling gait when crossing the paths of the lasers.

Second, the Y maze was used to establish if any spatial reference memory defect was present. As gross hippocampal and CA1 dendritic spine anatomy was normal, no defect was expected in the mutant. Consistent with this, there was no significant difference in performance between mutant and WT (T test of time spent exploring novel arm; t (df) =0.76 (15**)**, P =0.46, 95% CI = +16.2 to -34).

Figure 78: *Sox1-CreCxcr4* -/- mice display increased activity



E

Statistics

Mutant vs. WT (Paired T test)			
Comparison	**t (df)**	**P value**	**95% CI**
Total beam breaks	3.1 (16)	<0.01	+441 to +2352
Total cross-overs	3.04 (16)	<0.01	+77 to +429
Beam breaks across experiment	8.3 (23)	<0.0001	+44 to +73
Cross-over count across experiment	8.8 (23)	<0.0001	+8 to +13

Figure 78: *Total beam breaks (A). Total crossovers (B). Beam breaks and cross overs across experiment plotted in 5 minute intervals (C, D). Table of statistics (E). n = 10 WT (5M, 5F), 10 MUT (5M, 5F). Histogram summary: **P<0.01*

Future work plans for *Sox1-CreCxcr4*

My work in *Sox1-CreCxcr4* -/- mice generates several questions. Are *CXCR4* mutations causal to neurological disease in humans? As non-conditional null mutations in mice are embryonically lethal, it seems reasonable to speculate that ubiquitous null mutations would also fatally compromise human brain development. However, there are mechanisms through which congenital and/or progressive disease could theoretically occur. A mutation could arise in a progenitor cell leading to the generation of a subset of brain cells featuring a *CXCR4* defect. It may also be the case that missense *CXCR4* mutations could predispose a patient to disease later in life by impairing the brain's ability to remyelinate.

In order to assess if *CXCR4* mutations underlie cerebellar malformations in humans, I have shared my data with Dr Andrea Nemeth, clinical genetics consultant at the Churchill hospital in Oxford. She has supplied patient samples for sequencing. We have agreed to sequence all *CXCR4* exons (and adjacent splice sites) in these patients and to assess the pathogenicity of any polymorphisms discovered. In order to exclude polymorphisms prevalent in the unaffected population, I would discount *CXCR4* mutations reported in the 1000 genomes project database (Siva, 2008). To assess potential pathogenicity, I would verify if a mutation resulted in one of the following: a non-synonymous change at an evolutionary conserved residue; a change in splicing; a change in the reading frame; a premature stop codon. Assuming consent for a fresh tissue sample could be obtained, I would extract RNA from any patient featuring a putative pathogenic mutation in *CXCR4*. Using the method described in Drogemuller *et al.* 2011, I would then convert the RNA into cDNA. Subsequently, I would use *CXCR4* specific primers to amplify all *CXCR4* transcripts via PCR. Each transcript would then be isolated via gel electrophoresis and sequenced. This would ascertain if the genomic mutations in *CXCR4* resulted in alterations in the mRNA.

Additionally, I would assess how coding mutations might affect the structure and function of the CXCR4 protein. In order to do this, I would generate a 3D model by inputting the sequence of the affected protein domain into the PHYRE2 server (Kelley and Sternberg, 2009).

Other important questions are: how does *Cxcr4* expression lead to the maturation of oligodendrocyte precursor cells? If the mechanism were discovered, could it be pharmacologically exploited to increase remyelination in diseases such as multiple sclerosis? Indeed, the importance of finding the mechanism by which Cxcr4 leads to remyelination has been stressed by other authors who have shown it's protective role in viral and drug induced mouse models of demyelination (Patel *et al.*, 2010, Carbajal *et al.*, 2011). It is therefore crucial to assess if it is only *Cxcr4* expressed within the oligodendrocyte precursors that play a role in remyelination. In order to ascertain this, *cre* should be driven by a marker for oligodendrocyte precursor cells, such as O4 (Wolswijk, 2002). If *O4-creCxcr4 -/- mice* also display a myelination defect, it suggests Cxcr4 expressed within oligodendrocyte precursor cells is sufficient to induce maturation into oligodendrocytes (rather than maturation being induced indirectly via Cxcr4 expression in other cell types). Assuming *O4-creCxcr4 -/-* were viable, they would serve as an excellent model to test remyelinating therapeutics. Deverman and colleagues show that intracranial injections of adenoviruses expressing LIF (Leukemia inhibitory factor) increase oligodendrocyte precursor cell levels and boost remyelination in a cuprizone-induced model of demyelination(Deverman and Patterson, 2012). Using the same technology, I would assess if injections of adenoviruses expressing *Cxcr4* were sufficient to boost myelination in *O4-creCxcr4 -/- mice* and WT mice treated with cuprizone. I would also assess if co-administration with LIF expressing adenoviruses further increased remyelination. If successful, it may have implications for gene therapy in demyelinating disease.

Summary

I have demonstrated that embryonic lethality in *Cxcr4* -/- can be bypassed using *Sox1-Cre* to generate a brain specific KO. This method could be applied to floxed lines generated by Sanger in order to evaluate neuroanatomy and behaviour in lines with confounding somatic complications.

Sox1-Cre Cxcr4 -/- mice exhibit hypomyelination, disrupted cerebellar myeloarchitecture with a lack of distinction between molecular and granular layers, and simplified Purkinje cell branching. These anatomical defects result in poor performance in balance tests including the rotarod, running wheel and inverted grid. My data suggests that *Cxcr4* expression is required for at least two major functions. First, it is required for physiologically normal levels of myelination during development. This is consistent with previous studies suggesting Cxcr4 is needed for the maturation of oligodendrocyte precursor cells post pharmacologically induced damage (Patel *et al.*, 2010). Second, the simplification of Purkinje cell branching and disorganisation of cerebellar layering is consistent with a failure of Bergmann glia to adequately serve their physiological role as scaffolding cells and radial glia. The mechanism underling this failure remains to be explored.

Chapter 8

Discussion

Analysis of results, conclusions and final thoughts

Introduction

The aim of this thesis was to find genetic mutations which cause neuroanatomical defects. The rationale behind this was that such mutations would be informative about developmental neurobiology and the biological basis of behaviour. To achieve my aim, I conducted ENU mutagenesis and transgenic KO screens in adult mice.

This chapter has four sections: First, a summary of the yield rates of my screens; Second, an assessment of my neuroanatomical method; Third, the relative strengths and weaknesses of my ENU and KO screens; Fourth, the gene-phenotype associations made in my screens and their importance.

Summary of the yield rates

The yields of my screens are summarised in **Figure 79**. In this chapter, comparisons of screen efficacy shall be between the ENU screen and BL/6 KO data. Non BL/6 lines will not be compared. This is due to the influence of mixed 129 background effects.

Figure 79: Overview ENU and KO screen yield (from chapters 3 & 4)

	ENU screen	**KO screen * (BL/6 lines)**	**KO screen*† (Non BL/6 lines)**
Total animals qualitatively assessed for ectopias	1,912 (125 pedigrees)	1172 (239 KO lines)	168 (18 KO lines)
Total animals quantified	703 (38 pedigrees)	690 (6 + 16 wk cohorts = 366 + 324)	98 (6 + 16 wk cohorts = 87 + 11)
Ectopia phenotype yield	0.8 % (1hit in 125 pedigrees)	0%	0%
Quantified phenotype yield	15.8% (6 hit lines in 38 pedigrees screened)	8.7% (20 hit lines in 229 genes screened)	38.8% (7 hit lines in 18 genes screened)
Number of gene-phenotype associations established	1 mutation (+2 lines with identified candidate mutations)	20 (65% of hits have literature support for CNS role including 15% which have been linked to human CNS disease)	7 (29% of hits have literature support for CNS role)
Gene-phenotype associations per thousand animals sacrificed	0.5 (1.5 if *Pinky* and *Marble* candidate genes confirmed)	17.1	42

Figure79: ** 6 and 16 week old cohort data combined. † Non-BL/6 lines more likely to generate false positive due to mixed 129 background effects.*

Assessment of my neuroanatomical screening method

ENU screens for behavioural phenotypes have, at best, produced yields of ~2% (Nolan *et al.*, 2000). Screens of thousands of animals for complex behaviours such as alcohol preference, anxiety or memory defects have been almost entirely fruitless (Keays, 2005, Pawlak *et al.*, 2008, Reijmers *et al.*, 2006). These low yields are a consequence of small effect sizes and limited statistical power. My approach sought to bypass these problems by screening for highly penetrant morphological phenotypes. This proved successful with my ENU and KO screens generating hit rates of 15.8% and 8.7% respectively. I also successfully used the *Whirligig* and *Diminuendo* lines in **chapter 5** to prove that phenotypes detected using my neuroanatomical screening method can accompany behavioural defects.

Further advantages of my adult neuroanatomical screening method are highlighted by my results in **chapters 3 and 4**. The V4858E hydin mutant has progressive hydrocephalous and would have not been detected if screened embryonically. Another key feature of **chapters 3 and 4** was the range of phenotypes detected. For example: pyramidal cell layer ectopia in *Marble*; corpus callosum agenesis in *Pinky* and *Wdr47* -/-; cortical thinning in *Mcph1* -/- and thickening in *Farp2* -/-; ventricle enlargement in *Hydin* and *Ap4le* -/-; microcephally in *Ube3b* -/- and *Mysm1* -/-.

The pattern of my results highlights two important points. First, yield reflects the diversity of structures screened. Expanding analysis to encompass additional brain regions could only increase yield rate. This is a considerable advantage over both embryonic screening and behavioural screening. Embryonic screens are limited in their scope as intricate structures within the brain are not readily discernable. Behavioural screens are limited to assessing phenotypes that can be assessed at high throughput (Stottmann and Beier, 2010, Nolan *et al.*, 1997).

Second, both of my screens yielded lines which mirror anatomical defects which may be informative about human mental retardation pathology. Cortical malformations and other neuroanatomical abnormalities associated with mental retardation can arise due to abnormal levels of neurogenesis, inappropriate apoptosis and defective neuronal migration (Francis *et al.*, 2006, Pang *et al.*, 2008, Manzini and Walsh, 2011, Poulton *et al.*, 2011). As the dentate gyrus is a site of neurogenesis, it is reasonable to propose that lines which featured defects in dentate gyrus size may also feature alterations in their level of neurogenesis. If there is a severe reduction in neurogenesis, brain section area or hippocampus area may also be reduced. Lines which featured a reduction in both dentate gyrus length and total brain section area included *Mysm1*, *Atpif1* and *Ube3b*. *Ube3b* is related to *UBE3A*, the gene which underlies Angelman syndrome. My work in *Git2* and *Mbd2* further suggested that abnormal hippocampal anatomy can be associated with changes in neurogenesis: neurogenesis and stratum radiatum thickness are both elevated in *Git2* -/- and both decreased in *Mbd2* -/-. However, changes in anatomical thickness can also be due to alterations in cell size or atrophy from excessive cell death.

Work in the *Jenna* mouse, a model for type 1 lissencephaly, highlighted that *Tuba1* mutations are associated with increased levels of cell death (Keays *et al.*, 2007, Edwards *et al.*, 2011). As neurogenesis levels are normal in *Jenna* mutants, elevated cell death in addition to defective neuronal migration has been proposed as a pathophysiological mechanism in tubulinopathies (Edwards *et al.*, 2011, Keays *et al.*, 2010). Evidence from *TUBA1* mutant patients is consistent with this: several display progressive microcephally despite featuring a normal biparietal diameter in their third trimester (Morris-Rosendahl *et al.*, 2008, Bahi-Buisson *et al.*, 2008). Whilst my screens do not directly measure cell death, elevations in apoptosis level can result in tissue atrophy and lead to significant reductions in cortical and hippocampal thickness (Moriya *et al.*, 2011, Potkin *et al.*, 2009, Hickey and

Chesselet, 2003). Elevated apoptosis can also be associated with ventricle enlargement (Niklasson *et al.*, 2010, Feng *et al.*, 2004). As shown in **chapter 4**, many hit genes are associated with abnormal cortical thickness, hippocampal area or ventricle size including *Sptbn1* and *Slx4*. *Sptbn1* is related to *SPTAN1*, a gene which is implicated in human West Syndrome, an epileptic condition associated with cognitive impairment (Saitsu *et al.*, 2010). Similarly, *SLX4* mutations in patients have been associated with Fanconi anaemia, a condition which features microcephally (Stoepker *et al.*, 2011).

Enlargement of the ventricles can also occur in human ciliopathies associated with mental retardation, such as Joubert syndrome and Dandy-Walker syndrome, due to defective cerebrospinal fluid flow (Putoux *et al.*, 2011, Spennato *et al.*, 2011, Bachmann-Gagescu *et al.*, 2012). As primary cilia play a role in axon guidance, ciliopathies can also be associated with corpus callosum agenesis (Engle, 2010, Putoux *et al.*, 2011, Juric-Sekhar *et al.*, 2012). My screens were able to detect lines with these anatomical defects. The *Hydin* line features progressive hydrocephalous and the *Wdr47* -/- line features corpus callosum agenesis.

Another pathophysiological mechanism underlying mental retardation is neuronal migration defects. Mutations in *TUBA3*, *LIS1*, *RELN* and *DCX* all cause cortical malformation in humans (Keays *et al.*, 2007, Hong *et al.*, 2000, Dobyns *et al.*, 1993, Sossey-Alaoui *et al.*, 1998, Willemsen *et al.*, 2012). Mutations in the mouse homologs of these genes also result in neuroanatomical defects. Specifically; *Jenna*, *Lis1*, *Reeler* and *Dcx* mice, all feature disruption to the hippocampal pyramidal cell layer (Boyle *et al.*, 2011, Keays *et al.*, 2007, Hirotsune *et al.*, 1998, Bazelot *et al.*, 2012). The *Marble* mouse also displays similar pyramidal cell layer ectopia, inviting the possibility that *Pik3r4* may play a role in neuronal migration. Furthermore, neuronal migration defects lead to a shortened dentate gyrus in the *Legs at odd angles* (*Loa*) line (Ori-McKenney and Vallee, 2011). *Loa* mice feature a mutation

in *Dync1h1*. Mutations in *DYNC1H1* cause mental retardation with defective neuronal migration in humans (Willemsen *et al.*, 2012).

In summary, various anatomical measures used in my screen may be altered by the same pathogenic mechanisms which underlie mental retardation syndromes. One, aberrant levels of neurogenesis and cell death can result in abnormal thickness measurements. This is evident from studies in *Git2*, *Mbd2* and *Jenna*. Two, mutations leading to hydrocephalous will result in lines with enlarged ventricles such as the *Hydin* line. Three, neuronal migration defects can result in lines with pyramidal cell layer ectopias; *Jenna*, *Lis1*, *Reeler* and *Dcx*. Mutations in the human homologues of these lines cause mental retardation with cortical malformation. The *Marble* line ectopia closely resembles the hippocampal ectopia previously reported in the *Jenna* mouse (Keays *et al.*, 2007). Given these points, abnormal mouse lines have the potential to suggest candidate genes that underlie mental retardation syndromes.

Historically, several factors have slowed progress in establishing novel genetic causes of syndromic autosomal mental retardation in humans: Mutations are typically *de novo* or only present in small pedigrees (Ropers, 2010, Chelly *et al.*, 2006); Near-identical disease phenotypes are a barrier to forming well matched cohorts for screening (Francis *et al.*, 2006, Walsh, 1999). Previous studies have shown that genetic mutations in mice which are associated with neuroanatomical defects can have human homologs associated with mental retardation and related disorders (Keays *et al.*, 2007, Edwards, 2008, Corbo *et al.*, 2002, Assadi *et al.*, 2003).

This leads to my first five conclusions:

1. *Neuroanatomical screening in adult ENU pedigrees and KO lines produces a far higher yield than direct behavioural screening.*
2. *Detected lines can be bred and tested in sufficient numbers in behavioural paradigms to find behavioural defects relating to their anatomical abnormalities. This allows for small effect size behaviours with a neuroanatomical basis to be assessed with adequate power.*
3. *Genetic causes underlying non-congenital progressive disorders such as hydrocephalus can be detected using my screening method.*
4. *Genetic mutations can cause a wide variety of neuroanatomical defects in multiple structures. Optimal detection of gene-phenotype requires multiple brain structures to be quantified.*
5. *My method can be used to collect data on the range of genetic mutations that cause specific anatomical phenotypes and may be useful in highlighting candidate genes which cause human mental retardation.*

Strengths and weaknesses of my screens

Both screens led to novel gene-phenotype associations. The ENU project led to the discovery of a novel mutation in the *Hydin* gene, a gene involved in cilia function (Dawe *et al.*, 2007). The affected mouse develops hydrocephalus in adulthood unlike the previously discovered *Hy3* mutant that typically dies in infancy (Davy and Robinson, 2003). As fatality is delayed, the extent to which cilia defects impact on adult tissues could be studied. From this, we found that homozygous animals were infertile. Sperm from affected males are tailless and fully immobile. As a result, our findings suggest that *Hydin* may be an infertility gene in addition to its role in the brain. This highlights two strengths of ENU. First, it can create mutations which are informative about the importance of specific amino acid residues. Second, it can produce mutations which give rise to milder phenotypes than those produced from truncated alleles. This is useful in evaluating the role of a gene if the KO allele is embryonic or perinatal lethal.

A third strength of the ENU screen was the high rate of phenotypic hits: 15.8%. This is nearly double the 8.7% phenotypic hit rate of the KO screen. Arguably, this ENU phenotypic hit rate is substantially less than might be expected. Of the 25-40 gene mutations typically carried by ENU G1 founder males, 8-12 mutations are predicted to result in null alleles or transcript disruption (Keays *et al.*, 2006, Acevedo-Arozena *et al.*, 2008). However, the ENU phenotype hit rate was far from 8 to 12 fold higher than the rate of the KO screen. This is likely due to the conservative threshold set for detecting phenotypic animals in the ENU screen.

This conservative threshold was put in place due to the following three weaknesses of the ENU approach. First, phenotypes need to be strong enough to map to a genetic interval. Weak phenotypes could lead to affected animals being classed as unaffected and vice versa. This would lead to inaccurate mapping. Second, the potential consequences of wrongly

classing a pedigree as mutation bearing are substantially worse than the consequences of making a false negative. ENU mutation mapping requires substantial breeding and phenotyping. Abandoning the mapping process due to a false positive represents a significant waste of time and resources. Third, minor variation in G3 measurements could arise due to mixed C3H:BL/6 background effects and age. There was no such thing as a WT control in the ENU screen. All animal bore a plethora of mutations which may have collectively had a minor effect on their anatomy. This created potential contamination bias. Consequently, the threshold of significance in the ENU screen has higher to counter the elevated experimental noise.

A fourth weakness of the ENU was the rate that phenotypic hits could be translated into gene-phenotype associations. The genetic cause of pathology was only proven for the *Hydin* line. Whilst it is likely that the *Marble* phenotype is caused by a mutation in *Pik3r4*, confirmation studies have not yet been completed (despite several years of work). The *Pinky* line perfectly demonstrates why making gene-phenotype associations can be so slow using the ENU approach: induced mutations need to be segregated in order to prove a causative monogenic link. This is particularly frustrating if multiple ENU induced mutations are proximal and inherited together through linkage. In the *Pinky* line, two candidate mutations are present within the mapped interval. Establishing which genes are causal to a phenotype, and which are not, is a profound strength of the KO screen.

A fifth weakness of ENU screening can be seen from my results. The *Pik3r4* SNP in *Marble* and the Fnbp1l SNP in *Pinky* would result in premature stop codons likely to lead to nonsense mediated decay. This means that half of my ENU candidate SNPs would likely result in null alleles. This suggests a high proportion of findings from an ENU screen would be superfluous to a KO screen.

When a phenotype is identified in a KO line, the gene-phenotype association is known immediately. In stark contrast to the single gene-phenotype association made using the ENU approach, the KO approach made twenty positive associations. In addition, hundreds of genes were verified as not being associated with specific anatomical defects (at least not in 6 or 16 week old animals). If *Fnbp1l* -/- and *Ndst3* -/- KOs were available for screening I could verify in neither, one or both of the *Pinky* candidate mutations was causative.

As genotypes were known, the KO approach had further strengths. First, results could be critically evaluated. If a WT sample was found to have spontaneous hydrocephalous it could be excluded from the analysis. If only one of three mutant samples was abnormal for a given KO line, sources of potential experimental error such as inaccurate measuring could be investigated.

Second, it was possible to establish if individual KO lines were adequately powered. If only one KO sample survived processing, additional samples could be requested from the Sanger. Lines, such as *Git2*, that neared significance and had subtle morphological abnormalities could be retested with a greater n.

It could be argued that a weakness of the KO approach was that it was limited to lines where null alleles were not embryonic lethal. An ENU induced missense mutation in the same gene may result in a milder, viable, phenotype. **Chapter 7** demonstrates that the cre lox system can be used to create brain specific conditional KO mutants to bypass somatic causes of lethality. As Sanger's KO lines are generated via the knock out first method they can readily be converted into conditional mutants (Testa *et al.*, 2004).

This leads me to conclusions six to ten of my thesis:

6. *While ENU generates a higher rate of phenotypic hits, the bottleneck in identifying causative mutations cripples the rate at which gene-phenotype associations can be established.*
7. *The source of this bottleneck is the same factor which leads to the high phenotypic yield in ENU pedigrees: dozens of coding mutations are induced per gamete. Mutations are produced in a chaotic, a priori, manner. This randomness can lead to multiple candidate mutations being within a mapped interval, frustrating assessment of SNP pathogenicity.*
8. *Half of my ENU candidate genes contain SNPs likely to result in null alleles. This suggests that a high proportion of findings from ENU screens would be more readily found in a large scale KO screen.*
9. *KO screening has several key advantages over ENU screening: animal numbers can be controlled to boost statistical power; samples can be critically evaluated in an informed manner allowing for biasing effects to be filtered; negative results are informative about which genes do not have an effect on mouse neuroanatomy.*
10. *KO screening has no significant disadvantages to ENU screening. If a null allele is lethal due to somatic causes, conditional mutants can be generated.*

My findings and their importance

It is beyond the scope of my thesis to investigate the mechanisms by which my mutations induce pathology. It is also beyond the scope of my thesis to establish if mutations in human homologs lead to CNS defects. This said, several of my hit genes may be worth screening in patient cohorts. Despite more than 300 genes being implicated in human mental retardation, it is speculated that thousands of novel genetic links may remain to be discovered (Inlow and Restifo, 2004).

From the ENU screen, the *Marble* mouse bears a mutation likely to result in null expression of *Pik3r4*. This line features hippocampal ectopia similar to that of the *Jenna* mouse (Keays *et al.*, 2007). Mutations in *TUBA3*, the human homolog of the mutated *Jenna Tuba1* gene, are causal to lissencephaly. Pik3 activity is also up-regulated in the mouse model of Fragile X syndrome (Gross *et al.*, 2010). As a consequence, I consider it a suitable candidate for screening in human patient cohorts.

15% of hit genes detected in my KO screen have already been associated with CNS defects in humans. These include *AP4E1*, *MCPH1* and *SLX4* (Stoepker *et al.*, 2011, Jackson *et al.*, 2002, Abou Jamra *et al.*, 2011). This suggests that the KO screen is reliable and that in many instances gene-phenotypes associations translate across the species barrier. Of the remaining KO hit genes with supporting literature evidence, I consider three genes to be the most worthy of screening in patient cohorts.

First, *UBE3b* as it has been reported to be included in a 12q22-q24 deletion interval in a patient with mental retardation (Petek *et al.*, 2003). Angelman syndrome is caused by disruption of the maternal *UBA3a* allele and is associated with profound mental retardation with microcephaly (Williams *et al.*, 2010a). My data shows the *Ube3b* -/- also features microcephally in mice.

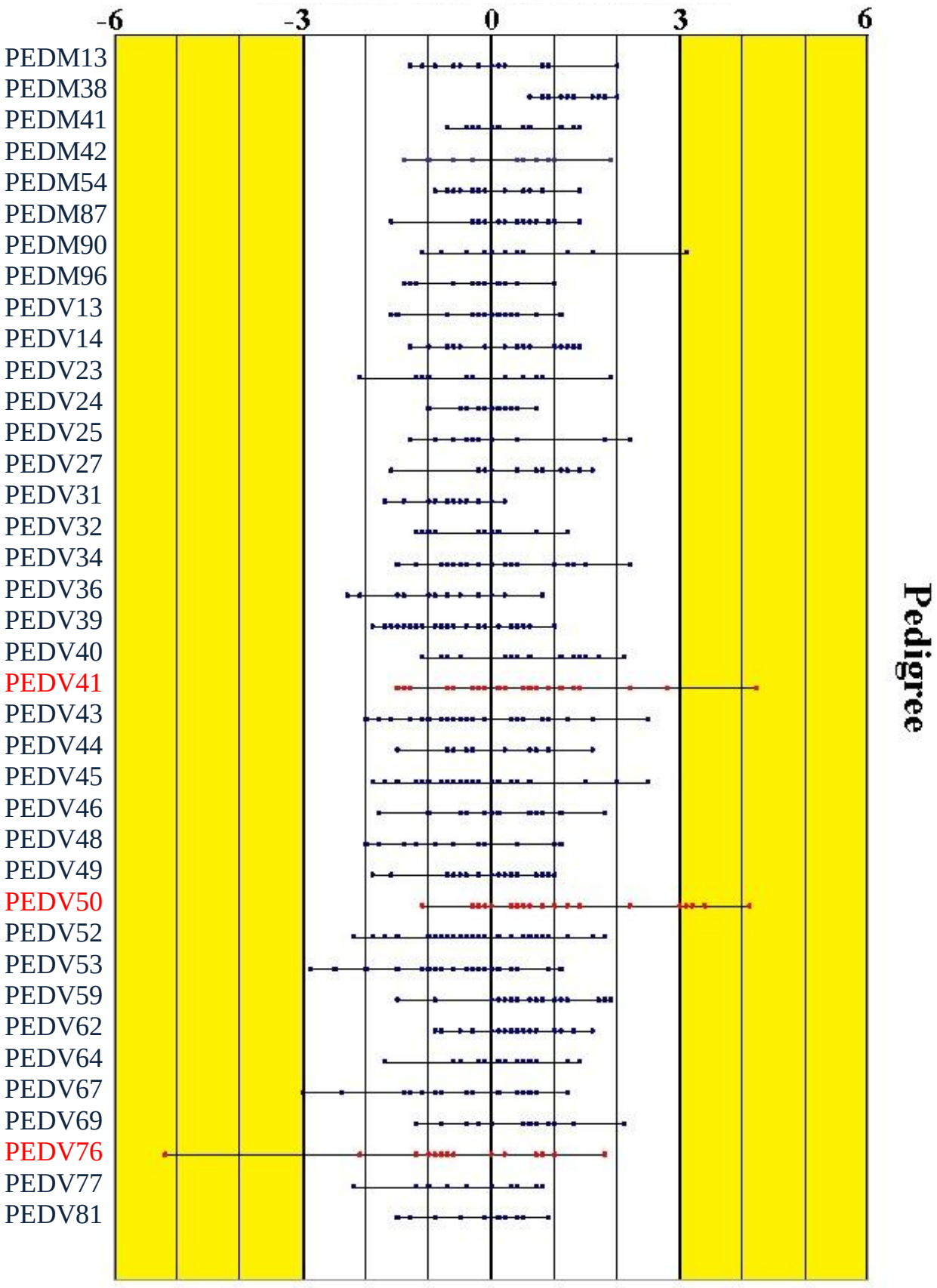
Second, *Wdr47* as several WD repeat proteins have been implicated in mental retardation. These include LIS1, CSA and WDR62 (Li and Roberts, 2001, Bilguvar *et al.*, 2010). *WDR62* mutations have been associated with microcephaly, cortical malformations and corpus callosum hypoplasia (Bilguvar *et al.*, 2010). Additionally, Wdr47 is reported to be a putative ligand for the N-terminal *Reeler* domain of Reelin (McGillewie, 2009).

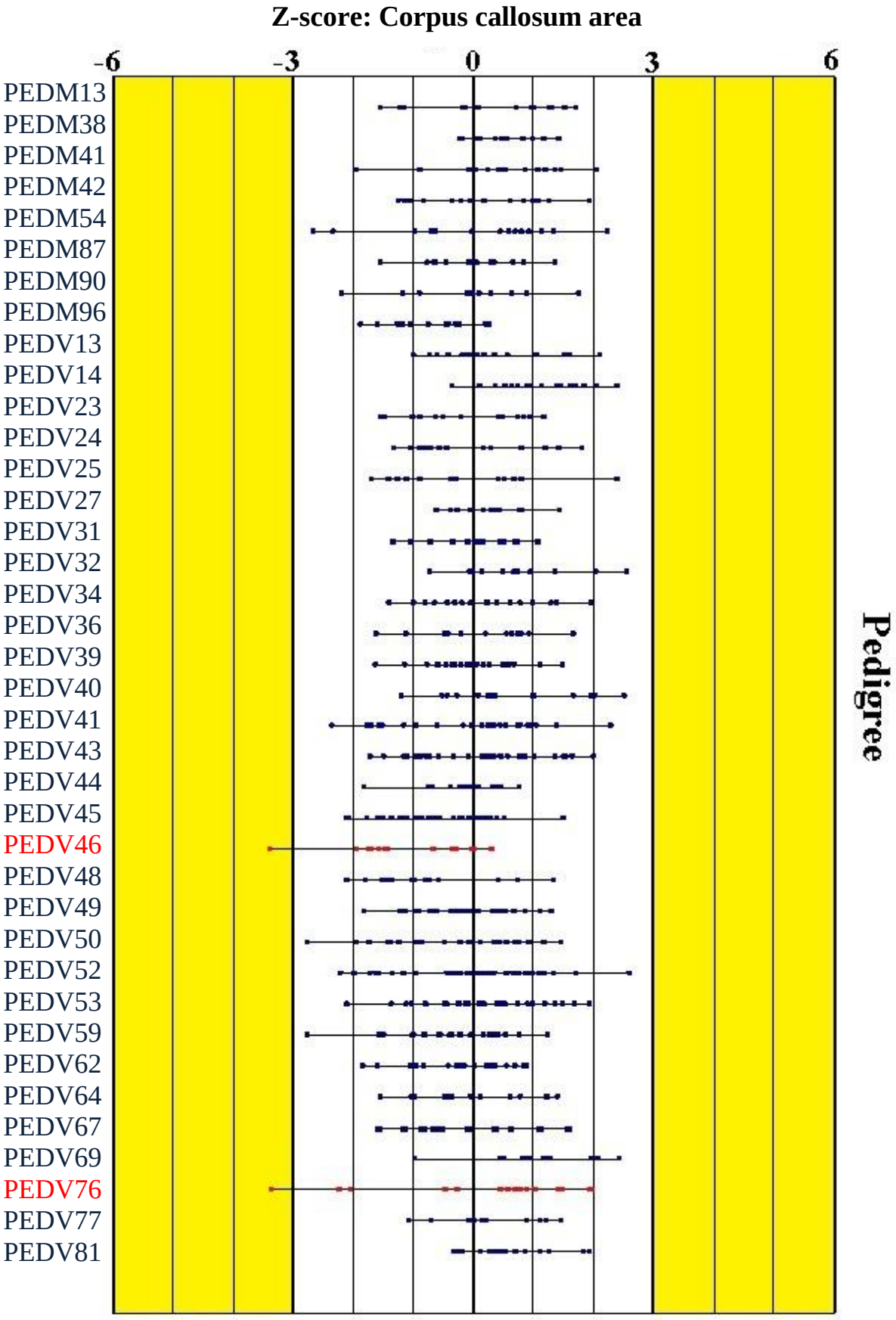
Third, *SPTBN1* as mutations in the related binding partner *SPTAN1* have been implicated in West syndrome (Saitsu *et al.*, 2010). This condition is associated with mental retardation, cortical and cerebellar atrophy, corpus callosum malformation, hypomyelination, poor visual attention and epilepsy.

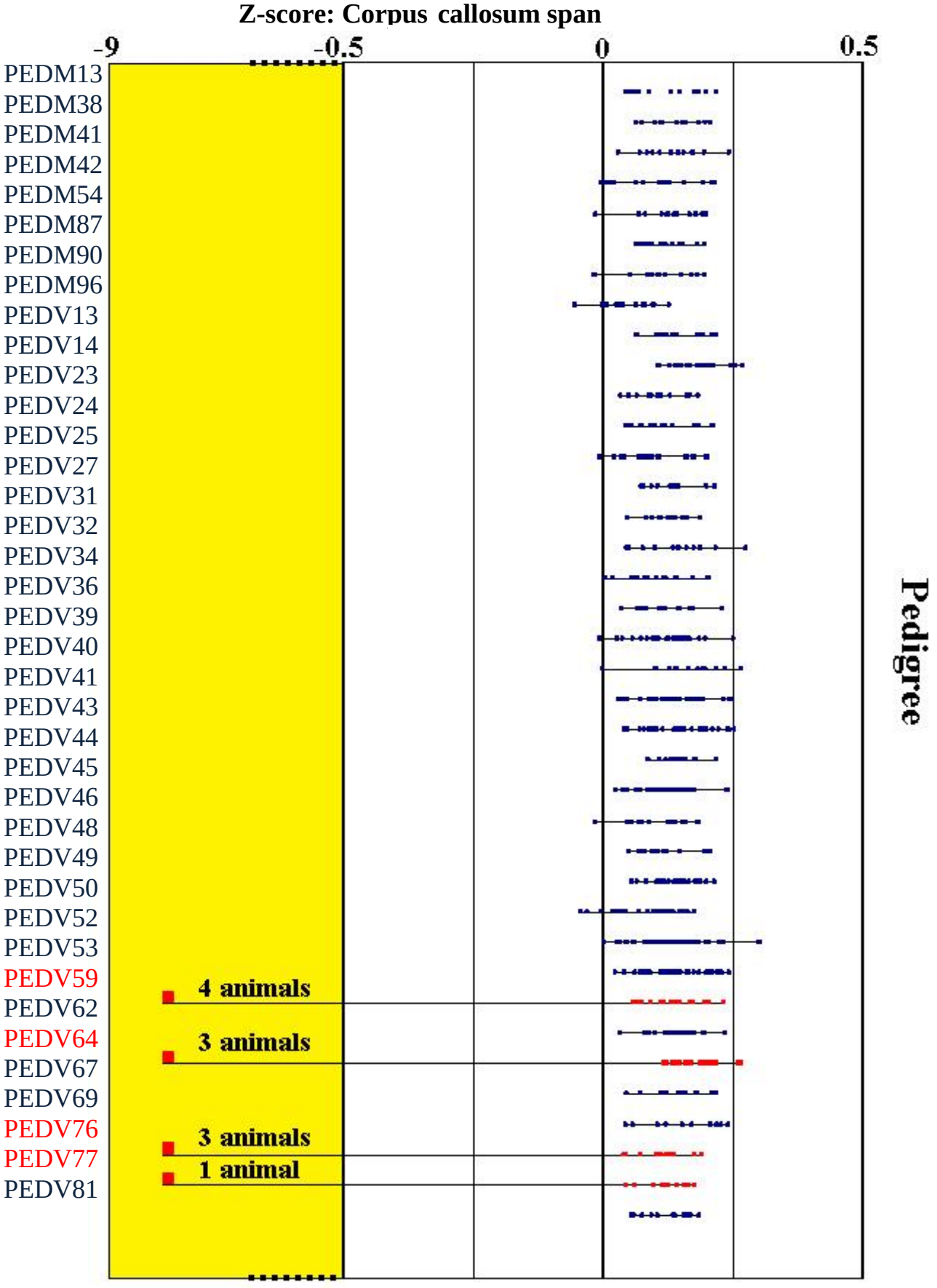
This leads to my eleventh and twelfth conclusion, the final conclusions of my thesis:

11. *KO screen found defects in mice bearing mutations in homologs of genes known to cause human mental retardation.*
12. *PIK3R4, UBE3b, WDR47 and SPTBN1 may be worth screening in human patient cohorts.*

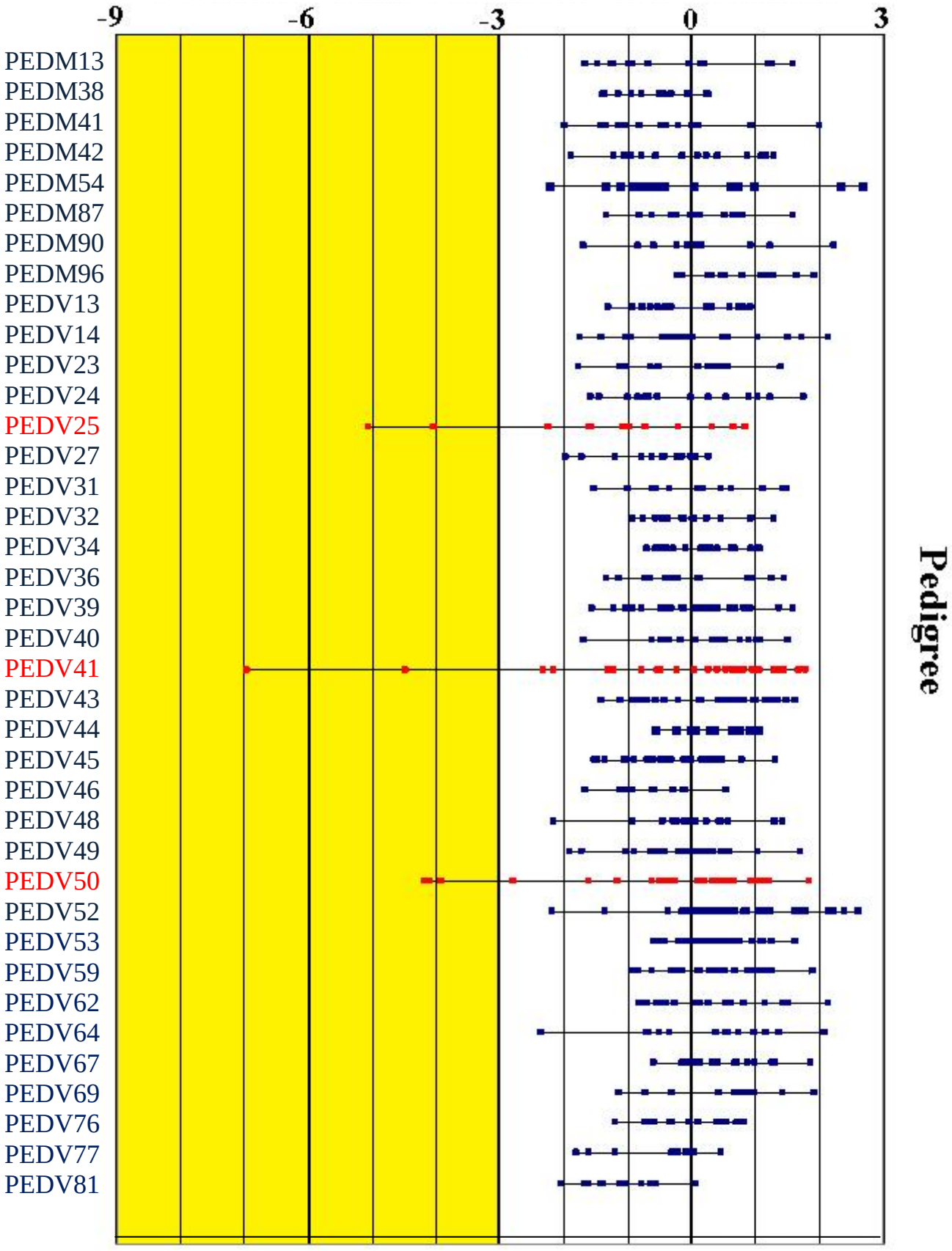
Appendix 1: ENU screen Z-score plots

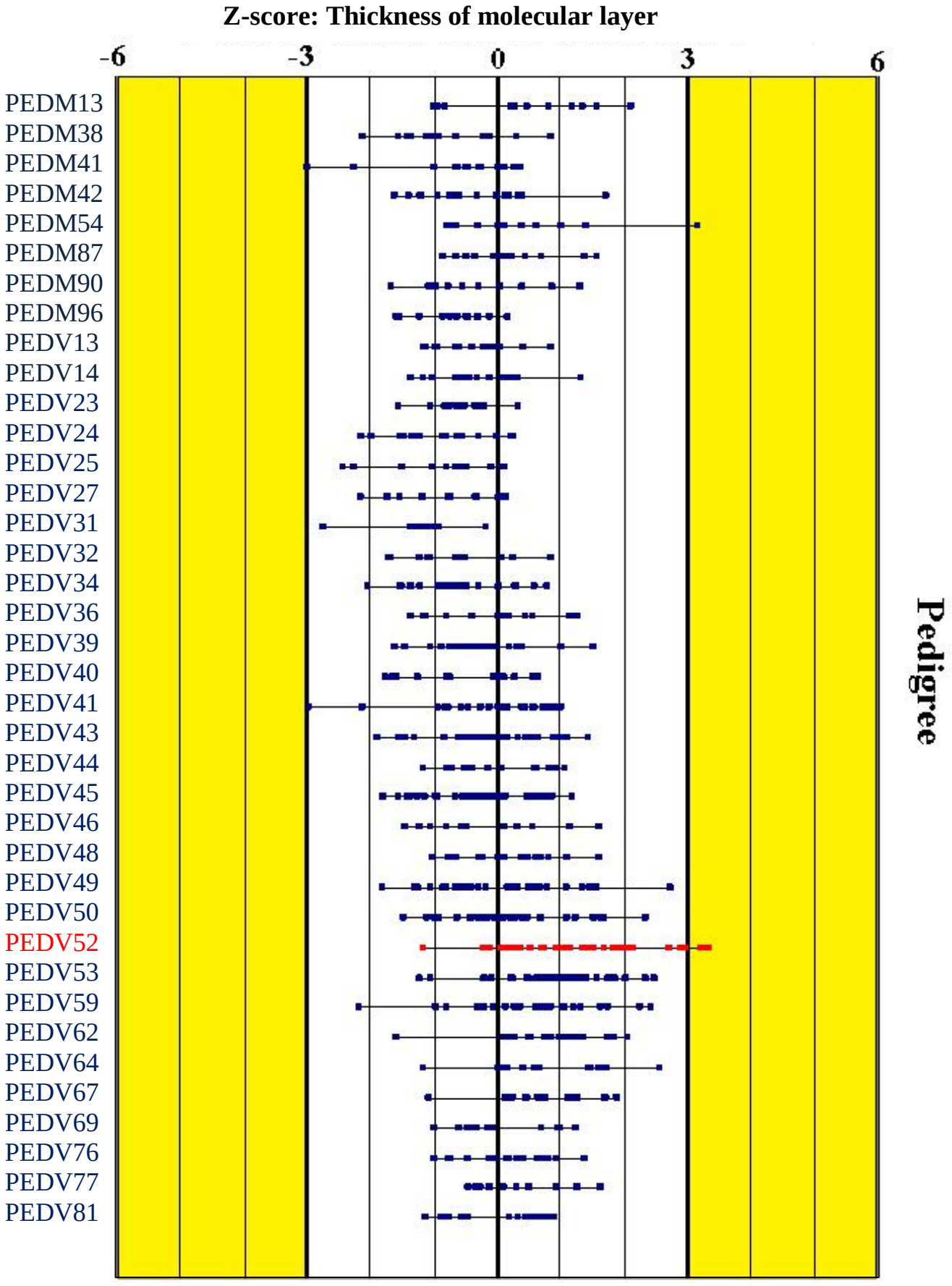


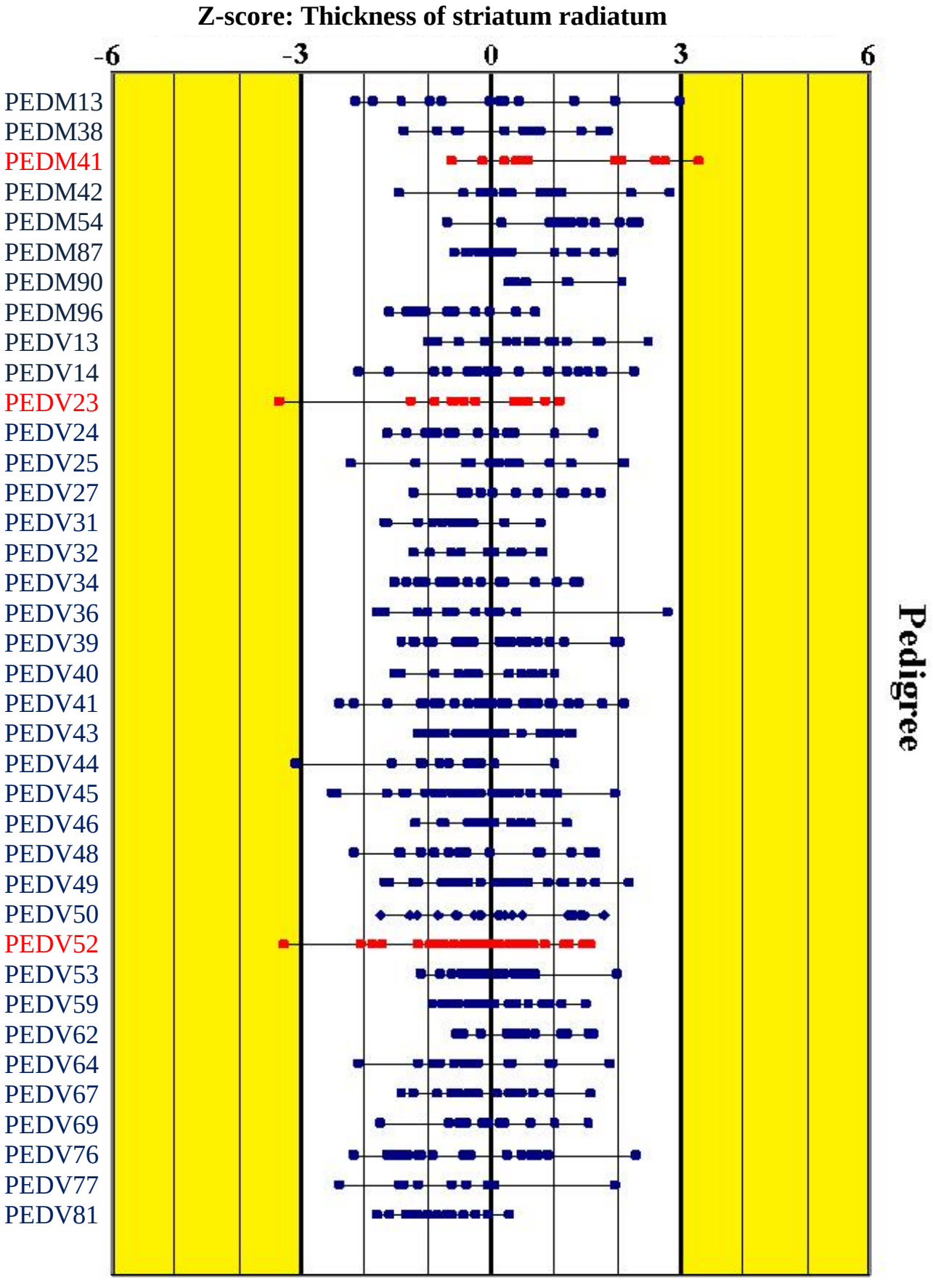

Z-score: Corpus callosum area
-6
-3
0
3
6
PEDM13
PEDM38
PEDM41
PEDM42
PEDM54
PEDM87
PEDM90
PEDM96
PEDV13
PEDV14
PEDV23
PEDV24
PEDV25
PEDV27
PEDV31
PEDV32
PEDV34
PEDV36
PEDV39
PEDV40
PEDV41
PEDV43
PEDV44
PEDV45
PEDV46
PEDV48
PEDV49
PEDV50
PEDV52
PEDV53
PEDV59
PEDV62
PEDV64
PEDV67
PEDV69
PEDV76
PEDV77
PEDV81
Pedigree

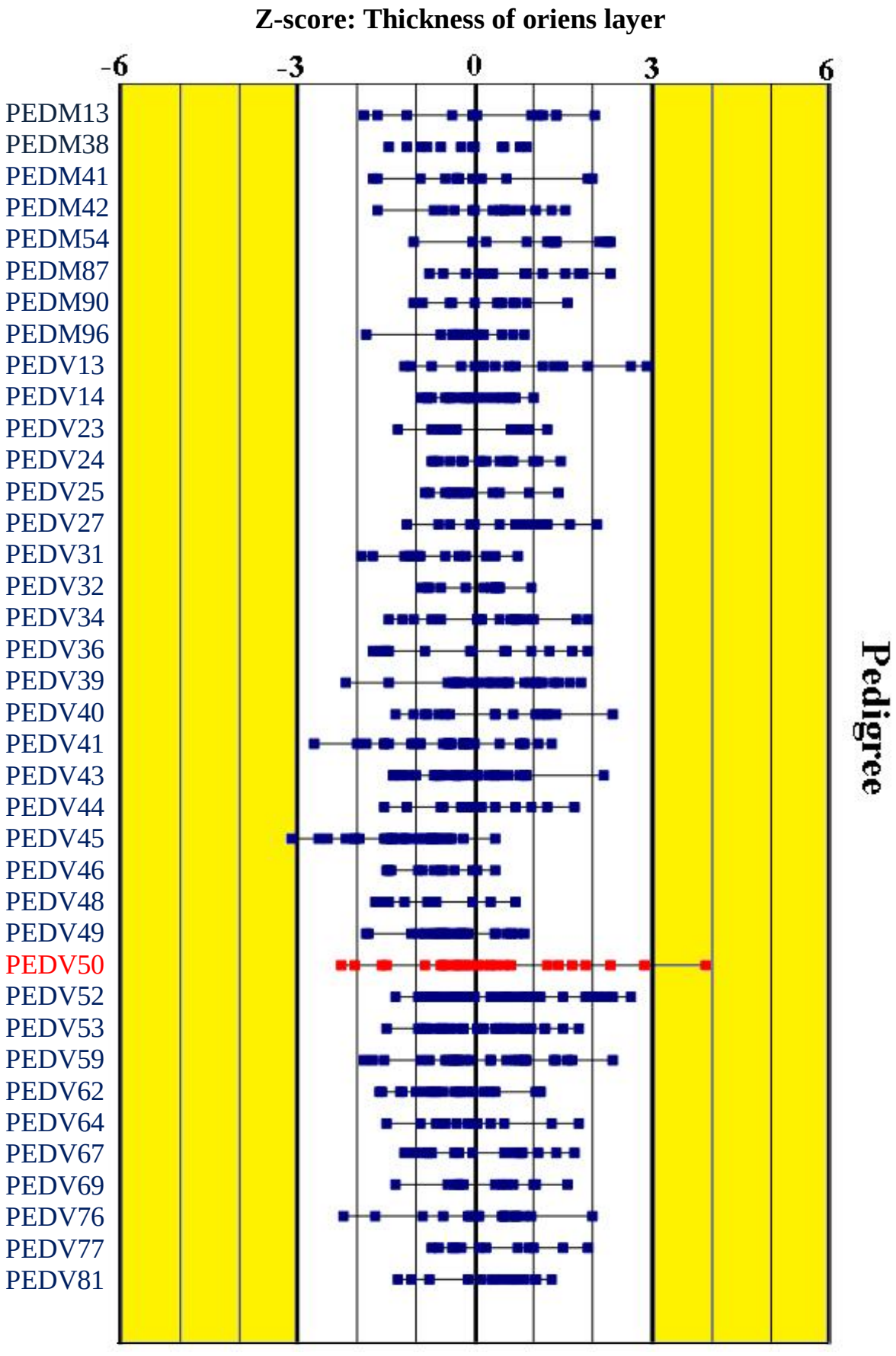

Z-score: Corpus callosum span
-9
-0.5
0
0.5
PEDM13
PEDM38
PEDM41
PEDM42
PEDM54
PEDM87
PEDM90
PEDM96
PEDV13
PEDV14
PEDV23
PEDV24
PEDV25
PEDV27
PEDV31
PEDV32
PEDV34
PEDV36
PEDV39
PEDV40
PEDV41
PEDV43
PEDV44
PEDV45
PEDV46
PEDV48
PEDV49
PEDV50
PEDV52
PEDV53
PEDV59
PEDV62
PEDV64
PEDV67
PEDV69
PEDV76
PEDV77
PEDV81
4 animals
3 animals
3 animals
1 animal
Pedigree

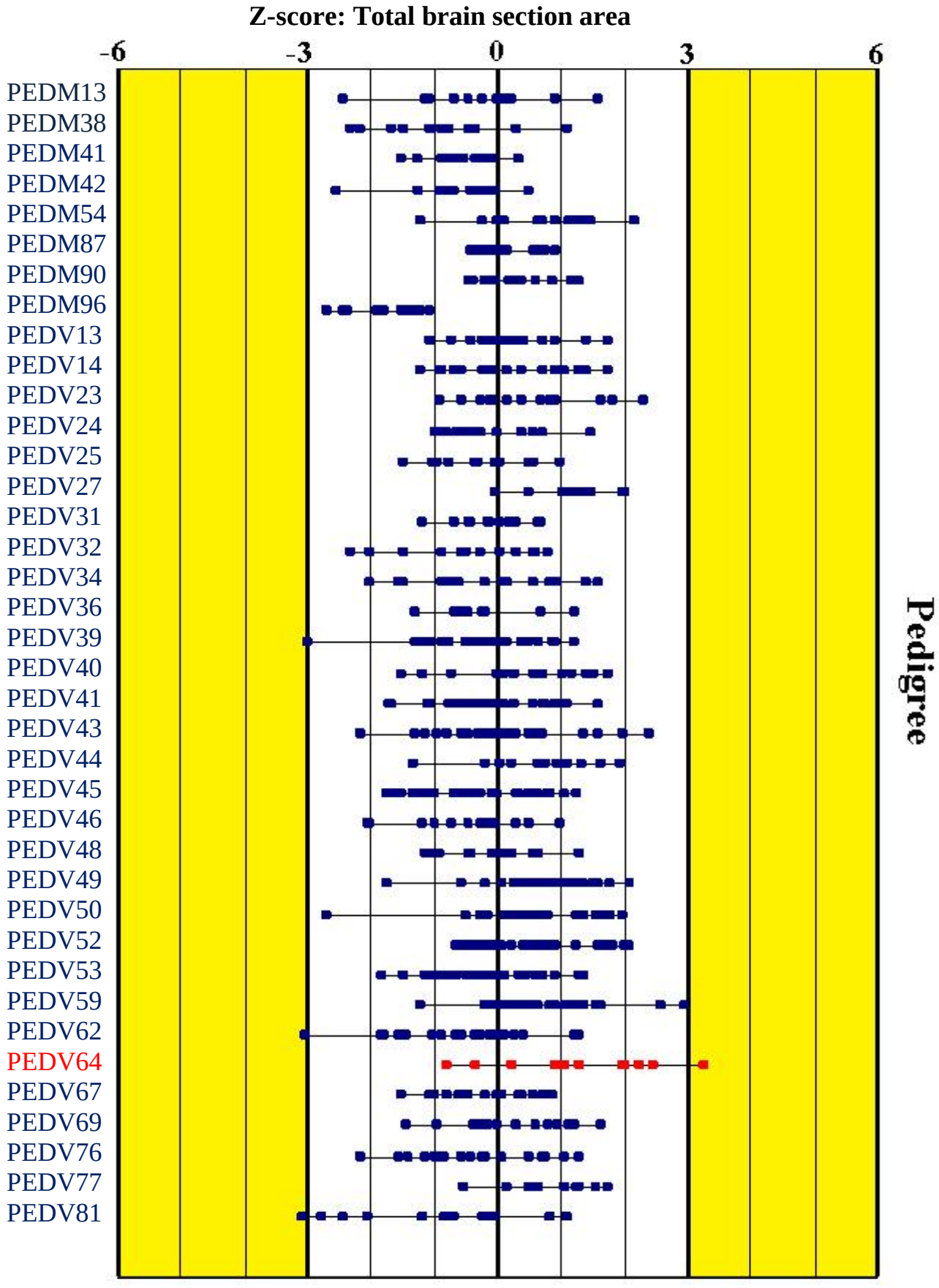
Z-score: Length of pyramidal cell layer

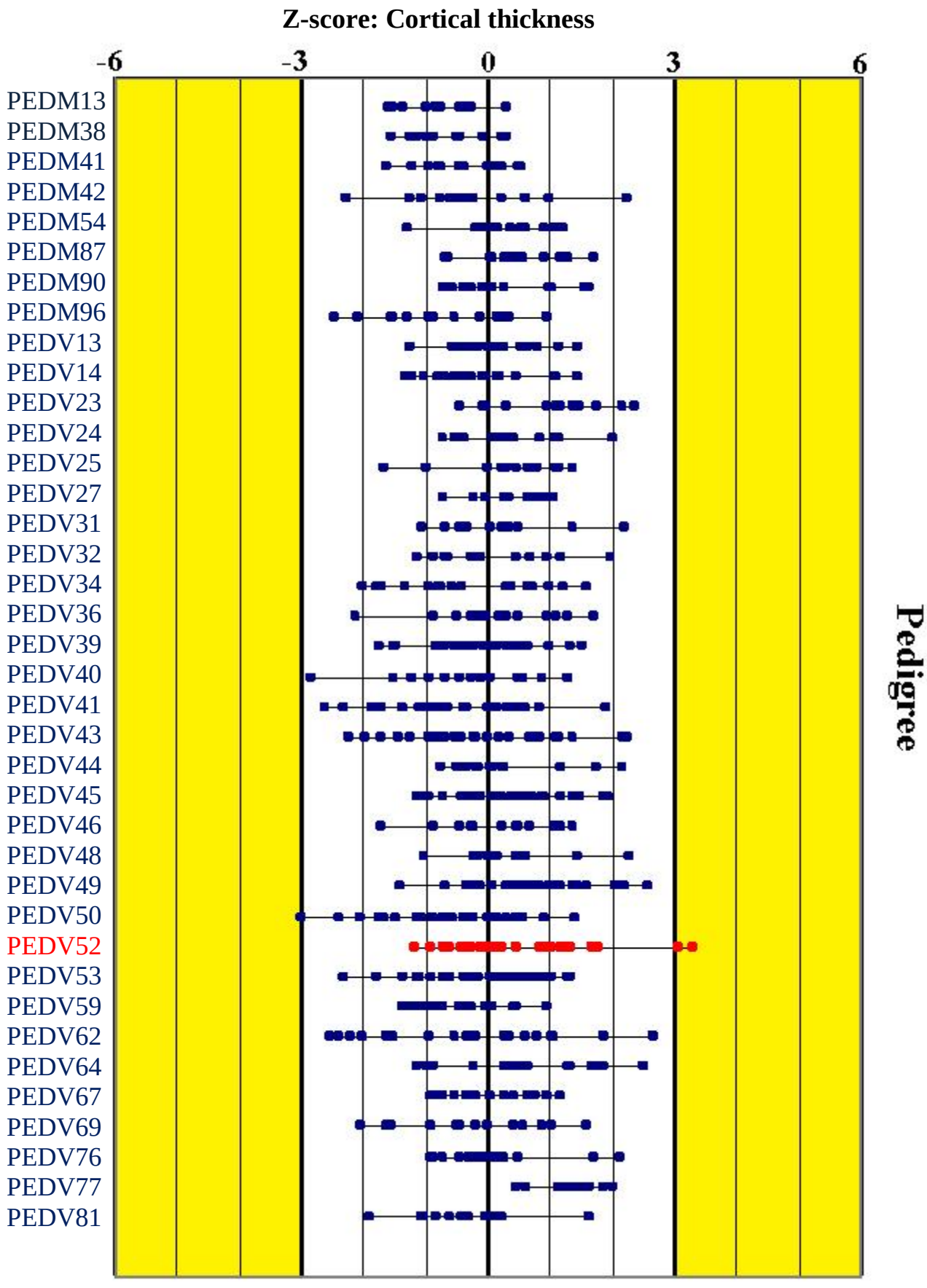



Z-score: Thickness of molecular layer
-6
-3
0
3
6
PEDM13
PEDM38
PEDM41
PEDM42
PEDM54
PEDM87
PEDM90
PEDM96
PEDV13
PEDV14
PEDV23
PEDV24
PEDV25
PEDV27
PEDV31
PEDV32
PEDV34
PEDV36
PEDV39
PEDV40
PEDV41
PEDV43
PEDV44
PEDV45
PEDV46
PEDV48
PEDV49
PEDV50
PEDV52
PEDV53
PEDV59
PEDV62
PEDV64
PEDV67
PEDV69
PEDV76
PEDV77
PEDV81
Pedigree


Z-score: Thickness of striatum radiatum
-6
-3
0
3
6
PEDM13
PEDM38
PEDM41
PEDM42
PEDM54
PEDM87
PEDM90
PEDM96
PEDV13
PEDV14
PEDV23
PEDV24
PEDV25
PEDV27
PEDV31
PEDV32
PEDV34
PEDV36
PEDV39
PEDV40
PEDV41
PEDV43
PEDV44
PEDV45
PEDV46
PEDV48
PEDV49
PEDV50
PEDV52
PEDV53
PEDV59
PEDV62
PEDV64
PEDV67
PEDV69
PEDV76
PEDV77
PEDV81
Pedigree


Z-score: Thickness of oriens layer
-6
-3
0
3
6
PEDM13
PEDM38
PEDM41
PEDM42
PEDM54
PEDM87
PEDM90
PEDM96
PEDV13
PEDV14
PEDV23
PEDV24
PEDV25
PEDV27
PEDV31
PEDV32
PEDV34
PEDV36
PEDV39
PEDV40
PEDV41
PEDV43
PEDV44
PEDV45
PEDV46
PEDV48
PEDV49
PEDV50
PEDV52
PEDV53
PEDV59
PEDV62
PEDV64
PEDV67
PEDV69
PEDV76
PEDV77
PEDV81
Pedigree


Z-score: Total brain section area
-6
-3
0
3
6
PEDM13
PEDM38
PEDM41
PEDM42
PEDM54
PEDM87
PEDM90
PEDM96
PEDV13
PEDV14
PEDV23
PEDV24
PEDV25
PEDV27
PEDV31
PEDV32
PEDV34
PEDV36
PEDV39
PEDV40
PEDV41
PEDV43
PEDV44
PEDV45
PEDV46
PEDV48
PEDV49
PEDV50
PEDV52
PEDV53
PEDV59
PEDV62
PEDV64
PEDV67
PEDV69
PEDV76
PEDV77
PEDV81
Pedigree


Z-score: Cortical thickness
-6
-3
0
3
6
PEDM13
PEDM38
PEDM41
PEDM42
PEDM54
PEDM87
PEDM90
PEDM96
PEDV13
PEDV14
PEDV23
PEDV24
PEDV25
PEDV27
PEDV31
PEDV32
PEDV34
PEDV36
PEDV39
PEDV40
PEDV41
PEDV43
PEDV44
PEDV45
PEDV46
PEDV48
PEDV49
PEDV50
PEDV52
PEDV53
PEDV59
PEDV62
PEDV64
PEDV67
PEDV69
PEDV76
PEDV77
PEDV81
Pedigree

Appendix 2: KO screen non-CNS phenotypes (6 wks)

KO line	Significant findings from Sanger's other pipelines
Akt2	*Akt2* -/- mice have low glucose tolerance. Both -/- and +/- mice are reduced in body weight and feature a weak grip
Ampd3	Abnormalities in peripheral blood lymphocytes
Brd7	*Brd7* -/- mice are subviable
Cadm1	*Cadm1* -/- male mice are infertile
Dusp3	*Dusp3* -/- mice are of normal weight but have a higher percentage of fat mass. Mice also feature malformations of the spine and their immune system is less efficient in clearing infection
Epc1	*Epc1* -/- mice are subviable. Heterozygous animals are significantly reduced in weight and males have elevated energy expenditure relative to WT
Epc2	*Epc2* -/- mice are homozygous lethal
Farp2	*Farp2* mutants are feature skin abnormalities
Git2	*Git2* -/- mice are less sensitive to heat and have significantly reduced white blood cell counts
Hmx3	*Hmx3* -/- mice are hyperactive, subfertile, perform poorly on the rotarod, and are reduced in both weight and length
Kctd10	*Kctd10* -/- mice are homozygous lethal. Heterozygous mice feature joint abnormalities and a weakened grip
Magi2	*Magi2* -/- mice are homozygous lethal
Mgst3	No physiological or behavioural have been reported
Mta1	*Mta1*-/- mice feature weakened grip strength. Both -/- and +/- mice feature elevated heart rate and spinal defects
Mysm1	*Mysm1* -/- mice are subviable, reduced in weight and length, have a lower percentage fat mass, move significantly less in the open field, have elevated energy expenditure, and are insensitive to heat. Mice also perform poorly on the rotarod suggesting a balance defect. They feature abnormal coat colour and limb/tail malformations. Red and white blood cell counts are reduced whilst mean corpuscular haemoglobin and platelet counts are elevated. Additionally, female KOs develop cataracts.
Ncaph2	*Ncaph2* -/- mice are homozygous lethal. The ENU derived *Nessy* mice, which feature a homozygous mutation in Ncaph2, feature low T-cell counts and altered CD4:CD8 profiles (Gosling *et al.*, 2008)
Prkcz	High incidence of eye abnormalities (Bergmeister's papilla) in *Prkcz* -/- mice. KOs have been reported have a significantly weakened immune response when immunised with to T-cell dependant antigen (Martin *et al.*, 2002)
Psmb2	No physiological or behavioural have been reported
Slx4	*Slx4* -/- mice are subviable, subfertile, are significantly reduced in weight and length, have fused spinal vertebra, have abnormal eye size and pigmentation, have reduced platelet counts and significantly lighter hearts
Sptbn1	*Sptbn1* -/- mice are homozygous lethal
Smyd2	*Smyd1* -/- mice have elevated blood cholesterol
Ube3b	*Ube3b* -/- mice have reduced viability and have significantly reduced body weight. Mice have a weaker grip, reduced sensitivity to heat and abnormal skull morphology
Wdr47	*Wdr47* -/- mice have significantly elevated energy expenditure levels

Appendix 3: KO screen gene expression (6 wks)

KO line	Allen Brain Atlas expression summary
Akt2	Expressed in the dentate gyrus, subventricular zones and cerebellum of adult mice. No information on embryonic expression is available.
Ampd3	*Ampd3* is not extensively expressed in the adult mouse brain. No information on embryonic expression is available.
Brd7	Expressed in the pyramidal cell layer and dentate gyrus of adult mice. No information on embryonic expression is available.
Cadm1	Is expressed throughout the adult mouse brain. Staining is most intense at the pyramidal cell layer, dentate gyrus and cortex.
Dusp3	*Dusp3* is widely expressed in the adult mouse brain. Expression is particularly strong in the pyramidal cell layer at CA3 and in layer IV of the cortex.
Epc1	*Epc1* is not widely expressed in the adult mouse brain. No information on embryonic expression is available.
Epc2	*Epc2* is not widely expressed in the adult mouse brain. No information on embryonic expression is available.
Farp2	*Farp2* is not widely expressed in the adult mouse brain. No information on embryonic expression is available.
Git2	Highly expressed in the subventricular zone of the lateral ventricles, olfactory bulbs, dentate gyrus and cerebellum in adult mice. These areas are associated with neurogenesis or the migration of newly formed cells (Ponti *et al.*, 2008, Schlessinger *et al.*, 1975, Bovetti *et al.*, 2011).
Hmx3	*Hmx3* is expressed in throughout the adult mouse brain. Staining is most intense in the cerebellum, thalamus, brainstem and layers 3 & 4 of the cerebral cortex.
Kctd10	*Kctd10* is not widely expressed in the adult mouse brain. No information on embryonic expression is available.
Magi2	*Magi2* is strongly expressed throughout the adult mouse brain.
Mgst3	*Mgst3* is expressed in the cortex, thalamus and pyramidal cell layer.
Mta1	*Mta1* is expressed throughout the adult mouse brain. Expression is strongest in the dentate gyrus, pyramidal cell layer, cortex and cerebellum.
Mysm1	*Mysm1* is not widely expressed in the adult mouse brain. No information on embryonic expression is available.
Ncaph2	No information on *Ncaph2* expression is available.
Prkcz	No information on *Prkcz* expression is available.
Psmb2	*Psmb2* is expressed in the pyramidal cell layer and dentate gyrus of adult mice.
Slx4	*Slx4* is expressed in the pyramidal cell layer and dentate gyrus of adult mice.
Sptbn1	*Sptbn1* is widely expressed in the adult mouse brain. Expression is strongest in the pyramidal cell layer, dentate gyrus and cerebellum.
Smyd2	*Smyd2* is expressed throughout the adult mouse brain. Staining is most intense in the pyramidal cell layer, dentate gyrus, cortex and cerebellum.
Ube3b	*Ube3b* is widely expressed in the adult mouse brain and includes the hippocampus, dentate gyrus, olfactory bulbs, cerebellum and cortex.
Wdr47	*Wdr47* is expressed in the pyramidal cell layer and dentate gyrus of adult mice.

Appendix 4: KO screen non-CNS phenotypes (16 wks)

KO line	Significant findings from Sanger's other pipelines
Ap4e1	*Ap4e1* -/- mice rear significantly less in the open field. They also feature reduced mean corpuscular haemoglobin levels and elevated platelet volume.
Arl4d	*Arl4d* -/- mice feature skeletal malformations and significantly reduced bone mineralisation. Heart weight is also significantly lighter.
Atpif1	*Atpif1* -/- mice rest significantly less in the open field maze.
Gm468	No physiological or behavioural have been reported.
Mcph1	*Mcph1* **-/-** mice are infertile, commonly feature cataracts and have significantly compromised hearing.
Mta1	This gene scored positive for both age cohorts. See 6 week cohort dataset for information.
Sfrs4	*Sfrs4* -/- mice are subviable.
Src	No physiological or behavioural have been reported.

Appendix 5: KO screen gene expression (16 wks)

KO line	Allen Brain Atlas expression summary
Ap4e1	*Ap4e1* is not widely expressed in the adult mouse brain. No information on embryonic expression is available.
Arl4d	The gene is lightly expressed in the pyramidal cell layer, dentate gyrus and cortex in adult mice. No information on embryonic expression is available.
Atpif1	The gene is ubiquitously expressed in the adult mouse brain.
Atp5a1	The gene is expressed throughout the adult mouse brain. Staining is most intense at the pyramidal cell layer, dentate gyrus and layers 3 and 4 of the cortex.
Gm468	No information on *Gm468* expression is available.
Mcph1	The gene is ubiquitously expressed in the adult mouse brain.
Mta1	This gene scored positive for both age cohorts. See 6 week cohort dataset for information.
Sfrs4	This gene is expressed in the cortex, pyramidal cell layer, dentate gyrus and cerebellum.
Src	The gene is expressed throughout the adult mouse brain. Staining is most intense at the pyramidal cell layer, dentate gyrus and the superficial layers of the cortex.

References

ABOU JAMRA, R., PHILIPPE, O., RAAS-ROTHSCHILD, A., ECK, S. H., GRAF, E., BUCHERT, R., BORCK, G., EKICI, A., BROCKSCHMIDT, F. F., NOTHEN, M. M., MUNNICH, A., STROM, T. M., REIS, A. & COLLEAUX, L. 2011. Adaptor protein complex 4 deficiency causes severe autosomal-recessive intellectual disability, progressive spastic paraplegia, shy character, and short stature. *Am J Hum Genet,* 88, 788-95.

ACEVEDO-AROZENA, A., WELLS, S., POTTER, P., KELLY, M., COX, R. D. & BROWN, S. D. 2008. ENU mutagenesis, a way forward to understand gene function. *Annu Rev Genomics Hum Genet,* 9, 49-69.

AKIYAMA, M., KOUZU, Y., TAKAHASHI, S., WAKAMATSU, H., MORIYA, T., MAETANI, M., WATANABE, S., TEI, H., SAKAKI, Y. & SHIBATA, S. 1999. Inhibition of light- or glutamate-induced mPer1 expression represses the phase shifts into the mouse circadian locomotor and suprachiasmatic firing rhythms. *J Neurosci,* 19, 1115-21.

ALCOCK, J. & SOTTILE, V. 2009. Dynamic distribution and stem cell characteristics of Sox1-expressing cells in the cerebellar cortex. *Cell Res,* 19, 1324-33.

ALLADA, R., WHITE, N. E., SO, W. V., HALL, J. C. & ROSBASH, M. 1998. A mutant Drosophila homolog of mammalian Clock disrupts circadian rhythms and transcription of period and timeless. *Cell,* 93, 791-804.

ANGEVINE, J. B., JR. & SIDMAN, R. L. 1961. Autoradiographic study of cell migration during histogenesis of cerebral cortex in the mouse. *Nature,* 192, 766-8.

ANTENOR-DORSEY, J. A. & O'MALLEY, K. L. 2012. WldS but not Nmnat1 protects dopaminergic neurites from MPP+ neurotoxicity. *Mol Neurodegener,* 7, 5.

ANTROBUS, R. & BORNER, G. H. 2011. Improved elution conditions for native co-immunoprecipitation. *PLoS One,* 6, e18218.

ASSADI, A. H., ZHANG, G., BEFFERT, U., MCNEIL, R. S., RENFRO, A. L., NIU, S., QUATTROCCHI, C. C., ANTALFFY, B. A., SHELDON, M., ARMSTRONG, D. D., WYNSHAW-BORIS, A., HERZ, J., D'ARCANGELO, G. & CLARK, G. D. 2003. Interaction of reelin signaling and Lis1 in brain development. *Nat Genet,* 35, 270-6.

AVERY, M. A., ROONEY, T. M., PANDYA, J. D., WISHART, T. M., GILLINGWATER, T. H., GEDDES, J. W., SULLIVAN, P. G. & FREEMAN, M. R. 2012. Wld(S) Prevents Axon Degeneration through Increased Mitochondrial Flux and Enhanced Mitochondrial Ca(2+) Buffering. *Curr Biol*.

BACHMANN-GAGESCU, R., ISHAK, G. E., DEMPSEY, J. C., ADKINS, J., O'DAY, D., PHELPS, I. G., GUNAY-AYGUN, M., KLINE, A. D., SZCZALUBA, K., MARTORELL, L., ALSWAID, A., ALRASHEED, S., PAI, S., IZATT, L., RONAN, A., PARISI, M. A., MEFFORD, H., GLASS, I. & DOHERTY, D. 2012. Genotype-phenotype correlation in CC2D2A-related Joubert syndrome reveals an association with ventriculomegaly and seizures. *J Med Genet,* 49, 126-37.

BAHI-BUISSON, N., POIRIER, K., BODDAERT, N., SAILLOUR, Y., CASTELNAU, L., PHILIP, N., BUYSE, G., VILLARD, L., JORIOT, S., MARRET, S., BOURGEOIS, M., VAN ESCH, H., LAGAE, L., AMIEL, J., HERTZ-PANNIER, L., ROUBERTIE, A., RIVIER, F., PINARD, J. M., BELDJORD, C. & CHELLY, J. 2008. Refinement of cortical dysgeneses spectrum associated with TUBA1A mutations. *J Med Genet,* 45, 647-53.

BALLING, R. 2001. ENU mutagenesis: analyzing gene function in mice. *Annu Rev Genomics Hum Genet,* 2, 463-92.

BALOGH, S. A., MCDOWELL, C. S., STAVNEZER, A. J. & DENENBERG, V. H. 1999. A behavioral and neuroanatomical assessment of an inbred substrain of 129 mice with behavioral comparisons to C57BL/6J mice. *Brain Res,* 836, 38-48.

BAUDAT, F., BUARD, J., GREY, C., FLEDEL-ALON, A., OBER, C., PRZEWORSKI, M., COOP, G. & DE MASSY, B. 2010. PRDM9 is a major determinant of meiotic recombination hotspots in humans and mice. *Science,* 327, 836-40.

BAZELOT, M., SIMONNET, J., DINOCOURT, C., BRUEL-JUNGERMAN, E., MILES, R., FRICKER, D. & FRANCIS, F. 2012. Cellular anatomy, physiology and epileptiform activity in the CA3 region of Dcx knockout mice: a neuronal lamination defect and its consequences. *Eur J Neurosci,* 35, 244-56.

BEDROSIAN, T. A., FONKEN, L. K., WALTON, J. C., HAIM, A. & NELSON, R. J. 2011. Dim light at night provokes depression-like behaviors and reduces CA1 dendritic spine density in female hamsters. *Psychoneuroendocrinology,* 36, 1062-9.

BEKESY, G. V., WEVER, E. G., RAHM, W. E., JR. & RAMBO, J. H. 1961. A new method of perfusion for the fixation of tissues. *Laryngoscope,* 71, 1534-47.

BENTLEY, D. R., BALASUBRAMANIAN, S., SWERDLOW, H. P., SMITH, G. P., MILTON, J., BROWN, C. G., HALL, K. P., EVERS, D. J., BARNES, C. L., BIGNELL, H. R., BOUTELL, J. M., BRYANT, J., CARTER, R. J., KEIRA CHEETHAM, R., COX, A. J., ELLIS, D. J., FLATBUSH, M. R., GORMLEY, N. A., HUMPHRAY, S. J., IRVING, L. J., KARBELASHVILI, M. S., KIRK, S. M., LI, H., LIU, X., MAISINGER, K. S., MURRAY, L. J., OBRADOVIC, B., OST, T., PARKINSON, M. L., PRATT, M. R., RASOLONJATOVO, I. M., REED, M. T., RIGATTI, R., RODIGHIERO, C., ROSS, M. T., SABOT, A., SANKAR, S. V., SCALLY, A., SCHROTH, G. P., SMITH, M. E., SMITH, V. P., SPIRIDOU, A., TORRANCE, P. E., TZONEV, S. S., VERMAAS, E. H., WALTER, K., WU, X., ZHANG, L., ALAM, M. D., ANASTASI, C., ANIEBO, I. C., BAILEY, D. M., BANCARZ, I. R., BANERJEE, S., BARBOUR, S. G., BAYBAYAN, P. A., BENOIT, V. A., BENSON, K. F., BEVIS, C., BLACK, P. J., BOODHUN, A., BRENNAN, J. S., BRIDGHAM, J. A., BROWN, R. C., BROWN, A. A., BUERMANN, D. H., BUNDU, A. A., BURROWS, J. C., CARTER, N. P., CASTILLO, N., CHIARA, E. C. M., CHANG, S., NEIL COOLEY, R., CRAKE, N. R., DADA, O. O., DIAKOUMAKOS, K. D., DOMINGUEZ-FERNANDEZ, B., EARNSHAW, D. J., EGBUJOR, U. C., ELMORE, D. W., ETCHIN, S. S., EWAN, M. R., FEDURCO, M., FRASER, L. J., FUENTES FAJARDO, K. V., SCOTT FUREY, W., GEORGE, D., GIETZEN, K. J., GODDARD, C. P., GOLDA, G. S., GRANIERI, P. A., GREEN, D. E., GUSTAFSON, D. L., HANSEN, N. F., HARNISH, K., HAUDENSCHILD, C. D., HEYER, N. I., HIMS, M. M., HO, J. T., HORGAN, A. M., *et al.* 2008. Accurate whole human genome sequencing using reversible terminator chemistry. *Nature,* 456, 53-9.

BERGMAN, J. E., BOSMAN, E. A., VAN RAVENSWAAIJ-ARTS, C. M. & STEEL, K. P. 2010. Study of smell and reproductive organs in a mouse model for CHARGE syndrome. *Eur J Hum Genet,* 18, 171-7.

BERNSTEIN, V. & DENNO, L. S. 2005. Repetitive behaviors in CHARGE syndrome: differential diagnosis and treatment options. *Am J Med Genet A,* 133A, 232-9.

BILGUVAR, K., OZTURK, A. K., LOUVI, A., KWAN, K. Y., CHOI, M., TATLI, B., YALNIZOGLU, D., TUYSUZ, B., CAGLAYAN, A. O., GOKBEN, S., KAYMAKCALAN, H., BARAK, T., BAKIRCIOGLU, M., YASUNO, K., HO,

W., SANDERS, S., ZHU, Y., YILMAZ, S., DINCER, A., JOHNSON, M. H., BRONEN, R. A., KOCER, N., PER, H., MANE, S., PAMIR, M. N., YALCINKAYA, C., KUMANDAS, S., TOPCU, M., OZMEN, M., SESTAN, N., LIFTON, R. P., STATE, M. W. & GUNEL, M. 2010. Whole-exome sequencing identifies recessive WDR62 mutations in severe brain malformations. ***Nature,*** **467, 207-10.**

BLISS, T. V. & ERRINGTON, M. L. 1977. "Reeler" mutant mice fail to show spontaneous alternation. ***Brain Res,*** **124, 168-70.**

BOLAND, E., CLAYTON-SMITH, J., WOO, V. G., MCKEE, S., MANSON, F. D., MEDNE, L., ZACKAI, E., SWANSON, E. A., FITZPATRICK, D., MILLEN, K. J., SHERR, E. H., DOBYNS, W. B. & BLACK, G. C. 2007. Mapping of deletion and translocation breakpoints in 1q44 implicates the serine/threonine kinase AKT3 in postnatal microcephaly and agenesis of the corpus callosum. ***Am J Hum Genet,*** **81, 292-303.**

BOSMAN, E. A., PENN, A. C., AMBROSE, J. C., KETTLEBOROUGH, R., STEMPLE, D. L. & STEEL, K. P. 2005. Multiple mutations in mouse Chd7 provide models for CHARGE syndrome. ***Hum Mol Genet,*** **14, 3463-76.**

BOUTROS, R. & BYRNE, J. A. 2005. D53 (TPD52L1) is a cell cycle-regulated protein maximally expressed at the G2-M transition in breast cancer cells. ***Exp Cell Res,*** **310, 152-65.**

BOVETTI, S., GRIBAUDO, S., PUCHE, A. C., DE MARCHIS, S. & FASOLO, A. 2011. From progenitors to integrated neurons: Role of neurotransmitters in adult olfactory neurogenesis. ***J Chem Neuroanat.***

BOYCOTT, K. M., FLAVELLE, S., BUREAU, A., GLASS, H. C., FUJIWARA, T. M., WIRRELL, E., DAVEY, K., CHUDLEY, A. E., SCOTT, J. N., MCLEOD, D. R. & PARBOOSINGH, J. S. 2005. Homozygous deletion of the very low density lipoprotein receptor gene causes autosomal recessive cerebellar hypoplasia with cerebral gyral simplification. ***Am J Hum Genet,*** **77, 477-83.**

BOYLE, M. P., BERNARD, A., THOMPSON, C. L., NG, L., BOE, A., MORTRUD, M., HAWRYLYCZ, M. J., JONES, A. R., HEVNER, R. F. & LEIN, E. S. 2011. Cell-type-specific consequences of Reelin deficiency in the mouse neocortex, hippocampus, and amygdala. ***J Comp Neurol,*** **519, 2061-89.**

BRENNAN, P. A. & KEVERNE, E. B. 1997. Neural mechanisms of mammalian olfactory learning. ***Prog Neurobiol,*** **51, 457-81.**

BRUNETTI-PIERRI, N., BERG, J. S., SCAGLIA, F., BELMONT, J., BACINO, C. A., SAHOO, T., LALANI, S. R., GRAHAM, B., LEE, B., SHINAWI, M., SHEN, J., KANG, S. H., PURSLEY, A., LOTZE, T., KENNEDY, G., LANSKY-SHAFER, S., WEAVER, C., ROEDER, E. R., GREBE, T. A., ARNOLD, G. L., HUTCHISON, T., REIMSCHISEL, T., AMATO, S., GERAGTHY, M. T., INNIS, J. W., OBERSZTYN, E., NOWAKOWSKA, B., ROSENGREN, S. S., BADER, P. I., GRANGE, D. K., NAQVI, S., GARNICA, A. D., BERNES, S. M., FONG, C. T., SUMMERS, A., WALTERS, W. D., LUPSKI, J. R., STANKIEWICZ, P., CHEUNG, S. W. & PATEL, A. 2008. Recurrent reciprocal 1q21.1 deletions and duplications associated with microcephaly or macrocephaly and developmental and behavioral abnormalities. ***Nat Genet,*** **40, 1466-71.**

BU, W., LIM, K. B., YU, Y. H., CHOU, A. M., SUDHAHARAN, T. & AHMED, S. 2010. Cdc42 interaction with N-WASP and Toca-1 regulates membrane tubulation, vesicle formation and vesicle motility: implications for endocytosis. ***PLoS One,*** **5, e12153.**

BURNETTE, W. N. 1981. "Western blotting": electrophoretic transfer of proteins from sodium dodecyl sulfate--polyacrylamide gels to unmodified nitrocellulose and radiographic detection with antibody and radioiodinated protein A. *Anal Biochem,* 112, 195-203.

CARBAJAL, K. S., MIRANDA, J. L., TSUKAMOTO, M. R. & LANE, T. E. 2011. CXCR4 signaling regulates remyelination by endogenous oligodendrocyte progenitor cells in a viral model of demyelination. *Glia,* 59, 1813-21.

CAROTHERS, A. M., URLAUB, G., MUCHA, J., GRUNBERGER, D. & CHASIN, L. A. 1989. Point mutation analysis in a mammalian gene: rapid preparation of total RNA, PCR amplification of cDNA, and Taq sequencing by a novel method. *Biotechniques,* 7, 494-6, 498-9.

CAVINESS, V. S., JR. & SIDMAN, R. L. 1973a. Retrohippocampal, hippocampal and related structures of the forebrain in the reeler mutant mouse. *J Comp Neurol,* 147, 235-54.

CAVINESS, V. S., JR. & SIDMAN, R. L. 1973b. Time of origin or corresponding cell classes in the cerebral cortex of normal and reeler mutant mice: an autoradiographic analysis. *J Comp Neurol,* 148, 141-51.

CERUSO, M. A. & WEINSTEIN, H. 2002. Structural mimicry of proline kinks: tertiary packing interactions support local structural distortions. *J Mol Biol,* 318, 1237-49.

CHAKRABARTI, L., GALDZICKI, Z. & HAYDAR, T. F. 2007. Defects in embryonic neurogenesis and initial synapse formation in the forebrain of the Ts65Dn mouse model of Down syndrome. *J Neurosci,* 27, 11483-95.

CHELLY, J., KHELFAOUI, M., FRANCIS, F., CHERIF, B. & BIENVENU, T. 2006. Genetics and pathophysiology of mental retardation. *Eur J Hum Genet,* 14, 701-13.

CHEN, C. P., LIN, S. P., CHERN, S. R., TSAI, F. J., WU, P. C., LEE, C. C., CHEN, Y. T., CHEN, W. L. & WANG, W. 2010. A de novo 7.9 Mb deletion in 22q13.2-->qter in a boy with autistic features, epilepsy, developmental delay, atopic dermatitis and abnormal immunological findings. *Eur J Med Genet,* 53, 329-32.

CHEN, X. J., KOVACEVIC, N., LOBAUGH, N. J., SLED, J. G., HENKELMAN, R. M. & HENDERSON, J. T. 2006. Neuroanatomical differences between mouse strains as shown by high-resolution 3D MRI. *Neuroimage,* 29, 99-105.

CHESLER, E. J., WILSON, S. G., LARIVIERE, W. R., RODRIGUEZ-ZAS, S. L. & MOGIL, J. S. 2002. Influences of laboratory environment on behavior. *Nat Neurosci,* 5, 1101-2.

COOPER, J. D. 2003. Progress towards understanding the neurobiology of Batten disease or neuronal ceroid lipofuscinosis. *Curr Opin Neurol,* 16, 121-8.

CORBO, J. C., DEUEL, T. A., LONG, J. M., LAPORTE, P., TSAI, E., WYNSHAW-BORIS, A. & WALSH, C. A. 2002. Doublecortin is required in mice for lamination of the hippocampus but not the neocortex. *J Neurosci,* 22, 7548-57.

CRABBE, J. C., WAHLSTEN, D. & DUDEK, B. C. 1999. Genetics of mouse behavior: interactions with laboratory environment. *Science,* 284, 1670-2.

CRAWLEY, J. N. 1985. Exploratory behavior models of anxiety in mice. *Neurosci Biobehav Rev,* 9, 37-44.

D'ARCANGELO, G., MIAO, G. G., CHEN, S. C., SOARES, H. D., MORGAN, J. I. & CURRAN, T. 1995. A protein related to extracellular matrix proteins deleted in the mouse mutant reeler. *Nature,* 374, 719-23.

DAHMANE, N. & RUIZ I ALTABA, A. 1999. Sonic hedgehog regulates the growth and patterning of the cerebellum. *Development,* 126, 3089-100.

DAS NEVES, L., DUCHALA, C. S., TOLENTINO-SILVA, F., HAXHIU, M. A., COLMENARES, C., MACKLIN, W. B., CAMPBELL, C. E., BUTZ, K. G. & GRONOSTAJSKI, R. M. 1999. Disruption of the murine nuclear factor I-A gene (Nfia) results in perinatal lethality, hydrocephalus, and agenesis of the corpus callosum. *Proc Natl Acad Sci U S A,* 96, 11946-51.

DAVIDSSON, J., JAHNKE, K., FORSGREN, M., COLLIN, A. & SOLLER, M. 2010. dup(19)(q12q13.2): array-based genotype-phenotype correlation of a new possibly obesity-related syndrome. *Obesity (Silver Spring),* 18, 580-7.

DAVIS, M., GENDELMAN, D. S., TISCHLER, M. D. & GENDELMAN, P. M. 1982. A primary acoustic startle circuit: lesion and stimulation studies. *J Neurosci,* 2, 791-805.

DAVY, B. E. & ROBINSON, M. L. 2003. Congenital hydrocephalus in hy3 mice is caused by a frameshift mutation in Hydin, a large novel gene. *Hum Mol Genet,* 12, 1163-70.

DAWE, H. R., SHAW, M. K., FARR, H. & GULL, K. 2007. The hydrocephalus inducing gene product, Hydin, positions axonemal central pair microtubules. *BMC Biol,* 5, 33.

DEACON, R. M. 2011. Hyponeophagia: a measure of anxiety in the mouse. *J Vis Exp*.

DES PORTES, V., PINARD, J. M., BILLUART, P., VINET, M. C., KOULAKOFF, A., CARRIE, A., GELOT, A., DUPUIS, E., MOTTE, J., BERWALD-NETTER, Y., CATALA, M., KAHN, A., BELDJORD, C. & CHELLY, J. 1998. A novel CNS gene required for neuronal migration and involved in X-linked subcortical laminar heterotopia and lissencephaly syndrome. *Cell,* 92, 51-61.

DEVERMAN, B. E. & PATTERSON, P. H. 2012. Exogenous leukemia inhibitory factor stimulates oligodendrocyte progenitor cell proliferation and enhances hippocampal remyelination. *J Neurosci,* 32, 2100-9.

DOBYNS, W. B., REINER, O., CARROZZO, R. & LEDBETTER, D. H. 1993. Lissencephaly. A human brain malformation associated with deletion of the LIS1 gene located at chromosome 17p13. *JAMA,* 270, 2838-42.

DROGEMULLER, C., REICHART, U., SEUBERLICH, T., OEVERMANN, A., BAUMGARTNER, M., KUHNI BOGHENBOR, K., STOFFEL, M. H., SYRING, C., MEYLAN, M., MULLER, S., MULLER, M., GREDLER, B., SOLKNER, J. & LEEB, T. 2011. An unusual splice defect in the mitofusin 2 gene (MFN2) is associated with degenerative axonopathy in Tyrolean Grey cattle. *PLoS One,* 6, e18931.

DROST, J., MANTOVANI, F., TOCCO, F., ELKON, R., COMEL, A., HOLSTEGE, H., KERKHOVEN, R., JONKERS, J., VOORHOEVE, P. M., AGAMI, R. & DEL SAL, G. 2010. BRD7 is a candidate tumour suppressor gene required for p53 function. *Nat Cell Biol,* 12, 380-9.

DUMONT, B. L., WHITE, M. A., STEFFY, B., WILTSHIRE, T. & PAYSEUR, B. A. 2011. Extensive recombination rate variation in the house mouse species complex inferred from genetic linkage maps. *Genome Res,* 21, 114-25.

DUNLAP, J. C. 1993. Genetic analysis of circadian clocks. *Annu Rev Physiol,* 55, 683-728.

DUNLAP, J. C. 1999. Molecular bases for circadian clocks. *Cell,* 96, 271-90.

EDWARDS, A. 2008. Neuronal ceroid lipofuscinosis pathology and the role of the synapse in pathogenesis. *University of Edinburgh; MRes Thesis*.

EDWARDS, A., TREIBER, C. D., BREUSS, M., PIDSLEY, R., HUANG, G. J., CLEAK, J., OLIVER, P. L., FLINT, J. & KEAYS, D. A. 2011. Cytoarchitectural

disruption of the superior colliculus and an enlarged acoustic startle response in the Tuba1a mutant mouse. ***Neuroscience,*** **195, 191-200.**

EDWARDS, M. A., CAVINESS, V. S., JR. & SCHNEIDER, G. E. 1986. Development of cell and fiber lamination in the mouse superior colliculus. ***J Comp Neurol,*** **248, 395-409.**

ENGLE, E. C. 2010. Human genetic disorders of axon guidance. ***Cold Spring Harb Perspect Biol,*** **2, a001784.**

FAIZI, M., BADER, P. L., TUN, C., ENCARNACION, A., KLESCHEVNIKOV, A., BELICHENKO, P., SAW, N., PRIESTLEY, M., TSIEN, R. W., MOBLEY, W. C. & SHAMLOO, M. 2011. Comprehensive behavioral phenotyping of Ts65Dn mouse model of Down Syndrome: Activation of B1-adrenergic receptor by xamoterol as a potential cognitive enhancer. ***Neurobiology of Disease,*** **43, 397-413.**

FELDER, B., RADLWIMMER, B., BENNER, A., MINCHEVA, A., TODT, G., BEYER, K. S., SCHUSTER, C., BOLTE, S., SCHMOTZER, G., KLAUCK, S. M., POUSTKA, F., LICHTER, P. & POUSTKA, A. 2009. FARP2, HDLBP and PASK are downregulated in a patient with autism and 2q37.3 deletion syndrome. ***Am J Med Genet A,*** **149A, 952-9.**

FENG, R., WANG, H., WANG, J., SHROM, D., ZENG, X. & TSIEN, J. Z. 2004. Forebrain degeneration and ventricle enlargement caused by double knockout of Alzheimer's presenilin-1 and presenilin-2. ***Proc Natl Acad Sci U S A,*** **101, 8162-7.**

FERNELL, E., OLSSON, V. A., KARLGREN-LEITNER, C., NORLIN, B., HAGBERG, B. & GILLBERG, C. 1999. Autistic disorders in children with CHARGE association. ***Dev Med Child Neurol,*** **41, 270-2.**

FINE, E. J., IONITA, C. C. & LOHR, L. 2002. The history of the development of the cerebellar examination. ***Semin Neurol,*** **22, 375-84.**

FLECK, M. W., HIROTSUNE, S., GAMBELLO, M. J., PHILLIPS-TANSEY, E., SUARES, G., MERVIS, R. F., WYNSHAW-BORIS, A. & MCBAIN, C. J. 2000. Hippocampal abnormalities and enhanced excitability in a murine model of human lissencephaly. ***J Neurosci,*** **20, 2439-50.**

FLINT, J. & MOTT, R. 2008. Applying mouse complex-trait resources to behavioural genetics. ***Nature,*** **456, 724-7.**

FONKEN, L. K., XU, X., WEIL, Z. M., CHEN, G., SUN, Q., RAJAGOPALAN, S. & NELSON, R. J. 2011. Air pollution impairs cognition, provokes depressive-like behaviors and alters hippocampal cytokine expression and morphology. ***Mol Psychiatry,*** **16, 987-95, 973.**

FRANCIS, F., MEYER, G., FALLET-BIANCO, C., MORENO, S., KAPPELER, C., SOCORRO, A. C., TUY, F. P., BELDJORD, C. & CHELLY, J. 2006. Human disorders of cortical development: from past to present. ***Eur J Neurosci,*** **23, 877-93.**

FREDENS, K. 1981. Genetic variation in the histoarchitecture of the hippocampal region of mice. ***Anat Embryol (Berl),*** **161, 265-81.**

FRICKE, R., GOHL, C., DHARMALINGAM, E., GREVELHORSTER, A., ZAHEDI, B., HARDEN, N., KESSELS, M., QUALMANN, B. & BOGDAN, S. 2009. Drosophila Cip4/Toca-1 integrates membrane trafficking and actin dynamics through WASP and SCAR/WAVE. ***Curr Biol,*** **19, 1429-37.**

FUJITA, E., DAI, H., TANABE, Y., ZHILING, Y., YAMAGATA, T., MIYAKAWA, T., TANOKURA, M., MOMOI, M. Y. & MOMOI, T. 2010. Autism spectrum disorder is related to endoplasmic reticulum stress induced by mutations in the synaptic cell adhesion molecule, CADM1. ***Cell Death Dis,*** **1, e47.**

GADISSEUX, J. F., KADHIM, H. J., VAN DEN BOSCH DE AGUILAR, P., CAVINESS, V. S. & EVRARD, P. 1990. Neuron migration within the radial glial fiber system of the developing murine cerebrum: an electron microscopic autoradiographic analysis. ***Brain Res Dev Brain Res,*** **52, 39-56.**

GAMBINO, J., BERGEN, L. G. & MORRIS, N. R. 1984. Effects of mitotic and tubulin mutations on microtubule architecture in actively growing protoplasts of Aspergillus nidulans. ***J Cell Biol,*** **99, 830-8.**

GARAVELLI, L., ZOLLINO, M., MAINARDI, P. C., GURRIERI, F., RIVIERI, F., SOLI, F., VERRI, R., ALBERTINI, E., FAVARON, E., ZIGNANI, M., ORTESCHI, D., BIANCHI, P., FARAVELLI, F., FORZANO, F., SERI, M., WISCHMEIJER, A., TURCHETTI, D., POMPILII, E., GNOLI, M., COCCHI, G., MAZZANTI, L., BERGAMASCHI, R., DE BRASI, D., SPERANDEO, M. P., MARI, F., ULIANA, V., MOSTARDINI, R., CECCONI, M., GRASSO, M., SASSI, S., SEBASTIO, G., RENIERI, A., SILENGO, M., BERNASCONI, S., WAKAMATSU, N. & NERI, G. 2009. Mowat-Wilson syndrome: facial phenotype changing with age: study of 19 Italian patients and review of the literature. ***Am J Med Genet A,*** **149A, 417-26.**

GARCIA-FUSTER, M. J., PARKS, G. S., CLINTON, S. M., WATSON, S. J., AKIL, H. & CIVELLI, O. 2011. The melanin-concentrating hormone (MCH) system in an animal model of depression-like behavior. ***Eur Neuropsychopharmacol*****.**

GILLINGWATER, T. H., INGHAM, C. A., PARRY, K. E., WRIGHT, A. K., HALEY, J. E., WISHART, T. M., ARBUTHNOTT, G. W. & RIBCHESTER, R. R. 2006. Delayed synaptic degeneration in the CNS of Wlds mice after cortical lesion. ***Brain,*** **129, 1546-56.**

GODINHO, S. I. & NOLAN, P. M. 2006. The role of mutagenesis in defining genes in behaviour. ***Eur J Hum Genet,*** **14, 651-9.**

GOSLING, K. M., GOODNOW, C. C., VERMA, N. K. & FAHRER, A. M. 2008. Defective T-cell function leading to reduced antibody production in a kleisin-beta mutant mouse. ***Immunology,*** **125, 208-17.**

GRAHAM, J. M., JR., ROSNER, B., DYKENS, E. & VISOOTSAK, J. 2005. Behavioral features of CHARGE syndrome (Hall-Hittner syndrome) comparison with Down syndrome, Prader-Willi syndrome, and Williams syndrome. ***Am J Med Genet A,*** **133A, 240-7.**

GREY, C., BARTHES, P., CHAUVEAU-LE FRIEC, G., LANGA, F., BAUDAT, F. & DE MASSY, B. 2011. Mouse PRDM9 DNA-binding specificity determines sites of histone H3 lysine 4 trimethylation for initiation of meiotic recombination. ***PLoS Biol,*** **9, e1001176.**

GROSS, C., NAKAMOTO, M., YAO, X., CHAN, C. B., YIM, S. Y., YE, K., WARREN, S. T. & BASSELL, G. J. 2010. Excess phosphoinositide 3-kinase subunit synthesis and activity as a novel therapeutic target in fragile X syndrome. ***J Neurosci,*** **30, 10624-38.**

GRUNEBERG, H. 1943. Two new mutant genes in the house mouse. ***J Genet.,*** **45, 22-28.**

GUAN, C., YE, C., YANG, X. & GAO, J. 2010. A review of current large-scale mouse knockout efforts. ***Genesis,*** **48, 73-85.**

HALL, J. C. 1990. Genetics of circadian rhythms. ***Annu Rev Genet,*** **24, 659-97.**

HARDIN, P. E., HALL, J. C. & ROSBASH, M. 1990. Feedback of the Drosophila period gene product on circadian cycling of its messenger RNA levels. ***Nature,*** **343, 536-40.**

HASTINGS, M. H. 1997. Central clocking. ***Trends Neurosci,*** **20, 459-64.**

HATTORI, M., ADACHI, H., TSUJIMOTO, M., ARAI, H. & INOUE, K. 1994. Miller-Dieker lissencephaly gene encodes a subunit of brain platelet-activating factor acetylhydrolase [corrected]. *Nature,* 370, 216-8.

HERRON, B. J., LU, W., RAO, C., LIU, S., PETERS, H., BRONSON, R. T., JUSTICE, M. J., MCDONALD, J. D. & BEIER, D. R. 2002. Efficient generation and mapping of recessive developmental mutations using ENU mutagenesis. *Nat Genet,* 30, 185-9.

HICKEY, M. A. & CHESSELET, M. F. 2003. Apoptosis in Huntington's disease. *Prog Neuropsychopharmacol Biol Psychiatry,* 27, 255-65.

HIROTSUNE, S., FLECK, M. W., GAMBELLO, M. J., BIX, G. J., CHEN, A., CLARK, G. D., LEDBETTER, D. H., MCBAIN, C. J. & WYNSHAW-BORIS, A. 1998. Graded reduction of Pafah1b1 (Lis1) activity results in neuronal migration defects and early embryonic lethality. *Nat Genet,* 19, 333-9.

HONG, S. E., SHUGART, Y. Y., HUANG, D. T., SHAHWAN, S. A., GRANT, P. E., HOURIHANE, J. O., MARTIN, N. D. & WALSH, C. A. 2000. Autosomal recessive lissencephaly with cerebellar hypoplasia is associated with human RELN mutations. *Nat Genet,* 26, 93-6.

HONG, Y., PIAO, F., ZHAO, Y., LI, S., WANG, Y. & LIU, P. 2009. Subchronic exposure to arsenic decreased Sdha expression in the brain of mice. *Neurotoxicology,* 30, 538-43.

INLOW, J. K. & RESTIFO, L. L. 2004. Molecular and comparative genetics of mental retardation. *Genetics,* 166, 835-81.

ISAACS, A. M., OLIVER, P. L., JONES, E. L., JEANS, A., POTTER, A., HOVIK, B. H., NOLAN, P. M., VIZOR, L., GLENISTER, P., SIMON, A. K., GRAY, I. C., SPURR, N. K., BROWN, S. D., HUNTER, A. J. & DAVIES, K. E. 2003. A mutation in Af4 is predicted to cause cerebellar ataxia and cataracts in the robotic mouse. *J Neurosci,* 23, 1631-7.

JACKSON, A. P., EASTWOOD, H., BELL, S. M., ADU, J., TOOMES, C., CARR, I. M., ROBERTS, E., HAMPSHIRE, D. J., CROW, Y. J., MIGHELL, A. J., KARBANI, G., JAFRI, H., RASHID, Y., MUELLER, R. F., MARKHAM, A. F. & WOODS, C. G. 2002. Identification of microcephalin, a protein implicated in determining the size of the human brain. *Am J Hum Genet,* 71, 136-42.

JAGLIN, X. H. & CHELLY, J. 2009. Tubulin-related cortical dysgeneses: microtubule dysfunction underlying neuronal migration defects. *Trends Genet,* 25, 555-66.

JEANS, A. F., OLIVER, P. L., JOHNSON, R., CAPOGNA, M., VIKMAN, J., MOLNAR, Z., BABBS, A., PARTRIDGE, C. J., SALEHI, A., BENGTSSON, M., ELIASSON, L., RORSMAN, P. & DAVIES, K. E. 2007. A dominant mutation in Snap25 causes impaired vesicle trafficking, sensorimotor gating, and ataxia in the blind-drunk mouse. *Proc Natl Acad Sci U S A,* 104, 2431-6.

JENSEN-SEAMAN, M. I., FUREY, T. S., PAYSEUR, B. A., LU, Y., ROSKIN, K. M., CHEN, C. F., THOMAS, M. A., HAUSSLER, D. & JACOB, H. J. 2004. Comparative recombination rates in the rat, mouse, and human genomes. *Genome Res,* 14, 528-38.

JOHN B, S. 1967. Relation of lifespan to brain weight, body weight, and metabolic rate among inbred mouse strains. *Experimental Gerontology,* 2, 173-182.

JONES, B. J. & ROBERTS, D. J. 1968. The quantiative measurement of motor inco-ordination in naive mice using an acelerating rotarod. *J Pharm Pharmacol,* 20, 302-4.

JURIC-SEKHAR, G., ADKINS, J., DOHERTY, D. & HEVNER, R. F. 2012. Joubert syndrome: brain and spinal cord malformations in genotyped cases and

implications for neurodevelopmental functions of primary cilia. ***Acta Neuropathol*.**

KAIDANOVICH-BEILIN, O., LIPINA, T., VUKOBRADOVIC, I., RODER, J. & WOODGETT, J. R. 2011. Assessment of social interaction behaviors. ***J Vis Exp*.**

KAS, M. J. & VAN REE, J. M. 2004. Dissecting complex behaviours in the post-genomic era. ***Trends Neurosci,*** **27, 366-9.**

KASARSKIS, A., MANOVA, K. & ANDERSON, K. V. 1998. A phenotype-based screen for embryonic lethal mutations in the mouse. ***Proc Natl Acad Sci U S A,*** **95, 7485-90.**

KEAYS, D. A. 2005. The Identification and Characterisation of Novel ENU Induced Behavioural Mouse Mutants. ***DPhil thesis, University of Oxford*.**

KEAYS, D. A. 2007. Neuronal migration: unraveling the molecular pathway with humans, mice, and a fungus. ***Mamm Genome,*** **18, 425-30.**

KEAYS, D. A., CLARK, T. G. & FLINT, J. 2006. Estimating the number of coding mutations in genotypic- and phenotypic-driven N-ethyl-N-nitrosourea (ENU) screens. ***Mamm Genome,*** **17, 230-8.**

KEAYS, D. A., CLEAK, J., HUANG, G. J., EDWARDS, A., BRAUN, A., TREIBER, C. D., PIDSLEY, R. & FLINT, J. 2010. The role of Tuba1a in adult hippocampal neurogenesis and the formation of the dentate gyrus. ***Dev Neurosci,*** **32, 268-77.**

KEAYS, D. A. & NOLAN, P. M. 2003. N-ethyl-N-nitrosourea mouse mutants in the dissection of behavioural and psychiatric disorders. ***Eur J Pharmacol,*** **480, 205-17.**

KEAYS, D. A., TIAN, G., POIRIER, K., HUANG, G. J., SIEBOLD, C., CLEAK, J., OLIVER, P. L., FRAY, M., HARVEY, R. J., MOLNAR, Z., PINON, M. C., DEAR, N., VALDAR, W., BROWN, S. D., DAVIES, K. E., RAWLINS, J. N., COWAN, N. J., NOLAN, P., CHELLY, J. & FLINT, J. 2007. Mutations in alpha-tubulin cause abnormal neuronal migration in mice and lissencephaly in humans. ***Cell,*** **128, 45-57.**

KELLEY, L. A. & STERNBERG, M. J. 2009. Protein structure prediction on the Web: a case study using the Phyre server. ***Nat Protoc,*** **4, 363-71.**

KING, D. P. & TAKAHASHI, J. S. 2000. Molecular genetics of circadian rhythms in mammals. ***Annu Rev Neurosci,*** **23, 713-42.**

KING, D. P., ZHAO, Y., SANGORAM, A. M., WILSBACHER, L. D., TANAKA, M., ANTOCH, M. P., STEEVES, T. D., VITATERNA, M. H., KORNHAUSER, J. M., LOWREY, P. L., TUREK, F. W. & TAKAHASHI, J. S. 1997. Positional cloning of the mouse circadian clock gene. ***Cell,*** **89, 641-53.**

KOCH, M. 1999. The neurobiology of startle. ***Prog Neurobiol,*** **59, 107-28.**

KOCH, S., MOLCHANOVA, S. M., WRIGHT, A. K., EDWARDS, A., COOPER, J. D., TAIRA, T., GILLINGWATER, T. H. & TYYNELA, J. 2011. Morphologic and functional correlates of synaptic pathology in the cathepsin D knockout mouse model of congenital neuronal ceroid lipofuscinosis. ***J Neuropathol Exp Neurol,*** **70, 1089-96.**

KOMATSU, S., IMOTO, I., TSUDA, H., KOZAKI, K. I., MURAMATSU, T., SHIMADA, Y., AIKO, S., YOSHIZUMI, Y., ICHIKAWA, D., OTSUJI, E. & INAZAWA, J. 2009. Overexpression of SMYD2 relates to tumor cell proliferation and malignant outcome of esophageal squamous cell carcinoma. ***Carcinogenesis,*** **30, 1139-46.**

KONOPKA, R. J. & BENZER, S. 1971. Clock mutants of Drosophila melanogaster. ***Proc Natl Acad Sci U S A,*** **68, 2112-6.**

KROON, J. A. & CAROBREZ, A. P. 2009. Olfactory fear conditioning paradigm in rats: effects of midazolam, propranolol or scopolamine. ***Neurobiol Learn Mem,*** **91, 32-40.**

KUBO, T., KIM, S. R., SAI, K., SAITO, Y., NAKAJIMA, T., MATSUMOTO, K., SAITO, H., SHIRAO, K., YAMAMOTO, N., MINAMI, H., OHTSU, A., YOSHIDA, T., SAIJO, N., OHNO, Y., OZAWA, S. & SAWADA, J. 2005. Functional characterization of three naturally occurring single nucleotide polymorphisms in the CES2 gene encoding carboxylesterase 2 (HCE-2). ***Drug Metab Dispos,*** **33, 1482-7.**

KUBO, T., YAMASHITA, T., YAMAGUCHI, A., SUMIMOTO, H., HOSOKAWA, K. & TOHYAMA, M. 2002. A novel FERM domain including guanine nucleotide exchange factor is involved in Rac signaling and regulates neurite remodeling. ***J Neurosci,*** **22, 8504-13.**

LECHTRECK, K. F., DELMOTTE, P., ROBINSON, M. L., SANDERSON, M. J. & WITMAN, G. B. 2008. Mutations in Hydin impair ciliary motility in mice. ***J Cell Biol,*** **180, 633-43.**

LECHTRECK, K. F. & WITMAN, G. B. 2007. Chlamydomonas reinhardtii hydin is a central pair protein required for flagellar motility. ***J Cell Biol,*** **176, 473-82.**

LEIN, E. S., HAWRYLYCZ, M. J., AO, N., AYRES, M., BENSINGER, A., BERNARD, A., BOE, A. F., BOGUSKI, M. S., BROCKWAY, K. S., BYRNES, E. J., CHEN, L., CHEN, T. M., CHIN, M. C., CHONG, J., CROOK, B. E., CZAPLINSKA, A., DANG, C. N., DATTA, S., DEE, N. R., DESAKI, A. L., DESTA, T., DIEP, E., DOLBEARE, T. A., DONELAN, M. J., DONG, H. W., DOUGHERTY, J. G., DUNCAN, B. J., EBBERT, A. J., EICHELE, G., ESTIN, L. K., FABER, C., FACER, B. A., FIELDS, R., FISCHER, S. R., FLISS, T. P., FRENSLEY, C., GATES, S. N., GLATTFELDER, K. J., HALVERSON, K. R., HART, M. R., HOHMANN, J. G., HOWELL, M. P., JEUNG, D. P., JOHNSON, R. A., KARR, P. T., KAWAL, R., KIDNEY, J. M., KNAPIK, R. H., KUAN, C. L., LAKE, J. H., LARAMEE, A. R., LARSEN, K. D., LAU, C., LEMON, T. A., LIANG, A. J., LIU, Y., LUONG, L. T., MICHAELS, J., MORGAN, J. J., MORGAN, R. J., MORTRUD, M. T., MOSQUEDA, N. F., NG, L. L., NG, R., ORTA, G. J., OVERLY, C. C., PAK, T. H., PARRY, S. E., PATHAK, S. D., PEARSON, O. C., PUCHALSKI, R. B., RILEY, Z. L., ROCKETT, H. R., ROWLAND, S. A., ROYALL, J. J., RUIZ, M. J., SARNO, N. R., SCHAFFNIT, K., SHAPOVALOVA, N. V., SIVISAY, T., SLAUGHTERBECK, C. R., SMITH, S. C., SMITH, K. A., SMITH, B. I., SODT, A. J., STEWART, N. N., STUMPF, K. R., SUNKIN, S. M., SUTRAM, M., TAM, A., TEEMER, C. D., THALLER, C., THOMPSON, C. L., VARNAM, L. R., VISEL, A., WHITLOCK, R. M., WOHNOUTKA, P. E., WOLKEY, C. K., WONG, V. Y., WOOD, M., ***et al.*** **2007. Genome-wide atlas of gene expression in the adult mouse brain.** ***Nature,*** **445, 168-76.**

LEWIS, M. A., QUINT, E., GLAZIER, A. M., FUCHS, H., DE ANGELIS, M. H., LANGFORD, C., VAN DONGEN, S., ABREU-GOODGER, C., PIIPARI, M., REDSHAW, N., DALMAY, T., MORENO-PELAYO, M. A., ENRIGHT, A. J. & STEEL, K. P. 2009. An ENU-induced mutation of miR-96 associated with progressive hearing loss in mice. ***Nat Genet,*** **41, 614-8.**

LI, C. C., CHIANG, T. C., WU, T. S., PACHECO-RODRIGUEZ, G., MOSS, J. & LEE, F. J. 2007. ARL4D recruits cytohesin-2/ARNO to modulate actin remodeling. ***Mol Biol Cell,*** **18, 4420-37.**

LI, D. & ROBERTS, R. 2001. WD-repeat proteins: structure characteristics, biological function, and their involvement in human diseases. *Cell Mol Life Sci,* 58, 2085-97.

LI, H., BERLIN, Y., HART, R. P. & GRUMET, M. 2003. Microtubules are critical for radial glial morphology: possible regulation by MAPs and MARKs. *Glia,* 44, 37-46.

LI, M., PEVNY, L., LOVELL-BADGE, R. & SMITH, A. 1998. Generation of purified neural precursors from embryonic stem cells by lineage selection. *Curr Biol,* 8, 971-4.

LI, S. H., TIAN, H., YUE, W. M., LI, L., LI, W. J., CHEN, Z. T., HU, W. S., ZHU, Y. C. & QI, L. 2011. Overexpression of Metastasis-Associated Protein 1 is Significantly Correlated with Tumor Angiogenesis and Poor Survival in Patients with Early-Stage Non-Small Cell Lung Cancer. *Ann Surg Oncol,* 18, 2048-56.

LIVY, D. J. & WAHLSTEN, D. 1997. Retarded formation of the hippocampal commissure in embryos from mouse strains lacking a corpus callosum. *Hippocampus,* 7, 2-14.

LOCK, E. A., GYTE, A., DUFFELL, S. & WYATT, I. 2001. The effect of postnatal age on L-2-chloropropionic acid-induced cerebellar granule cell necrosis in the rat. *Arch Toxicol,* 74, 783-8.

LORDKIPANIDZE, T. & DUNAEVSKY, A. 2005. Purkinje cell dendrites grow in alignment with Bergmann glia. *Glia,* 51, 229-34.

LOWE, J., LI, H., DOWNING, K. H. & NOGALES, E. 2001. Refined structure of alpha beta-tubulin at 3.5 A resolution. *J Mol Biol,* 313, 1045-57.

LU, M., GROVE, E. A. & MILLER, R. J. 2002. Abnormal development of the hippocampal dentate gyrus in mice lacking the CXCR4 chemokine receptor. *Proc Natl Acad Sci U S A,* 99, 7090-5.

LU, Z. X., JIANG, P. & XING, Y. 2011. Genetic variation of pre-mRNA alternative splicing in human populations. *Wiley Interdiscip Rev RNA*.

LUDUENA, R. F., SHOOTER, E. M. & WILSON, L. 1977. Structure of the tubulin dimer. *J Biol Chem,* 252, 7006-14.

MACK, T. G., REINER, M., BEIROWSKI, B., MI, W., EMANUELLI, M., WAGNER, D., THOMSON, D., GILLINGWATER, T., COURT, F., CONFORTI, L., FERNANDO, F. S., TARLTON, A., ANDRESSEN, C., ADDICKS, K., MAGNI, G., RIBCHESTER, R. R., PERRY, V. H. & COLEMAN, M. P. 2001. Wallerian degeneration of injured axons and synapses is delayed by a Ube4b/Nmnat chimeric gene. *Nat Neurosci,* 4, 1199-206.

MAGNUSSON, K. P., SANDSTROM, M., STAHLBERG, M., LARSSON, M., FLYGARE, J., HELLGREN, D., WIMAN, K. G. & LJUNGQUIST, S. 2000. p53 splice acceptor site mutation and increased HsRAD51 protein expression in Bloom's syndrome GM1492 fibroblasts. *Gene,* 246, 247-54.

MANDILLO, S., TUCCI, V., HOLTER, S. M., MEZIANE, H., BANCHAABOUCHI, M. A., KALLNIK, M., LAD, H. V., NOLAN, P. M., OUAGAZZAL, A. M., COGHILL, E. L., GALE, K., GOLINI, E., JACQUOT, S., KREZEL, W., PARKER, A., RIET, F., SCHNEIDER, I., MARAZZITI, D., AUWERX, J., BROWN, S. D., CHAMBON, P., ROSENTHAL, N., TOCCHINI-VALENTINI, G. & WURST, W. 2008. Reliability, robustness, and reproducibility in mouse behavioral phenotyping: a cross-laboratory study. *Physiol Genomics,* 34, 243-55.

MANZINI, M. C. & WALSH, C. A. 2011. What disorders of cortical development tell us about the cortex: one plus one does not always make two. *Curr Opin Genet Dev,* 21, 333-9.

MAR, L., RIVKIN, E., KIM, D. Y., YU, J. Y. & CORDES, S. P. 2005. A genetic screen for mutations that affect cranial nerve development in the mouse. ***J Neurosci,*** **25, 11787-95.**

MARSHALL, C. R., YOUNG, E. J., PANI, A. M., FRECKMANN, M. L., LACASSIE, Y., HOWALD, C., FITZGERALD, K. K., PEIPPO, M., MORRIS, C. A., SHANE, K., PRIOLO, M., MORIMOTO, M., KONDO, I., MANGUOGLU, E., BERKER-KARAUZUM, S., EDERY, P., HOBART, H. H., MERVIS, C. B., ZUFFARDI, O., REYMOND, A., KAPLAN, P., TASSABEHJI, M., GREGG, R. G., SCHERER, S. W. & OSBORNE, L. R. 2008. Infantile spasms is associated with deletion of the MAGI2 gene on chromosome 7q11.23-q21.11. ***Am J Hum Genet,*** **83, 106-11.**

MARTIN, P., DURAN, A., MINGUET, S., GASPAR, M. L., DIAZ-MECO, M. T., RENNERT, P., LEITGES, M. & MOSCAT, J. 2002. Role of zeta PKC in B-cell signaling and function. ***EMBO J,*** **21, 4049-57.**

MARTINEZ-FINLEY, E. J., ALI, A. M. & ALLAN, A. M. 2009. Learning deficits in C57BL/6J mice following perinatal arsenic exposure: consequence of lower corticosterone receptor levels? ***Pharmacol Biochem Behav,*** **94, 271-7.**

MCGILLEWIE, L. 2009. Identification of novel ligands of WDR47, using yeast two-hybrid analysis.

MCILWAIN, K. L., MERRIWEATHER, M. Y., YUVA-PAYLOR, L. A. & PAYLOR, R. 2001. The use of behavioral test batteries: effects of training history. ***Physiol Behav,*** **73, 705-17.**

MELONI, E. G. & DAVIS, M. 2000. GABA in the deep layers of the superior Colliculus/Mesencephalic reticular formation mediates the enhancement of startle by the dopamine D1 receptor agonist SKF 82958 in rats. ***J Neurosci,*** **20, 5374-81.**

MENON, P., DEANE, R., SAGARE, A., LANE, S. M., ZARCONE, T. J., O'DELL, M. R., YAN, C., ZLOKOVIC, B. V. & BERK, B. C. 2010. Impaired spine formation and learning in GPCR kinase 2 interacting protein-1 (GIT1) knockout mice. ***Brain Res,*** **1317, 218-26.**

MILLER, N. D., NANCE, M. A., WOHLER, E. S., HOOVER-FONG, J. E., LISI, E., THOMAS, G. H. & PEVSNER, J. 2009. Molecular (SNP) analyses of overlapping hemizygous deletions of 10q25.3 to 10qter in four patients: evidence for HMX2 and HMX3 as candidate genes in hearing and vestibular function. ***Am J Med Genet A,*** **149A, 669-80.**

MOINUDDIN, S. M. & TADA, T. 2000. Study of cerebrospinal fluid flow dynamics in TGF-beta 1 induced chronic hydrocephalic mice. ***Neurol Res,*** **22, 215-22.**

MORENO-DE-LUCA, A., HELMERS, S. L., MAO, H., BURNS, T. G., MELTON, A. M., SCHMIDT, K. R., FERNHOFF, P. M., LEDBETTER, D. H. & MARTIN, C. L. 2011. Adaptor protein complex-4 (AP-4) deficiency causes a novel autosomal recessive cerebral palsy syndrome with microcephaly and intellectual disability. ***J Med Genet,*** **48, 141-4.**

MORIARTY, O., ROCHE, M., MCGUIRE, B. E. & FINN, D. P. 2012. Validation of an air-puff passive-avoidance paradigm for assessment of aversive learning and memory in rat models of chronic pain. ***J Neurosci Methods,*** **204, 1-8.**

MORIYA, J., CHEN, R., YAMAKAWA, J., SASAKI, K., ISHIGAKI, Y. & TAKAHASHI, T. 2011. Resveratrol improves hippocampal atrophy in chronic fatigue mice by enhancing neurogenesis and inhibiting apoptosis of granular cells. ***Biol Pharm Bull,*** **34, 354-9.**

MORRIS-ROSENDAHL, D. J., NAJM, J., LACHMEIJER, A. M., SZTRIHA, L., MARTINS, M., KUECHLER, A., HAUG, V., ZESCHNIGK, C., MARTIN, P., SANTOS, M., VASCONCELOS, C., OMRAN, H., KRAUS, U., VAN DER KNAAP, M. S., SCHUIERER, G., KUTSCHE, K. & UYANIK, G. 2008. Refining the phenotype of alpha-1a Tubulin (TUBA1A) mutation in patients with classical lissencephaly. *Clin Genet,* 74, 425-33.

MUNOZ-ABELLAN, C., DAVIU, N., RABASA, C., NADAL, R. & ARMARIO, A. 2009. Cat odor causes long-lasting contextual fear conditioning and increased pituitary-adrenal activation, without modifying anxiety. *Horm Behav,* 56, 465-71.

MUNROE, R. J., PRABHU, V., ACLAND, G. M., JOHNSON, K. R., HARRIS, B. S., O'BRIEN, T. P., WELSH, I. C., NODEN, D. M. & SCHIMENTI, J. C. 2009. Mouse H6 Homeobox 1 (Hmx1) mutations cause cranial abnormalities and reduced body mass. *BMC Dev Biol,* 9, 27.

MYERS, S., FREEMAN, C., AUTON, A., DONNELLY, P. & MCVEAN, G. 2008. A common sequence motif associated with recombination hot spots and genome instability in humans. *Nat Genet,* 40, 1124-9.

NAGY, Z. M. & MISANIN, J. R. 1970. Visual perception in the retinal degenerate C3H mouse. *J Comp Physiol Psychol,* 72, 306-10.

NAKAHATA, S., SAITO, Y., HAMASAKI, M., HIDAKA, T., ARAI, Y., TAKI, T., TANIWAKI, M. & MORISHITA, K. 2009. Alteration of enhancer of polycomb 1 at 10p11.2 is one of the genetic events leading to development of adult T-cell leukemia/lymphoma. *Genes Chromosomes Cancer,* 48, 768-76.

NEWBY, L. M. & JACKSON, F. R. 1993. A new biological rhythm mutant of Drosophila melanogaster that identifies a gene with an essential embryonic function. *Genetics,* 135, 1077-90.

NICHOLAS, J. 2005. Can specific deficits in executive functioning explain the behavioral characteristics of CHARGE syndrome: a case study. *Am J Med Genet A,* 133A, 300-5.

NIEVEL, J. G. & CUMINGS, J. N. 1967. Nissl substance and ribosomal aggregates. *Nature,* 214, 1123-4.

NIKLASSON, M., BERGSTROM, T., ZHANG, X. Q., GUSTAFSDOTTIR, S. M., SJOGREN, M., EDQVIST, P. H., VENNSTROM, B., FORSBERG, M. & FORSBERG-NILSSON, K. 2010. Enlarged lateral ventricles and aberrant behavior in mice overexpressing PDGF-B in embryonic neural stem cells. *Exp Cell Res,* 316, 2779-89.

NOLAN, P. M., KAPFHAMER, D. & BUCAN, M. 1997. Random mutagenesis screen for dominant behavioral mutations in mice. *Methods,* 13, 379-95.

NOLAN, P. M., PETERS, J., STRIVENS, M., ROGERS, D., HAGAN, J., SPURR, N., GRAY, I. C., VIZOR, L., BROOKER, D., WHITEHILL, E., WASHBOURNE, R., HOUGH, T., GREENAWAY, S., HEWITT, M., LIU, X., MCCORMACK, S., PICKFORD, K., SELLEY, R., WELLS, C., TYMOWSKA-LALANNE, Z., ROBY, P., GLENISTER, P., THORNTON, C., THAUNG, C., STEVENSON, J. A., ARKELL, R., MBURU, P., HARDISTY, R., KIERNAN, A., ERVEN, A., STEEL, K. P., VOEGELING, S., GUENET, J. L., NICKOLS, C., SADRI, R., NASSE, M., ISAACS, A., DAVIES, K., BROWNE, M., FISHER, E. M., MARTIN, J., RASTAN, S., BROWN, S. D. & HUNTER, J. 2000. A systematic, genome-wide, phenotype-driven mutagenesis programme for gene function studies in the mouse. *Nat Genet,* 25, 440-3.

O'BRYANT, S. E., EDWARDS, M., MENON, C. V., GONG, G. & BARBER, R. 2011. Long-term low-level arsenic exposure is associated with poorer

neuropsychological functioning: a Project FRONTIER study. *Int J Environ Res Public Health,* 8, 861-74.

OHL, F. & KECK, M. E. 2003. Behavioural screening in mutagenised mice--in search for novel animal models of psychiatric disorders. *Eur J Pharmacol,* 480, 219-28.

OLIVER, P. L. & DAVIES, K. E. 2005. Analysis of human neurological disorders using mutagenesis in the mouse. *Clin Sci (Lond),* 108, 385-97.

ORI-MCKENNEY, K. M. & VALLEE, R. B. 2011. Neuronal migration defects in the Loa dynein mutant mouse. *Neural Dev,* 6, 26.

OUAGAZZAL, A. M., MOREAU, J. L., PAULY-EVERS, M. & JENCK, F. 2003. Impact of environmental housing conditions on the emotional responses of mice deficient for nociceptin/orphanin FQ peptide precursor gene. *Behav Brain Res,* 144, 111-7.

PACIORKOWSKI, A. R., THIO, L. L., ROSENFELD, J. A., GAJECKA, M., GURNETT, C. A., KULKARNI, S., CHUNG, W. K., MARSH, E. D., GENTILE, M., REGGIN, J. D., WHELESS, J. W., BALASUBRAMANIAN, S., KUMAR, R., CHRISTIAN, S. L., MARINI, C., GUERRINI, R., MALTSEV, N., SHAFFER, L. G. & DOBYNS, W. B. 2011. Copy number variants and infantile spasms: evidence for abnormalities in ventral forebrain development and pathways of synaptic function. *Eur J Hum Genet.*

PALAY, S. L., MC, G.-R. S., GORDON, S., JR. & GRILLO, M. A. 1962. Fixation of neural tissues for electron microscopy by perfusion with solutions of osmium tetroxide. *J Cell Biol,* 12, 385-410.

PALLERLA, S. R., LAWRENCE, R., LEWEJOHANN, L., PAN, Y., FISCHER, T., SCHLOMANN, U., ZHANG, X., ESKO, J. D. & GROBE, K. 2008. Altered heparan sulfate structure in mice with deleted NDST3 gene function. *J Biol Chem,* 283, 16885-94.

PANG, T., ATEFY, R. & SHEEN, V. 2008. Malformations of cortical development. *Neurologist,* 14, 181-91.

PARK, H. J., KONG, J. H., KANG, Y. S., PARK, W. M., JEONG, S. A., PARK, S. M., LIM, J. K. & JEON, C. J. 2002. The distribution and morphology of calbindin D28K- and calretinin-immunoreactive neurons in the visual cortex of mouse. *Mol Cells,* 14, 143-9.

PATEL, J. R., MCCANDLESS, E. E., DORSEY, D. & KLEIN, R. S. 2010. CXCR4 promotes differentiation of oligodendrocyte progenitors and remyelination. *Proc Natl Acad Sci U S A,* 107, 11062-7.

PAWLAK, C. R., SANCHIS-SEGURA, C., SOEWARTO, D., WAGNER, S., HRABE DE ANGELIS, M. & SPANAGEL, R. 2008. A phenotype-driven ENU mutagenesis screen for the identification of dominant mutations involved in alcohol consumption. *Mamm Genome,* 19, 77-84.

PAXINOS, G. A. F., K. 2007. *The Mouse Brain in Stereotaxic Coordinates*.

PAYLOR, R., HIROTSUNE, S., GAMBELLO, M. J., YUVA-PAYLOR, L., CRAWLEY, J. N. & WYNSHAW-BORIS, A. 1999. Impaired learning and motor behavior in heterozygous Pafah1b1 (Lis1) mutant mice. *Learn Mem,* 6, 521-37.

PELLOW, S., CHOPIN, P., FILE, S. E. & BRILEY, M. 1985. Validation of open:closed arm entries in an elevated plus-maze as a measure of anxiety in the rat. *J Neurosci Methods,* 14, 149-67.

PETEK, E., WINDPASSINGER, C., MACH, M., RAUTER, L., SCHERER, S. W., WAGNER, K. & KROISEL, P. M. 2003. Molecular characterization of a 12q22-

q24 deletion associated with congenital deafness: confirmation and refinement of the DFNA25 locus. *Am J Med Genet A,* 117A, 122-6.

PEVNY, L. H., SOCKANATHAN, S., PLACZEK, M. & LOVELL-BADGE, R. 1998. A role for SOX1 in neural determination. *Development,* 125, 1967-78.

PILUSO, G., D'AMICO, F., SACCONE, V., BISMUTO, E., ROTUNDO, I. L., DI DOMENICO, M., AURINO, S., SCHWARTZ, C. E., NERI, G. & NIGRO, V. 2009. A missense mutation in CASK causes FG syndrome in an Italian family. *Am J Hum Genet,* 84, 162-77.

PISTORIO, A. L., HENDRY, S. H. & WANG, X. 2006. A modified technique for high-resolution staining of myelin. *J Neurosci Methods,* 153, 135-46.

PITTENDRIGH, C. S. 1993. Temporal organization: reflections of a Darwinian clock-watcher. *Annu Rev Physiol,* 55, 16-54.

PONTI, G., PERETTO, P. & BONFANTI, L. 2008. Genesis of neuronal and glial progenitors in the cerebellar cortex of peripuberal and adult rabbits. *PLoS One,* 3, e2366.

POPOV, V. I., KLESCHEVNIKOV, A. M., KLIMENKO, O. A., STEWART, M. G. & BELICHENKO, P. V. 2011. Three-dimensional synaptic ultrastructure in the dentate gyrus and hippocampal area CA3 in the Ts65Dn mouse model of Down syndrome. *J Comp Neurol,* 519, 1338-54.

PORTER, A. G. & JANICKE, R. U. 1999. Emerging roles of caspase-3 in apoptosis. *Cell Death Differ,* 6, 99-104.

POTKIN, S. G., GUFFANTI, G., LAKATOS, A., TURNER, J. A., KRUGGEL, F., FALLON, J. H., SAYKIN, A. J., ORRO, A., LUPOLI, S., SALVI, E., WEINER, M. & MACCIARDI, F. 2009. Hippocampal atrophy as a quantitative trait in a genome-wide association study identifying novel susceptibility genes for Alzheimer's disease. *PLoS One,* 4, e6501.

POULTON, C. J., SCHOT, R., KIA, S. K., JONES, M., VERHEIJEN, F. W., VENSELAAR, H., DE WIT, M. C., DE GRAAFF, E., BERTOLI-AVELLA, A. M. & MANCINI, G. M. 2011. Microcephaly with simplified gyration, epilepsy, and infantile diabetes linked to inappropriate apoptosis of neural progenitors. *Am J Hum Genet,* 89, 265-76.

PRICE, J. L., BLAU, J., ROTHENFLUH, A., ABODEELY, M., KLOSS, B. & YOUNG, M. W. 1998. double-time is a novel Drosophila clock gene that regulates PERIOD protein accumulation. *Cell,* 94, 83-95.

PRUT, L. & BELZUNG, C. 2003. The open field as a paradigm to measure the effects of drugs on anxiety-like behaviors: a review. *Eur J Pharmacol,* 463, 3-33.

PUTOUX, A., THOMAS, S., COENE, K. L., DAVIS, E. E., ALANAY, Y., OGUR, G., UZ, E., BUZAS, D., GOMES, C., PATRIER, S., BENNETT, C. L., ELKHARTOUFI, N., FRISON, M. H., RIGONNOT, L., JOYE, N., PRUVOST, S., UTINE, G. E., BODUROGLU, K., NITSCHKE, P., FERTITTA, L., THAUVIN-ROBINET, C., MUNNICH, A., CORMIER-DAIRE, V., HENNEKAM, R., COLIN, E., AKARSU, N. A., BOLE-FEYSOT, C., CAGNARD, N., SCHMITT, A., GOUDIN, N., LYONNET, S., ENCHA-RAZAVI, F., SIFFROI, J. P., WINEY, M., KATSANIS, N., GONZALES, M., VEKEMANS, M., BEALES, P. L. & ATTIE-BITACH, T. 2011. KIF7 mutations cause fetal hydrolethalus and acrocallosal syndromes. *Nat Genet,* 43, 601-6.

QUWAILID, M. M., HUGILL, A., DEAR, N., VIZOR, L., WELLS, S., HORNER, E., FULLER, S., WEEDON, J., MCMATH, H., WOODMAN, P., EDWARDS, D., CAMPBELL, D., RODGER, S., CAREY, J., ROBERTS, A., GLENISTER, P., LALANNE, Z., PARKINSON, N., COGHILL, E. L., MCKEONE, R., COX, S.,

WILLAN, J., GREENFIELD, A., KEAYS, D., BRADY, S., SPURR, N., GRAY, I., HUNTER, J., BROWN, S. D. & COX, R. D. 2004. A gene-driven ENU-based approach to generating an allelic series in any gene. ***Mamm Genome,*** **15, 585-91.**

RALPH, M. R. & MENAKER, M. 1988. A mutation of the circadian system in golden hamsters. ***Science,*** **241, 1225-7.**

REEVES, R. H., IRVING, N. G., MORAN, T. H., WOHN, A., KITT, C., SISODIA, S. S., SCHMIDT, C., BRONSON, R. T. & DAVISSON, M. T. 1995. A mouse model for Down syndrome exhibits learning and behaviour deficits. ***Nat Genet,*** **11, 177-84.**

REIJMERS, L. G., COATS, J. K., PLETCHER, M. T., WILTSHIRE, T., TARANTINO, L. M. & MAYFORD, M. 2006. A mutant mouse with a highly specific contextual fear-conditioning deficit found in an N-ethyl-N-nitrosourea (ENU) mutagenesis screen. ***Learn Mem,*** **13, 143-9.**

REINER, O., CARROZZO, R., SHEN, Y., WEHNERT, M., FAUSTINELLA, F., DOBYNS, W. B., CASKEY, C. T. & LEDBETTER, D. H. 1993. Isolation of a Miller-Dieker lissencephaly gene containing G protein beta-subunit-like repeats. ***Nature,*** **364, 717-21.**

RESTREPO, D., ARELLANO, J., OLIVA, A. M., SCHAEFER, M. L. & LIN, W. 2004. Emerging views on the distinct but related roles of the main and accessory olfactory systems in responsiveness to chemosensory signals in mice. ***Horm Behav,*** **46, 247-56.**

RICE, D. S. & CURRAN, T. 2001. Role of the reelin signaling pathway in central nervous system development. ***Annu Rev Neurosci,*** **24, 1005-39.**

ROBINSON, M. L., ALLEN, C. E., DAVY, B. E., DURFEE, W. J., ELDER, F. F., ELLIOTT, C. S. & HARRISON, W. R. 2002. Genetic mapping of an insertional hydrocephalus-inducing mutation allelic to hy3. ***Mamm Genome,*** **13, 625-32.**

RODERICK, T. H., WIMER, R. E., WIMER, C. C. & SCHWARTZKROIN, P. A. 1973. Genetic and phenotypic variation in weight of brain and spinal cord between inbred strains of mice. ***Brain Res,*** **64, 345-53.**

RODGERS, R. J. & DALVI, A. 1997. Anxiety, defence and the elevated plus-maze. ***Neurosci Biobehav Rev,*** **21, 801-10.**

ROGERS, D. C., FISHER, E. M., BROWN, S. D., PETERS, J., HUNTER, A. J. & MARTIN, J. E. 1997. Behavioral and functional analysis of mouse phenotype: SHIRPA, a proposed protocol for comprehensive phenotype assessment. ***Mamm Genome,*** **8, 711-3.**

ROPERS, H. H. 2010. Genetics of early onset cognitive impairment. ***Annu Rev Genomics Hum Genet,*** **11, 161-87.**

ROSENFELD, J. A., CROLLA, J. A., TOMKINS, S., BADER, P., MORROW, B., GORSKI, J., TROXELL, R., FORSTER-GIBSON, C., CILLIERS, D., HISLOP, R. G., LAMB, A., TORCHIA, B., BALLIF, B. C. & SHAFFER, L. G. 2010. Refinement of causative genes in monosomy 1p36 through clinical and molecular cytogenetic characterization of small interstitial deletions. ***Am J Med Genet A,*** **152A, 1951-9.**

RUSSELL, W. L., KELLY, E. M., HUNSICKER, P. R., BANGHAM, J. W., MADDUX, S. C. & PHIPPS, E. L. 1979. Specific-locus test shows ethylnitrosourea to be the most potent mutagen in the mouse. ***Proc Natl Acad Sci U S A,*** **76, 5818-9.**

RUTILA, J. E., SURI, V., LE, M., SO, W. V., ROSBASH, M. & HALL, J. C. 1998. CYCLE is a second bHLH-PAS clock protein essential for circadian rhythmicity and transcription of Drosophila period and timeless. ***Cell,*** **93, 805-14.**

SAITSU, H., TOHYAMA, J., KUMADA, T., EGAWA, K., HAMADA, K., OKADA, I., MIZUGUCHI, T., OSAKA, H., MIYATA, R., FURUKAWA, T., HAGINOYA, K., HOSHINO, H., GOTO, T., HACHIYA, Y., YAMAGATA, T., SAITOH, S., NAGAI, T., NISHIYAMA, K., NISHIMURA, A., MIYAKE, N., KOMADA, M., HAYASHI, K., HIRAI, S., OGATA, K., KATO, M., FUKUDA, A. & MATSUMOTO, N. 2010. Dominant-negative mutations in alpha-II spectrin cause West syndrome with severe cerebral hypomyelination, spastic quadriplegia, and developmental delay. ***Am J Hum Genet,*** **86, 881-91.**

SALINGER, W. L., LADROW, P. & WHEELER, C. 2003. Behavioral phenotype of the reeler mutant mouse: effects of RELN gene dosage and social isolation. ***Behav Neurosci,*** **117, 1257-75.**

SANDERSON, D. J., GRAY, A., SIMON, A., TAYLOR, A. M., DEACON, R. M., SEEBURG, P. H., SPRENGEL, R., GOOD, M. A., RAWLINS, J. N. & BANNERMAN, D. M. 2007. Deletion of glutamate receptor-A (GluR-A) AMPA receptor subunits impairs one-trial spatial memory. ***Behav Neurosci,*** **121, 559-69.**

SCHELL-APACIK, C. C., WAGNER, K., BIHLER, M., ERTL-WAGNER, B., HEINRICH, U., KLOPOCKI, E., KALSCHEUER, V. M., MUENKE, M. & VON VOSS, H. 2008. Agenesis and dysgenesis of the corpus callosum: clinical, genetic and neuroimaging findings in a series of 41 patients. ***Am J Med Genet A,*** **146A, 2501-11.**

SCHLESSINGER, A. R., COWAN, W. M. & GOTTLIEB, D. I. 1975. An autoradiographic study of the time of origin and the pattern of granule cell migration in the dentate gyrus of the rat. ***J Comp Neurol,*** **159, 149-75.**

SCHMALZIGAUG, R., RODRIGUIZ, R. M., PHILLIPS, L. E., DAVIDSON, C. E., WETSEL, W. C. & PREMONT, R. T. 2009. Anxiety-like behaviors in mice lacking GIT2. ***Neurosci Lett,*** **451, 156-61.**

SEHGAL, A., PRICE, J. L., MAN, B. & YOUNG, M. W. 1994. Loss of circadian behavioral rhythms and per RNA oscillations in the Drosophila mutant timeless. ***Science,*** **263, 1603-6.**

SHIFMAN, S., BELL, J. T., COPLEY, R. R., TAYLOR, M. S., WILLIAMS, R. W., MOTT, R. & FLINT, J. 2006. A high-resolution single nucleotide polymorphism genetic map of the mouse genome. ***PLoS Biol,*** **4, e395.**

SIVA, N. 2008. 1000 Genomes project. ***Nat Biotechnol,*** **26, 256.**

SOLLBERGER, A. 1965. Biological Rhythm Research. ***New York, Elsevier Publishing Company.***

SOSSEY-ALAOUI, K., HARTUNG, A. J., GUERRINI, R., MANCHESTER, D. K., POSAR, A., PUCHE-MIRA, A., ANDERMANN, E., DOBYNS, W. B. & SRIVASTAVA, A. K. 1998. Human doublecortin (DCX) and the homologous gene in mouse encode a putative Ca2+-dependent signaling protein which is mutated in human X-linked neuronal migration defects. ***Hum Mol Genet,*** **7, 1327-32.**

SPENNATO, P., MIRONE, G., NASTRO, A., BUONOCORE, M. C., RUGGIERO, C., TRISCHITTA, V., ALIBERTI, F. & CINALLI, G. 2011. Hydrocephalus in Dandy-Walker malformation. ***Childs Nerv Syst,*** **27, 1665-81.**

SPIEGELMAN, B. M., PENNINGROTH, S. M. & KIRSCHNER, M. W. 1977. Turnover of tubulin and the N site GTP in Chinese hamster ovary cells. ***Cell,*** **12, 587-600.**

STANEWSKY, R., KANEKO, M., EMERY, P., BERETTA, B., WAGER-SMITH, K., KAY, S. A., ROSBASH, M. & HALL, J. C. 1998. The cryb mutation identifies cryptochrome as a circadian photoreceptor in Drosophila. ***Cell,*** **95, 681-92.**

STOEPKER, C., HAIN, K., SCHUSTER, B., HILHORST-HOFSTEE, Y., ROOIMANS, M. A., STELTENPOOL, J., OOSTRA, A. B., EIRICH, K., KORTHOF, E. T., NIEUWINT, A. W., JASPERS, N. G., BETTECKEN, T., JOENJE, H., SCHINDLER, D., ROUSE, J. & DE WINTER, J. P. 2011. SLX4, a coordinator of structure-specific endonucleases, is mutated in a new Fanconi anemia subtype. ***Nat Genet,*** **43, 138-41.**

STOTTMANN, R. W. & BEIER, D. R. 2010. Using ENU mutagenesis for phenotype-driven analysis of the mouse. ***Methods Enzymol,*** **477, 329-48.**

STOTTMANN, R. W., MORAN, J. L., TURBE-DOAN, A., DRIVER, E., KELLEY, M. & BEIER, D. R. 2011. Focusing Forward Genetics: A Tri-partite ENU Screen for Neurodevelopmental Mutations in the Mouse. ***Genetics*****.**

TAKAHASHI, J. S. 1995. Molecular neurobiology and genetics of circadian rhythms in mammals. ***Annu Rev Neurosci,*** **18, 531-53.**

TAKAYANAGI, Y., FUJITA, E., YU, Z., YAMAGATA, T., MOMOI, M. Y., MOMOI, T. & ONAKA, T. 2010. Impairment of social and emotional behaviors in Cadm1-knockout mice. ***Biochem Biophys Res Commun,*** **396, 703-8.**

TARANTINO, L. M., GOULD, T. J., DRUHAN, J. P. & BUCAN, M. 2000. Behavior and mutagenesis screens: the importance of baseline analysis of inbred strains. ***Mamm Genome,*** **11, 555-64.**

TESTA, G., SCHAFT, J., VAN DER HOEVEN, F., GLASER, S., ANASTASSIADIS, K., ZHANG, Y., HERMANN, T., STREMMEL, W. & STEWART, A. F. 2004. A reliable lacZ expression reporter cassette for multipurpose, knockout-first alleles. ***Genesis,*** **38, 151-8.**

THONGNOPPAKHUN, A., RUNGROJ, N., WILAIRAT, P., VAREESANGTHIP, K., SIRINAVIN, C. & YENCHITSOMANUS, P. T. 2000. A novel splice-acceptor site mutation (IVS13-2A>T) of polycystic kidney disease 1 (PKD1) gene resulting in an RNA processing defect with a 74-nucleotide deletion in exon 14 of the mRNA transcript. ***Hum Mutat,*** **15, 115.**

TOYOFUKU, T., YOSHIDA, J., SUGIMOTO, T., ZHANG, H., KUMANOGOH, A., HORI, M. & KIKUTANI, H. 2005. FARP2 triggers signals for Sema3A-mediated axonal repulsion. ***Nat Neurosci,*** **8, 1712-9.**

TSUNEKAWA, N., YANAGAWA, Y. & OBATA, K. 2005. Development of GABAergic neurons from the ventricular zone in the superior colliculus of the mouse. ***Neurosci Res,*** **51, 243-51.**

VADOLAS, J., WARDAN, H., BOSMANS, M., ZAIBAK, F., JAMSAI, D., VOULLAIRE, L., WILLIAMSON, R. & IOANNOU, P. A. 2005. Transgene copy number-dependent rescue of murine beta-globin knockout mice carrying a 183 kb human beta-globin BAC genomic fragment. ***Biochim Biophys Acta,*** **1728, 150-62.**

VALLIER, L., MANCIP, J., MARKOSSIAN, S., LUKASZEWICZ, A., DEHAY, C., METZGER, D., CHAMBON, P., SAMARUT, J. & SAVATIER, P. 2001. An efficient system for conditional gene expression in embryonic stem cells and in their in vitro and in vivo differentiated derivatives. ***Proc Natl Acad Sci U S A,*** **98, 2467-72.**

VAN BON, B. W., KOOLEN, D. A., BRUETON, L., MCMULLAN, D., LICHTENBELT, K. D., ADES, L. C., PETERS, G., GIBSON, K., MOLONEY, S., NOVARA, F., PRAMPARO, T., DALLA BERNARDINA, B., ZOCCANTE, L., BALOTTIN, U., PIAZZA, F., PECILE, V., GASPARINI, P., GUERCI, V., KETS, M., PFUNDT, R., DE BROUWER, A. P., VELTMAN, J. A., DE LEEUW, N., WILSON, M., ANTONY, J., REITANO, S., LUCIANO, D., FICHERA, M.,

ROMANO, C., BRUNNER, H. G., ZUFFARDI, O. & DE VRIES, B. B. 2010. The 2q23.1 microdeletion syndrome: clinical and behavioural phenotype. *Eur J Hum Genet,* 18, 163-70.

VAN DEN BERG, R. & HOOGENRAAD, C. C. 2012. Molecular motors in cargo trafficking and synapse assembly. *Adv Exp Med Biol,* 970, 173-96.

VENTER, J. C., ADAMS, M. D., MYERS, E. W., LI, P. W., MURAL, R. J., SUTTON, G. G., SMITH, H. O., YANDELL, M., EVANS, C. A., HOLT, R. A., GOCAYNE, J. D., AMANATIDES, P., BALLEW, R. M., HUSON, D. H., WORTMAN, J. R., ZHANG, Q., KODIRA, C. D., ZHENG, X. H., CHEN, L., SKUPSKI, M., SUBRAMANIAN, G., THOMAS, P. D., ZHANG, J., GABOR MIKLOS, G. L., NELSON, C., BRODER, S., CLARK, A. G., NADEAU, J., MCKUSICK, V. A., ZINDER, N., LEVINE, A. J., ROBERTS, R. J., SIMON, M., SLAYMAN, C., HUNKAPILLER, M., BOLANOS, R., DELCHER, A., DEW, I., FASULO, D., FLANIGAN, M., FLOREA, L., HALPERN, A., HANNENHALLI, S., KRAVITZ, S., LEVY, S., MOBARRY, C., REINERT, K., REMINGTON, K., ABU-THREIDEH, J., BEASLEY, E., BIDDICK, K., BONAZZI, V., BRANDON, R., CARGILL, M., CHANDRAMOULISWARAN, I., CHARLAB, R., CHATURVEDI, K., DENG, Z., DI FRANCESCO, V., DUNN, P., EILBECK, K., EVANGELISTA, C., GABRIELIAN, A. E., GAN, W., GE, W., GONG, F., GU, Z., GUAN, P., HEIMAN, T. J., HIGGINS, M. E., JI, R. R., KE, Z., KETCHUM, K. A., LAI, Z., LEI, Y., LI, Z., LI, J., LIANG, Y., LIN, X., LU, F., MERKULOV, G. V., MILSHINA, N., MOORE, H. M., NAIK, A. K., NARAYAN, V. A., NEELAM, B., NUSSKERN, D., RUSCH, D. B., SALZBERG, S., SHAO, W., SHUE, B., SUN, J., WANG, Z., WANG, A., WANG, X., WANG, J., WEI, M., WIDES, R., XIAO, C., YAN, C., *et al.* 2001. The sequence of the human genome. *Science,* 291, 1304-51.

VISSERS, L. E., VAN RAVENSWAAIJ, C. M., ADMIRAAL, R., HURST, J. A., DE VRIES, B. B., JANSSEN, I. M., VAN DER VLIET, W. A., HUYS, E. H., DE JONG, P. J., HAMEL, B. C., SCHOENMAKERS, E. F., BRUNNER, H. G., VELTMAN, J. A. & VAN KESSEL, A. G. 2004. Mutations in a new member of the chromodomain gene family cause CHARGE syndrome. *Nat Genet,* 36, 955-7.

VITATERNA, M. H., KING, D. P., CHANG, A. M., KORNHAUSER, J. M., LOWREY, P. L., MCDONALD, J. D., DOVE, W. F., PINTO, L. H., TUREK, F. W. & TAKAHASHI, J. S. 1994. Mutagenesis and mapping of a mouse gene, Clock, essential for circadian behavior. *Science,* 264, 719-25.

VORHEES, C. V. & WILLIAMS, M. T. 2006. Morris water maze: procedures for assessing spatial and related forms of learning and memory. *Nat Protoc,* 1, 848-58.

WAGER-SMITH, K. & KAY, S. A. 2000. Circadian rhythm genetics: from flies to mice to humans. *Nat Genet,* 26, 23-7.

WAHLSTEN, D., HUDSPETH, W. J. & BERNHARDT, K. 1975. Implications of genetic variation in mouse brain structure for electrode placement by stereotaxic surgery. *J Comp Neurol,* 162, 519-31.

WALSH, C. A. 1999. Genetic malformations of the human cerebral cortex. *Neuron,* 23, 19-29.

WANG, J. Y., YEH, C. L., CHOU, H. C., YANG, C. H., FU, Y. N., CHEN, Y. T., CHENG, H. W., HUANG, C. Y., LIU, H. P., HUANG, S. F. & CHEN, Y. R. 2011. Vaccinia H1-related phosphatase is a phosphatase of ErbB receptors and is down-regulated in non-small cell lung cancer. *J Biol Chem,* 286, 10177-84.

WANG, W., CHAN, E. K., BARON, S., VAN DE WATER, T. & LUFKIN, T. 2001. Hmx2 homeobox gene control of murine vestibular morphogenesis. *Development,* 128, 5017-29.

WANG, Y., ZHENG, Y., LUO, F., FAN, X., CHEN, J., ZHANG, C. & HUI, R. 2009. KCTD10 interacts with proliferating cell nuclear antigen and its down-regulation could inhibit cell proliferation. *J Cell Biochem,* 106, 409-13.

WATAKABE, A., ICHINOHE, N., OHSAWA, S., HASHIKAWA, T., KOMATSU, Y., ROCKLAND, K. S. & YAMAMORI, T. 2007. Comparative analysis of layer-specific genes in Mammalian neocortex. *Cereb Cortex,* 17, 1918-33.

WATERSTON, R. H., LINDBLAD-TOH, K., BIRNEY, E., ROGERS, J., ABRIL, J. F., AGARWAL, P., AGARWALA, R., AINSCOUGH, R., ALEXANDERSSON, M., AN, P., ANTONARAKIS, S. E., ATTWOOD, J., BAERTSCH, R., BAILEY, J., BARLOW, K., BECK, S., BERRY, E., BIRREN, B., BLOOM, T., BORK, P., BOTCHERBY, M., BRAY, N., BRENT, M. R., BROWN, D. G., BROWN, S. D., BULT, C., BURTON, J., BUTLER, J., CAMPBELL, R. D., CARNINCI, P., CAWLEY, S., CHIAROMONTE, F., CHINWALLA, A. T., CHURCH, D. M., CLAMP, M., CLEE, C., COLLINS, F. S., COOK, L. L., COPLEY, R. R., COULSON, A., COURONNE, O., CUFF, J., CURWEN, V., CUTTS, T., DALY, M., DAVID, R., DAVIES, J., DELEHAUNTY, K. D., DERI, J., DERMITZAKIS, E. T., DEWEY, C., DICKENS, N. J., DIEKHANS, M., DODGE, S., DUBCHAK, I., DUNN, D. M., EDDY, S. R., ELNITSKI, L., EMES, R. D., ESWARA, P., EYRAS, E., FELSENFELD, A., FEWELL, G. A., FLICEK, P., FOLEY, K., FRANKEL, W. N., FULTON, L. A., FULTON, R. S., FUREY, T. S., GAGE, D., GIBBS, R. A., GLUSMAN, G., GNERRE, S., GOLDMAN, N., GOODSTADT, L., GRAFHAM, D., GRAVES, T. A., GREEN, E. D., GREGORY, S., GUIGO, R., GUYER, M., HARDISON, R. C., HAUSSLER, D., HAYASHIZAKI, Y., HILLIER, L. W., HINRICHS, A., HLAVINA, W., HOLZER, T., HSU, F., HUA, A., HUBBARD, T., HUNT, A., JACKSON, I., JAFFE, D. B., JOHNSON, L. S., JONES, M., JONES, T. A., JOY, A., KAMAL, M., KARLSSON, E. K., *et al.* 2002. Initial sequencing and comparative analysis of the mouse genome. *Nature,* 420, 520-62.

WEBER, J. S., SALINGER, A. & JUSTICE, M. J. 2000. Optimal N-ethyl-N-nitrosourea (ENU) doses for inbred mouse strains. *Genesis,* 26, 230-3.

WERNER, M., CHOTT, A., FABIANO, A. & BATTIFORA, H. 2000. Effect of formalin tissue fixation and processing on immunohistochemistry. *Am J Surg Pathol,* 24, 1016-9.

WILLEMSEN, M. H., VISSERS, L. E., WILLEMSEN, M. A., VAN BON, B. W., KROES, T., DE LIGT, J., DE VRIES, B. B., SCHOOTS, J., LUGTENBERG, D., HAMEL, B. C., VAN BOKHOVEN, H., BRUNNER, H. G., VELTMAN, J. A. & KLEEFSTRA, T. 2012. Mutations in DYNC1H1 cause severe intellectual disability with neuronal migration defects. *J Med Genet,* 49, 179-83.

WILLIAMS, C. A., DRISCOLL, D. J. & DAGLI, A. I. 2010a. Clinical and genetic aspects of Angelman syndrome. *Genet Med,* 12, 385-95.

WILLIAMS, S. R., MULLEGAMA, S. V., ROSENFELD, J. A., DAGLI, A. I., HATCHWELL, E., ALLEN, W. P., WILLIAMS, C. A. & ELSEA, S. H. 2010b. Haploinsufficiency of MBD5 associated with a syndrome involving microcephaly, intellectual disabilities, severe speech impairment, and seizures. *Eur J Hum Genet,* 18, 436-41.

WIMER, R. E., WIMER, C. C. & RODERICK, T. H. 1969. Genetic variability in forebrain structures between inbred strains of mice. *Brain Res,* 16, 257-64.

WISHART, T. M., PARSON, S. H. & GILLINGWATER, T. H. 2006. Synaptic vulnerability in neurodegenerative disease. ***J Neuropathol Exp Neurol,*** **65, 733-9.**

WOLSWIJK, G. 2002. Oligodendrocyte precursor cells in the demyelinated multiple sclerosis spinal cord. ***Brain,*** **125, 338-49.**

YAMADA, K. & WATANABE, M. 2002. Cytodifferentiation of Bergmann glia and its relationship with Purkinje cells. ***Anat Sci Int,*** **77, 94-108.**

YAMADA, Y., GOTO, H., WAKAMATSU, N. & OGASAWARA, N. 2001. A rare case of complete human erythrocyte AMP deaminase deficiency due to two novel missense mutations in AMPD3. ***Hum Mutat,*** **17, 78.**

YAMAUCHI, J., MIYAMOTO, Y., TORII, T., MIZUTANI, R., NAKAMURA, K., SANBE, A., KOIDE, H., KUSAKAWA, S. & TANOUE, A. 2009. Valproic acid-inducible Arl4D and cytohesin-2/ARNO, acting through the downstream Arf6, regulate neurite outgrowth in N1E-115 cells. ***Exp Cell Res,*** **315, 2043-52.**

YEANEY, N. K., HE, M., TANG, N., MALOUF, A. T., O'RIORDAN, M. A., LEMMON, V. & BEARER, C. F. 2009. Ethanol inhibits L1 cell adhesion molecule tyrosine phosphorylation and dephosphorylation and activation of pp60(src). ***J Neurochem,*** **110, 779-90.**

YU, A., ZHAO, C., FAN, Y., JANG, W., MUNGALL, A. J., DELOUKAS, P., OLSEN, A., DOGGETT, N. A., GHEBRANIOUS, N., BROMAN, K. W. & WEBER, J. L. 2001. Comparison of human genetic and sequence-based physical maps. ***Nature,*** **409, 951-3.**

ZHANG, X., ZHU, J., YANG, G. Y., WANG, Q. J., QIAN, L., CHEN, Y. M., CHEN, F., TAO, Y., HU, H. S., WANG, T. & LUO, Z. G. 2007. Dishevelled promotes axon differentiation by regulating atypical protein kinase C. ***Nat Cell Biol,*** **9, 743-54.**

ZHENG, J., XU, D. F., LI, K., WANG, H. T., SHEN, P. C., LIN, M., CAO, X. H. & WANG, R. 2011. Neonatal exposure to fluoxetine and fluvoxamine alteres spine density in mouse hippocampal CA1 pyramidal neurons. ***Int J Clin Exp Pathol,*** **4, 162-8.**

ZHU, P., ZHOU, W., WANG, J., PUC, J., OHGI, K. A., ERDJUMENT-BROMAGE, H., TEMPST, P., GLASS, C. K. & ROSENFELD, M. G. 2007. A histone H2A deubiquitinase complex coordinating histone acetylation and H1 dissociation in transcriptional regulation. ***Mol Cell,*** **27, 609-21.**

ZOU, Y. R., KOTTMANN, A. H., KURODA, M., TANIUCHI, I. & LITTMAN, D. R. 1998. Function of the chemokine receptor CXCR4 in haematopoiesis and in cerebellar development. ***Nature,*** **393, 595-9.**

ZYGOURAKIS, C. C. & ROSEN, G. D. 2003. Quantitative trait loci modulate ventricular size in the mouse brain. ***J Comp Neurol,*** **461, 362-9.**